An Experimental Study of Dimuons Produced in High Energy Neutrino Interactions

by

Karol Lang

Submitted in Partial Fulfillment

of the

Requirements for the Degree

Doctor of Philosophy

Supervised by Arie Bodek
Department of Physics and Astronomy
College of Arts and Sciences

University of Rochester

Rochester, New York

1985

Curriculum Vitae

Karol Lang, born 21 May 1955 in Warsaw, Poland, graduated from the XIV Warsaw High School in 1974. He attended the Department of Physics and Astronomy of the Warsaw University, Warsaw, Poland, and graduated in 1979 with the degree Master of Science. In 1979-1981 he worked in the High Energy Physics group of the Institute of Nuclear Research in Warsaw. Since 1981, he has been a graduate student at the University of Rochester in Rochester, New York, where he has done research in high energy neutrino physics and received the degree of Doctor of Philosophy.

Acknowledgments

All high energy physics experiments are efforts of teams of people. All members of CCFRR collaboration (full list in Appendix A) are warmly acknowledged for their contributions to both E616 and E701 experiments.

The results presented in this work are culmination of the three year efforts of my close collaborators : Arie Bodek, Frank Merritt, Frank Sciulli, Mike Shaevitz and Wesley Smith. Without their help and support the task would have not been achieved.

My special thanks go first to Wesley Smith whose tremendous enthusiasm and contribution in all stages of the analysis will be always for me an example difficult to follow. I have benefitted enormously from often discussions with Mike Shaevitz. His clear overview of the analysis and clarity of argumentation always made things easier.

My advisor Arie Bodek at all times provided me with solutions to encountered problems. I have been always impressed by his deep physical insight and have learned a lot from frequent discussions.

Tom Ferbel and Adam Para are kindly acknowledged for their good will in helping me start my studies at the University of Rochester. Tom and Barbara Ferbel's help at the very beginning enabled me to painlessly overcome all adjustment problems.

I am grateful to my parents for their support and encouragement throughout my entire academic carrier.

Finally, I want to thank my wife, Małgorzata, for her constant support, patience and sacrifice over the past few years. The short whiles of my free time shared with her and our daughter Marta made my effort possible.

Abstract

Results on production of dimuon events in high energy neutrino interactions are presented.

The 18 observed like sign dimuon events with muon momentum cut of 9 GeV/c have a calculated background of 11.4±2.2 events. This yields an average rate for prompt like sign dimuon production of $(1.0\pm0.7)\times10^{-4}$ per charged current event. Some of the distributions of the kinematical variables indicate that not all observed events originate from the hadron shower background.

The opposite-sign dimuon signal is consistent with the charm production model in which the second muon originates from the production and semileptonic decays of charm particles. The rate for such a process rises with energy and reaches a value of $(9.0\pm1.1)\times10^{-3}$ at $E_\nu=200$ GeV.

The opposite-sign dimuon data were used for the extraction of the strange sea fraction in the nucleon expressed by the parameter $\kappa=2s(x)/(\bar{u}(x)+\bar{d}(x))$. The data yield $\kappa=0.42^{+0.13}_{-0.10}$ over the full neutrino energy range

30-230 GeV, where errors include uncertainties due to statistics, hadron shower background subtraction, and charm quark mass and fragmentation.

These parameters were unexpectedly found to be energy dependent : $\kappa=0.19^{+0.18}_{-0.14}$ in 30-100 GeV energy range, and $\kappa=0.52^{+0.17}_{-0.15}$ in 100-230 GeV range.

The opposite-sign dimuon data were also used to measure the semileptonic branching ratio of neutrino produced charm particles decaying into muons. The measured value of $B_1=0.093^{+0.022}_{-0.020}$ is consistent with the results extracted from the e^+e^- and ν-emulsion experiments.

Table of Contents

page

Chapter 1: Introduction.....1
1.1 Deep Inelastic Neutrino Scattering 5
1.2 Neutrino Cross-Section 7
1.3 Neutrino Induced Dimuon Cross-Section 9

Chapter 2: Neutrino Beam and Apparatus.....15
2.1 Neutrino Beam 15
2.2 Neutrino Detector 21

Chapter 3: Event Reconstruction and Data Sample..... 29
3.1 Event Reconstruction 33
3.1.1 Hadron Energy Determination 33
3.1.2 Muon Energy Determination 35
3.2 Dimuon Selection and Reconstruction 36
3.3 Cuts 39
3.3.1 Cuts on the Beam 39
3.3.2 Cuts on Events 40
3.4 Acceptance Corrections 44
3.5 Final Data Set and Its Characteristics 51
3.5.1 1μ Charged Current Data 52
3.5.2 Dimuon Data 57

Chapter 4: Background Calculation.....64
4.1 Fragmentation Functions from BEBC 69
4.2 Relative Fragmentation Functions from EMC 71
4.3 Lund Monte Carlo Calculations 74
4.4 Muon Rates from the Fermiiab Experiment E379 80
4.5 Interaction and Decay Lengths of Primary Hadrons 84
4.6 Outline of the Background Calculation 86
4.7 Systematic Errors on the Background Rate 95

Chapter 5: Neutrino Charm Production Monte Carlo.....97
5.1 Single-Muon Charged Current Monte Carlo 99
5.2 Monte Carlo for Production of Opposite-Sign Dimuons 106
5.2.1 The Fragmentation Function of Charm Quarks 108
5.2.2 The Semileptonic Branching Ratio $B_1(c\to\mu X)$ 113
5.2.3 Outline of the Charm Monte Carlo Calculation 116
5.3 Outline of the Background Monte Carlo 119

Chapter 6: Results on Like-Sign Dimuons.....121
6.1 Like-Sign Dimuon Rates 125
6.2 Like-Sign Dimuon Kinematics 135

Chapter 7: Results on Opposite-Sign Dimuons.....159
7.1 Rates of Opposite-Sign Dimuons 161
7.2 The Fraction of the Strange Sea in the Nucleon 171
7.3 The Determination of the Semileptonic Branching Ratio of Charm->Muons in Neutrino Interactions 174
7.4 Energy Dependence of κ 175
7.5 Effect of a Semileptonic Branching Ratio, Charm Quark Mass, and Fragmentation 178
7.6 Effect of Like-Sign Dimuons on the Extraction of the Strange Sea 187
7.7 Kinematics of Opposite-Sign Dimuons 189
7.8 Conclusions 195

References 197

Appendix A: Participants in the CCFRR Collaboration 203
Appendix B: Parametrization of the BEBC Fragmentation Functions 205
Appendix C: Multiplicities Used in the Background Calculations 207
Appendix D: Muon Rates from E379 209
Appendix E: Decay and Interaction Lengths of Pions and Kaons 217
Appendix F: Mean x Values Used in the Background Calculations 220
Appendix G: Final Tables and Fits of the Muon Rates from Neutrino and Antineutrino Showers 221
Appendix H: Like-Sign Dimuon Sample 245

List of Tables

page

Table 3.1 Definitions of energy bins used in the analysis 51
Table 3.2 Number of 1μ Events (CLASS 1, ν) 53
Table 3.3 Number of 1μ Events (CLASS 1, anti-ν) 53
Table 3.4 Number of 1μ Events (CLASS 2 & 3, ν) 53
Table 3.5 Number of 1μ Events (CLASS 2 & 3, anti-ν) 53
Table 3.6 Characteristics of 1μ Events (CLASS 1, ν) 54
Table 3.7 Characteristics of 1μ Events (CLASS 1, anti-ν) 54
Table 3.8 Characteristics of 1μ Events (CLASS 2,3, ν) 55
Table 3.9 Characteristics of 1μ Events (CLASS 2,3, anti-ν) 55
Table 3.10 Mean neutrino energies (CLASS 1) 56
Table 3.11 Mean antineutrino energies (CLASS 1) 56
Table 3.12 Mean neutrino energies (CLASS 2 & 3) 56
Table 3.13 Mean antineutrino energies (CLASS 2 & 3) 57
Table 3.14 Number of 2μ neutrino events(p>4.3GeV/c) 57
Table 3.15 Number of 2μ antineutrino events (p>4.3GeV/c) 57
Table 3.16 Number of 2μ neutrino events (p>9GeV/c) 58
Table 3.17 Number of 2μ antineutrino events (p>9GeV/c) 58
Table 3.18 Number of like-sign dimuons (p>9GeV/c) 58
Table 3.19 Characteristics of neutrino 2μ (p>4.3 GeV/c) 59
Table 3.20 Characteristics of antineutrino 2μ (p>4.3GeV/c) 60
Table 3.21 Characteristics of neutrino 2μ (p>9GeV/c) 61
Table 3.22 Characteristics of antineutrino 2μ (p>9GeV/c) 62
Table 3.23 Characteristics of like-sign 2μ (p>4GeV/c) 63
Table 6.1 Number and mean energies of 1μ and $\mu^-\mu^-$ events 122
Table 6.2 Kinematics of 1μ and $\mu^-\mu^-$ events 123
Table 6.3 Comparison of the like-sign dimuon data from several experiments 125
Table 6.4 Proposed mechanisms for $\mu^-\mu^-$ production and experimental limits 126
Table 6.5 Rates of like-sign dimuons from CCFRR 131
Table 6.6 Comparison like-sign dimuons from several experiments 133
Table 6.7 Means of kinematics of like-sign dimuon data, hadron shower background, and hadron shower background with c-c 136
Table 6.8 Comparison of kinematics of opposite-sign dimuons with p > 9 GeV/c and charm Monte Carlo 151
Table 7.1 Number of background events for opposite-sign dimuons with p > 4.3 GeV/c 160
Table 7.2 Calculation of opposite-sign dimuon rates from neutrino interactions 165

Table 7.3 Calculation of opposite-sign dimuon rates from antineutrino interactions 165
Table 7.4 Rates of opposite-sign dimuons corrected for slow rescaling with m_c=1.0,1.5,and 1.9 GeV/c^2 168
Table 7.5 Energy dependence of κ 175
Table 7.6 Effect of $c-\bar{c}$ contamination on κ 177
Table 7.7 Effect of charm quark mass on κ 182
Table 7.8 Effect of fragmentation function on κ 185
Table 7.9 Effect of fragmentation function in the form δ(z-0.68) on κ 186

List of Figures

		page
Figure 1.1	Schematic deep inelastic neutrino scattering from a nucleon	4
Figure 1.2	Diagram for opposite-sign dimuon production	10
Figure 2.1	The layout of the Fermilab neutrino narrow band beam	16
Figure 2.2	The flux of neutrinos at the Fermilab Lab E detector from 200 GeV/c primary beam	18
Figure 2.3	The separation of pion and kaon neutrino events	19
Figure 2.4	Overview of the Lab E detector	23
Figure 2.5	The detailed structure of the Lab E target cart	24
Figure 2.6	The structure of the target and spectrometer of the Lab E detector	25
Figure 2.7	The E701 configuration of the Lab E detector	27
Figure 3.1	A computer display of a dimuon event with both muons momentum analyzed	31
Figure 3.2	A computer display of a dimuon event with the second muon ranging out	32
Figure 3.3	Distribution of $\theta_{\mu 1}$	45
Figure 3.4	Distribution of $\theta_{\mu 2}$	46
Figure 3.5	Illustration of the geometric acceptance calculation	48
Figure 4.1	Illustration of the hadron shower development as a source of the second muon production	67
Figure 4.2	EMC fragmentation functions	72
Figure 4.3	BEBC and Lund MC fragmentation functions	76
Figure 4.4	Charged kaons fragmentation functions from Lund MC and fits to the BEBC/EMC data	77
Figure 4.5	Neutral kaon fragmentation functions compared with five measurements	79
Figure 4.6	Muon rates from E379	81-82
Figure 4.7	Total probability of a muon production from neutrino induced hadron showers	89-90
Figure 4.8	Total probability of a muon production from antineutrino induced hadron showers	91-92
Figure 4.9	Comparison of muon rates from E379 and the calculation	93-94
Figure 5.1	F_2 and xF_3 structure functions	100
Figure 5.2	The x distributions of valence and sea quarks	101
Figure 5.3	Distribution of measured neutrino energy in 1μ charged current events	102
Figure 5.4	Distribution of measured hadron energy in 1μ charged current events	103
Figure 5.5	The Bjorken x distribution as measured in single-muon charged current events	104
Figure 5.6	Distribution of y from single-muon charged current events	105
Figure 5.7	Distribution of W^2 as measured in single-muon charged current events	110
Figure 5.8	Fragmentation of D^{*+} meson as measured by the ARGUS collaboration	111
Figure 6.1	Proposed diagrams for like-sign dimuon production	127-129
Figure 6.2	Like-sign dimuon rates	134
Figure 6.3	Distributions of several kinematic quantities from like-sign dimuons and hadron shower background events (ϕ_{12}, p_{Tmin}^2, $p_{\mu 2}$, E_{mis}, $z_{\mu 2}$, M_{12})	137-142
Figure 6.4	Distributions of several kinematic quantities from like-sign dimuons and background events from hadron shower and $c-\bar{c}$ (ϕ_{12}, p_{Tmin}^2, $p_{\mu 2}$, E_{mis}, $z_{\mu 2}$, M_{12})	144-149
Figure 6.5	Distribution of missing energy in 1μ events	150
Figure 6.6	Distributions of several kinematic quantities from opposite-sign dimuons and charm Monte Carlo (ϕ_{12}, p_{Tmin}^2, $p_{\mu 2}$, E_{mis}, $z_{\mu 2}$, M_{12})	152-157
Figure 7.1	Rates of opposite-sign dimuons in neutrino interactions	162
Figure 7.2	Rates of opposite-sign dimuons in antineutrino interactions	163
Figure 7.3	Rates of opposite-sign dimuons corrected for slow rescaling with m_c=1.0, 1.5, and 1.9 GeV/c^2	167
Figure 7.4	Opposite-sign neutrino dimuon rates from CCFRR and CDHS collaborations	169
Figure 7.5	Opposite-sign antineutrino dimuon rates from CCFRR and CDHS collaborations	170
Figure 7.6	1,2,3 σ contours in κ-B_1 χ^2 plane	173
Figure 7.7	Correlation κ-B_1	179
Figure 7.8	Correlation κ-B_1 for m_c=1.0, 1.5, and 1.9 GeV/c^2	180
Figure 7.9	Correlation κ-B_1 for ε=0.09, 0.19, and 0.29	183
Figure 7.10	Correlation κ-B_1 for $\delta(z-0.68)$ charm fragmentation function	184
Figure 7.11	The x distribution of opposite-sign dimuons and charm Monte Carlo	190

Figure 7.12 The ϕ_{12} distribution of opposite-sign dimuons and charm Monte Carlo 191
Figure 7.13 The $z_{\mu 2}$ distribution of opposite-sign dimuons and charm Monte Carlo 192
Figure 7.14 The missing energy distribution of opposite-sign dimuons and charm Monte Carlo 193
Figure 7.15 The distribution of transverse second muon momentum with respect to the hadron shower direction 194

Chapter 1

Introduction

The first observation of neutrino interactions with two muons of opposite sign in the final state occurred in the summer of 1974. The two reported events [1.1] could not be explained by processes known at that time. The origins of neutrino dimuons events were understood only after charm particles were discovered [1.2], and significant data samples were collected [1.2].

Production of dimuons in neutrino interactions was expected within the framework of a four quark model. The second muon originates from the production and subsequent semileptonic decay of a heavy charm quark [1.4, 1.5].

Initially, other competing mechanisms such as production of a new heavy neutral lepton [1.6], production of a weak intermediate vector or scalar boson [1.7], or charm production through the right-handed currents [1.8] were proposed. These "exotic" models were later ruled out by high statistics experiments, which established the interpretation of the observed $\mu^-\mu^+$ events in terms of charm particle production [1.9,1.10,1.11,1.3f,1.3g].

Additional confirmation of the semileptonic decay of charm particles as the source of opposite-sign dimuons came from the observation of an opposite-sign muon-electron (μe) pair in neutrino interactions in bubble chamber experiments [1.12].

The origin of opposite-sign dimuons is fairly well understood. Dimuons of the same sign, however [1.13,1.10,1.11], have stimulated a lot of interest since they could possibly originate from an unknown process. Experimental data reported so far are not conclusive; most reported results quote a 2 standard deviation prompt signal above the background at a level of 10^{-4} to 10^{-3} of the single muon rate. The situation regarding the production of like-sign μe pairs in bubble chambers (which may originate from the same source as like-sign dimuons) is similarly inconclusive [1.14].

At present, there is no theoretical model which predicts a level of prompt like-sign dimuons at such high rates.

This work reports results on neutrino dimuon production from an experiment performed at Fermilab by the Columbia - Chicago - Fermilab - Rochester - Rockefeller (CCFRR) collaboration (the full list of participants is given in Appendix A). Neutrino production of prompt like-sign dimuons is discussed. Studies of charm particle production leading to opposite-sign dimuons, and information about the extraction of the fraction of the strange sea in the nucleon are presented.

A brief introduction of deep inelastic neutrino scattering is given in Chapter 1. The neutrino beam and neutrino detector are presented in Chapter 2. The collected data sample and its main characteristics are given in Chapter 3. Details about hadron shower background calculation are outlined in Chapter 4. A description of Monte Carlo calculations of opposite-sign dimuons through charm quark production is given in Chapter 5. Prompt like-sign dimuon production is discussed in Chapter 6, and the results on the strange sea in the nucleon, and conclusions are presented in Chapter 7.

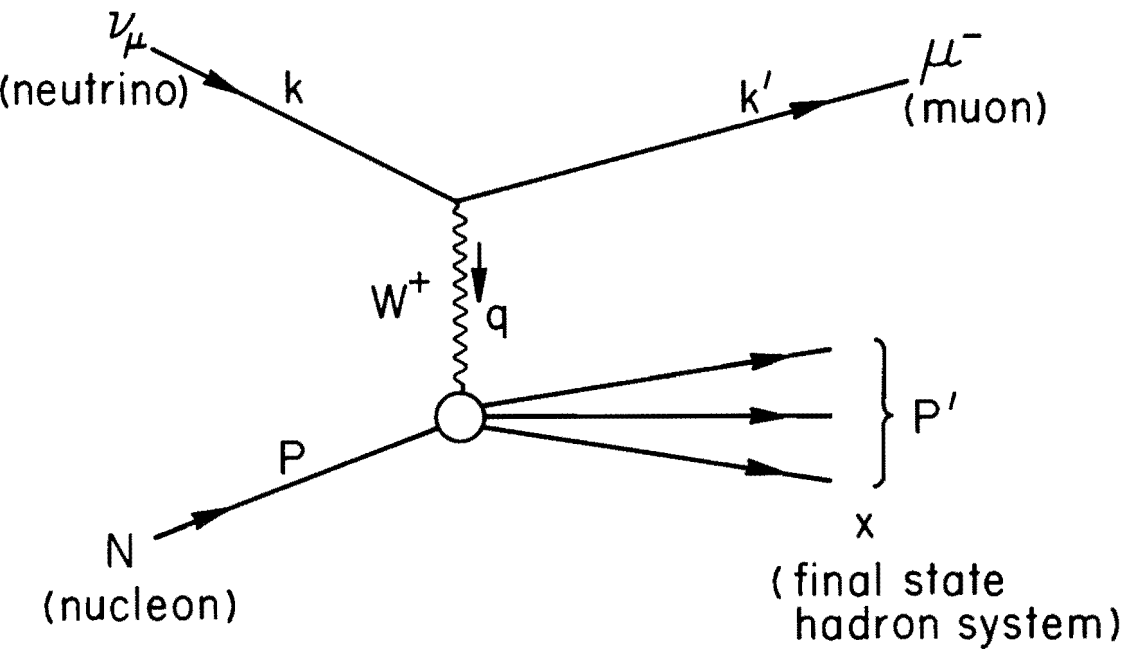

Figure 1.1 Schematic deep inelastic neutrino scattering from a nucleon.

1.1 Deep Inelastic Neutrino Scattering

Fig.1.1 schematically depicts a charged current neutrino interaction. The 4-momenta of the incident neutrino (k), the outgoing muon (k'), the target proton (p), and the final state hadron system (p') are:

$$k = (E_\nu, 0, 0, E_\nu) \tag{1.1.1a}$$

$$k' = (E_\mu, p_\mu \sin\theta_\mu \cos\Phi_\mu, p_\mu \sin\theta_\mu \cos\Phi_\mu, p_\mu \cos\Phi_\mu) \tag{1.1.1b}$$

$$p = (M, 0, 0, 0) \tag{1.1.1c}$$

$$p' = p+q = p+(k-k') = (M+E_\nu-E_\mu, -p_\mu \sin\theta_\mu \cos\Phi_\mu, -p_\mu \sin\theta_\mu \cos\Phi_\mu, E_\nu - p_\mu \cos\Phi_\mu) \tag{1.1.1d}$$

here $q = k-k'$ is the 4-momentum transferred to the nucleon, E_ν is the neutrino energy in the lab, E_μ and p_μ are the energy and momentum of the outgoing muon, and θ_μ and Φ_μ are the polar and azimuthal angles of the muon (in the lab) with respect to the neutrino direction. The Lorentz invariant quantities often used are:

the center of mass energy:

$$s = (p+k)^2 = M^2 + 2ME_\nu \approx 2ME_\nu \; ; \tag{1.1.2}$$

the neutrino energy loss in the lab :

$$\nu = qp/M = E_\nu - E_\mu \; ; \tag{1.1.3}$$

the square of 4-momentum transfer:

$$Q^2 = -q^2 = -(k-k')^2 = 2E_\mu E_\mu - 2E_\nu p_\mu \cos\theta_\mu - m_\mu{}^2 =$$
$$= 2E_\nu E_\mu(1-\cos\theta_\mu) = 4E_\nu E_\mu \sin^2\theta_\mu{}^2/2 \; ; \qquad (1.1.4)$$

the square of the mass of the system recoiling against the lepton (= invariant mass of the hadronic system):

$$W^2 = p'^2 = (p+q)^2 = M^2 + 2M\nu - Q^2 \; ; \qquad (1.1.5)$$

the Bjorken variable x:

$$x = Q^2/2M\nu \; ; \qquad (1.1.6)$$

and the fraction of the neutrino energy lost in the lab:

$$y = qp/kp = \nu/E_\nu \; . \qquad (1.1.7)$$

In the quark-parton model the variable x (or x_{Bj}) is the fraction of the target nucleon's momentum carried by the struck quark. For the case where the struck quark has negligible mass but the outgoing quark has a significant mass m_q :

$$(q+x'p)^2 = m_q{}^2 \; , \qquad (1.1.8)$$

and therefore:

$$-Q^2 + 2M\nu x' + x'^2M^2 = m_q{}^2 \; . \qquad (1.1.9)$$

Neglecting the term x'^2M^2 yields

$$x' = Q^2/2M\nu + m_q{}^2/2M\nu \; , \qquad (1.1.10)$$

or

$$x' = x_{Bj} + m_q{}^2/2M\nu . \qquad (1.1.11)$$

In the case of heavy quark production the fractional momentum carried by the struck quark is x', as given by (1.1.11). This redefinition carries the name of slow rescaling [1.15].

1.2 Neutrino Cross Section

In a simple scaling model the high energy cross section of neutrinos interacting with an isoscalar target (equal number of neutrons and protons) can be expressed as :

$$\frac{d^2\sigma^\nu}{dxdy} = \frac{G^2 s}{2\pi}[q^\nu(x) + \bar{q}^\nu(x)(1-y)^2 + 2k(x)(1-y)] \qquad (1.2.1)$$

and for antineutrinos:

$$\frac{d^2\sigma^{\bar{\nu}}}{dxdy} = \frac{G^2 s}{2\pi}[q^{\bar{\nu}}(x)(1-y)^2 + \bar{q}^{\bar{\nu}}(x) + 2k(x)(1-y)] \qquad (1.2.2)$$

where $q(x)dx = x\rho_q(x)dx$ is the distribution in fractional momentum x, multiplied by x, of spin-1/2 constituents in the nucleon (and $\bar{q}(x)$ their antiparticles), and k(x) denotes spin-0 type constituents.

Within the framework of the quark-parton model (with 4 quarks) tne nucleon spin-1/2 constituents are identified with quarks and antiquarks (the four quarks being: up (u) (charge=+2/3); down (d) (charge=-1/3), strange (s) (charge=-1/3); charm (c) (charge=+2/3)). The definitions of quark distributions in the nucleon are:

$$q(x) = u(x) + d(x) + s(x) + c(x) \qquad (1.2.3a)$$

$$\bar{q}(x) = \bar{u}(x) + \bar{d}(x) + \bar{s}(x) + \bar{c}(x) \qquad (1.2.3b)$$

and

$$q^{\nu}=q(x)-c(x)+s(x)=u(x)+d(x)+2s(x) \qquad (1.2.4a)$$

$$\bar{q}^{\nu}=\bar{q}(x)+\bar{c}(x)-\bar{s}(x)=\bar{u}(x)+\bar{d}(x)+2\bar{c}(x) \qquad (1.2.4b)$$

$$q^{\nu}=q(x)+c(x)-s(x)=u(x)+d(x)+2c(x) \qquad (1.2.4c)$$

$$\bar{q}^{\nu}=\bar{q}(x)-\bar{c}(x)+\bar{s}(x)=\bar{u}(x)+\bar{d}(x)+2\bar{s}(x) \qquad (1.2.4d)$$

In this language the structure functions of the nucleon are:

$$F_2(x,Q^2) = q(x) + \bar{q}(x) + 2k(x) \qquad (1.2.5)$$

$$2xF_1(x,Q^2) = q(x) + \bar{q}(x) \qquad (1.2.6)$$

$$xF_3(x,Q^2) = q(x) - \bar{q}(x) \qquad (1.2.7)$$

and the measure of spin-0 constituents is:

$$R'(x,Q^2) = 2k(x)/(q(x)+\bar{q}(x)) \qquad (1.2.8)$$

The F_2 structure function is therefore a measure of all spin 0 and 1/2 constituents in the nucleon, $2xF_1$ is a measure of spin-1/2 constituents, and xF_3 represents valence spin-1/2 components. The cross section written in terms of structure functions is:

$$\frac{d\sigma^{\nu(\bar{\nu})}}{dxdy}=\frac{G^2ME_{\nu}}{\pi}\left\{\left(1-y-\frac{Mxy}{2E_{\nu}}\right)F_2^{\nu(\bar{\nu})}(x,Q^2) + \frac{y^2}{2}\,2xF_1^{\nu(\bar{\nu})}(x,Q^2) \pm y\left(1-\frac{y}{2}\right)xF_3^{\nu(\bar{\nu})}(x,Q^2)\right\} \qquad (1.2.9)$$

1.3 Neutrino Induced Dimuon Cross Section

The dominant source of the second oppositely charged muon in neutrino (antineutrino) interactions with two muons in the final state is the semileptonic decay of a charm particle. This requires that a charm (anticharm) quark is produced in the neutrino (antineutrino) scattering.

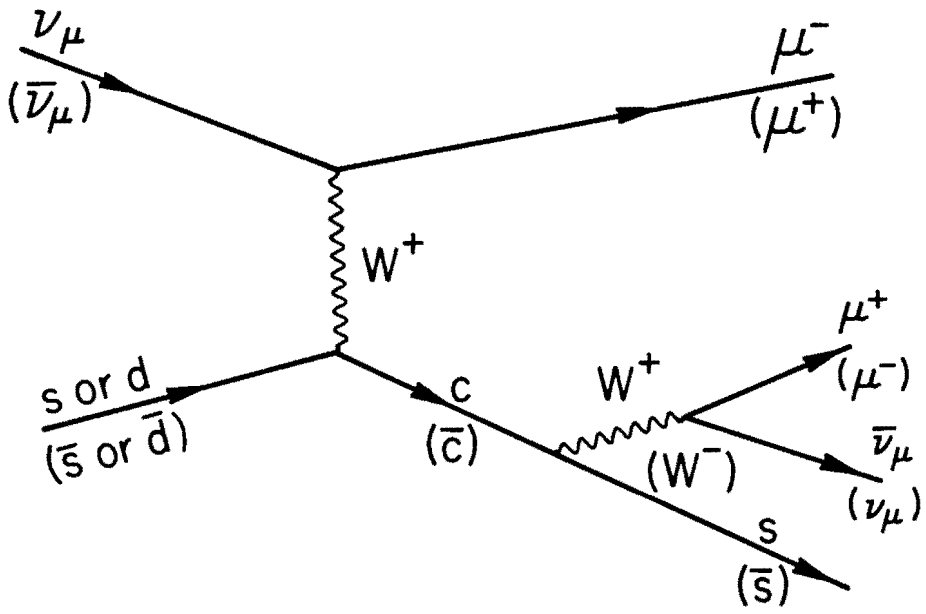

Figure 1.2 Diagram for opposite-sign dimuon production through charm quark production and its semileptonic decay.

Fig.1.2 illustrates this process. The production of a charm quark by neutrinos can occur only on s or d quarks, and production of an anticharm quark on $\bar{s}$ or $\bar{d}$ antiquarks. In the absence of threshold effects (assuming negligible charm quark mass) the cross section for charm production can be expressed as:

$$\frac{d\sigma^{\nu}(\text{charm})}{dxdy} = \frac{G^2 M E_\nu}{2\pi}\left[(u(x)+d(x))\sin^2\theta_c + 2s(x)\cos^2\theta_c\right] \tag{1.3.1}$$

$$\frac{d\sigma^{\bar{\nu}}(\text{charm})}{dxdy} = \frac{G^2 M E_{\bar{\nu}}}{2\pi}\left[(\bar{u}(x)+\bar{d}(x))\sin^2\theta_c + 2\bar{s}(x)\cos^2\theta_c\right] \tag{1.3.2}$$

where θ_c is Cabibbo angle ($\sin^2\theta_c$=0.053; $\cos^2\theta_c$=0.947) which reflects the weak interaction selection rules.

The significant charm quark mass (expected to be of the order of 1.5 GeV/c^2) requires the slow rescaling substitution (1.1.8-1.1.11):

$$x \rightarrow x' = x + m_c^2/2M\nu \qquad (m_c\text{=charm quark mass}).$$

This procedure naturally introduces threshold effects for heavy quark production.

The full expression for <u>dimuon</u> production has to contain a factor for charm quark fragmentation into charm particles, and the semileptonic decay branching ratio of charm particles into muons (B_l(charm -> μX). For an isoscalar target the neutrino cross section to produce opposite-sign dimuons can be written in the following form [1.15, 1.16, 1.17, 1.18, 1.19].

$$\frac{d^3\sigma(\mu^-\mu^+)}{dx'dydz} = \frac{G^2 ME_\nu}{2\pi}\,[x'(u(x')+d(x'))\sin^2\theta_c +$$

$$+ 2s(x')\cos^2\theta_c][1-\frac{m_c^2}{2ME_\nu x'}]D(z_D)B_l(\text{charm} \to \mu X) \qquad (1.3.3)$$

Here the fragmentation of charm quark is described by the function $D(z_D)$, where z_D $(0<z_D<1)$ is the ratio of the momentum of the charm particle (predominantly D mesons) to the maximum possible momentum of this particle in the W-boson - nucleon center of mass:

$$z_D = p_D^*/p_{max}^* \qquad (1.3.4)$$

where

$$p_{max}^{*2} = W^2/4 - M_D^2 , \qquad (1.3.5)$$

M_D is the charm particle mass, and W^2 is defined by (1.1.5)

Details of the assumptions about structure functions, fragmentation functions, and semileptonic branching ratios used in the Monte Carlo model of dimuon production are discussed in Chapter 5.

The primary physics goal of studies of neutrino induced opposite-sign dimuons is the determination of the strange sea content of the nucleon. The commonly used parameters that can be extracted from the data are:

$$\kappa = 2s(x)/(\bar{u}(x)+\bar{d}(x)) \qquad (1.3.6)$$

and a quantity which is closely related to the measured dimuon and single-muon cross sections:

$$\eta_s = 2S/(U+D) \quad , \qquad (1.3.7)$$

where

$$S = \int_0^1 s(x)dx, \quad D = \int_0^1 d(x)dx, \text{ and } \quad U = \int_0^1 u(x)dx. \qquad (1.3.8)$$

The extraction of the strange sea is done under the assumption that, aside from the relative normalization, the shape of the sea components ($u_s(x)$, $d_s(x)$, and $s(x)$) are the same. Results for κ and η_s from this experiment are discussed in Chapter 7.

Chapter 2

Neutrino Beam and Apparatus

The Fermilab neutrino narrow band beam (NBB) has been described in detail in several publications [2.1-2.6]. The neutrino detector used for this experiment has also been presented previously [2.7,2.4,2.5]. Therefore, only brief description necessary to understand the nature of the experimental set-up is given.

2.1 Neutrino Beam

Fig.2.1 shows the layout of the Fermilab narrow band neutrino beam.

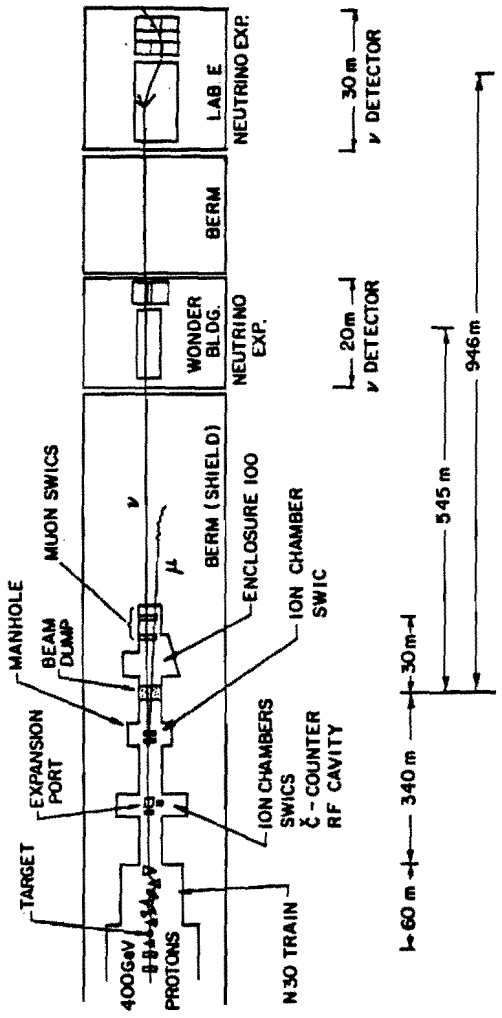

Figure 2.1 The layout of the Fermilab neutrino narrow band beam.

The 400 GeV primary proton beam with intensities of about 1×10^{13} protons per spill (monitored by Secondary Emission Monitor, inductive toroid, and RF cavity) was focused on a beryllium target producing secondary particles.

The secondary beam (mostly pions and kaons) passed through a magnetic train (system of dipole and quadrupole magnets on rails), which selected particles with the desired charge sign and momentum. In this experiment the train was set to select particles with charge/momentum of +100, ±120, ±140, ±165, ±200, and ±250 GeV/c. The RMS momentum spread of the accepted secondary beam was 10%.

Next, the beam traversed a 340m long evacuated tube (decay pipe), where decaying pions and kaons produced a flux of neutrinos. At the end of the decay pipe the beam was stopped in iron and earth shields.

Due to the mass difference between pions and kaons the flux of neutrinos had a dichromatic energy spectrum, i.e. a high energy band from kaons (called ν_K) well separated from a low energy band from pions (called ν_π). Kaon 3-body decays played an insignificant role. The neutrino energy E_ν^D

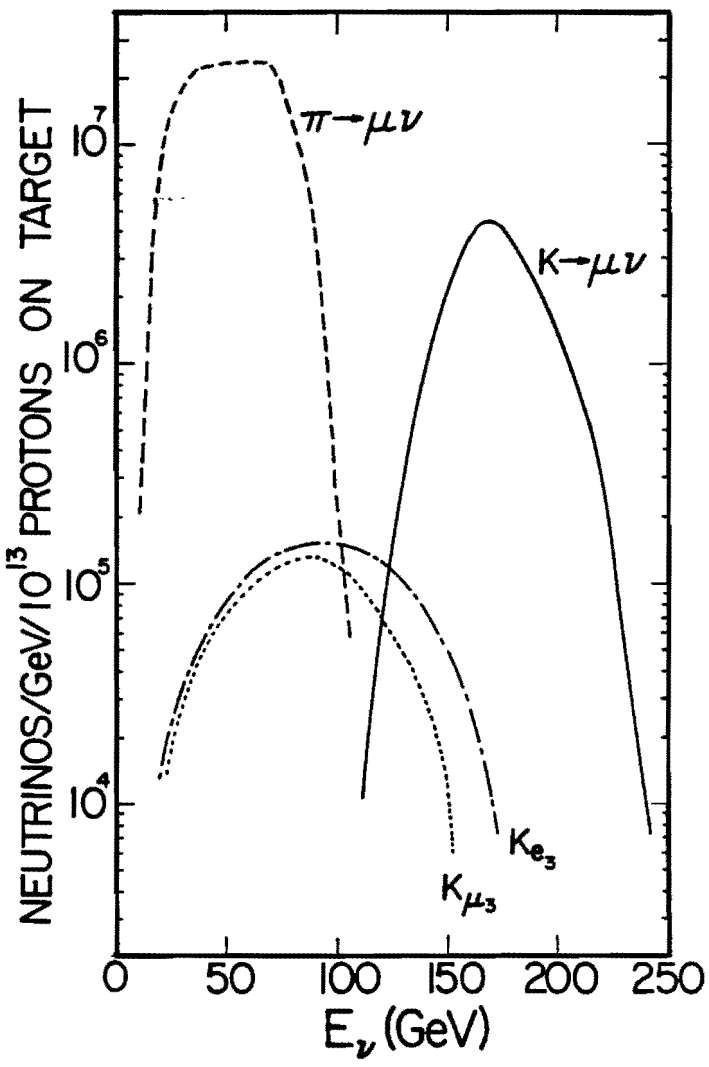

Figure 2.2 The flux of neutrinos at the Fermilab Lab E detector with the central hadron momentum selected at 200 GeV/c with positive electric charge. The dichromatic nature of the beam is clear. The small neutrino contamination from three-body kaon decays is also shown. Low-momentum decays before momentum selection of the meson beam produced additional background primarily below 20 GeV. This wide band contribution can be directly measured by stopping the dichromatic beam before its entry into the decay region.

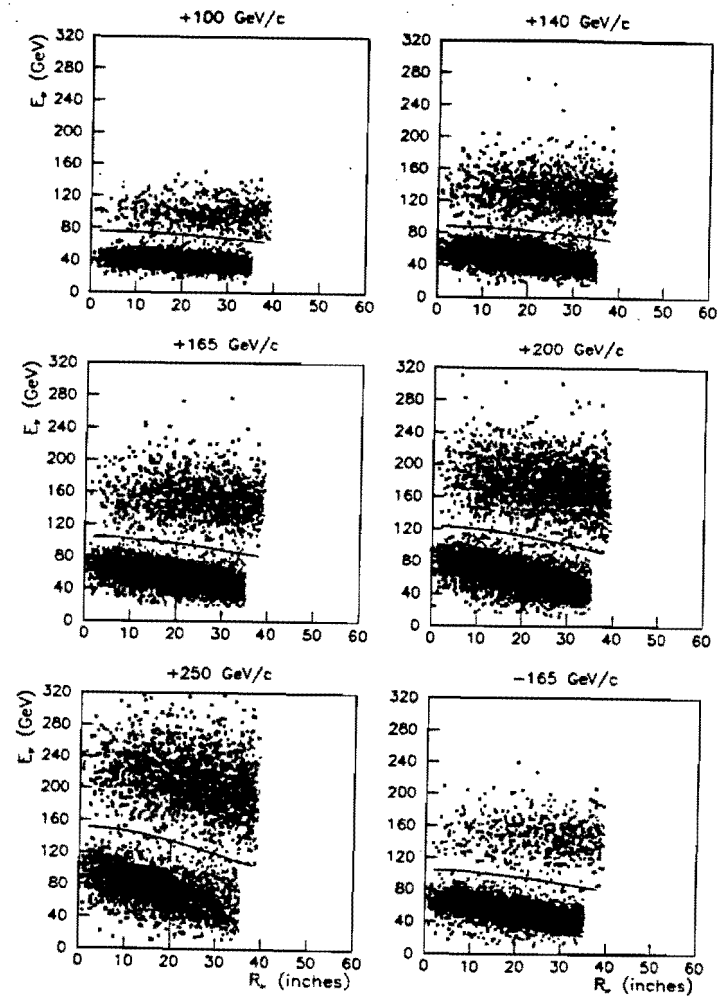

Figure 2.3 The separation of pion and kaon neutrino events as seen on the scatter plot of measured neutrino energy versus the radial position of the interaction in the detector. Plots shown come from the second running period (E701) with five train momentum settings.

and its angle θ in the lab (and therefore the radial event location, R, in the detector) are kinematically related as follows:

$$E_\nu = E_\nu(max)/(1+\gamma^2\theta^2) \qquad (2.1)$$

and

$$\theta^2 = R^2/L^2 \qquad (2.2)$$

where:

γ is the Lorentz transformation factor, L is the distance from the decay point (of the order of 1000 m) to the interaction point in the detector, R is the radial distance from the beam axis to the interaction vertex in the apparatus (of the order of 1.0 m), and

$$E_\nu(max) = E_{\pi,K}(1-(m_\mu/m_{\pi,K})^2) \ . \qquad (2.3)$$

Here $E_{\pi,K}, m_{\pi,K}, m_\mu$ are energies in the lab, and masses of pion, kaon, and muon respectively. From (2.3):

$$E_\nu^\pi(max) = 0.42E_\pi \quad \text{and} \quad E_\nu^K(max) = 0.95E_K \qquad (2.4)$$

Fig.2.2 shows an example of neutrino flux produced with the train set to +200 GeV/c, and passing through the Lab E apparatus. Fig.2.3 shows the ν_π and ν_K event separation as seen using the measured energy (E_ν) and radius (R) in the detector.

The dichromatic beam allows the measurement of missing energy in dimuon events. The quantity

$$E_{mis} = E_\nu^D - E_\nu \qquad (2.5)$$

is the difference between the neutrino beam energy (determined from the event radius) and the measured total energy in the detector. The average $\langle E_{mis}\rangle$ is expected to be zero for single muon charged current events.

The monitoring system of the secondary beam consisted of [2.2]: ion chambers, Segmented Wire Ionization Chambers (SWIC), an RF cavity, and a Cherenkov counter. These detectors were measuring intensity, composition, and position of the secondary beam. All the beam monitoring information was written on magnetic tape along with associated neutrino events.

2.2 Neutrino Detector

The neutrino detector, shown in Fig.2.4, 2.5, and 2.6, and described in details earlier [2.4, 2.5, 2.7] is located in the Lab E building, 1292m from the beginning of the decay pipe. The apparatus consists of a target calorimeter and forward muon spectrometer instrumented with scintillation counters and spark chambers.

The 690-ton target calorimeter is constructed of 168 3m × 3m × 5cm iron plates, 82 3m × 3m liquid scintillation counters (with a BBQ shifter bar readout and located every 10 cm of iron), and 42 3m × 3m magnetostrictive readout spark chambers (located every 20 cm of iron). Fig.2.5 and 2.6 illustrate the detector structure.

The muon spectrometer consisted of three 3m long toroidal magnets (containing 1.6m of iron each) with a 1.8m outer radius and a 12.7cm radius hole for the coils. The three half-toroid gaps were instrumented with 6 1.5m × 3m spark chambers each (in 3 planes). The space between toroid 1 and 2, and 2 and 3 was filled with four 1.5m × 3m chambers (in 2 planes) and one 3m × 3m spark chamber (total of 3 planes). After the third toroid there were four 1.5m × 3m (in 2 planes) and two 3m × 3m spark chambers. The total number of spark chamber planes was 19. In addition, located after each toroid iron slab (20cm of iron) were acrylic scintillation counters constructed of 4 symmetric squares. These were used to determine which toroid quadrant the muon passed through.

Some of the important parameters of the apparatus were:

1) the RMS hadron energy resolution: $\Delta E_H/E_H = 0.89/\sqrt{E_H}(\mathrm{GeV})$;
2) the RMS fractional muon momentum resolution (from the toroids): $\Delta p_\mu/p_\mu = 0.11$;
3) the spatial spark chamber resolution: 500μm;

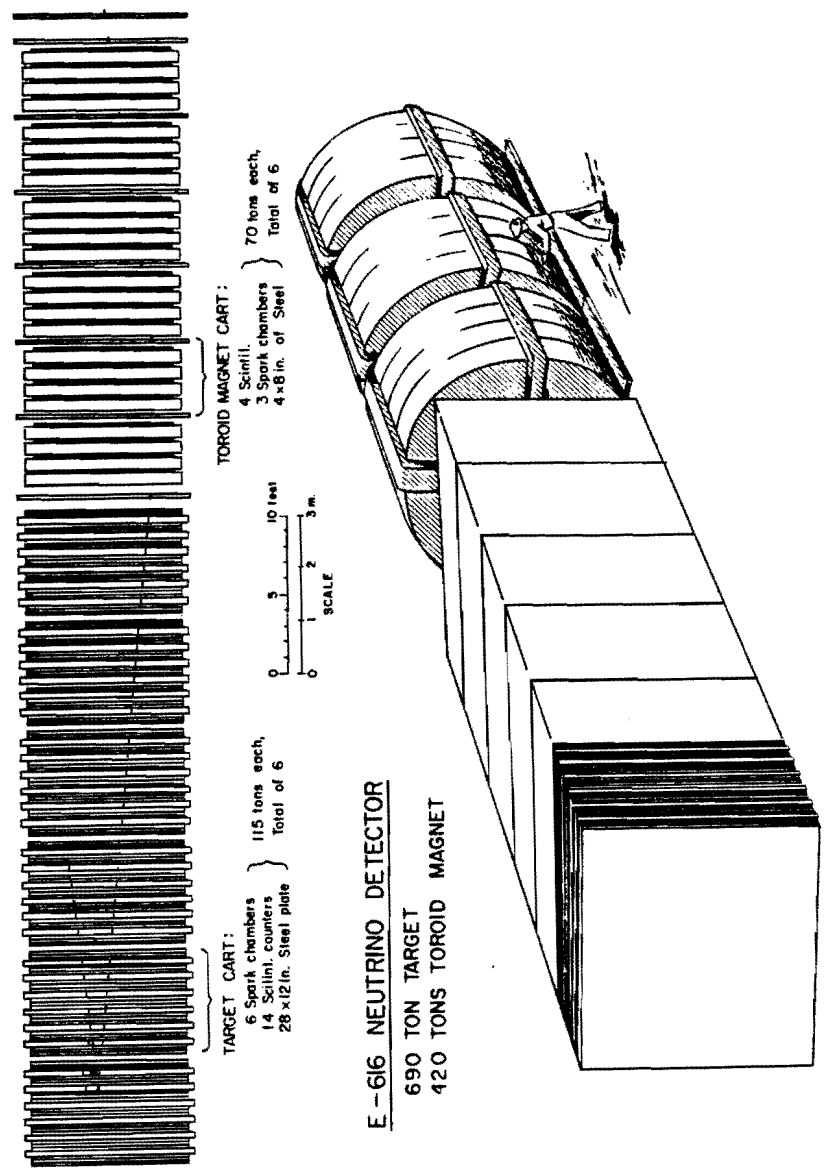

Figure 2.4 Overview of the Lab E neutrino detector consisted of 6 target carts and 3 toroidal magnets.

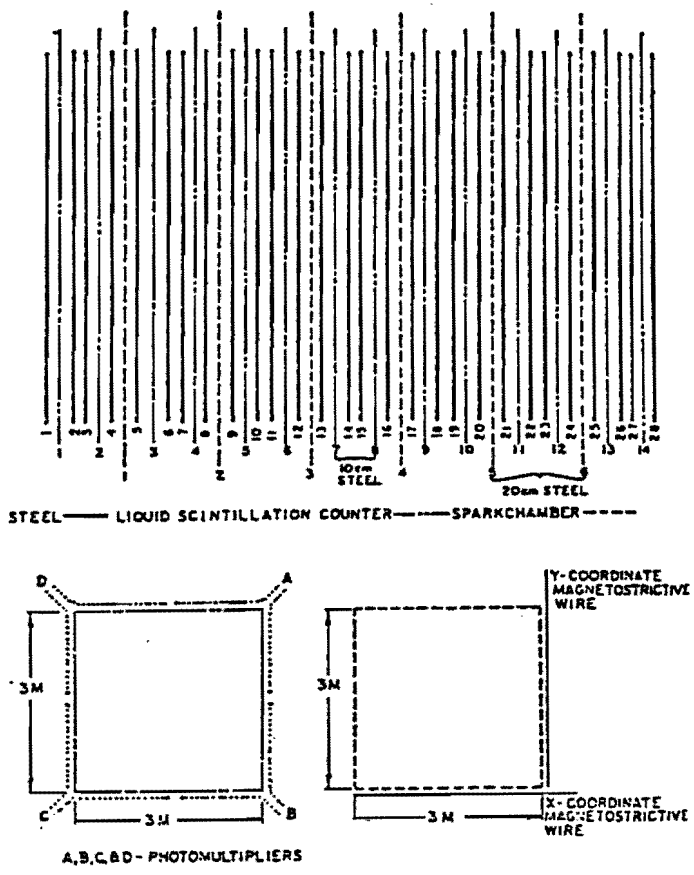

Figure 2.5 The detailed structure of the Lab E target cart showing the relative configuration of iron plates, scintillation counters, and spark chambers.

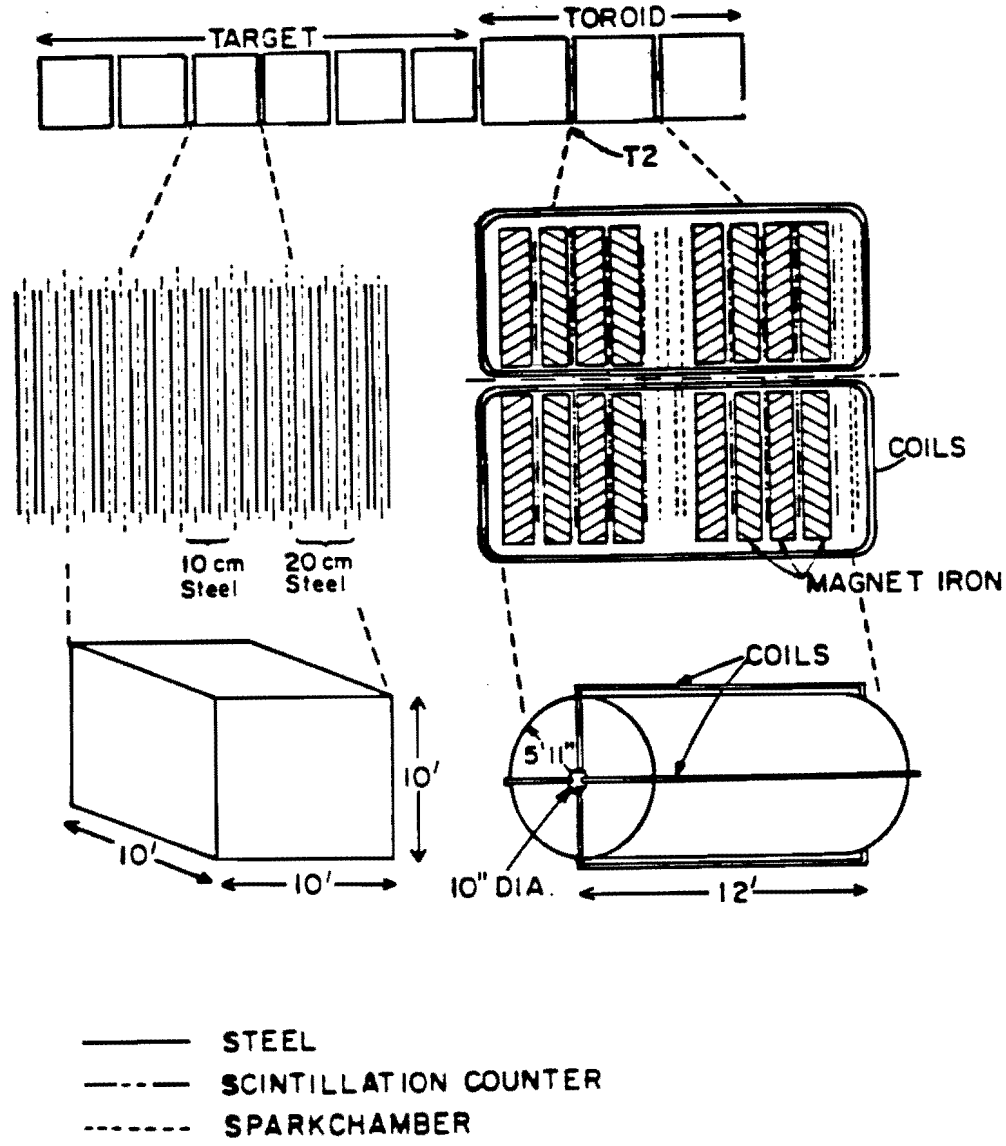

Figure 2.6 The overview of the Lab E detector indicating target and spectrometer details.

4) the angular resolution of the muon track:

$$\Delta\theta_\mu = 35\text{mrad}/p_\mu(\text{GeV}/c);$$

5) the total transverse momentum kick of the toroids:

$$p_t = 2.4\ \text{GeV}/c;$$

Data were collected over two periods of running: in 1979-1980 (experiment E616), and in 1982 (experiment E701). The Lab E apparatus was slightly modified for the second run (for which one of the main goals was the study of neutrino oscillations using two neutrino detectors). These changes included :

1) Only the 4 downstream target carts were used (2/3 of the previous fiducial volume);

2) The spectrometer spark chamber instrumentation was changed: there were no chambers in half-toroid gaps, but there were five 3m × 3m chambers after each toroid (total of 15 planes in the spectrometer).

Triggering of the apparatus used characteristic features of neutrino interactions. A charged current neutrino reaction has a characteristic topology consisting of a neutral incoming neutrino (i.e. no incoming charged particle) interacting in the target fiducial volume, and producing a penetrating muon, and a hadron shower.

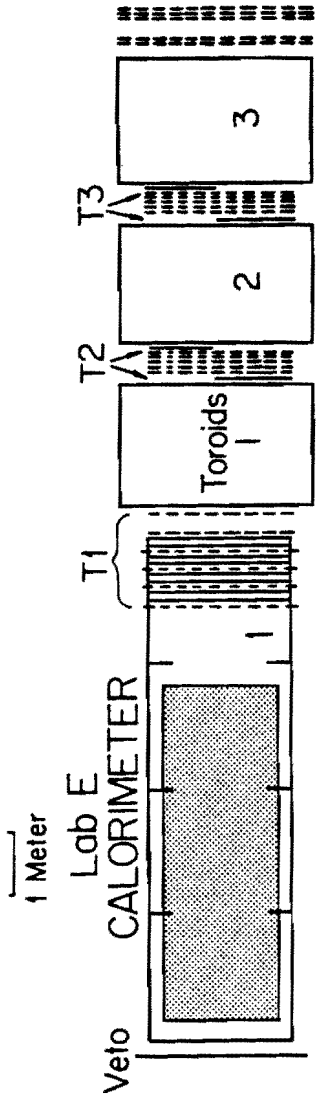

Figure 2.7 The active part of the detector used in the second period of running (E701). The trigger counters locations are marked T1 (logical OR of several counters), T2, and T3.

Charged current events were recorded using two triggers:

1) Trigger 1, called the "MUON TRIGGER", required the upstream veto counter to be off, at least one well defined minimum ionizing particle passing through several counters in the downstream end of the target, and a signal from trigger counter T2. The T2 requirement ensured that the muon momentum could be analyzed in the toroid.

2) Trigger 3, called the "PENETRATION TRIGGER", required the upstream veto counter to be off, a minimum ionizing particle in the target penetrating at least 16 counter planes (1.6m of iron), and a deposition of more than 4 GeV of hadronic energy. This trigger was designed to record events with muons which ranged out or escaped from the target.

For events passing all cuts (cuts are discussed in the next chapter), the efficiency of the triggers was found to be >99%.

Chapter 3

Event Reconstruction and Data Sample

The data used in this analysis were collected over two periods of running; the first, from June, 1979 through January, 1980 (Fermilab experiment E616), and the second, from January, 1982 through June, 1982 (Fermilab experiment E701). A total of 5.4×10^{18} and 3.6×10^{18} 400 GeV protons on target were delivered during each run, respectively, of which 2.5×10^{18} and 1.4×10^{18} protons were delivered with the train set to focus negative secondaries (yielding antineutrinos). The remaining running was with positive secondaries (yielding neutrinos).

During the E616 run data were taken with ten momentum settings of the train: +250, +200, +165, +140, +120 GeV/c and -250, -200, -165, -140, -120 GeV/c. During the E701 run the train was set at the six values of +250, +200, +165, +140, +100, and -165 GeV/c.

The off-line analysis was carried out on the Fermilab CDC Cyber 175 and 875 computers. The charged current event analysis was divided into two stages. The first, a cruncher stage, contained most of the track finding, and hadron energy determination. The output of this stage were event records which also retained much of the raw detector information. The second stage, the data summary tape (DST) writer, produced a summary record for each event which contained further processed physics and apparatus information.

Dimuon events were extracted from the total event sample by visually scanning a set of computer selected dimuon event candidates. All the accepted dimuon events were scanned and reconstructed using an interactive program.

A series of final cuts were then applied to the single and dimuon events to produce the data sample used in physics analysis.

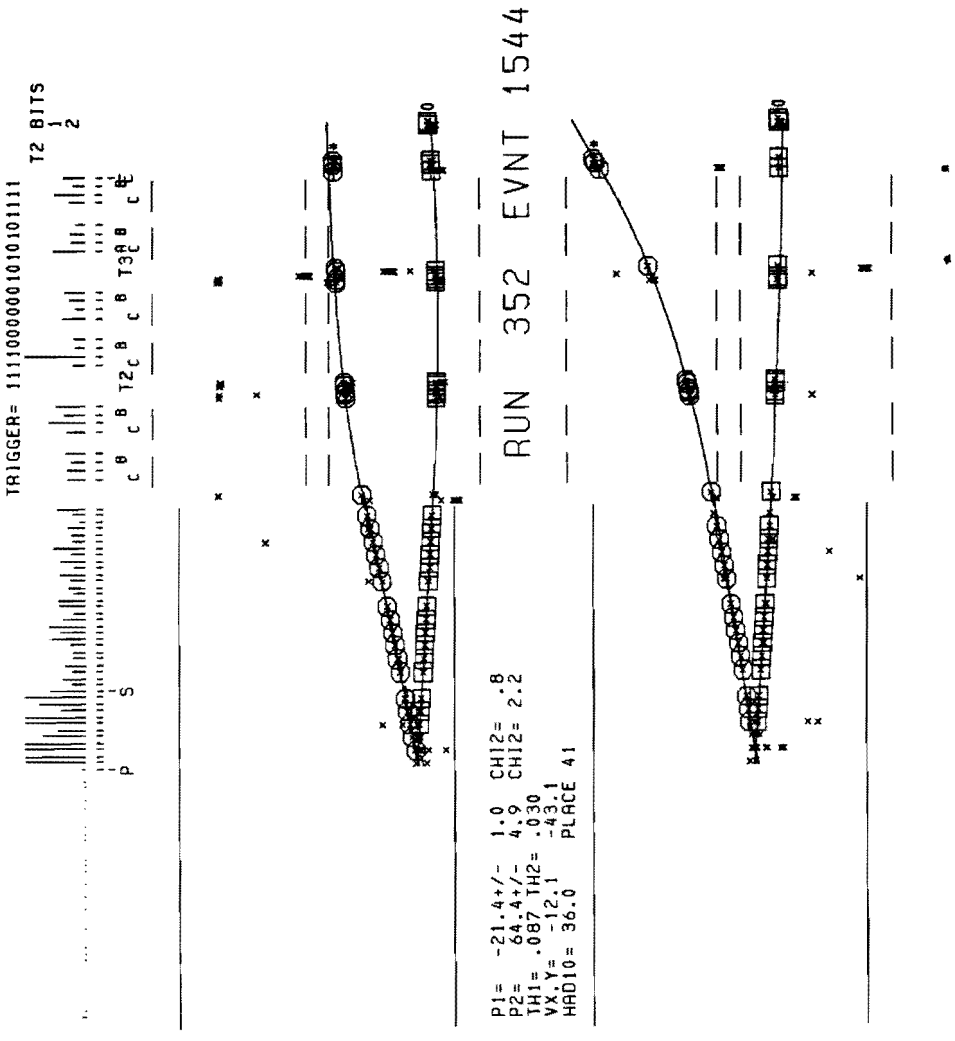

Figure 3.1 A computer display of a dimuon event with both muon momentum analyzed.

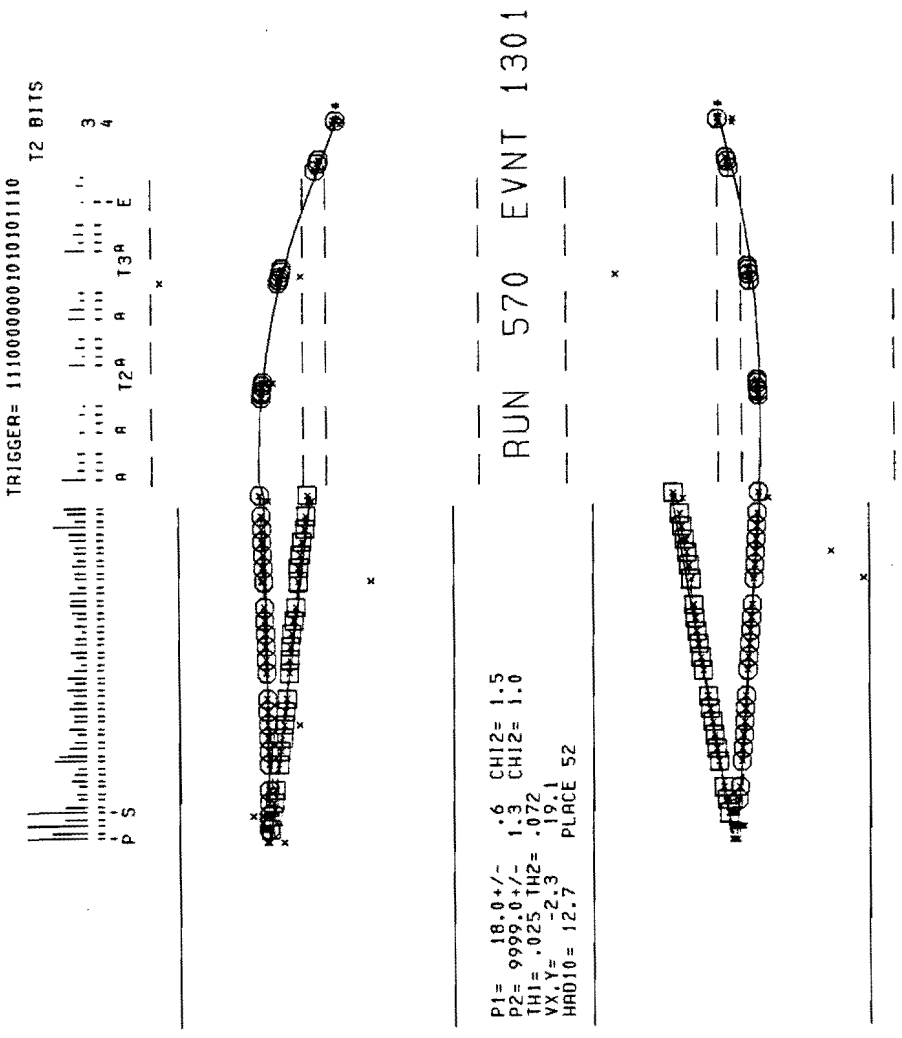

Figure 3.2 A computer display of a dimuon event with the second muon ranging out in the toroid.

3.1 Event Reconstruction

The reconstruction of events detected by the Lab E apparatus has been described in details in number of publications [2.5, 2.5, 3.1, 3.2]. Therefore only a brief review of the scheme applied to charged current events will be presented with emphasis on features important for dimuon events.

3.1.1 Hadron Energy Determination

In a typical charged current neutrino event, Fig.3.1, in the Lab E apparatus the target counters immediately downstream of the interaction point exhibited large pulse height (associated with the hadron shower development), the counters further downstream displayed pulse heights of almost constant (within fluctuations) level associated with the passing muon (a minimum ionizing particle).

The pulse height values from the photomultipliers were corrected by: a) pedestal subtraction, b) counter gain shifts (monitored by flasher system and change of response to muons), and c) light attenuation in counters (using a map of the spatial variation of counter response as determined from hadronic showers). The corrected pulse

height values were converted to a number of equivalent minimum ionizing particles.

The hadron energy was proportional to the sum of the corrected pulse heights in the shower region, defined for the apparatus as starting with the most upstream counter with pulse height greater than 0.25 times minimum ionizing, and ending with the most downstream counter of a series of six counters with pulse height less than 3 times minimum ionizing. The constant of proportionality, which converts this sum into energy in GeV, was obtained by using data obtained with a hadron calibration beam of known energy. These calibration data were also used to determine the RMS hadron energy resolution of the apparatus found to be:

$$\Delta E_H/E_H = 0.89/\sqrt{E_H(\mathrm{GeV})}$$

To correct for the energy deposition of a muon passing through counters within the hadron shower region, the energy loss of the minimum ionizing muon was subtracted from the hadron energy. In the case of a dimuon event, twice this value was subtracted. For this case the non-leading muon is considered as a part of the hadron shower , and total visible energy transfer to the target, ν_{vis}, is a sum of the hadron energy and the energy of the second muon.

3.1.2 Muon Energy Determination

The trajectories of charged particles passing through the Lab E apparatus were determined using the spark chambers in the target and the muon spectrometer.

The muon trajectory in the target was a straight line with deviations due to multiple Coulomb scattering. In the toroid, the bend in the magnetic field was used for the momentum determination. The fit of the muon momentum and the production angle utilized an error matrix method which included the contribution of multiple scattering. The RMS resolution on the muon momentum was about 11.0%.

The total muon energy was a sum of its target energy loss and momentum in the spectrometer. The target energy loss was the total energy loss (dE/dx) in all material downstream of the neutrino vertex to the beginning of the magnet.

For a muon ranging out or escaping from the target before reaching the toroid, the muon energy was obtained from the energy loss only. For muons escaping from the target this energy was only a fraction of the total muon energy, and therefore only a lower limit on the energy was determined.

The chambers in the shower region (where there were many charged particles) had many sparks. Therefore in this

region an unambiguous assignment of sparks to the muon trajectory was usually difficult. Beyond the end of the shower the number of sparks in the chambers was low, and in most cases the muon tracks were easily determined. For dimuon events, the track finding was a much more difficult software task, since it required good track separation and proper track segment (x and y view) matching.

The reconstruction program developed for the Lab E apparatus had an efficiency of about 95% in successfully fitting single muon event tracks. For dimuon events the efficiency was about 20%. This inefficiency required the special treatment of dimuon events discussed in the following section.

3.2 Dimuon Selection and Reconstruction

The processing of the dimuon data was divided into two parts. First, a specially selected subsample of all the data (containing computer selected dimuon candidates) was scanned and candidates for dimuon events sorted out. Next, these candidate events were closely examined on a high resolution graphics terminal and, if accepted, an interactive track reconstruction was performed.

As an illustration of the dimuon selection further details on the selection of events are presented for experiment E701. The E616 events were processed in a very similar way.

The selection of events for scanning was done by software requirements. Three independent subroutines were used on all charged current triggers (triggers 1 and 3).

The first subroutine selected candidates for scanning on the basis of the number of sparks per chamber view (downstream of the end of the hadron shower as determined by the scintillation counters). Events with an average of 3 or more sparks per view (over a set of at least 4 consecutive chambers in the target or toroid past the end of the shower) were selected.

In this subroutine toroid quadrant counter information was also used. Quadrant bits were set which required 2 out of 4 consecutive counters (a bit for each half-toroid). All events in which there were two quadrant bits set in at least one half-toroid were chosen for further scanning.

The second subroutine selected events on the basis of pulse heights in target counters. All events with long showers (longer than 17 counters, or ~1.7m of iron) were selected. In addition, events were selected if any consecutive set of 8 counters downstream of the shower end had an average pulse height $\geq$ 1.7 times minimum ionizing.

Events for which the pulse heights displayed a step function behavior (with a step longer than 8 counters), indicating a muon range-out, were also selected.

The third subroutine processed all the events using an algorithm developed for the same apparatus in the Fermilab experiment E595 [4.6a]. The algorithm of searching for multimuon events in experiment E595 (through finding steps in pulse height) was >99% efficient. In experiment E595 hadron showers were contained in an additional calorimeter, and the E616 detector was used as the muon identifier.

The first subroutine was used on all events. If a given event was not selected, it was processed by the second one, and then through the third.

Out of 190000 neutrino triggers 1 or 3, about 47000 events were selected for scanning. Out of 19000 antineutrino triggers 1 or 3, about 2500 events were sorted out. Most of selected events were ordinary charged current events chosen by the very loose selection requirements. The scanning of events (displayed on a paper printout) was fast and relatively effortless at a rate of about 2000 events per day. The scanning resulted in about 4500 neutrino dimuon candidates and 500 antineutrino dimuon candidates.

As a check of the selection efficiency a raw subsample of about 25000 events was scanned and checked for dimuon candidates which were missed by the three software

algorithms. No such events were found. The scanning inefficiency was also estimated by triple scanning a part of selected data (about 25000 events). The inefficiency was found to be smaller than 1% and therefore negligible.

Candidate dimuon events were then carefully examined on plotter pictures and on a high resolution graphics terminal. An event was selected as a legitimate dimuon candidate if both tracks were visible for a distance longer than ~2.2 m of iron (corresponding to 11 spark chambers). Accepted events were reconstructed using an interactive program by assigning sparks to two muon tracks. The rest of the reconstruction proceeded in exactly the same way as for the single muon charged current data sample.

3.3 Cuts

Several cuts were applied to the data in order to assure efficient reconstruction. Additional cuts were applied on the information from the beam monitoring devices.

3.3.1 Cuts on the Beam

Only beam pulses with good steering parameters were accepted (i.e. when the secondary beam in the decay pipe was aimed at the center of the apparatus). This was done by

looking at the split plate ion chambers read-outs and requiring that:

$$(\text{left}-\text{right})/(\text{left}+\text{right}) < 0.1$$

$$(\text{top}-\text{bottom})/(\text{top}+\text{bottom}) < 0.1$$

These requirements ensured a properly steered neutrino beam, centered to within ±4 inch square at the neutrino detector.

3.3.2 Cuts on Events

Dimuon events were divided into three classes

1) Class 1: opposite-sign dimuons with momenta > 4.3 GeV/c. This class contains: 1) events with both muons analyzed in the spectrometer (Fig.3.1); 2) events with second muon ranging out in the target or toroid and whose sign is not determined (Fig.3.2); 3) events where the second muon escaped the calorimeter, but had a minimum visible energy of at least 4.3 GeV (leaving its total energy and sign unknown). About 10% of events for which sign of the second muon is unknown are really same sign events from the hadronic shower background. This background and background subtraction are discussed in the next chapters.

2) Class 2: opposite-sign dimuons with momentum > 9 GeV/c and both muons analyzed in the spectrometer (Fig.3.1). This class contains only dimuons for which both muons have known sign and momentum.

3) Class 3: like-sign dimuons with momenta > 9 GeV/c and both muons analyzed in the spectrometer. Appendix H contains a complete list and computer displays of all accepted like-sign dimuon events.

Data events were selected by applying geometrical and kinematical cuts. In general, the criteria used in the structure function analysis as described in [3.1, 3.2] were closely followed. However, some cuts were loosened in order to increase the statistical sample.

A. Fiducial volume cuts:

1)Longitudinal fiducial volume: To ensure full shower containment in the calorimeter and to track the muon outside of the hadron shower a length of ~1.7m of iron before the forward spectrometer was required. Therefore, all events from class 2 and 3, occurring between counter number 17 (downstream) and 80 (upstream), have been accepted. For experiment E701 (having a shorter active target) the cut was 17 (downstream) and 54 (upstream). A more stringent cut for events of class 1 was required. The requirement of a visible muon energy of at least 4.3 GeV implies that a muon must traverse more than about 3m of iron. If neutrino interactions are required to occur upstream of counter 28, the muon would then traverse at least 3.2m of iron equivalent material (11.49 cm iron equivalent per mean distance between centers of the two consecutive counters)

before entering the toroid. Otherwise, absorption in the toroid might lead to an ambiguity in the minimum muon energy for low energy muons. In summary, the following longitudinal cuts which are expressed in terms of counter number. (Note that the counter 1 is the most downstream counter.)

	E616	E701	
class 1:	28-80	28-54	($\mu^-\mu^+$: p_μ>4.3 GeV/c)
class 2:	20-80	17-54	($\mu^-\mu^+$: p_μ>9.0 GeV/c)
class 3:	17-80	17-54	($\mu^-\mu^-$: p_μ>9.0 GeV/c)

2) Transverse fiducial volume: Cuts were imposed to ensure the transverse containment of hadronic showers. In addition, because of the sensitivity of the neutrino flux at large radius to uncertainties in beam dispersion and steering, more stringent transverse fiducial volume cuts were imposed. The cuts were different for interactions of neutrinos originating from pion and kaon decays. Both, a transverse vertex cut, which was a square centered on the apparatus (for energy containment), and a radial cut centered on the beam axis (to reduce the flux uncertainty) were applied. The following cut values were used:

CLASS 1: ($\mu^-\mu^+$: p_μ>4.3 GeV/c)

	RADIUS CUT	SQUARE CUT
pion ν	30.0in	-60.0in - +60.0in
kaon ν	50.0in	-60.0in - +60.0in

CLASS 2 & 3: ($\mu^-\mu^+$: p_μ>9GeV/c and $\mu^-\mu^-$: p_μ>9GeV/c)

	RADIUS CUT	SQUARE CUT
pion ν	30.0in	-60.0in - +60.0in
kaon ν	60.0in	-60.0in - +60.0in

Note that less stringent cuts were applied to the like-sign dimuon data sample in order to increase the statistics.

B. Geometric cuts: To ensure good quality event reconstruction additional geometrical cuts were imposed: 1) the straight line extrapolation of the leading muon track in the target had to intercept the front face of the toroid at radius smaller than 64.0in (the toroid radius was 69.0in); 2) the same straight line extrapolation through the first toroid was required to be outside the coil hole for more than 70% of its toroid path (the radius of the toroid hole was 5.0in). 3) the straight line extrapolation also had to intercept the active area of the T2 counter at the rear face of the first toroid within ±58in in the x and y views. Since all leading muons were focussed by the toroidal magnet, these cuts ensured a geometrical acceptance which is independent of the muon momentum.

C. Angle cuts: For class 1 events (p_μ>4.3GeV/c) leading muons with angles < 0.150 mrad (see Fig.3.3) and second muons with angles < 0.350 mrad (see Fig.3.4) with respect to the incident neutrino direction were accepted. For class 2 and 3 (p_μ>9GeV/c) both muons were required to have angles < 0.250 mrad and momentum analyzed in the toroid.

D. Kinematic cuts: For comparisons with the quark-parton model, only single muon events with hadron energy $E_H(=\nu+M)$ > 2 GeV were accepted. These cuts did not remove any dimuon events from the sample. In addition, only events with a properly reconstructed leading muon were used.

3.4 Acceptance Corrections

The extraction of single muon and dimuon production cross sections from the data sample requires corrections for geometric and momentum acceptance, as well as for kinematic cuts (P_μ > 4.3 or 9.0 GeV/c, E_H > 2 GeV). These acceptance corrections were calculated using a Monte Carlo program, which is discussed in detail in Chapter 5. However, some geometrical contributions to the acceptance corrections can be checked by using the observed data directly. These checks are described below.

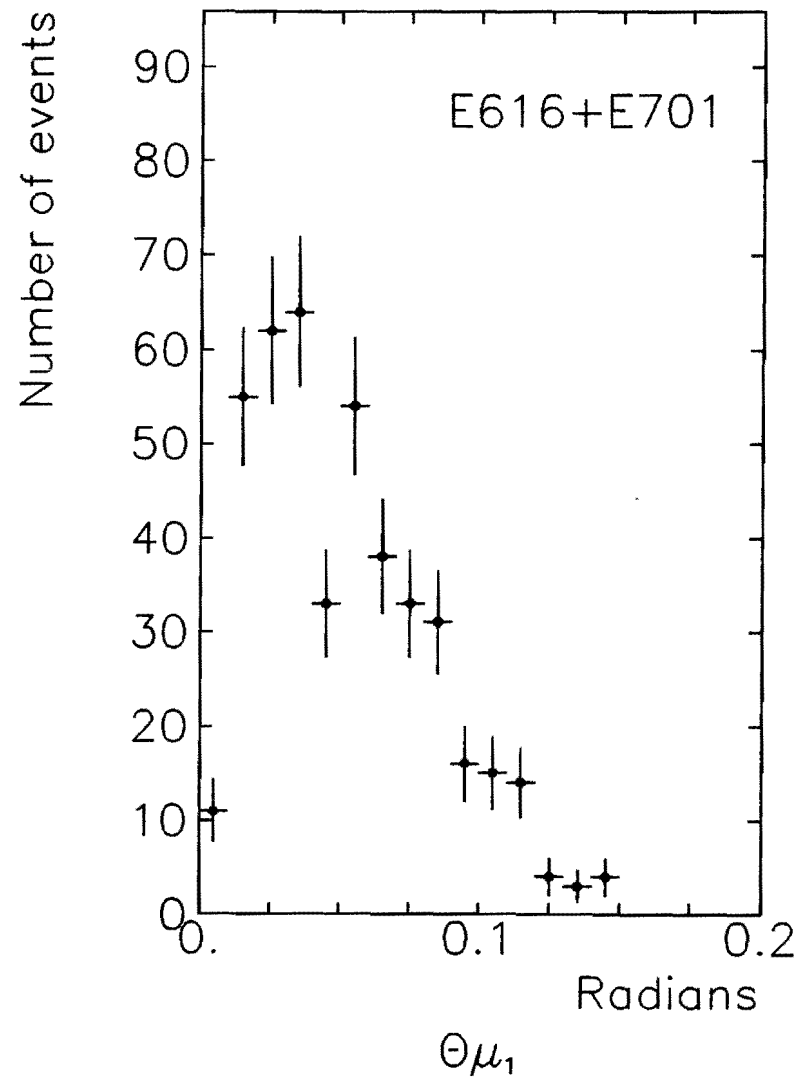

Figure 3.3 Distribution of the leading muon angle with respect to the incident direction for events with p_μ > 4.3 GeV/c.

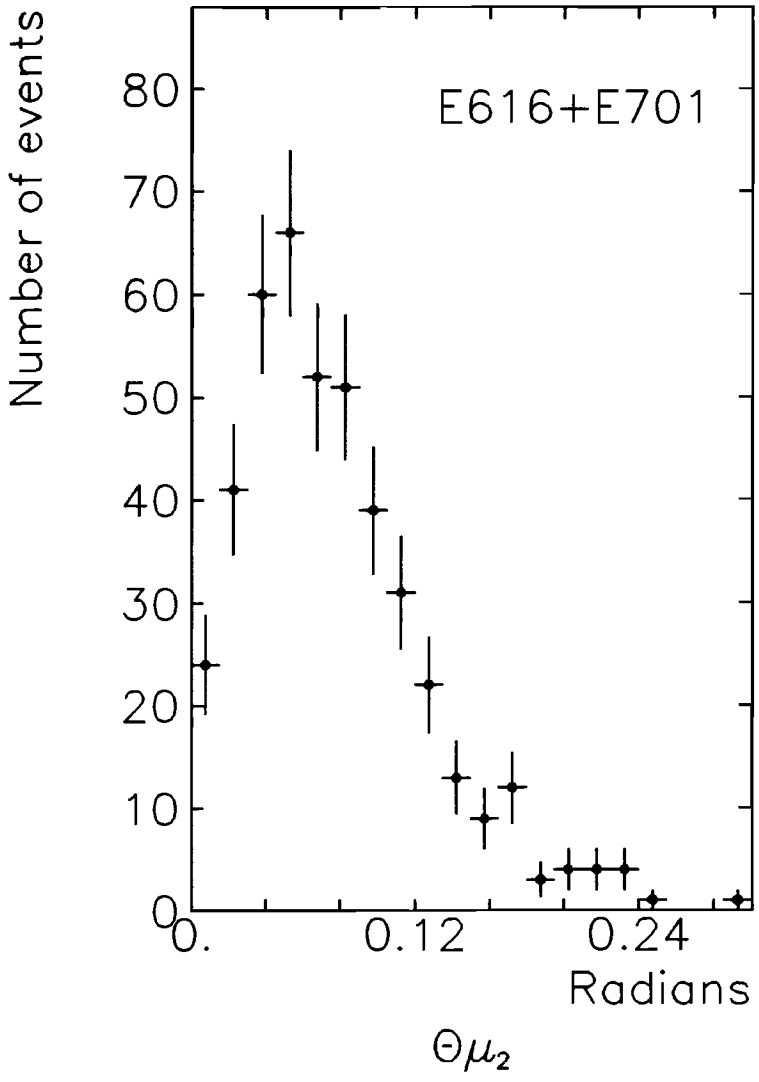

Figure 3.4 Distribution of the second muon angle with respect to the incident neutrino direction for events with $p_\mu > 4.3$ GeV/c.

Due to the finite size and geometry of the detector not all neutrino interactions occurring within the fiducial volume can trigger the apparatus. In particular, because of the square geometry of the triggering system, the acceptance depends on the azimuthal angle of the muon (or muons) and the transverse vertex position. In addition, the solid angle of the spectrometer as viewed from the interaction vertex depends on the longitudinal position of the vertex.

(a) Single muon events: The geometrical correction for single-muon events can be calculated directly from the data sample. The principle of the calculation is illustrated in Fig.3.5. For given x,y, and z position of an interaction the azimuthal acceptance of the event is equal to $\Phi/2\pi$. The event was then translated along the target from the beginning to the end of the longitudinal fiducial volume in small steps. The fraction of the translated events which pass all the geometric cuts yields the longitudinal acceptance. The combined ϕ and the longitudinal acceptance is the average acceptance of an event. The analysis of Monte Carlo generated events (for which the number of events in the fiducial volume is known) show that the procedure fully corrects for geometrical acceptance. This geometric acceptance was used only for comparisons between the two sets of data (E616 and E701).

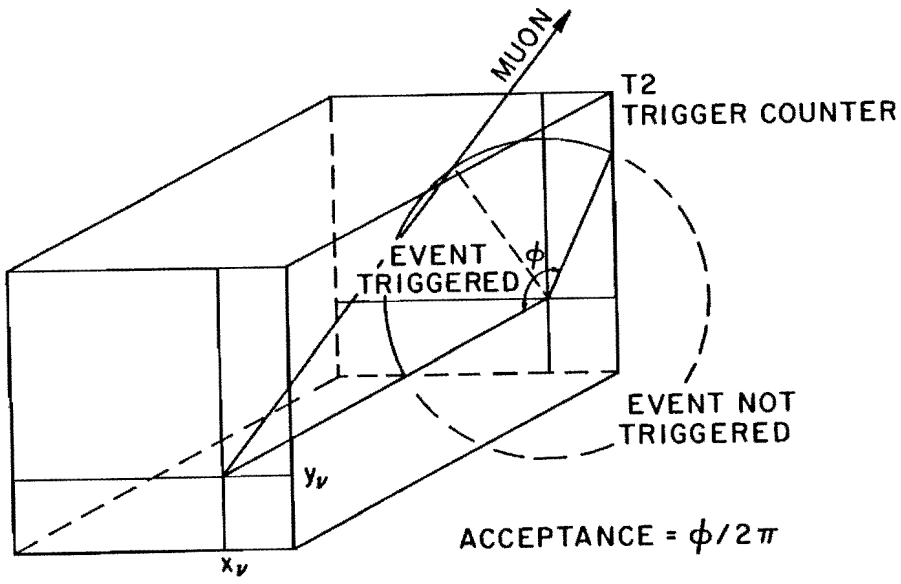

Figure 3.5 Illustration of the geometric acceptance calculation.

Corrections for kinematic cuts were obtained from the Monte Carlo program directly.

(b) Dimuon events: Accepted dimuon events with momentum > 4.3 GeV/c (class 1) were corrected for the acceptance of the leading muon using the above method. The geometrical efficiency for detecting a second muon with p_μ > 4.3 GeV/c was determined by a ϕ rotation of each event about the z axis (neutrino beam direction). The ϕ acceptance was the fraction for which the second muon could traverse 3m of iron (4.3 GeV range) before leaving the target. The analysis of the Monte Carlo events in the same way shows that this procedure fully corrects for geometrical acceptance for muons with θ_μ < 350 mrad. The angular distribution of second muons indicates that most of them have much smaller angles (see Fig.3.4). The corrections for missing second muons with $0<p_\mu<4.3$ GeV/c was obtained from a charm Monte Carlo model (see Chapter 5).

(c) Momentum analyzed muons (class 2 and 3): Momentum analyzed muons were corrected by translating each dimuon event to every single-muon vertex location and determining if at this new location the translated event can be reconstructed (requiring momentum at the front face of the toroid to be > 2.5 GeV/c, and momentum at the rear face of the first toroid to be > 300 MeV/c). The analysis of the charm Monte Carlo events in the same way indicates that this

procedure does not correct for dimuon events with a large opening angle between two muons. The additional corrections for these events (~20%) was obtained from the charm Monte Carlo.

In summary, the geometrical acceptance corrections for single-muon events and dimuon events were used for comparisons between the two sets of data (E616 and E701). Rates of dimuon events was calculated by applying Monte Carlo corrections to raw data events passing standard series of cuts:

$$\text{Rate}(2\mu/1\mu) = \frac{[2\mu\ \text{d-bkg}]_{cuts}\ \dfrac{[2\mu\ \text{MC model}]_{\text{fiducial v. cuts}}}{[2\mu\ \text{MC model}]_{cuts}}}{[1\mu\ \text{d}]_{cuts}\ \dfrac{[1\mu\ \text{MC model}]_{\text{fiducial v. cuts}}}{[1\mu\ \text{MC model}]_{cuts}}} \qquad (3.4.1)$$

where d=data, bkg=dimuon background events. For opposite-sign dimuon rates the charm quark production model was used (details are presented in Chapter 5). For like-sign dimuon rates (whose origins are not fully understood) 3 different models were used: the shower background model, the c-$\bar{c}$ production through the gluon bremsstrahlung model, and the

D^0-$\bar{D}^0$ mixing model. Details are presented in Chapters 5,6, and 7. Extraction of the fraction of the strange sea in the nucleon was obtained by comparison of raw data and raw Monte Carlo dimuon events passing a series of standard cuts.

3.5 Final Raw Data Set and its Characteristics

In this section the number of raw events passing cuts and their basic characteristics are given. Events are presented in bins of measured neutrino energy as defined in Table 3.1.

Table 3.1 Definitions of energy bins used in the analysis.

For CLASS 1: (p_μ > 4.3 GeV/c)

low energy pion ν	:	E_ν < 70.0 GeV
high energy pion ν	:	E_ν > 70.0 GeV
low energy kaon ν	:	E_ν < 180.0 GeV
high energy kaon ν	:	E_ν > 180.0 GeV

For CLASS 2 & 3: (p_μ > 9 GeV/c spectrometer analyzed)

all energy pion ν	:	all pion neutrino energies
low energy kaon ν	:	E_ν < 200.0 GeV
high energy kaon ν	:	E_ν > 200.0 GeV

The measured variables are expressed in the following units: the measured neutrino energy (E_ν), the measured hadronic shower energy (E_H), and the missing energy E_{mis} (see eqn.2.5) are in GeV; the measured muon momenta ($p_{\mu 1}$ and $p_{\mu 2}$) are in GeV/c, and the four momentum transfer Q^2 is in GeV^2/c^2. The invariant hadronic mass W^2 is in GeV^2/c^4, the

polar muon angles ($\theta_{\mu 1}$ and $\theta_{\mu 2}$) are in radians, the azimuthal angle between two muons, ϕ_{12}, in degrees, and the transverse momentum of the second muon with respect to the hadron shower direction p_T is in GeV/c. The fragmentation variable $z_u = p_{\mu 2}/E_\nu$, Bjorken x, and variable y are dimensionless. The abbreviation <corr> is for the mean geometrical acceptance correction for each subsample.

3.5.1 1μ Charged Current Data

Tables 3.2-3.13 show the number of single-muon charged current events (passing cuts described previously) corresponding to the 3 classes of dimuon events and their mean characteristics. The data shown are broken into the classes of events described above, and are also presented separately and together for the two data runs (experiment E616 and E701). The numbers in parenthesis are the statistical errors only. Note that the neutrino beams in experiments E616 and E701 were not identical due to changes in specific magnet locations and exact energy settings. Also, since the fiducial cuts for the two experiments were not the same, the mean characteristics are expected to be different.

The comparison of distributions with Monte Carlo calculation is given in Chapter 5.

TABLE 3.2: The number of 1μ charged current neutrino events for CLASS 1.

		E616	E701	E616+E701
1	low π	19826	14137	33963
2	high π	12483	5812	18295
3	low K	11633	8094	19727
4	high K	13311	5450	18761
5	all π	32309	19949	52258
6	all K	24944	13544	38488
7	TOTAL	57253	33493	90746

TABLE 3.3: The number of 1μ charged current antineutrino events for CLASS 1.

		E616	E701	E616+E701
1	all π	6310	2336	8646
2	all K	1582	695	2277
3	TOTAL	7892	3031	10923

TABLE 3.4: The number of 1μ charged current neutrino events for CLASSES 2 and 3.

		E616	E701	E616+E701
1	all π	37943	28147	66090
2	low K	20397	17530	37927
3	high K	8980	4042	13022
4	all K	29377	21572	50949
5	TOTAL	67320	49719	117039

TABLE 3.5: The number of 1μ charged current antineutrino events for CLASSES 2 and 3.

		E616	E701	E616+E701
1	all π	7296	3274	10570
2	all K	1854	1142	2996
3	TOTAL	9150	4416	13566

TABLE 3.6: Characteristics of 1μ charged current neutrino data for CLASS 1:

		E616	E701	E616+E701
1	$\langle E_\nu \rangle$	115.6(0.3)	102.7(0.4)	110.9(0.2)
2	$\langle E_H \rangle$	45.8(0.2)	42.2(0.3)	44.5(0.2)
3	$\langle P_\mu \rangle$	70.2(0.2)	60.8(0.3)	66.7(0.2)
4	$\langle Q^2 \rangle$	15.8(0.1)	14.3(0.1)	15.3(0.1)
5	$\langle W^2 \rangle$	70.9(0.3)	65.5(0.4)	68.9(0.3)
6	$\langle x_{Bj} \rangle$	0.207(0.001)	0.209(0.001)	0.208(0.001)
7	$\langle y \rangle$	0.385(0.001)	0.403(0.001)	0.392(0.001)
8	$\langle \theta_\mu \rangle$	0.047(0.001)	0.054(0.002)	0.050(0.001)
9	$\langle corr \rangle$	1.264(0.003)	1.185(0.002)	1.236(0.002)

TABLE 3.7: Characteristics of 1μ charged current antineutrino data for CLASS 1:

		E616	E701	E616+E701
1	$\langle E_\nu \rangle$	82.2(0.7)	79.3(1.0)	80.3(0.6)
2	$\langle E_H \rangle$	26.0(0.4)	25.0(0.6)	25.3(0.3)
3	$\langle P_\mu \rangle$	56.4(0.5)	52.6(0.8)	55.4(0.5)
4	$\langle Q^2 \rangle$	7.7(0.2)	7.8(0.3)	7.7(0.1)
5	$\langle W^2 \rangle$	41.6(0.7)	38.5(1.0)	40.7(0.5)
6	$\langle x_{Bj} \rangle$	0.199(0.002)	0.209(0.004)	0.202(0.002)
7	$\langle y \rangle$	0.311(0.003)	0.318(0.005)	0.313(0.002)
8	$\langle \theta_\mu \rangle$	0.043(0.001)	0.045(0.001)	0.044(0.001)
9	$\langle corr \rangle$	1.178(0.006)	1.114(0.006)	1.161(0.005)

TABLE 3.8: Characteristics of 1μ charged current neutrino data for CLASSES 2 and 3.

		E616	E701	E616+E701
1	$\langle E_\nu \rangle$	115.7(0.3)	105.8(0.4)	111.5(0.2)
2	$\langle E_H \rangle$	46.5(0.2)	43.3(0.2)	45.1(0.1)
3	$\langle P_\mu \rangle$	69.6(0.2)	62.7(0.3)	66.6(0.2)
4	$\langle Q^2 \rangle$	16.7(0.1)	16.1(0.1)	16.4(0.1)
5	$\langle W^2 \rangle$	71.2(0.3)	65.8(0.3)	68.9(0.2)
6	$\langle x_{Bj} \rangle$	0.212(0.001)	0.220(0.001)	0.215(0.001)
7	$\langle y \rangle$	0.389(0.001)	0.399(0.001)	0.394(0.001)
8	$\langle \theta_\mu \rangle$	0.049(0.001)	0.055(0.001)	0.052(0.001)

TABLE 3.9: Characteristics of 1μ charged current antineutrino data for CLASSES 2 and 3:

		E616	E701	E616+E701
1	$\langle E_\nu \rangle$	82.2(0.6)	79.3(0.8)	81.2(0.5)
2	$\langle E_H \rangle$	26.0(0.4)	25.0(0.5)	25.6(0.3)
3	$\langle P_\mu \rangle$	56.6(0.5)	54.6(0.7)	55.9(0.4)
4	$\langle Q^2 \rangle$	8.1(0.2)	8.2(0.2)	8.1(0.1)
5	$\langle W^2 \rangle$	41.6(0.6)	39.6(0.8)	40.9(0.5)
6	$\langle x_{Bj} \rangle$	0.203(0.002)	0.211(0.003)	0.206(0.002)
7	$\langle y \rangle$	0.310(0.002)	0.316(0.004)	0.312(0.002)
8	$\langle \theta_\mu \rangle$	0.043(0.001)	0.047(0.001)	0.045(0.001)

The following tables present the measured mean total energies and measured mean hadron energies for the bins previously defined:

TABLE 3.10: Mean neutrino and hadron energies for 4 bins of 1μ charged current neutrino events for CLASS 1.

		E616		E701		E616+E701	
		E_ν	E_H	E_ν	E_H	E_ν	E_H
1	low π:	56.7	20.5	52.0	19.9	54.7	20.2
2	high π:	80.9	31.5	77.1	31.8	79.7	31.6
3	low K:	151.9	60.2	143.7	59.0	148.5	59.7
4	high K:	204.3	84.4	200.6	86.1	203.2	84.9

TABLE 3.11: Mean antineutrino and hadron energies for 2 bins of 1μ charged current antineutrino events for CLASS 1.

		E616		E701		E616+E701	
		E_ν	E_H	E_ν	E_H	E_ν	E_H
1	all π:	62.3	19.4	56.1	17.8	60.6	19.0
2	all K:	159.7	51.3	144.4	45.5	155.0	49.5

TABLE 3.12: Mean neutrino and hadron energies for 3 bins of 1μ charged current neutrino events for CLASSES 2 and 3.

		E616		E701		E616+E701	
		E_ν	E_H	E_ν	E_H	E_ν	E_H
1	all π:	66.1	25.0	60.1	23.7	63.5	24.5
2	low K:	163.8	66.7	154.0	63.1	159.3	65.0
3	high K:	215.9	91.0	214.1	93.9	215.4	91.9

TABLE 3.13: Mean antineutrino and hadron energies for 2 bins of 1μ charged current antineutrino events for CLASS 2 and 3.

		E616		E701		E616+E701	
		E_ν	E_H	E_ν	E_H	E_ν	E_H
1	all π:	62.5	19.4	56.6	18.0	60.7	18.9
2	all K:	159.6	51.9	144.1	45.1	153.7	49.3

3.5.2 Dimuon Data

Tables 3.14-3.23 show number of dimuon events (passing cuts previously defined) in all 3 classes of events and their most important characteristics.

TABLE 3.14: The number of neutrino dimuon events with p_μ > 4.3 GeV/c (CLASS 1).

		E616	E701	E616+E701
1	low π	48	28	76
2	high π	34	25	59
3	low K	73	58	131
4	high K	122	49	171
5	all π	82	53	135
6	all K	195	107	302
7	TOTAL	277	160	437

TABLE 3.15: The number of antineutrino dimuon events with p_μ > 4.3 GeV/c (CLASS 1).

		E616	E701	E616+E701
1	all π	10	6	16
2	all K	10	5	15
3	TOTAL	20	11	31

TABLE 3.16: The number of neutrino opposite-sign dimuon events with both muons momentum analyzed in the toroid and $p_\mu > 9$ GeV/c (CLASS 2).

		E616	E701	E616+E701
1	all π	18	23	41
2	low K	50	58	108
3	high K	33	17	50
4	all K	83	75	158
5	TOTAL	101	98	199

TABLE 3.17: The number of antineutrino opposite-sign dimuon events with both muons momentum analyzed in the toroid and $p_\mu > 9$ GeV/c (CLASS 2).

		E616	E701	E616+E701
1	all π	2	2	4
2	all K	8	5	13
3	TOTAL	10	7	17

TABLE 3.18: The number of neutrino like-sign dimuon events with both muons momentum analyzed in the toroid and $p_\mu > 9$ GeV/c (CLASS 3).

		E616	E701	E616+E701
1	all π	2	0	2
2	low K	6	5	11
3	high K	2	3	5
4	all K	8	8	16
5	TOTAL	10	8	18

Tables 3.19-3.23 show the mean values of the most important characteristics of dimuon events (passing all the analysis cuts). The missing energy ($\langle E_{mis} \rangle$) and the transverse momentum of the second muon with respect to the hadron shower direction ($\langle p_T \rangle$) are given only for kaon-neutrino (ν_K) events for which these quantities are unambiguously determined.

TABLE 3.19: Characteristics of neutrino opposite-sign dimuon events with $p_\mu > 4.3$ GeV/c (CLASS 1). Missing energy is corrected for the corresponding 1μ off-set values.

		E616	E701	E616+E701
1	$\langle E_\nu \rangle$	138.6(3.4)	133.5(4.6)	136.7(2.7)
2	$\langle E_H \rangle$	59.2(2.5)	58.2(3.5)	58.8(2.0)
3	$\langle P_{\mu 1} \rangle$	67.7(2.6)	64.1(3.6)	66.4(2.1)
4	$\langle Q^2 \rangle$	19.6(1.2)	19.5(1.7)	19.5(1.0)
5	$\langle W^2 \rangle$	112.7(4.5)	110.5(6.2)	111.9(3.6)
6	$\langle x_{Bj} \rangle$	0.17(0.01)	0.17(0.01)	0.17(0.01)
7	$\langle y \rangle$	0.42(0.01)	0.43(0.02)	0.42(0.01)
8	$\langle \Theta_{\mu 1} \rangle$	0.051(0.002)	0.055(0.003)	0.052(0.002)
9	$\langle P_{\mu 2} \rangle$	11.7(0.8)	11.2(0.8)	11.5(0.6)
10	$\langle \Theta_{\mu 2} \rangle$	0.076(0.003)	0.078(0.004)	0.077(0.002)
11	$\langle \phi_{12} \rangle$	129.2(2.6)	125.0(3.7)	127.6(2.1)
12	$\langle z_\mu \rangle$	0.21(0.01)	0.21(0.01)	0.21(0.01)
13	$\langle p_T \rangle$	0.54(0.02)	0.54(0.03)	0.54(0.02)
14	$\langle E_{mis} \rangle$	19.2(1.7)	10.7(2.4)	16.7(1.4)
15	$\langle corr \rangle$	1.264(0.003)	1.185(0.002)	1.236(0.002)

TABLE 3.20: Characteristics of antineutrino opposite-sign dimuon events with p_μ > 4.3 GeV/c (CLASS 1). Missing energy is corrected for the corresponding 1μ off-set values.

		E616	E701	E616+E701
1	$\langle E_\nu \rangle$	105.3(10.9)	93.6(10.9)	101.1(8.1)
2	$\langle E_H \rangle$	39.1(5.6)	29.1(3.3)	35.5(3.9)
3	$\langle P_{\mu 1} \rangle$	56.6(6.5)	55.5(8.7)	56.2(5.2)
4	$\langle Q^2 \rangle$	9.9(2.6)	12.4(4.8)	10.8(2.4)
5	$\langle W^2 \rangle$	80.9(11.9)	58.8(7.3)	73.0(8.3)
6	$\langle x_{Bj} \rangle$	0.13(0.03)	0.17(0.05)	0.14(0.03)
7	$\langle y \rangle$	0.37(0.03)	0.33(0.03)	0.35(0.02)
8	$\langle \theta_{\mu 1} \rangle$	0.042(0.005)	0.052(0.011)	0.046(0.005)
9	$\langle P_{\mu 2} \rangle$	9.6(1.4)	9.0(1.5)	9.4(1.1)
10	$\langle \theta_{\mu 2} \rangle$	0.076(0.013)	0.077(0.012)	0.077(0.010)
11	$\langle \phi_{12} \rangle$	134.2(9.1)	143.7(9.5)	137.6(6.8)
12	$\langle z_\mu \rangle$	0.24(0.02)	0.24(0.03)	0.24(0.02)
13	$\langle p_T \rangle$	0.47(0.09)	0.48(0.14)	0.48(0.07)
14	$\langle E_{mis} \rangle$	20.0(5.9)	19.1(7.7)	19.7(4.7)
15	$\langle corr \rangle$	1.117(0.008)	1.368(0.016)	1.253(0.011)

TABLE 3.21: Characteristics of neutrino opposite-sign dimuon events analyzed in the toroid and with p_μ > 9 GeV/c (CLASS 2). Missing energy is corrected for the corresponding 1μ off-set values.

		E616	E701	E616+E701
1	$\langle E_\nu \rangle$	155.4(5.2)	147.8(5.1)	151.6(3.7)
2	$\langle E_H \rangle$	68.6(4.0)	61.2(3.7)	64.9(2.7)
3	$\langle P_{\mu 1} \rangle$	63.7(3.8)	61.9(3.8)	62.8(2.7)
4	$\langle Q^2 \rangle$	23.8(2.2)	20.6(2.5)	22.2(1.7)
5	$\langle W^2 \rangle$	147.8(7.3)	140.4(7.0)	144.2(5.0)
6	$\langle x_{Bj} \rangle$	0.15(0.02)	0.12(0.02)	0.14(0.01)
7	$\langle y \rangle$	0.43(0.02)	0.41(0.02)	0.42(0.01)
8	$\langle \theta_{\mu 1} \rangle$	0.054(0.003)	0.049(0.003)	0.052(0.002)
9	$\langle P_{\mu 2} \rangle$	23.1(1.7)	24.7(1.3)	23.9(1.1)
10	$\langle \theta_{\mu 2} \rangle$	0.045(0.002)	0.043(0.003)	0.044(0.002)
11	$\langle \phi_{12} \rangle$	135.5(4.2)	135.3(4.3)	135.4(3.0)
12	$\langle z_\mu \rangle$	0.29(0.02)	0.32(0.02)	0.31(0.01)
13	$\langle p_T \rangle$	0.62(0.04)	0.65(0.04)	0.63(0.03)
14	$\langle E_{mis} \rangle$	19.3(2.7)	7.7(2.7)	14.0(2.0)

TABLE 3.22: Characteristics of antineutrino opposite-sign dimuon events analyzed in the toroid with $p_\mu > 9$ GeV/c (CLASS 2). Missing energy is corrected for the corresponding 1μ off-set values.

		E616+E701
1	$\langle E_\nu \rangle$	134.1(11.9)
2	$\langle E_H \rangle$	49.9(8.3)
3	$\langle P_{\mu 1} \rangle$	63.4(7.0)
4	$\langle Q^2 \rangle$	18.3(4.2)
5	$\langle W^2 \rangle$	115.4(15.7)
6	$\langle x_{Bj} \rangle$	0.15(0.04)
7	$\langle y \rangle$	0.35(0.04)
8	$\langle \theta_{\mu 1} \rangle$	0.044(0.006)
9	$\langle P_{\mu 2} \rangle$	21.4(4.0)
10	$\langle \theta_{\mu 2} \rangle$	0.043(0.008)
11	$\langle \phi_{12} \rangle$	128.6(11.3)
12	$\langle z_\mu \rangle$	0.36(0.06)
13	$\langle p_T \rangle$	0.48(0.06)
14	$\langle E_{mis} \rangle$	14.9(4.5)

TABLE 3.23: Characteristics of neutrino like-sign dimuon events analyzed in the toroid with $p_\mu > 9$ GeV/c (CLASS 3). Missing energy is corrected for the corresponding 1μ off-set values.

		E616+E701
1	$\langle E_\nu \rangle$	151.2(10.1)
2	$\langle E_H \rangle$	78.4(9.2)
3	$\langle P_{\mu 1} \rangle$	56.3(8.7)
4	$\langle Q^2 \rangle$	39.0(7.6))
5	$\langle W^2 \rangle$	133.2(14.6)
6	$\langle x_{Bj} \rangle$	0.21(0.03)
7	$\langle y \rangle$	0.51(0.04)
8	$\langle \theta_{\mu 1} \rangle$	0.087(0.014)
9	$\langle P_{\mu 2} \rangle$	17.1(1.3)
10	$\langle \theta_{\mu 2} \rangle$	0.054(0.005)
11	$\langle \phi_{12} \rangle$	139.4(9.0)
12	$\langle z_\mu \rangle$	0.21(0.02)
13	$\langle p_T \rangle$	0.71(0.14)
14	$\langle E_{mis} \rangle$	17.5(4.5)

Chapter 4

Background Calculation

The main source of neutrino dimuon events is a charged current neutrino interaction with an additional muon from the semileptonic decay of a charm particle. Background dimuon events primarily originate from pion and kaon decays in the hadron shower cascade. Optical detectors in a magnetic field, such as high resolution bubble chambers or nuclear emulsions can observe individual particles and follow their tracks throughout the fiducial volume. In principle, some pion/kaon decays can be observed in a high resolution detectors by a change in the trajectory or curvature in a magnetic field. Such detailed information is

not available in a high density calorimetric apparatus, and an event-by-event determination of the origin of the second muon is not possible.

In the Lab E detector, muon tracks can be traced only if the particle penetrates beyond the end of the hadronic shower. Muons are the only particles which can traverse a sufficient distance in high density detectors to be observed beyond the range of a typical hadron shower.

The final state in an ordinary charged current neutrino interaction,

$$\nu + N \rightarrow \mu^- + \text{hadrons},$$

includes a muon emerging from the leptonic vertex, and primary hadrons produced in the fragmentation process of the scattered quark. Muons are identified as minimum ionizing particles which propagate through matter undergoing only multiple Coulomb scattering. Hadrons typically interact with a characteristic interaction length, but also a small fraction can decay. Products of secondary collisions may also decay or re-interact again. The overall picture resembles an avalanche with less and less energy in each subsequent step. Among the products of these secondary processes there may be an additional muon originating from a pion/kaon decay or from the production in secondary interactions. Such processes can lead to two or more muons in the final state.

In this analysis, a dimuon event is considered to be a background event if the second muon is produced from a secondary process in the hadronic shower, e.g. from pion, or kaon decays, or from meson and nucleon interactions in the calorimeter. An event-by-event separation of the background events from prompt dimuon events is impossible. Therefore the analysis requires a statistical subtraction of the background from the observed data. Details concerning the Monte Carlo calculation of the background are presented in the next chapter. Here, only the method and assumptions for the generation of the background dimuon events are described.

Fig.4.1 schematically shows the shower development, and serves as an illustration of the calculation of the background. Each neutrino interaction can be viewed as a two stage phenomenon: first, there are "prompt" hadrons coming from the fragmentation of the primary quark struck by the neutrino, then, the primary hadrons develop their own secondary reaction chain.

In the detector used in this experiment only muons with momentum greater than about 4 GeV/c can be observed and identified as the individual particles.

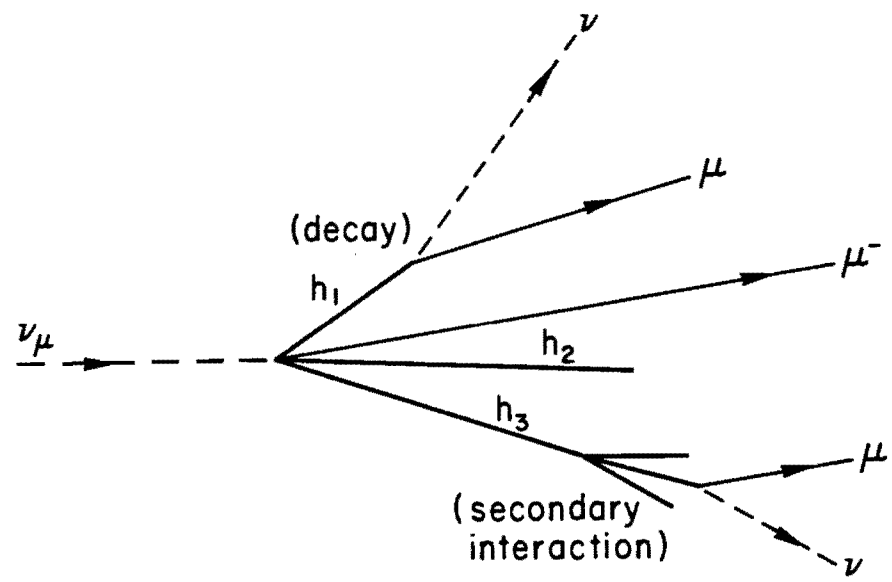

Figure 4.1 Illustration of the hadron shower development as a source of second muon production.

The kinematic distributions of primary hadrons can be described in terms of fragmentation functions (defined below). In the analysis, fragmentation functions obtained with the Lund Monte Carlo Program [4.4] were used and compared to fragmentation functions measured by Big European Bubble Chamber (BEBC) collaboration at CERN [4.1] and European Muon Collaboration at CERN [4.2].

Extraction of fragmentation functions from available data (i.e. BEBC and EMC data) used absolute normalizations (multiplicities) from the BEBC data and relative contributions of various particles from the EMC data. This method was necessary since the experimental information available from bubble chamber experiments is limited. In particular, neutrons are not observed and charged hadrons cannot be identified with momenta greater than about 1 GeV/c. In the background calculation the individual fractions of the total multiplicity due to pions, kaons and nucleons within the full available phase space of the interaction are important. This information was extracted from the results of the EMC which studied complete hadronic final states in deep inelastic muon scattering [4.2]. The assumption that the particle fractions in muon and neutrino interactions are similar is discussed on in section 4.2.

As mentioned, fragmentation functions describe the first stage of the reaction: primary hadrons. Information about prompt and non-prompt muons originating from secondaries in the hadronic shower cascade can be obtained from data with a hadron beam on a variable-density target. These data were obtained from Fermilab experiment E379 [4.3].

In the next two sections the extraction of fragmentation functions from existing data is discussed. Section 4.3 presents fragmentation functions obtained with the Lund Monte Carlo and comparison of both methods. Final results presented in Chapter 6 and 7 used hadron shower background calculated with the Lund MC fragmentation functions.

4.1 Fragmentation Functions from BEBC

The BEBC collaboration [4.1] has studied charged hadron production in charged current neutrino interactions on neon. Data were provided in the form of tables for all positive and all negative fragmentation functions. The fragmentation function is defined as:

$$D^h(z,W^2) = \frac{1}{N_{event}} \frac{dN_h}{dW^2 dz} \qquad (4.1.1)$$

where:

$h=\pi,K,p,n,...$ is a particle type,

and

$$z = \frac{E_h}{\sum_i E_{h_i}} \qquad (4.1.2)$$

is the fraction of a total hadron energy carried by a hadron h with energy E_h;

and

W^2 $(=2M\nu-Q^2+M^2)$ is the square of the invariant mass of the hadronic final state (notation as in Chapter 1, section 1.1);

$N_{event}(W^2)$ is a total number of events in the given W^2 bin; and

dN_h is a number of hadrons of type h observed in a given z and W^2 bin.

The data were binned in 5 W^2 values and 10 z bins for each W^2 range. These tables were parametrized under the constraint that the total multiplicity in given W^2 bin be conserved:

$$< n_h(W^2) > = \int_0^1 D^h(z,W^2)dz \qquad (4.1.3)$$

The form of the fit and resulting parameters are presented in Appendix B.

The data included information only about <u>all</u> positive and <u>all</u> negative particles. Individual contributions from various charged or neutral products of the ν-Ne reaction were not provided. The separation of pion, kaon (charged and neutral) and nucleon contributions was done using results from the EMC experiment.

4.2 Relative Fragmentation Functions from EMC

The European Muon Collaboration at CERN has studied final state hadrons in deep-inelastic muon scattering. In reference [4.2], results are presented for fragmentation functions for π^+, K^+, p, Λ, π^-, K^-, $\bar{p}$, $\bar{\Lambda}$, and K^0 as a function of Feynman variable x_F for all events in the range of W^2 from 16 GeV^2/c^4 to 400 GeV^2/c^4. The mean W^2 was about 130 GeV^2/c^4 (Fig.4.2).

On the basis of this figure, relations among pion, kaon, and proton fragmentation functions have been found to be:

$$D^{K^+}(z) = 0.066\times\exp(2.26z)\times D^{\pi^+}(z) \qquad (4.2.1)$$

$$D^{p}(z) = 0.223\times D^{\pi^+}(z) \qquad (4.2.2)$$

$$D^{K^-}(z) = 0.063\times\exp(1.60z)\times D^{\pi^-}(z) \qquad (4.2.3)$$

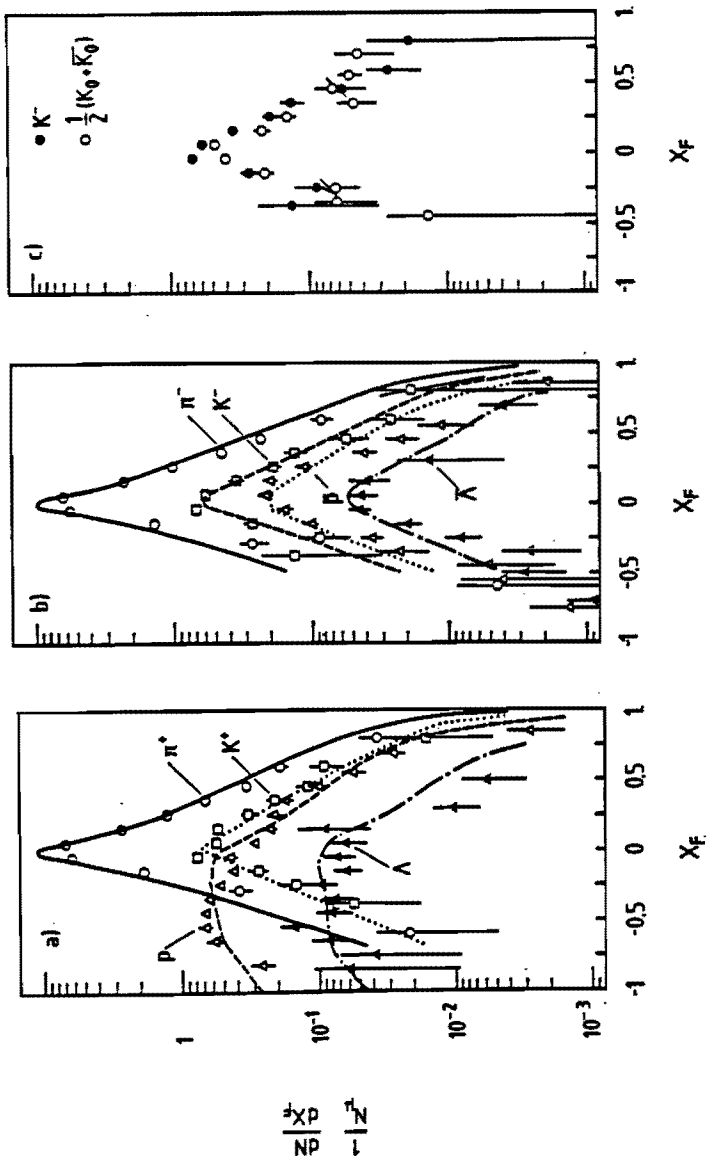

Figure 4.2 Fragmentation functions in variable x_F from the EMC collaboration [4.2]. Solid lines represent the Lund MC predictions.

$$D^{\bar{p}}(z) = 0.101 \times D^{\pi^-}(z) \qquad (4.2.4)$$

$$D^{K^0}(z) = \frac{1}{2} \times (D^{K^+}(z) + D^{K^-}(z)) \qquad (4.2.5)$$

An additional assumption was made:

$$D^{n}(z) = D^{p}(z) \quad \text{and} \quad D^{\bar{n}}(z) = D^{\bar{p}}(z) \qquad (4.2.6)$$

Several comments should be made about the use of the EMC data. These fragmentation functions are for μ-p scattering (ideally data from ν-Fe interaction should be used). According to ref.[4.5] forward fragmentation ($x_F > 0$) in ν-p is the same as forward fragmentation of μ-p and backward fragmentation ($x_F < 0$) in $\bar{\nu}$-p is equal to backward μ-p fragmentation. This can be easily understood in terms of the quark model. In both ν-p and μ-p collision the forward fragmentation is dominated by the u-quark while in $\bar{\nu}$-p and μ-p interaction, the backward fragmentation is dominated by the u-d diquark. Therefore μ-p and ν-p fragmentation functions should be very similar. The EMC data also indicates that the fragmentation functions for copper and carbon are the same (within errors). The μ-p data were only used for the z dependent ratios. The total charged hadron fragmentation is obtained from the neutrino-neon results. It

was assumed that these z dependent ratios hold over the whole range of W^2. It is clear from the error bars in Fig.4.2 that the relations among various hadrons fragmentation have considerable uncertainty.

In the calculations, contributions from charged pions, charged and neutral kaons, and nucleons were taken into account, and all other particles (e.g. Λ,Ω etc.) were neglected. The multiplicities versus W^2 are presented in Appendix C.

4.3 Lund Monte Carlo Calculations

The Lund Monte Carlo Program [4.4] provides a good description of many sets of experimental data [4.2,4.9-4.11]. Fragmentation functions predicted by this program agree with measured functions for many reactions. The agreement is good over a wide range of the variable z, and is worse for $z > 0.5$ [4.8a] (the program predicts too high values of fragmentation functions), see also Fig.4.2.

Many collaborations use Lund MC changing some of its fragmentation parameters to obtain the best agreement with the observed data. This experiment cannot "fit" Lund MC parameters, and therefore, with two exceptions, the default

version 4.3 of the Lund MC was used. Following recent suggestions [4.14,4.8a] two parameters were changed:

1. the minimum energy, E_{min}, above which creation of quark-antiquark pair is allowed was set to 0.2 GeV (the default value is 1.1 GeV);

2. a strangeness suppression parameter, λ, denoting the ratio of the probability γ_s of producing an $s\bar{s}$ pair to the probability γ_u (γ_d) of producing a $u\bar{u}$ ($d\bar{d}$) pair in the fragmentation chain (where $\gamma_u=\gamma_d$ due to isospin symmetry) was set to 0.2 [4.14] (the default value is 0.3). This parameter essentially controls the production of kaons and therefore is very important for the dimuon background. Since various collaboration use values ranging from 0.1 to 0.3, the effect of $\lambda=0.1$ and $\lambda=0.3$ was studied. This uncertainty is one the sources of the systematic error on the background. Values 0.1-0.3 bracket measurements in bubble chamber experiments (see Fig.4.5). Figure 4.3 shows fragmentation functions obtained from the BEBC/EMC data and compared to the Lund MC predictions. Figure 4.4 shows charged kaon fragmentation functions obtained from the BEBC/EMC data and compared to the Lund MC predictions with three values of the parameter $\lambda=0.1,0.2$, and 0.3. Figure 4.5 shows K^o fragmentation functions obtained from the BEBC/EMC

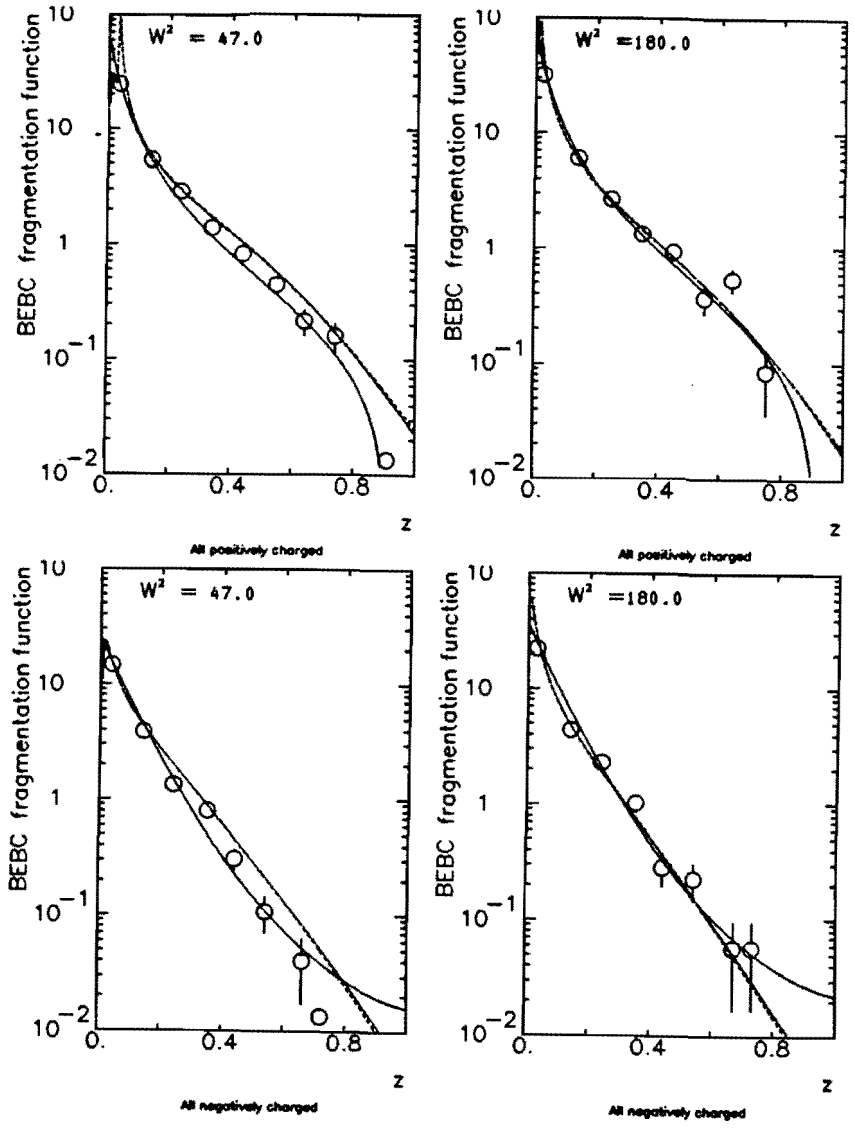

Figure 4.3 Positive and negative fragmentation functions from BEBC. The solid line shows the fit to these data, dashed-dotted lines represent fits to the fragmentation functions obtained with the Lund MC with λ=0.1,0.2, and 0.3.

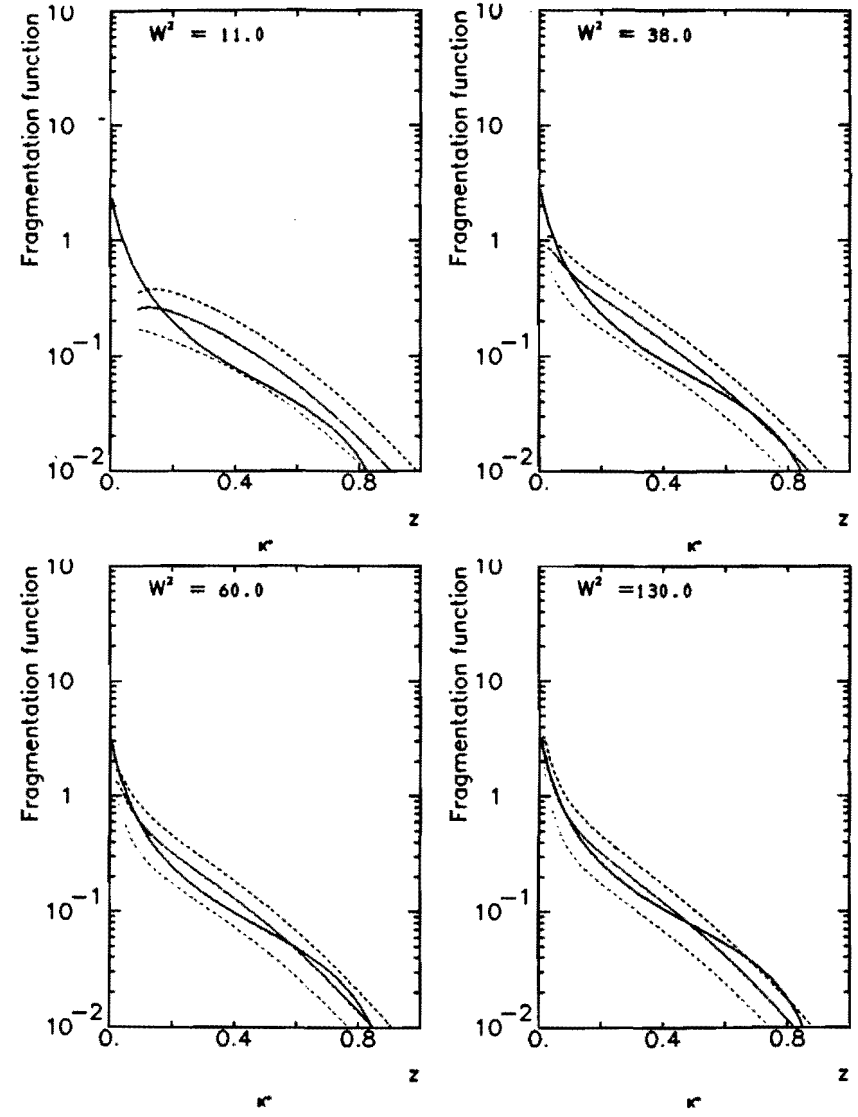

Figure 4.4a K^+ fragmentation functions from the BEBC/EMC data (solid line) and from the Lund MC (dashed-dotted lines: the top line is with λ=0.3, the middle one with λ=0.2, and the bottom one is with λ=0.1)

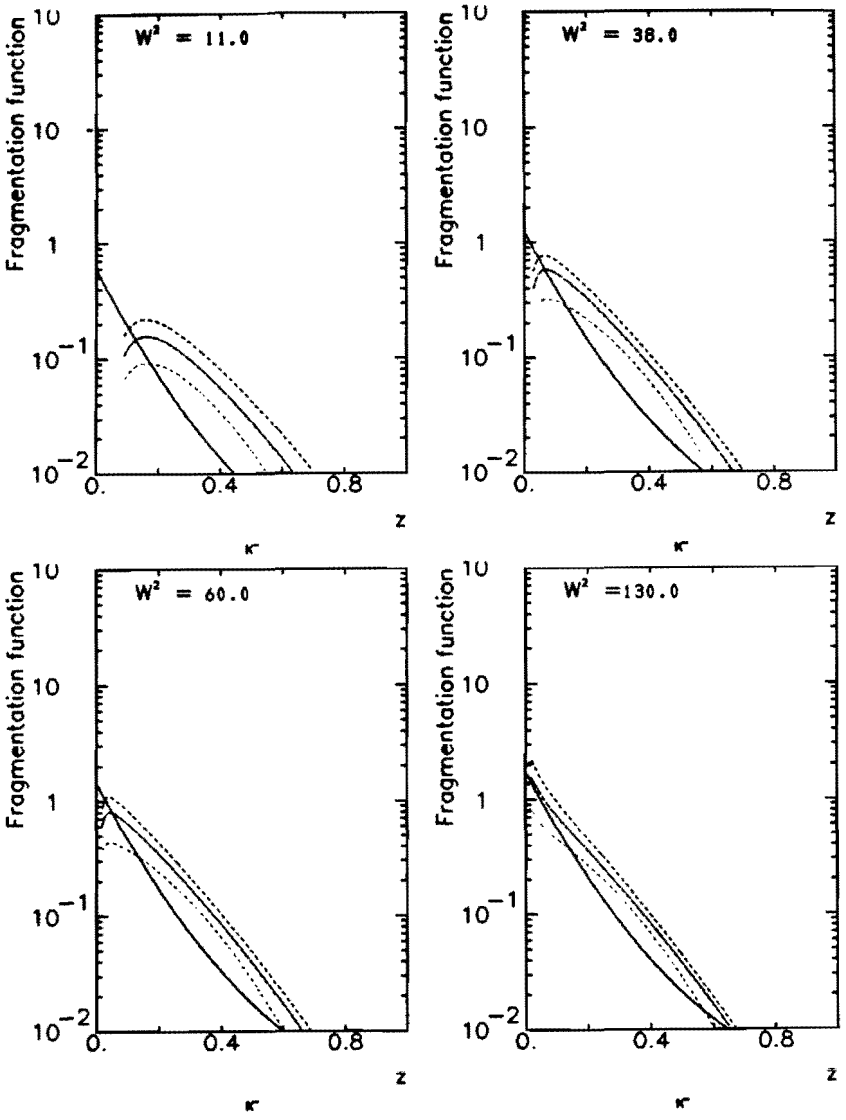

Figure 4.4b K^- fragmentation functions from the BEBC/EMC data (solid line) and from the Lund MC (dashed-dotted lines: the top line is with λ=0.3, the middle one with λ=0.2, and the bottom one is with λ=0.1)

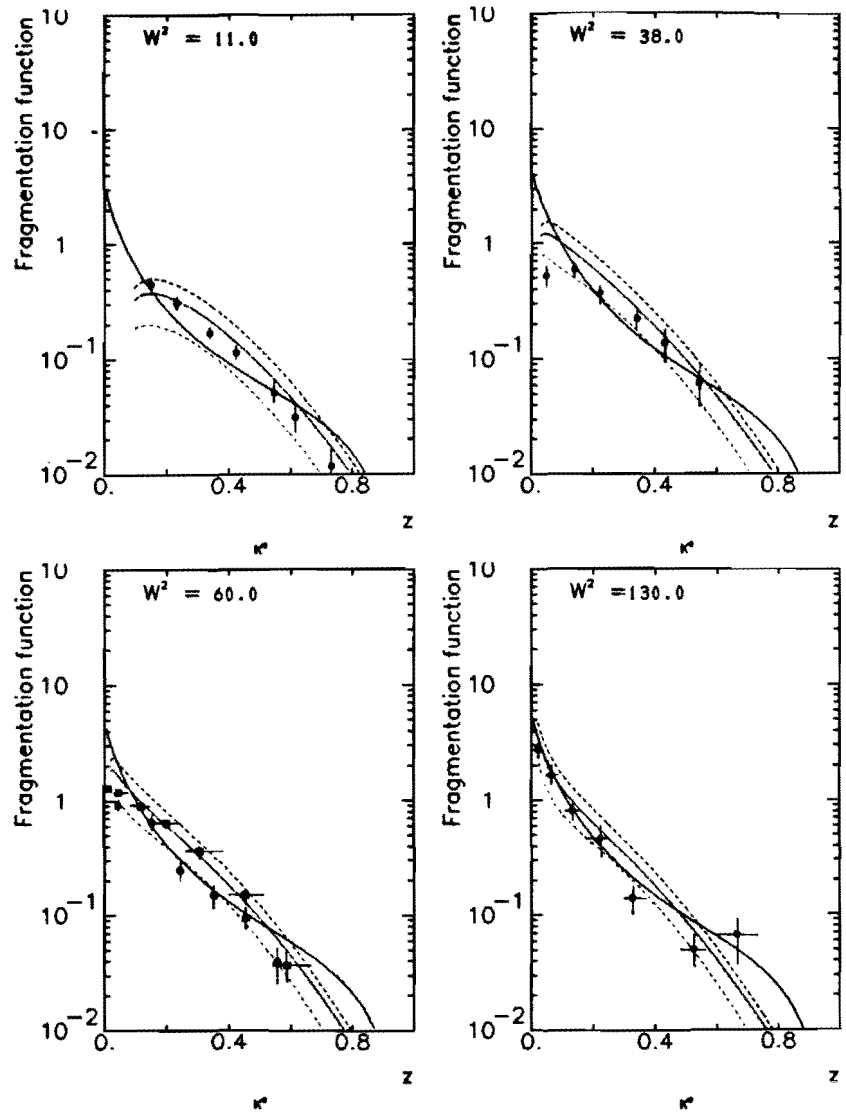

Figure 4.5 $K^o[=.5\times(K^o+\bar{K}^o)]$ fragmentation functions from the BEBC/EMC data (solid line) and from the Lund MC (dashed-dotted lines: the top line is with λ=0.3, the middle one with λ=0.2, and the bottom one is with λ=0.1). Data points are from: [4.16] in a, [4.17] in b, [4.18] (circles) and [4.20] (squares) in c, and from [4.19] in d.

data and compared to the Lund MC predictions with λ=0.1,0.2, and 0.3. Also shown are measurements from bubble chamber experiments at corresponding W^2 values [4.16-4.20].

4.4 Muon Rates from the Fermilab Experiment E379

Fermilab experiment E379 studied muon production by negative pions using a variable density target [4.3]. The existing data give a probability of observing a muon with momentum >4.26, >8.45, >9.45, > 15.45, and > 20.45 GeV/c from showers initiated by π^- beams with energies of 40, 75, 150 and 225 GeV. The sign of the muon was determined except at the lowest momentum cut of 4.26 GeV/c where the momentum was determined by range. Experiment E379 took data with two target densities allowing the separation of prompt and non-prompt muon rates. These data were used to interpolate the rates from the E379 target densities (ρ_1 = 6.12 g/cm^3, ρ_2 = 3.06 g/cm^3) to the density of the Lab E detector (ρ= 4.29 g/cm^3 for E616 run and ρ=4.24 g/cm^3 for E701 run). These rates were then parametrized for for all 5 cuts, p_{cut}, on muon momenta in a simple form (see Appendix D for details):

$$P^{\mu^\pm}_{shower} = a\left(1 - \frac{p_{cut}}{p_\pi}\right) E_\pi^b \qquad (4.4.1)$$

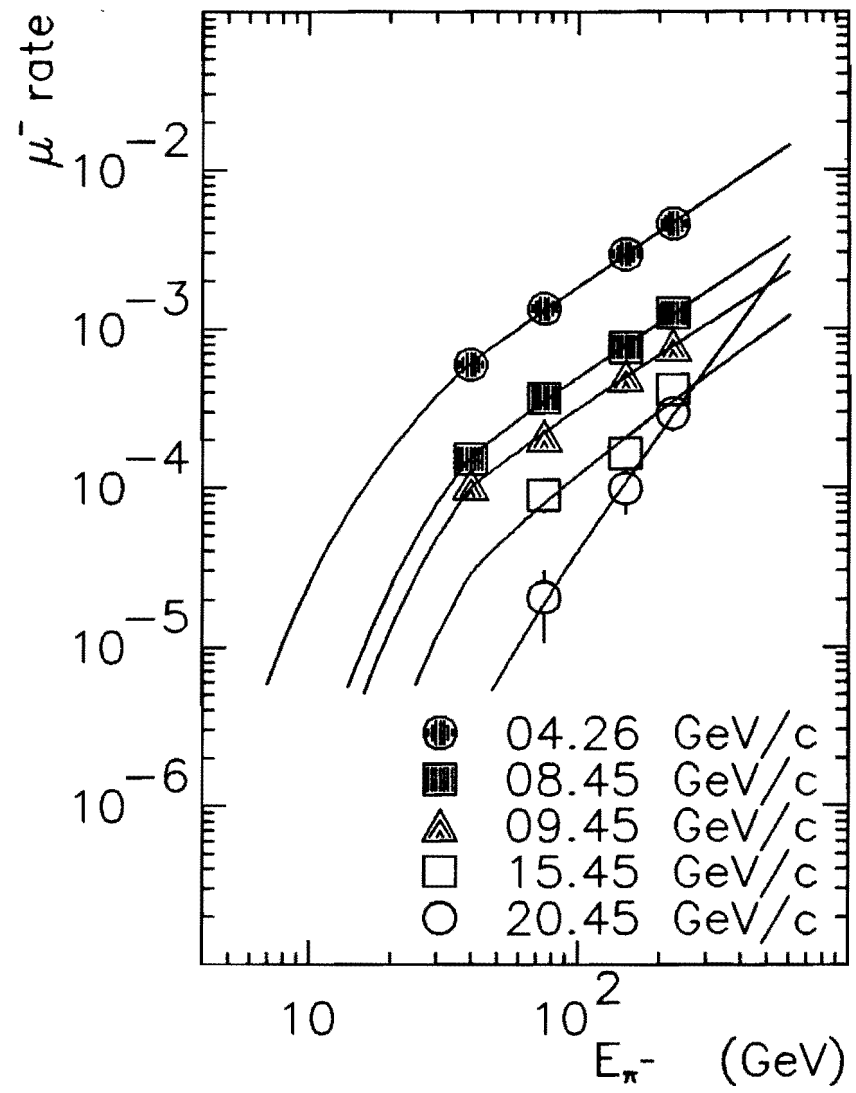

Figure 4.6a The points are the measurements for μ^- rates from Fermilab experiment E379 at five muon momenta cuts. Solid lines show the fit used in the background calculation.

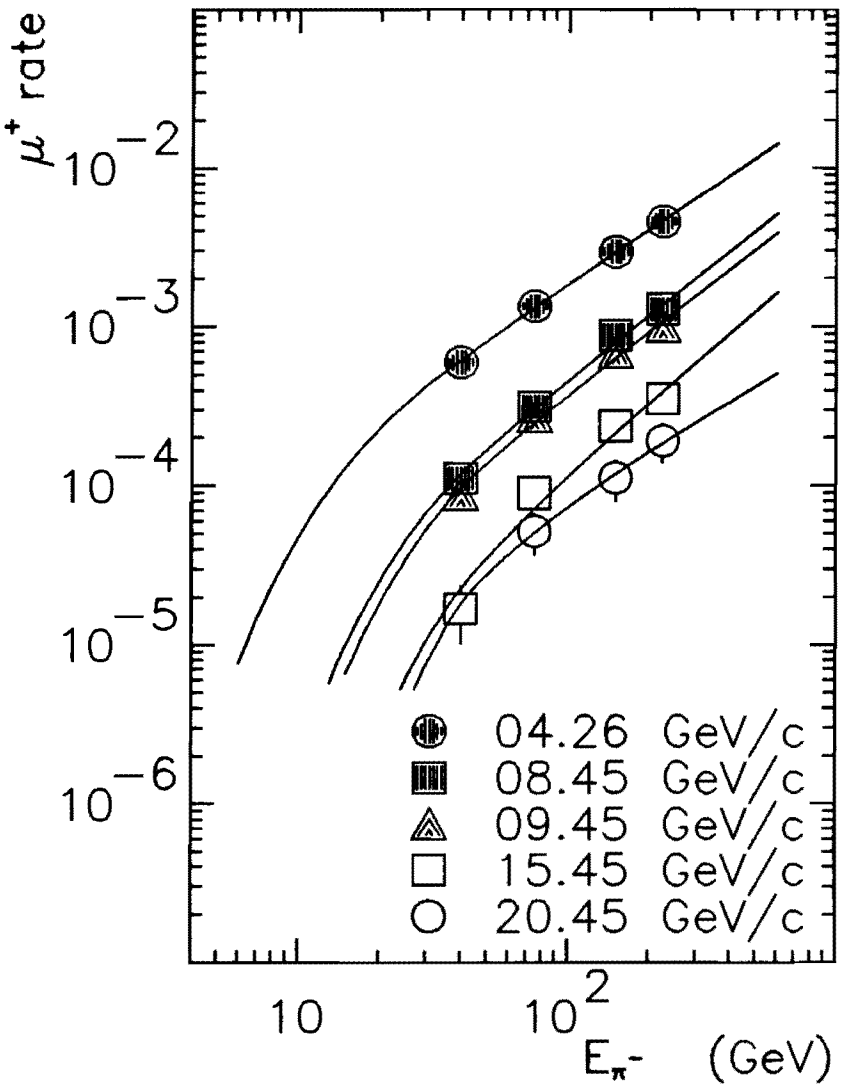

Figure 4.6b The points are the measurements for μ^+ rates from Fermilab experiment E379 at five muon momenta cuts. Solid lines show the fit used in the background calculation.

where a,b are constants, E_π, and p_π are energy and momentum of the pion beam. The E379 results are in good agreement with other data from experiments E595 at Fermilab [4.6a], and from the CDHS collaboration at CERN [4.6b].

It should be pointed out that the E379 data were obtained with negative pions only. It was assumed that rates for μ^- and μ^+ in a π^- beam are the same as the corresponding μ^+ and μ^- rates in a π^+ beam.

Lacking data on muon production from other beams and using results from refs. [4.6a] and [4.15] it was estimated that the muon yield from showers initiated by other particles can be obtained by correcting pion-initiated showers. The correcting factors used were:

a) for kaon showers: the pion-initiated muon rates were multiplied by a factor $F_K = (1-f) + A\times f/2$, where $f=(-1.45\pm0.10)g^2 + (2.42\pm0.13)g + (0.030\pm0.030)$, with $g=p_{cut}/E_K$, and $A = 3.73$. Factor f reflects differences in the particle yields from pion and kaon showers, and the constant A reflects kinematic differences between pions and kaons (i.e. difference in the ratio of the decay to interaction lengths, $\lambda_{int}/\lambda_{decay}$ (see next section), and difference in the muon spectrum from a kaon/pion decay). The factor F_K averages in calculations to about 1.8.

b) for proton showers: the pion-initiated μ^+ yield was multiplied by 1.17, and μ^- yield by 0.39.

c) for neutron showers: the pion-initiated muon yields (μ^+ and μ^-) were multiplied by 0.775.

An additional correction for the dimuon yield was applied by multiplying the total secondary shower yield by a factor 0.9.

These corrections together result in about 3% decrease in the total muon yield as compared to the case where secondary showers from all particles are assumed to be equal to the pion-initiated yields.

An additional assumption for the data with $p_\mu > 4.26$ GeV/c (where determination of the sign of a muon was not possible) was that rates of μ^- are equal to rates of μ^+.

4.5 Interaction and Decay Lengths of Primary Hadrons

The primary hadrons can interact with other nuclei in the medium or decay to a muon. To find the probability of muon production it is necessary to calculate the ratio:

$$r^h = \frac{\lambda^h_{int}}{\lambda^h_d} \qquad (4.5.1)$$

where λ_d^h is the decay length of a hadron h with energy E_h,

mass m_h, and proper mean lifetime $c\tau$, and λ^h_{int} is the mean interaction length of a hadron h in the medium of atomic mass A, the two defined as:

$$\lambda^h_d = \gamma\beta c\tau = \frac{E_h}{m_h} \cdot c\tau \qquad (4.5.2)$$

$$\lambda^h_{int} = \frac{A}{N\,\sigma^h \rho} \qquad (4.5.3)$$

where σ^h denotes the absorption cross section of hadron h in the medium, ρ is the density (in g/cm^3), and N is Avogadro's number.

Measurements from reference 4.7 were used for absorption cross sections of pions and kaons. More detailed information about calculation of the probabilities r^π and r^K may be found in Appendix E. For the mean density of the Lab E detector of 4.27 g/cm^3 it was found:

$$r^{\pi^\pm} = \frac{6.384}{E_\pi} \times 10^{-3} \qquad \text{for } p_\pi > 22 \text{ GeV/c} \qquad (4.5.4a)$$

$$r^{\pi^\pm} = \frac{3.730}{E_\pi(678 - 4.2\,p_\pi)} \qquad p_\pi < 22 \text{ GeV/c} \qquad (4.5.4b)$$

$$r^{K^+} = \frac{3.460 \cdot 10^{-2}}{E_K} + 0.212 \times r^\pi(E_\pi = \tfrac{1}{2}E_K) \qquad (4.5.5)$$

$$r^{K^-} = \frac{3.337 \cdot 10^{-2} f}{E_K} + 0.212 \times r^\pi(E_\pi = \tfrac{1}{2}E_K) \qquad (4.5.6)$$

The kinematics of the two-body decay of a hadron h,

$$h \rightarrow \mu + \nu \qquad (h = \pi \text{ or } K)$$

yields an energy distribution of muons in the range

$$(m_\mu^2/m_h^2)E_h < E_\mu < E_h \ .$$

To obtain the decay probability for the muon with the momentum cut p_{cut}, it is necessary to consider three cases:

1. $P_{decay}(p_{cut}, E_h) = 0$ for $p_{cut} > E_h$ (4.5.7)

2. $P_{decay}(p_{cut}, E_h) = r^h \dfrac{1 - p_{cut}/E_h}{1 - R_h}$ for $p_{cut} < E_h < R_h p_{cut}$ (4.5.8)

3. $P_{decay}(p_{cut}, E_h) = r^h$ for $E_h > R_h p_{cut}$ (4.5.9)

where

$$R_h = \frac{m_\mu^2}{m_h^2} \qquad (4.5.10)$$

For pions and kaons :

$$R_\pi = 1/1.744 \quad \text{and} \quad \frac{1}{1 - R_\pi} = 2.344$$

and

$$R_K = 1/21.830 \quad \text{and} \quad \frac{1}{1 - R_K} = 1.048$$

4.6 Outline of the Background Calculations

There are two main sources which can produce an additional background muon in charged current neutrino interactions: (a) muons from decays of primary hadrons, and (b) muons from production and decays in re-interactions.

Contributions from both processes have been included.

The Lund (and BEBC/EMC) fragmentation functions were parametrized in W^2 and z variables. The E379 results for hadron showers were given as a function of hadron (beam) energy E_h. According to (4.1.2)

$$E_h = z \sum_i E_{h_i} = zE_H \qquad (4.6.1)$$

where E_H is the total hadron energy of the collision.

As shown in Chapter 1:

$$W^2 = 2M\nu - Q^2 + M^2 \quad \text{and} \quad Q^2 = 2M\nu x \qquad (4.6.2)$$

hence

$$W^2 = 2M\nu(1-x) + M^2 \qquad (4.6.3)$$

and

$$E_H = \nu + M \ .$$

Thus, the energy of a hadron h as a function of z, x, and W^2 is:

$$E_h = zE_H = z(\nu + M) = z\left(\frac{W^2 - M^2}{2M\nu(1-x)} + M\right) \qquad (4.6.4)$$

The total probability of producing a muon from the hadronic shower in a neutrino interaction may be expressed in the form:

$$P_{total}(p_{cut}, \nu, x) = P_{total}^{shower}(p_{cut}, \nu, x) + P_{total}^{decay}(p'_{cut}, \nu, x) \qquad (4.6.5)$$

where

$$P^{shower}_{total}(p_{cut},\nu,x) = \sum_h \int_0^1 D^h(z,W^2(\nu,x))P_{shower}(p_{cut},E_h(z,\nu))dz \qquad (4.6.6)$$

and

$$P^{decay}_{total}(p_{cut},\nu,x) = \sum_h \int_0^1 D^h(z,W^2(z,\nu))P_{decay}(p'_{cut},E'_h(z,\nu))dz \qquad (4.6.7)$$

The quantities P_{shower} and P_{decay} are defined by formulae 4.4.1 and 4.5.7-4.5.10. Therefore, the total probability is a function of two variables, namely the hadron energy ν and the Bjorken x. The variables $p'_{cut} = p_{cut} - \Delta$ and $E_h' = E_h - \Delta$, where $\Delta = 0.29$ GeV for pions and $\Delta = 0.32$ GeV for kaons, correct for the muon decay point which is 1 interaction length (on average) downstream of the neutrino event vertex.

The probabilities were calculated as a function of ν for the five muon momentum cuts of 4.26, 8.45, 9.45, 15.45, and 20.45 GeV/c in 7 x bins over the range $0 < x < 1$. The mean x for each bin was calculated using the $F_2(x)$ structure function (details can be found in Appendix F).

The integrals for each x bin and muon momentum cut from eqs. 4.6.5-4.6.7 were evaluated and the results for the total probability of producing a muon were parametrized.

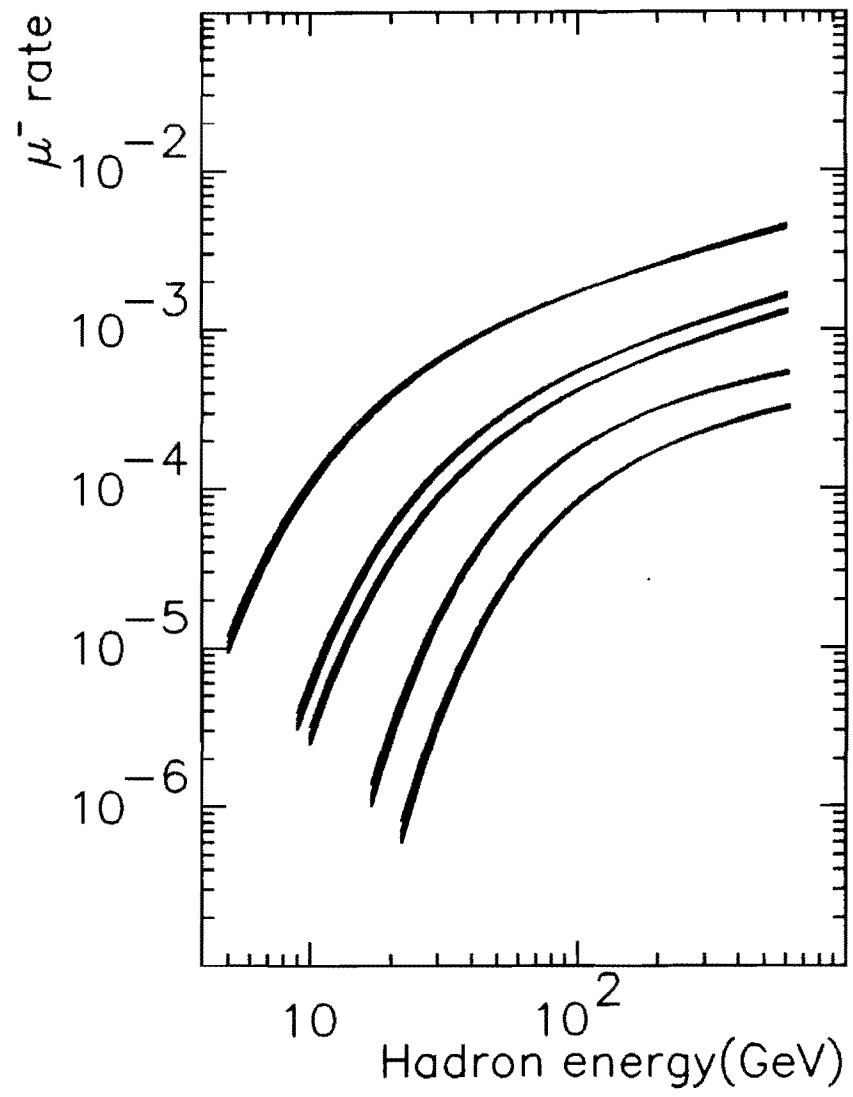

Figure 4.7a The curves for the final results for μ^- rates from neutrino induced showers obtained by the calculations described in this chapter. The five series of curves (each for 7 x bins) are for five muon momenta cuts of 4.26, 8.45, 9.45, 15.45, and 20.45 GeV/c.

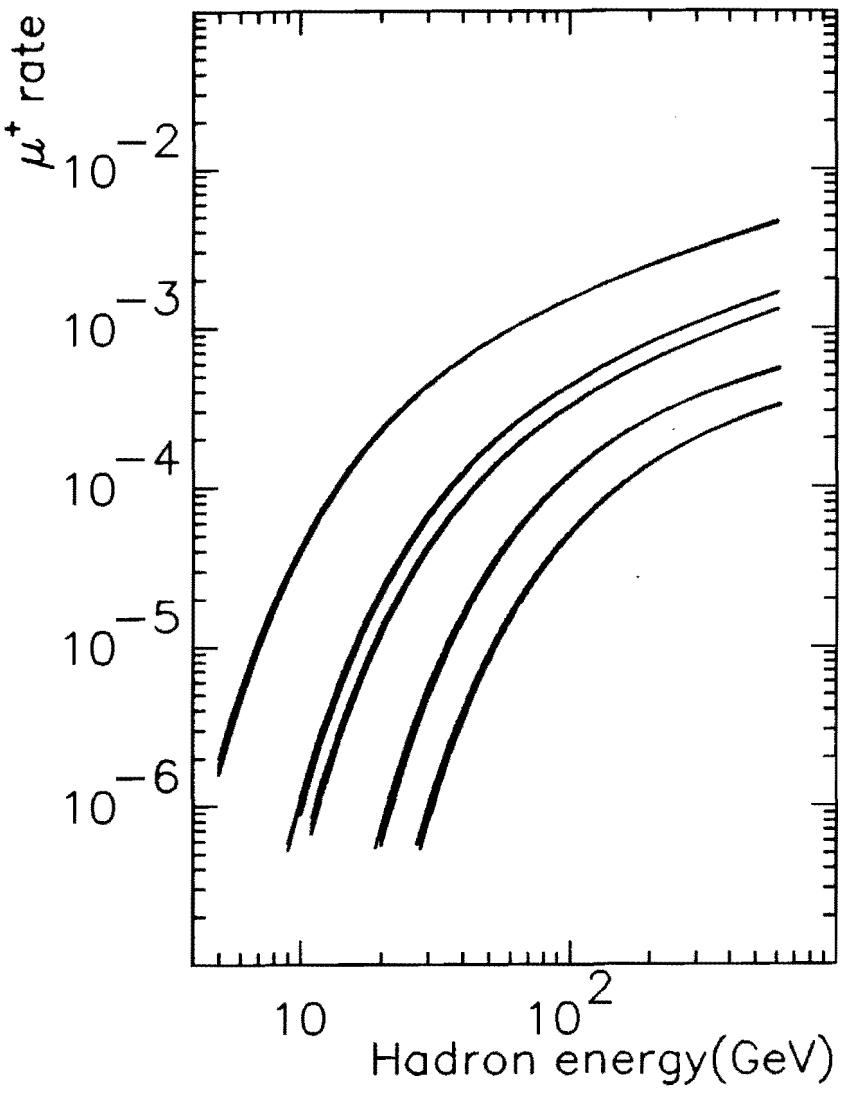

Figure 4.7b The curves show the final results for μ^+ rates from neutrino induced showers obtained by the calculations described in this chapter. The five series of curves (each for 7 x bins) are for five muon momenta cuts of 4.26, 8.45, 9.45, 15.45, and 20.45 GeV/c.

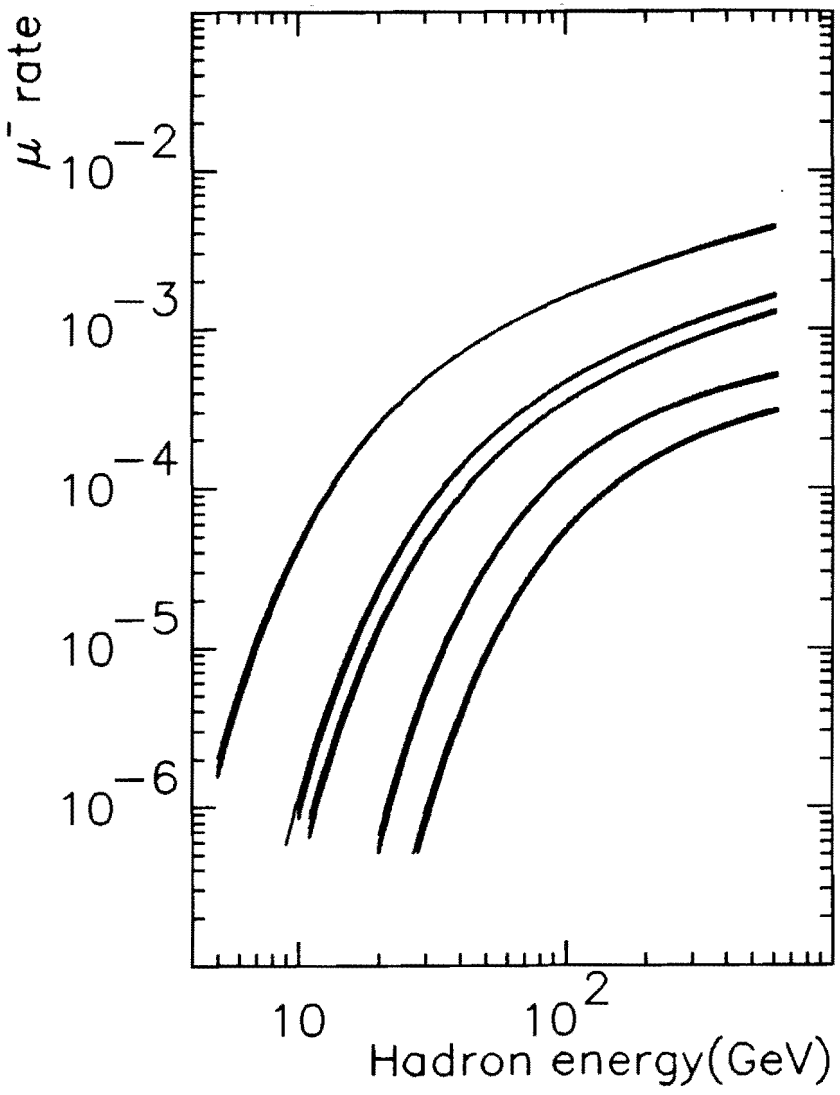

Figure 4.8a The curves show the final results for μ^- rates from antineutrino induced showers obtained by the calculations described in this chapter. The five series of curves (each for 7 x bins) are for five muon momenta cuts of 4.26, 8.45, 9.45, 15.45, and 20.45 GeV/c.

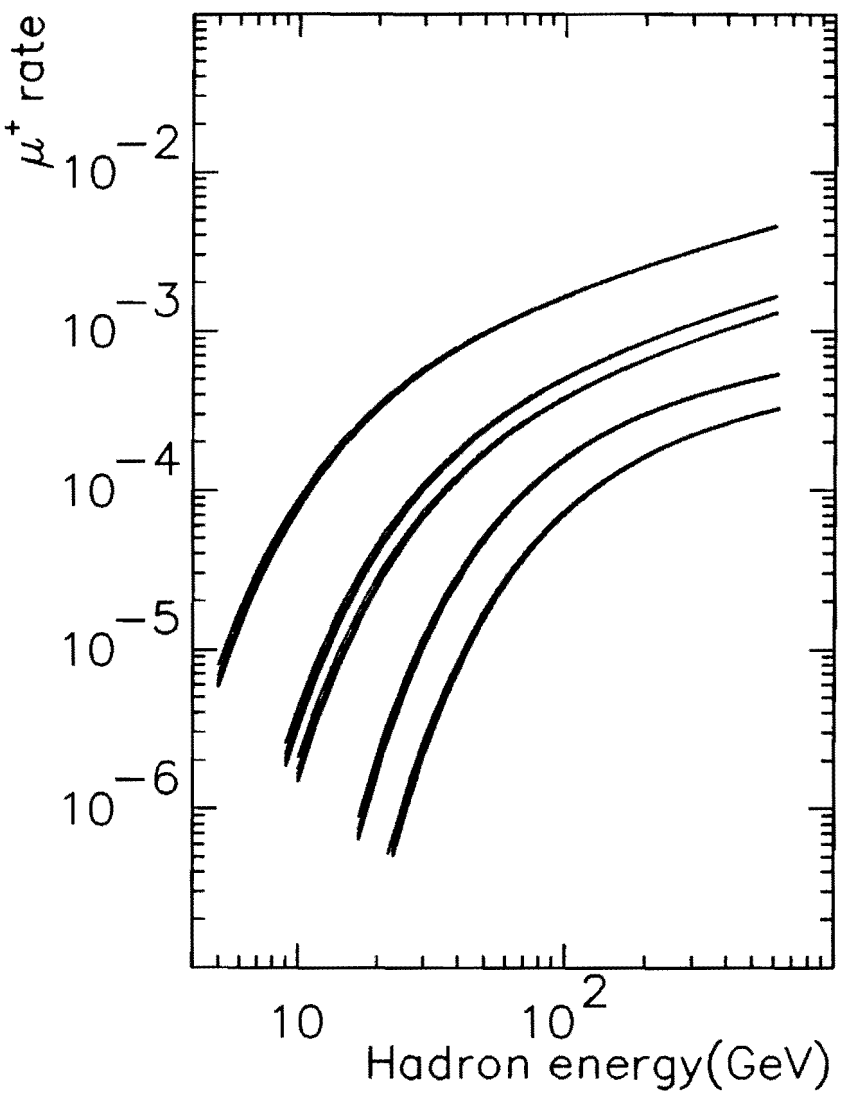

Figure 4.8b The curves show the final results for μ^+ rates from antineutrino induced showers obtained by the calculations described in this chapter. The five series of curves (each for 7 x bins) are for five muon momenta cuts of 4.26, 8.45, 9.45, 15.45, and 20.45 GeV/c.

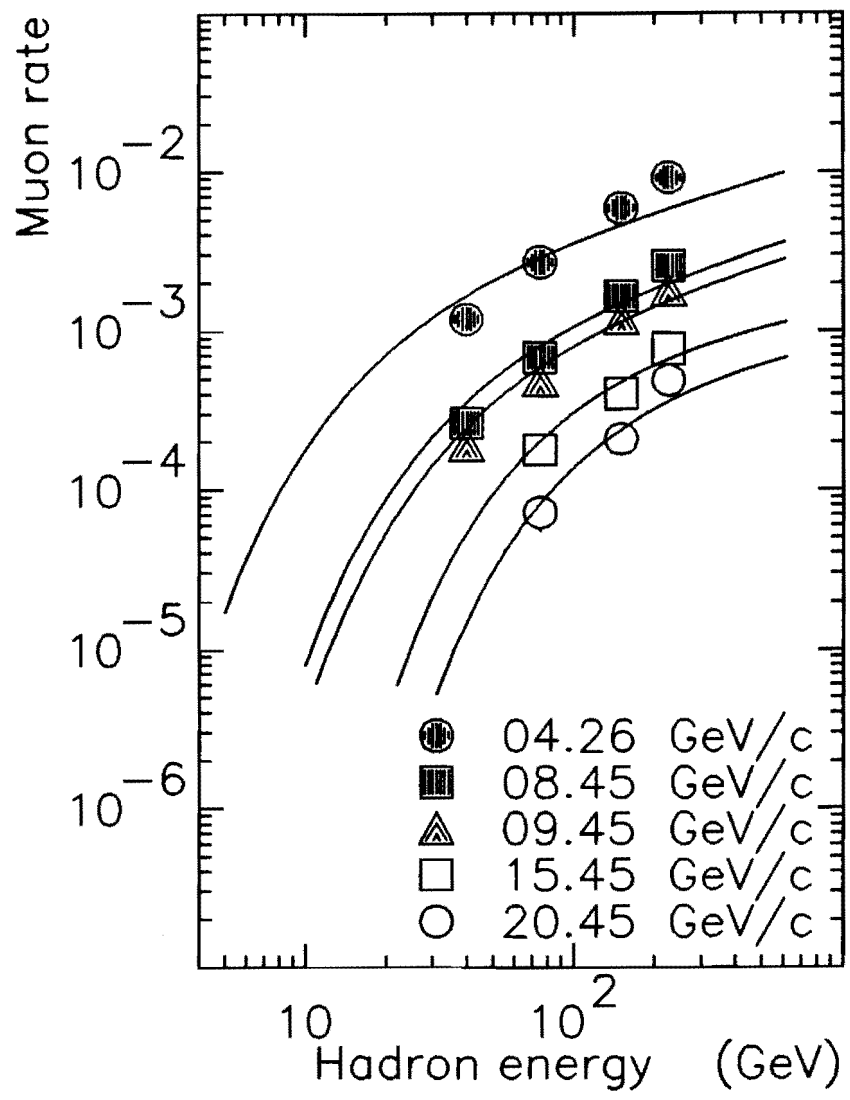

Figure 4.9a Total muon rates as a function of hadron energy as measured by Fermilab experiment E379 for five momenta cuts (full points). The curves represent neutrino hadron shower induced total muon rates obtained by the calculation described in this chapter (at x=0.2).

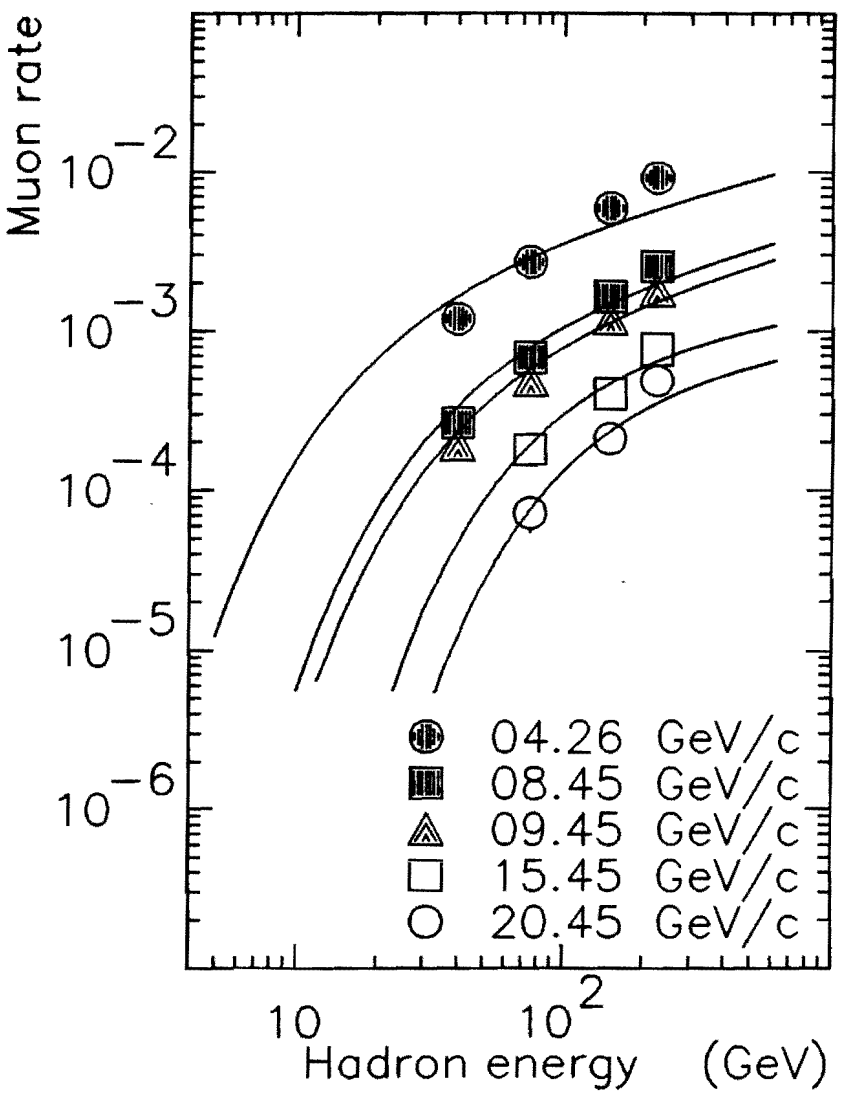

Figure 4.9b Total muon rates as a function of hadron energy as measured by Fermilab experiment E379 for five momenta cuts (full points). The curves represent antineutrino hadron shower induced total muon rates obtained by the calculation described in this chapter (at x=0.2).

The calculation was performed for the five momentum cuts and 7 x bins (35 functions altogether). The final results were parametrized as a function of a momentum cut p_{cut} in the form:

$$P_{total}(p_{cut}) = A\ \nu^{B}\ e^{-(-\frac{C}{\nu} + D)\ p_{cut}} \qquad (4.6.8)$$

which provided flexibility in varying the momentum cut continuously from 4 to 20 GeV/c.

Figs.4.7 - 4.9 show the results of the calculations. Appendix G contains detailed tables of rates and all the final fit parameters.

4.7 Systematic Errors on the Background Rate

There are experimental errors in the input data and theoretical uncertainties in the assumptions used in the background calculations. The effect of various parameters on the total probability of muon production in a neutrino-induced hadron shower was studied.

1. The Lund MC fragmentation functions are generated for neutrino-nucleon interactions (with small correction for non-isoscalar target). It was assumed that they are the same for neutrinos interacting on iron (ν-Fe). EMC measurements of fragmentation functions for various nuclear targets

[4.12] indicate that the uncertainty in this assumption leads to an error of ±15% in the total muon production probability.

2. A change of λ parameter in the Lund MC from 0.2 to 0.3 or 0.1 values leads to the ±6% change in the total muon production probability.

3. The uncertainty of ±2% in the decay probability and interaction lengths for mesons produced in the primary neutrino reaction leads to ±1% systematic error in the total muon production probability.

4. A ±10% systematic error on the total muon production probability is due to a ±20% uncertainty in the contribution of secondary interactions.

5. Parametrizations of fragmentation functions and final muon rates were obtained with ±5% precision leading to the same uncertainty in the background normalization.

All the above systematic uncertainties added in quadrature lead to a total systematic error on the background normalization of ±20%.

Chapter 5

Neutrino Charm Production Monte Carlo

One of the main physics goals of the experiment is the determination of the strange sea fraction in the nucleon. The extraction of this information from dimuon data requires a model for opposite-sign dimuon production. The input parameters to the model can be then compared to the observed data.

In the standard model of electroweak interactions, neutrino (antineutrino) events with opposite-sign dimuons in the final state originate from the production

and semileptonic decay of charm particles (see Fig.1.2). A background contamination from hadronic showers (discussed in Chapter 4) is also expected. Therefore, the interpretation of the data requires a model for neutrino charm production, and a model for the production of background muons in neutrino induced showers.

The input to the background model requires a knowledge of the rates for production of muons in neutrino (or antineutrino) induced showers as a function of the energy of the hadron shower and final state muon momentum. In addition, information about the transverse momentum of background muons (primarily from pion and kaon decays) is also required.

The charm particle production model in neutrino interactions requires several input parameters. Aside from the nucleon structure functions, important quantities are:

1. The strange sea content in the nucleon κ (as defined by (1.3.4)) ;
2. The mass of a charm quark, m_c;
3. The fragmentation function of a charm quark into charm particles, $D(z_D)$;
4. The average semileptonic decay branching ratio of charm particles into muons $B_l(c \to \mu X)$.

A detailed discussion of these parameters and the Monte Carlo is presented in this chapter.

5.1 Single-Muon Charged Current Monte Carlo

The construction of a model for neutrino charm production is based on single-muon charged current events generated by a Monte Carlo technique.

The neutrino beam Monte Carlo which reproduced the observed distributions in devices monitoring the secondary beam [2.6] was used as the input to the event Monte Carlo. Charged current interactions were generated according to eq.1.2.9. Structure functions were parametrized in a form suggested by Buras and Gaemers [5.1] with coefficients obtained from fits to the charged current data from the first run (experiment E616) [3.1, 3.2].

Generated events were processed through exactly the same reconstruction program as the data. The same geometrical and kinematical cuts were applied.

Fig.5.1 shows the structure functions at a four-momentum transfer (Q^2) of 20 GeV^2/c^2. Fig.5.2 shows the valence and sea contributions to the structure functions of the nucleon at the same four-momentum transfer.

There was a good agreement between the Monte Carlo generated events and the data. Figs.5.3-5.6 show comparison of few kinematic quantities.

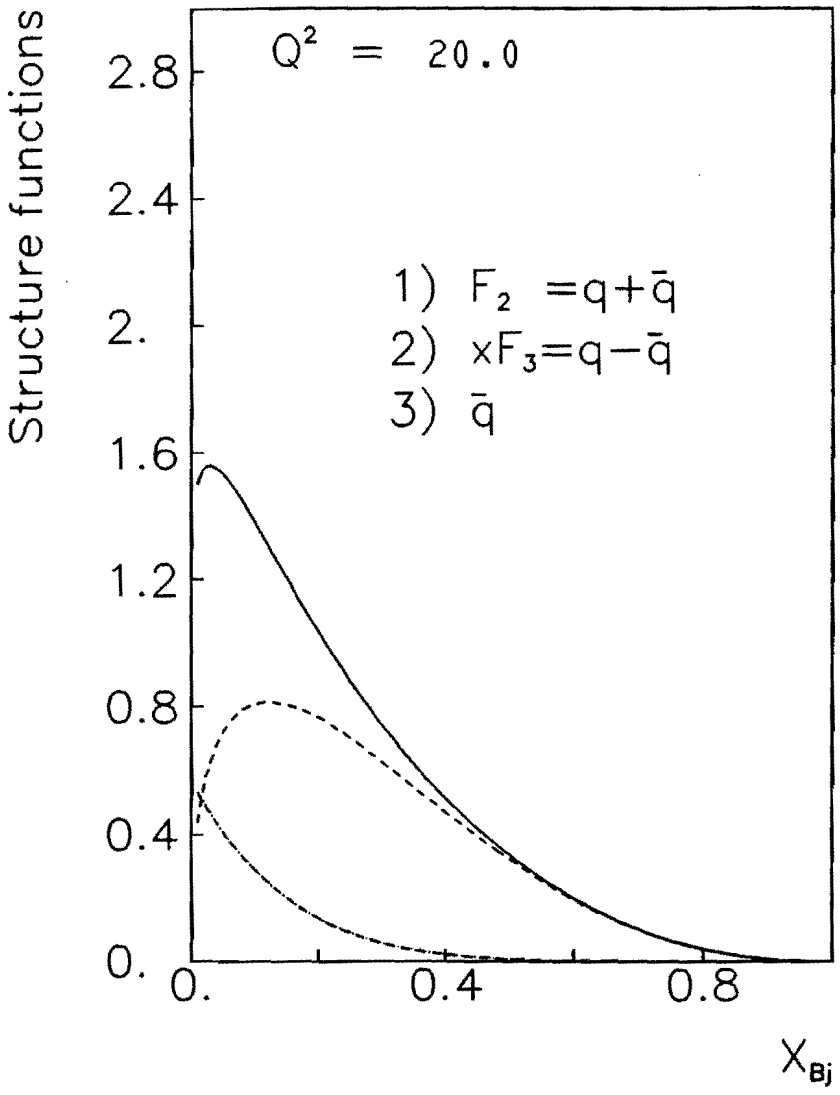

Figure 5.1 F_2 and xF_3 structure functions fits, and the antiquark distribution at Q^2 = 20 GeV^2/c^2 as measured in experiment E616.

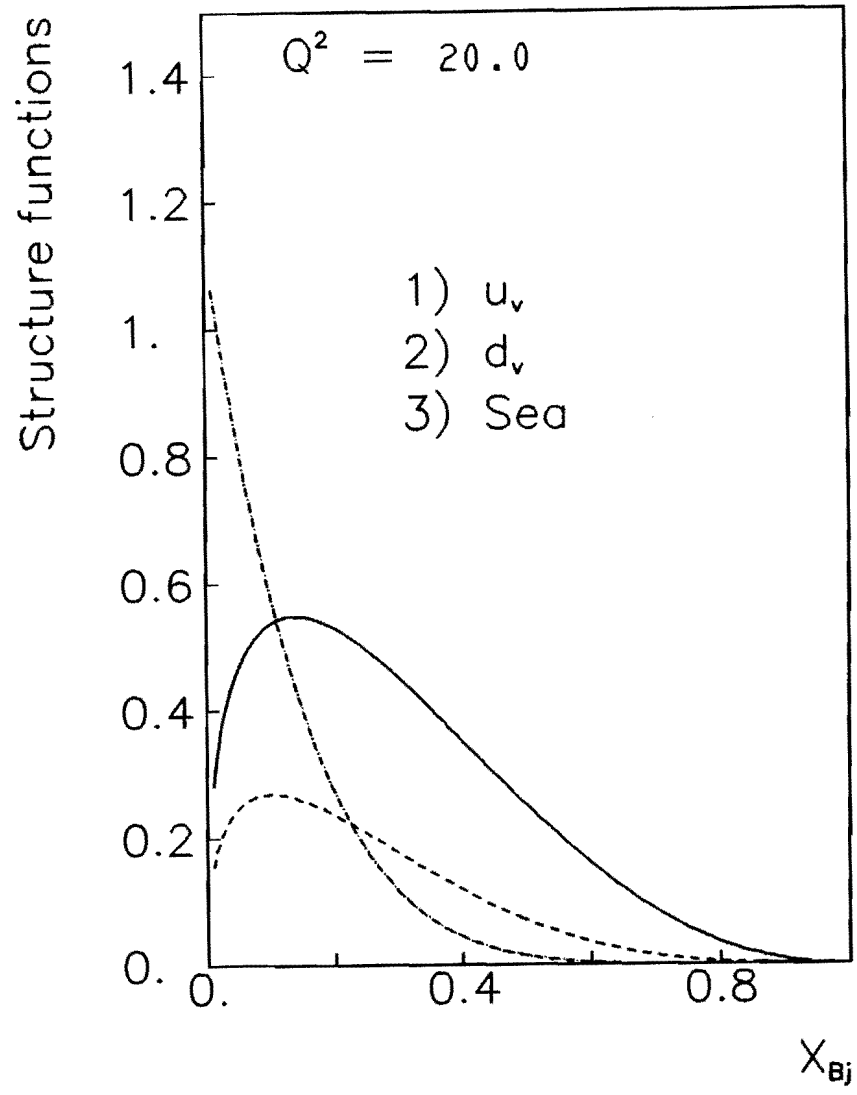

Figure 5.2 The x_2 distributions of valence and sea quarks in the nucleon at Q^2 = 20 GeV^2/c^2.

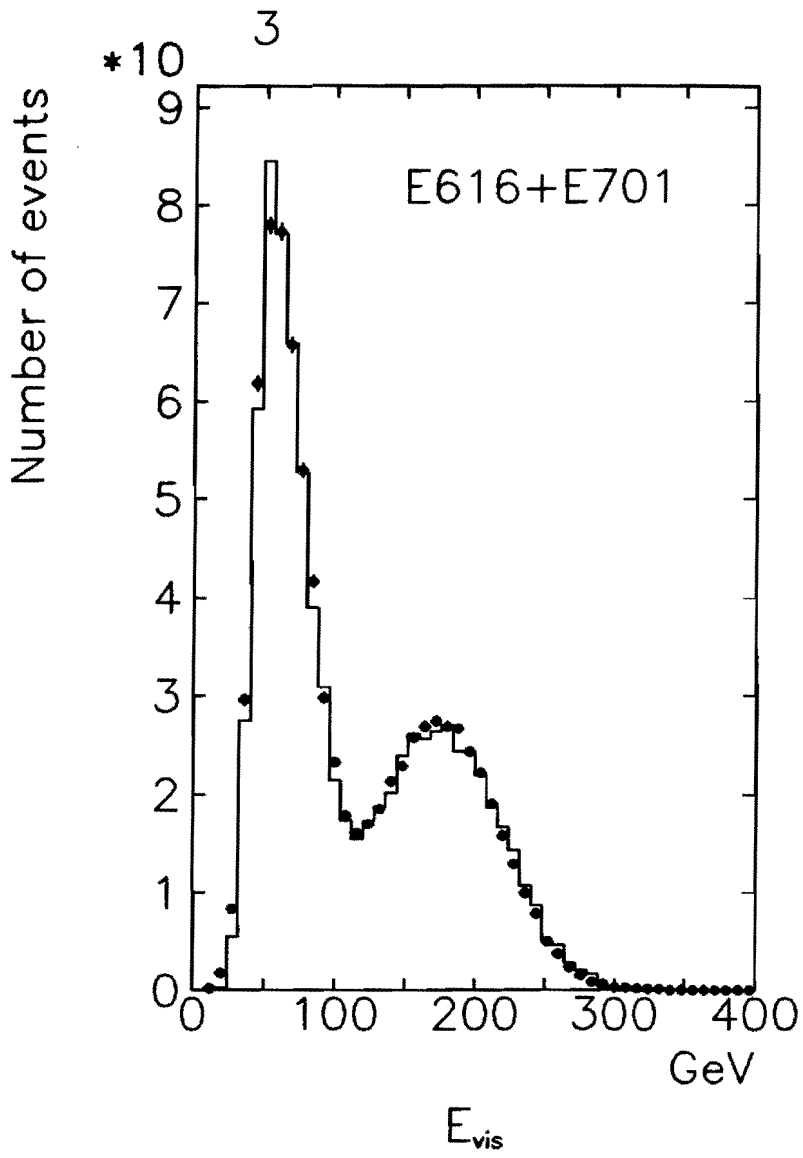

Figure 5.3 Distribution of measured neutrino energy in single-muon charged current events. The points with error bars represent the data, and the histogram represents the Monte Carlo events.

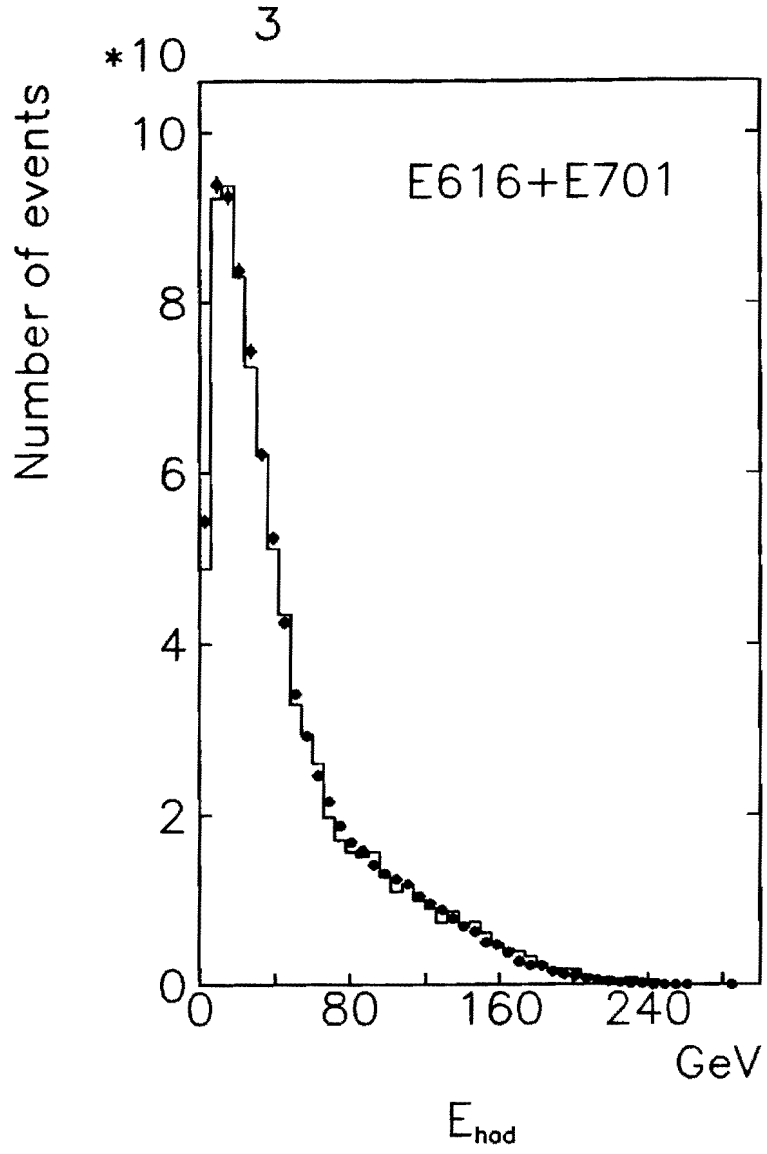

Figure 5.4 Distribution of measured hadron energy in single-muon charged current events. The points with error bars represent the data, and the histogram represents the Monte Carlo events.

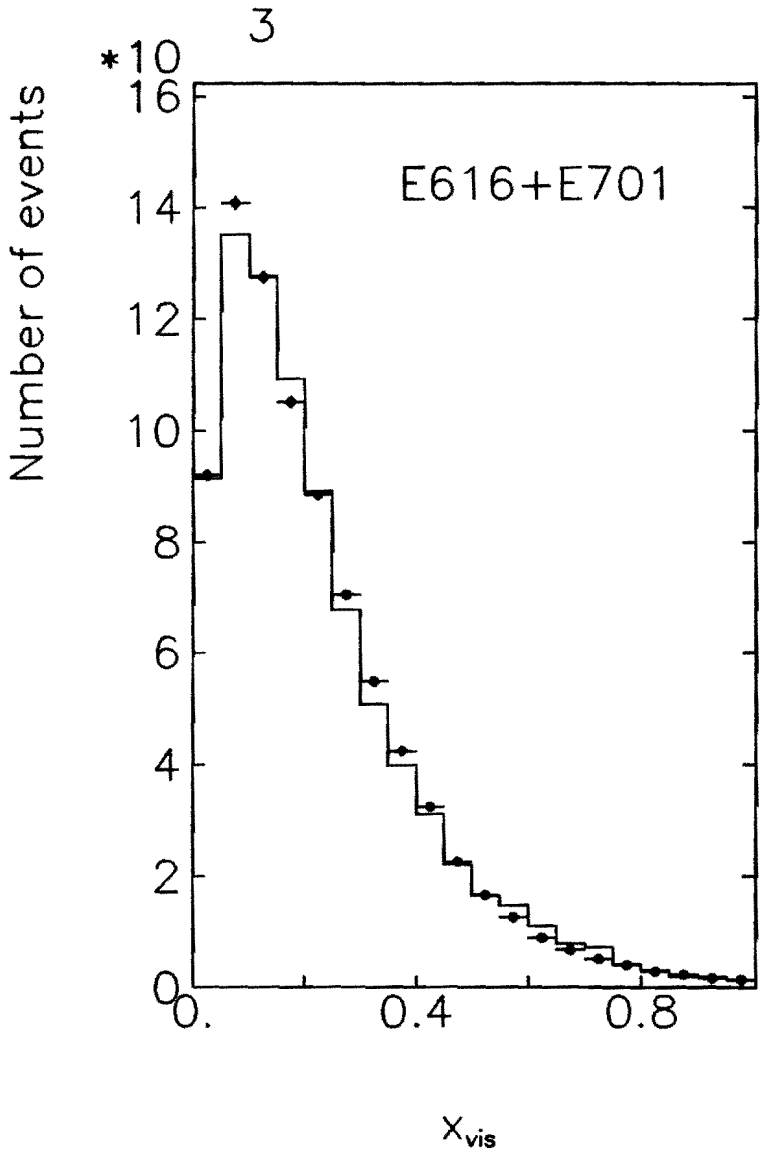

Figure 5.5 Bjorken x distribution as measured in single-muon charged current events. The points with error bars represent the data, and the histogram represents the Monte Carlo events.

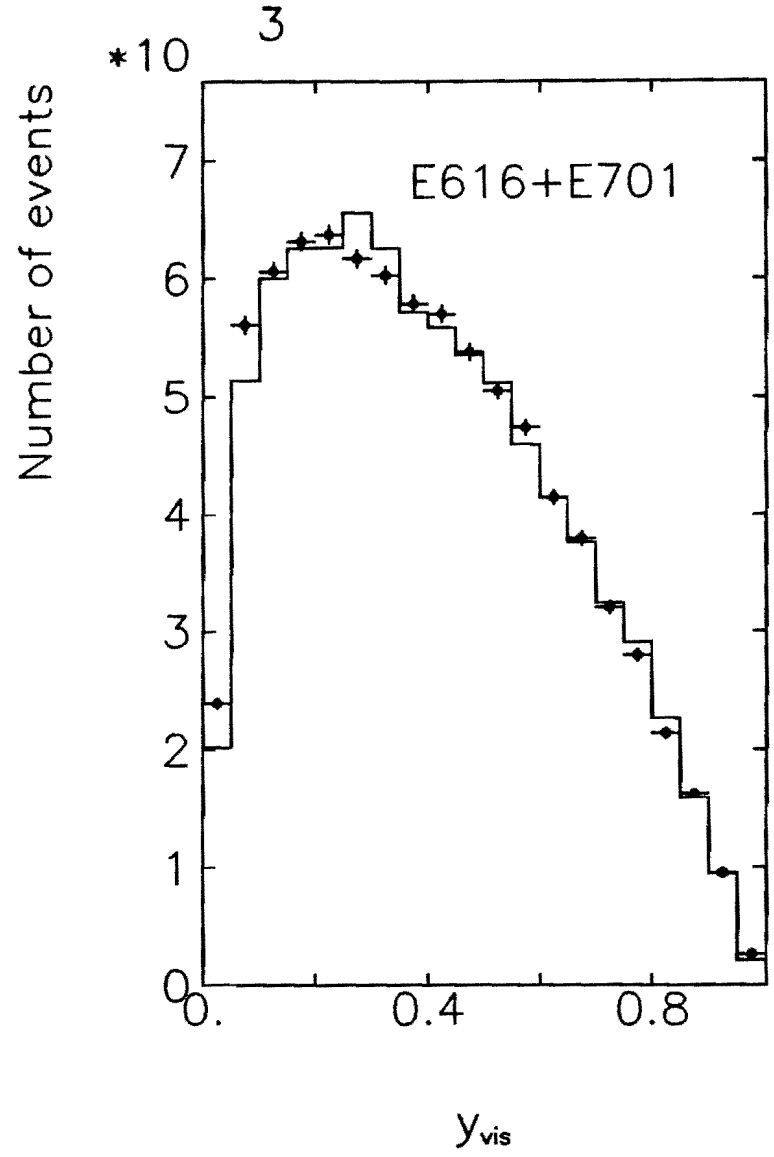

Figure 5.6 Distribution of the scaling variable y for single-muon charged current events. The points with error bars represent the data, and the histogram represents the Monte Carlo events.

5.2 Monte Carlo for Production of Opposite-Sign Dimuons

As outlined in Chapter 1, the model for neutrino production of opposite-sign dimuons is based on the production and semileptonic decay of charm particles. Production of charm particles occurs in a process shown in Fig.1.2 and the cross section is expressed by eqs.1.3.1 and 1.3.2.

Monte Carlo generated single-muon events were used as the input to the production of dimuon events. Each charged current event was assigned a weight equal to the ratio of the charm production cross section (eq.1.3.1.) to the charged current cross section (eq.1.2.1) for its particular x, y, and E_ν. This ratio was expressed in the form which used quark distributions parametrized separately for valence up quarks (u_v) , valence down quarks (d_v), and quarks in the nucleon sea. Equations 1.2.4a-d which express the quark distributions as "seen" by neutrinos or antineutrinos can be rewritten in the following form:

a) for the single-muon neutrino cross section

$$q^\nu = d_v + u_v + Sea(1+\kappa)/(2+\kappa) \qquad (5.2.1)$$

$$\bar{q}^\nu = Sea/(2+\kappa) \qquad (5.2.2)$$

and for antineutrinos

$$q^\nu = d_v + u_v + Sea/(2+\kappa) \qquad (5.2.3)$$

$$\bar{q}^\nu = Sea(1+\kappa)/(2+\kappa) \qquad (5.2.4)$$

b) for the charm production neutrino cross-section

$$q^\nu = \{[d_v' + u_v' + Sea'/(2+\kappa)]\sin^2\theta_c + [Sea'\kappa/(2+\kappa)]\cos^2\theta_c\}\{1-y + xy/x'\} \qquad (5.2.5)$$

$$\bar{q}^\nu = 0 \qquad (5.2.6)$$

and for antineutrinos

$$q^\nu = 0 \qquad (5.2.7)$$

$$\bar{q}^\nu = [Sea'/(2+\kappa)][\sin^2\theta_c + \kappa\cos^2\theta_c]\{1-y+xy/x'\} \qquad (5.2.8)$$

Quantities u_v, d_v, and Sea are functions of x and Q^2. Primed quantities are expressed as functions of Q^2 and the slow rescaling variable x' (1.1.11), where $x' = x + m_c^2/2M\nu$ (m_c is a mass of a charm quark).

For the Monte Carlo calculations a value of 1.5 GeV/c^2 for the charm quark mass was assumed. The effect of this parameter on the final results was studied and is discussed in Chapter 7.

A parameter κ $[\kappa=2s(x)/(\bar{u}(x)+\bar{d}(x))]$ expresses the fraction of the strange sea in the nucleon in terms of a ratio of strange sea to non-strange sea. The $\kappa=1$ corresponds to the so called "fully SU_3 symmetric sea" (i.e. strange quarks carry the same momentum fraction of the nucleon as u and d sea quarks), $\kappa=0.5$ corresponds to the so called "half-SU_3 symmetric sea" (i.e. strange quarks carry half the momentum fraction of the nucleon as u and d sea quarks), $\kappa=0$ means no strange sea in the nucleon. The κ parameter was a free parameter in the model. The shape and normalization of the x distributions of the dimuon data (with the hadron shower background subtracted) were used to obtain the value of κ which gives the best agreement between the model and the data. The results are discussed in Chapter 7.

5.2.1 Fragmentation Function of Charm Quarks

The diagram in Fig.1.2 illustrates the production and decay of a charm quark. However, free quark states have not been observed. The produced quarks initially progress through a stage of dressing to form color-singlet hadrons. This process is described by fragmentation functions.

Whereas light quark fragmentation into mesons is characterized by a behavior $(1-z)^2/z$, a different shape is expected for the fragmentation of heavy quarks (e.g. charm, bottom), (see Chapter 4 for the definition of z and examples of z distributions of pions and kaons as measured by the BEBC collaboration). From kinematical considerations, the fragmentation function is expected to peak at large z, as first pointed out by Bjorken and Suzuki [5.2]. The attachment of a light quark to a heavy charm quark only slightly decelerates the heavy quark in the fragmentation process. This has been observed experimentally in e^+e^- collisions [5.3-5.5], and neutrino reactions [1.9, 5.6].

For charm hadron production the fragmentation variable z_D was used as defined by eq.1.3.4.

$$z_D = p_D^*/p_{max}^* \qquad (5.2.9)$$

where p_{max}^* is the maximum possible momentum p_D^* of the charm particle with mass M_D in the W-boson - nucleon center of mass system:

$$p_{max}^{*2} = W^2/4 - M_D^2 \ . \qquad (5.2.10)$$

The variable z_D corresponds to the fragmentation variable x_p defined in the e^+e^- reactions (at electron storage rings)

$$x_p = p_D/\sqrt{(E_{beam}^2 - M_D^2)} \qquad (5.2.11)$$

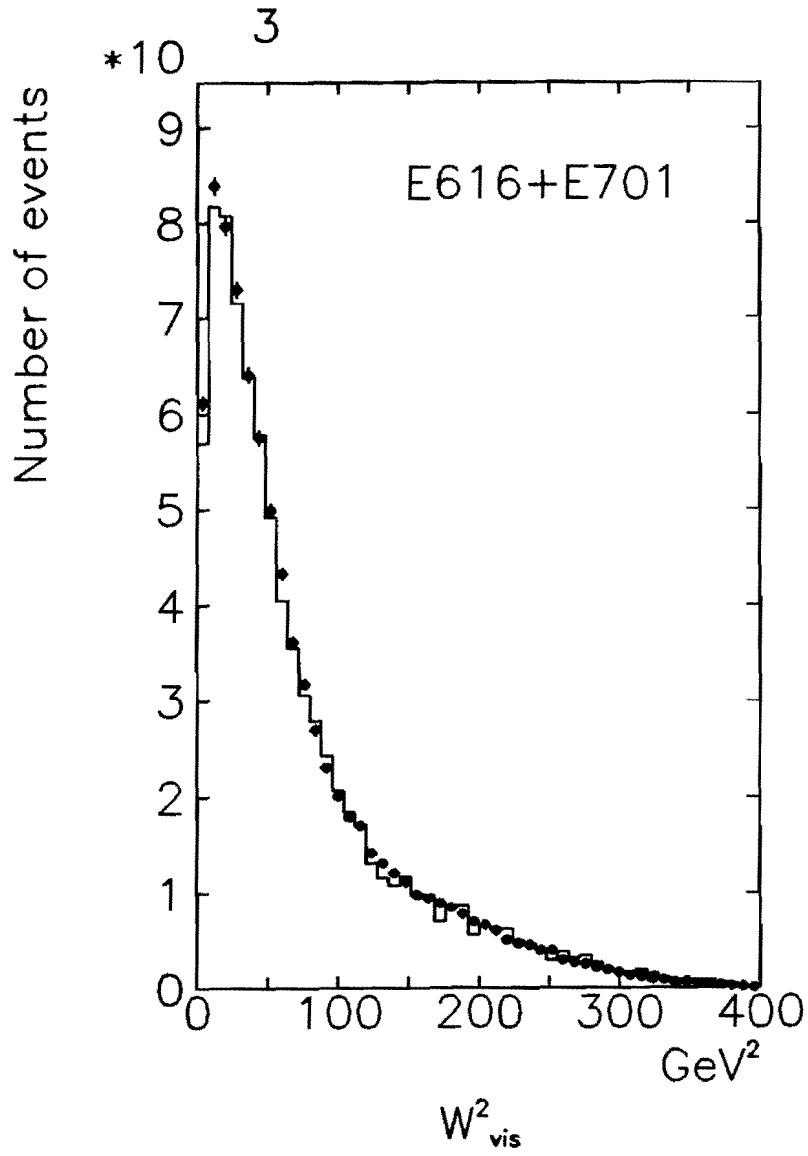

Figure 5.7 The measured distribution of the square of the invariant mass of the final hadron system, W^2, in single-muon charged current events. The points with error bars represent the data, and the histogram represents the Monte Carlo events.

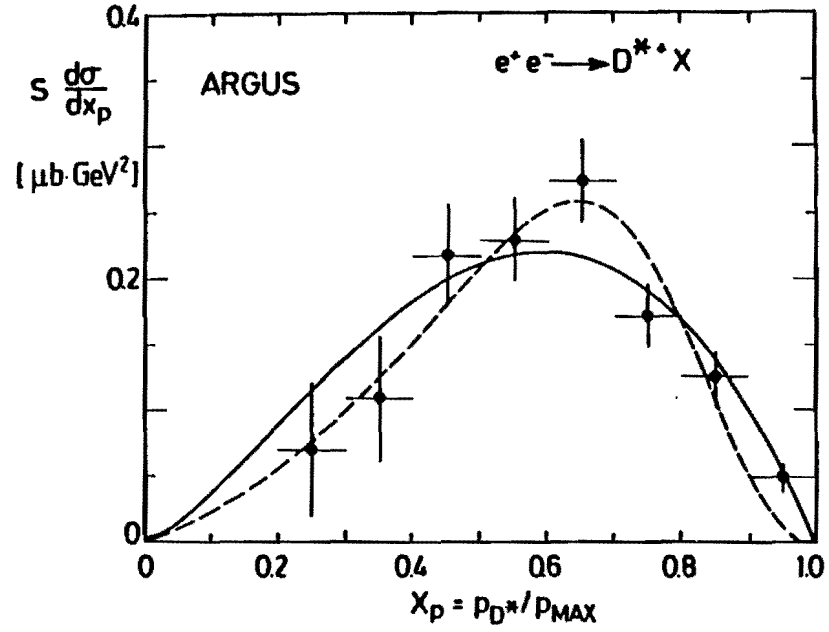

Figure 5.8 Fragmentation of D^{*+} mesons as measured by the ARGUS collaboration. The dotted curve is the fit to the Peterson et al. fragmentation function [5.7] with ϵ=0.19±0.3; the solid curve is the fit to the Kartvelishvili et al. fragmentation function [5.8] with α=1.5±0.2.

The mean $\sqrt{W^2}$ of single-muon events in experiments E616 and E701 is ~9 GeV (see Fig.5.7). Therefore fragmentation functions from a similar energy region were used. The fragmentation of charm quarks to D^* meson has been investigated in the ARGUS detector at the DORIS e^+e^- storage ring at DESY with E_{beam} = 5 GeV [5.6]. The ARGUS data have been compared to two fragmentation models. One is the model of Peterson et al. [5.7] where:

$$s\frac{d\sigma}{dx_p} \sim \frac{1}{x_p\left(1 - 1/x_p - \varepsilon/(1-x_p)\right)^2} \qquad (5.2.12)$$

and the second in the form of Kartvelishvili et al. [5.8] where:

$$s\frac{d\sigma}{dx_p} \sim x_p^{\alpha}(1 - x_p) \qquad (5.2.13)$$

The value of the ε parameter was found to be

$$\varepsilon = 0.19 \pm 0.03, \qquad (5.2.14)$$

and the value of the α parameter

$$\alpha = 1.5 \pm 0.2. \qquad (5.2.15)$$

Fig.5.8 presents the results of the ARGUS group.

In the dimuon Monte Carlo the fragmentation function proposed by Peterson et al. was used

$$D(z_D) \sim \frac{1}{z_D\left(1 - 1/z_D - \varepsilon/(1-z_D)\right)^2} \qquad (5.2.16)$$

with the value of ε = 0.19 as measured by the ARGUS group.

Several other experiments have reported similar charm fragmentation spectra [5.3, 5.9, 5.10] with mean value of z_D of ~0.6. The extracted parameters ε and α, though, have considerable uncertainties. The effect of changing the parameter ε in the dimuon Monte Carlo is not large, and is discussed in Chapter 7.

5.2.2 The Semileptonic Branching Ratio B_l(charm->μX)

Charm hadrons are short lived particles (~10^{-13} sec.) and therefore difficult to detect directly. Charm hadrons decay to strange and non-strange hadrons which have much longer lifetimes (~10^{-8} sec.). These decay products can be more easily identified in tracking detectors. However, such hadronic decay modes are not observable in neutrino counter experiments. In counter experiments charm particle decays are detected through their semileptonic decays resulting in dimuon events.

Only production of D mesons was considered as the source of prompt muons in the dimuon charm Monte Carlo. As reported by the Fermilab experiment E531 [5.11, 5.12] (which studied neutrino interactions using a hybrid emulsion spectrometer), D meson production is the dominant contributor at high neutrino energy. In particular, D meson production dominates in the forward x_F fragmentation region, and therefore contributes to energetic muons. Production of charm baryons Λ_c is important at low neutrino energies, and in the backward x_F region ($x_F \leq 0$).

The semileptonic branching fraction of the specific mixture of charm particles produced in neutrino interaction is not directly measured. However, it can be determined by combining data on branching ratios of charm particles into leptons (from e^+e^- collisions studied in colliding storage rings), with the information about composition of charm particles produced in neutrino interactions (e.g. as measured by emulsion experiment E531).

The Mark III Collaboration at SLAC has recently reported the following branching ratios [5.13]:

$$Br(D^+ \to e^+X) = 17.0 \pm 1.9 \pm 0.7\ \% \qquad (5.2.17)$$

$$Br(D^0 \to e^+X) = 7.5 \pm 1.1 \pm 0.4\ \% \qquad (5.2.18)$$

and the ratio of D^+ to D^0 lifetimes:

$$\tau^+/\tau^0 = 2.3 \begin{smallmatrix} +0.5 \\ -0.4 \end{smallmatrix} \begin{smallmatrix} +0.1 \\ -0.1 \end{smallmatrix} \qquad (5.2.19)$$

The ratio of the number of D^+ mesons to the number of D^0 mesons produced in e^+e^- collisions has been also measured to be [5.14]:

$$N_e^+/N_e^0 = 0.75 \pm 0.17$$

The lifetimes of D^0, D^+, F and Λ_c hadrons have been also measured [5.15]

$$\tau_{D^+} = 9.3 \begin{smallmatrix} +2.7 \\ -1.8 \end{smallmatrix} \times 10^{-13} \qquad (5.2.20)$$

$$\tau_{D^0} = 4.0 \begin{smallmatrix} +1.2 \\ -1.9 \end{smallmatrix} \times 10^{-13} \qquad (5.2.21)$$

$$\tau_{\Lambda_c} = 2.2 \begin{smallmatrix} +0.9 \\ -0.5 \end{smallmatrix} \times 10^{-13} \qquad (5.2.22)$$

$$\tau_F = 2.9 \begin{smallmatrix} +1.8 \\ -0.9 \end{smallmatrix} \times 10^{-13} \qquad (5.2.23)$$

Fermilab emulsion experiment (E531) has observed a total number of 25 charm particles produced in neutrino interactions with visible energy $E_\nu > 30$ GeV. In this sample, there are 12 neutral charm mesons (D^0 and $\bar{D}^0$), 10 D^+ mesons, 3 charm hyperons (2 identified Λ_c^+).

Using particle fractions from this experiment and the branching ratios (5.2.17-5.2.18) from e^+e^- reactions the average branching ratio into electrons of the neutrino produced mixture of charm particles was calculated to be

$$B_e(\text{charm} \to eX) = 10.9 \pm 1.4\ \% \qquad (5.2.24)$$

If charm baryons are excluded from this calculation, the

branching ratio results to be 11.4 ± 1.7 % (using $\sigma(D^{\pm})/\sigma(D^{o}(\bar{D}^{o})) = 0.7 \pm 0.4$ [5.11]). In the dimuon Monte Carlo it was assumed that the charm branching ratio into muons is equal to the charm branching ratio into electrons.

A direct measurement of the average branching ratio of charm particles into muons can also be extracted from neutrino dimuon interactions at large Bjorken x. The procedure and results are discussed in Chapter 7.

5.2.3 Outline of the Charm Monte Carlo Calculations

The input to the Monte Carlo model for dimuon production used generated single-muon charged current events. The deep inelastic scattering formalism (as described in Chapter 1) for charm quark production was applied. The transformation of charm quarks to charm hadrons is by far the least understood stage in the standard model. This transformation was parametrized using the Peterson et al. fragmentation function discussed in section 5.2.1. The D mesons were produced with a distribution of transverse momenta p_T with respect to the direction of the hadron shower of the form

$$dN_D/dp_T \sim \exp(-ap_T^2).$$

The value a=1.1 yields the best fit of the p_T^2 distribution of the second muon as measured in this experiment. Fermilab

experiment E531 obtained the best fit of $\exp(-3.1p_T^2)$, with limited statistics [5.11], and the CDHS collaboration used the form $\exp(-6(p_T^2+M_D^2)^{1/2})$ [1.9].

Experiments which study charm production with hadron (π^-) beams report several parametrizations of the p_T distributions. Fermilab experiment E595 finds that forms $\exp([-2.0\pm0.3]p_T)$, or $\exp([3.5\pm0.5][p_T^2+M_D^2]^{1/2})$, and $\exp([-0.70\pm0.15]p_T^2)$ yield a good description of the data. The LEBC EHS collaboration at CERN finds the best fit of $\exp(-1.1p_T^2)$ [5.16]. However, in hadron interactions charm particles originate from different processes than neutrino induced reactions. In hadronic collisions charm particles are produced in pairs and p_T is defined with respect to the incident hadron direction.

The semileptonic charm decay, $D \to \mu\nu X$, was modeled using the squared matrix element for $D \to K^*\mu\nu$ [5.17]:

$$|M|^2 \sim (2p_D p_\mu)(2p_D p_\nu) - (M_D^2 - 2M_x^2)(2p_\nu p_\mu) \quad (5.2.25)$$

The mass M_x was a free parameter chosen to be 0.65 GeV [1.17] to provide a reasonable fit to the inclusive D-decay electron yield measured at the $\psi''(3770)$ by the DELCO group at SLAC [5.18].

The semileptonic branching ratio of charm to muons was assumed to be 10.9 ± 1.4 %.

Using standard Monte Carlo technique, muons from charm particle decays were propagated with energy loss and multiple Coulomb scattering through the Lab E target calorimeter and the forward muon spectrometer. The kinematics of the generated events were smeared with the experimental resolutions and written on data summary tapes. The Monte Carlo events were normalized using the ratio of single-muon Monte Carlo events passing all the analysis cuts to the corresponding number of single-muon data events passing the same set of cuts. The number of generated dimuon events was about 20% of the number of single-muon data events. This was a factor of ~20 larger than the number of dimuon data events. Therefore, the error bars shown for the Monte Carlo distributions are larger than those for the data for single- muon distributions, and smaller for dimuon distributions.

The processed Monte Carlo events were compared with the data sample. This comparison between the model and the data was investigated as function of various values of Monte Carlo input parameters (such as κ, ε, m_c, B_1). Results are discussed in Chapter 7.

5.3 Outline of the Background Monte Carlo

The model for the background used the generated values of the hadron shower energy, E_H, and Bjorken x of single-muon charged current Monte Carlo events. Dimuon events with a particular weight and momentum of the second muon, $p_{\mu 2}$ were generated. The weight was taken as the total probability for producing a muon from neutrino shower as expressed by eqs.4.6.5, and 4.6.8 and calculated by the method described in Chapter 4 (see Figs.4.7-4.9). The momentum of the muon was generated with the formula

$$p_\mu = p_{cut} - \log(Rnd)/g \qquad (5.3.1)$$

where Rnd is a random number $0 \leq Rnd \leq 1$, and g is the coefficient of the exponent value from eq.4.6.8. It can be also shown that the momentum of a parent hadron which produces a muon is generated according to:

$$p_h = -\log[(1-Rnd)e^{-p_\mu g} + Rnd e^{-p_\mu m_h^2/m_\mu^2}]/g. \qquad (5.3.2)$$

The fraction of pion and kaon contributions was taken from calculations described in Chapter 4.

Missing energy of the background events was obtained by histogramming neutrino energy from primary hadrons decays at the stage of the calculations of the muon rates from hadron showers. Secondary showers (re-interactions of primary

hadrons) were assumed to result in the same missing energy distributions. Then, in the Monte Carlo the missing energy was generated according to thus obtained histograms.

The produced muon was given a p_T based on transverse momentum fits to final state hadrons from EMC μ-p data [5.19]. These data are in good agreement with other measurements using neutrino beams [5.20]. The gaussian smearing was generated with width:

$$p_\sigma = (0.7z + 0.1225f)^{1/2} \qquad (5.3.3)$$

where z is a standard fragmentation variable

$$z = p_h/(E_H{}^2 - W^2)^{1/2} \qquad (5.3.4)$$

and

$$f = 1.00 + 0.0055W^2 \quad (W^2 < 100\ \mathrm{GeV}^2/c^2) \qquad (5.3.5a)$$

$$f = 1.44 + 0.0011W^2 \quad (W^2 \geq 100\ \mathrm{GeV}^2/c^2) \qquad (5.3.5b)$$

The background events were processed in the same way as the charm Monte Carlo events (as described in the previous section). The systematic uncertainty on the absolute normalization of the background was 20% due to sources described in section 4.7 in Chapter 4.

In the analysis, the distributions of normalized background events were subtracted from corresponding data distributions. Charm Monte Carlo event distributions were then compared to the corrected data. The fit to the strange fraction of the sea was based on the x distributions. Details and results are discussed in Chapter 7.

Chapter 6

Results on Like-Sign Dimuons

The cross-section for production of like-sign dimuon events is small (~10% of opposite sign dimuon production, or ~0.5% of the charged current cross-section). Therefore, large data samples are difficult to obtain. In addition, the hadron shower background is large and comparable to the observed data [1.13f, 1.10].

The like-sign dimuon sample collected in experiments E616 and E701 contains 18 events. Both muons traverse at least one toroidal magnet and have momenta greater than 9 GeV/c. Both muons were required to pass all the single-muon cuts and have angles less than 250mrad with respect to the beam

axis (as described in Chapter 3). However, only one of the muons must satisfy the extrapolation condition to the muon trigger counter. In addition, muons must have fitted tracks which originate in a common vertex consistent with the counter pulse heights, and each track must be visible in the spark chambers after the first toroid. The last condition allows the determination of the sign of the muon. Appendix H contains computer drawn pictures and detailed information of all 18 events. Tables 6.1 and 6.2 show the number of events and mean values of important kinematic quantities for single-muon and dimuon events passing all cuts (events from CLASS 3 as discussed in Chapter 3).

Table 6.1 Number, mean measured total energy and mean hadronic energy of single-muon and dimuon events passing all cuts of the like-sign dimuon analysis. The events are binned by the neutrino energy calculated from the event radius. The errors in the means are shown only if they are greater than 0.5 GeV. The hadron energy cut is E_H=2GeV.

Energy Bin (GeV)	μ^- Events	μ^- E_ν (GeV)	μ^- E_H (GeV)	$\mu^-\mu^-$ Events	$\mu^-\mu^-$ E_ν (GeV)	$\mu^-\mu^-$ E_H (GeV)
30-100	66090	64.	25.	2	82±18	51±22
100-200	37927	159.	65.	11	147±12	68±11
200-230	13022	215.	92.	5	189±5	112±17
30-230	117039	112.	45.	18	151±10	78±10

Table 6.2 Kinematic quantities for single-muon and dimuon events used in the like-sign dimuon analysis.

Quantity	μ^-	$\mu^-\mu^-$
$p_{\mu 1}$(GeV/c)	66.6 ± 0.2	56.3 ± 8.7
Q^2(GeV^2/c^2)	16.4 ± 0.1	39.0 ± 7.6
W^2(GeV^2/c^2)	68.9 ± 0.2	133.2 ± 14.6
x_{Bj}	0.215 ± 0.001	0.21 ± 0.03
y	0.394 ± 0.001	0.51 ± 0.04
$\theta_{\mu 1}$(rad)	0.052 ± 0.001	0.087 ± 0.014

The principal background sources of like-sign dimuons are decays to muons of primary pions or kaons from the hadron shower in charged current events, and the production of prompt or non-prompt muons from the secondary interactions of the primary hadrons. Details regarding the calculation of this background has been described in Chapter 4. The Monte Carlo calculation has been outlined in Chapter 5.

The hadron shower background for the 18 like-sign dimuon events was calculated (with 20% systematic normalization uncertainties discussed in Chapter 4) to be 10.7 ± 2.1 events.

An additional background was due to misclassified trimuon events (originating primarily from hadronic and electromagnetic muon pair production [6.1,6.12]) for which

the third muon is hidden in the shower (and has momentum below the threshold for unambiguous identification). The number of possible misidentified trimuon events was estimated using the 9 trimuon events for which the sum of the energies of the two non-leading muons was greater than 9 GeV. It was assumed that the distribution of energy between the two non-leading muons was uniform. Trimuon events for which the energy of the third muon is less than 2 GeV would be misclassified dimuon events. This resulted in 0.6 ± 0.2 background events. It should be also pointed out for later considerations, that the missing energy for the 9 trimuon events is 1.0 ± 2.0 GeV. The background from spatially and temporally coincident single-muon charged current neutrino events was estimated to be 0.1 ± 0.1 events. Therefore the total prompt like-sign dimuon signal is 6.6 ± 4.8 events. For completeness it should be added that if fits based on the BEBC/EMC fragmentation functions are used in the background calculation, the hadron showers give 9.4 ± 1.9 background events what results in 7.9 ± 4.7 prompt like-sign dimuon signal.

Table 6.3 shows results on like-sign dimuons from other experiments.

Table 6.3 The comparison of the like-sign dimuon data samples from several of the highest statistics experiments. (NBB stands for narrow band beam, WBB stands for wide band horn focused beam, QTB stands for quadrupole triplet beam).

Experiment (Beam)	p_μ cut (GeV/c)	Events	Backgr.	Prompt	Ref.
CCFRR (NBB)	9.	18	11.4±2.2	6.6±4.8	this exp.
CDHS (WBB)	6.5	290±17	207±33	67±37	[1.13c]
CDHS (NBB)	4.5	47	30±8	17±11	[1.13a]
CHARM (WBB)	4.	-	-	74±17 [1*]	[1.10]
(WBB)	4.	-	-	52±13 [2*]	[1.10]
HPWFOR (QTB)	5.	-	-	52±13*	[1.13d]
(QTB)	10.	-	-	65±15*	[1.13d]
(QTB)	15.	-	-	37±11*	[1.13d]
CFNRR (QTB)	9.	10	4.3	5.7±3.3	[1.13f]

[1]) $\mu^-\mu^-$ from ν beam, [2]) $\mu^+\mu^+$ from $\bar{\nu}$ beam; * only the prompt signal is quoted.

6.1 Like-Sign Dimuon Rates

The calculation of the ratio of prompt like-sign dimuon production to single-muon production requires that the numbers of single-muon and prompt like-sign dimuons events be corrected for geometrical acceptance. This acceptance must rely on a specific model. Although each experiment is not statistically very significant, it is interesting that none of the experiments can explain the observed rates of like-sign dimuon events as totally background.

Several processes have been proposed to explain the production of like-sign dimuons in neutrino interactions. Although there are large uncertainties in the theoretical calculations (some of which are very sensitive to unknown parameters such as the value of the strong coupling constant α_s, and on the mass of the charm quark) none of the proposed mechanisms accounts for the observed rates. Table 6.4 and Figs.6.1a-f summarize the present theoretical and experimental situation.

Table 6.4 Summary of presently proposed mechanisms for neutrino production of like-sign dimuons with theoretical rates ($\sigma(\mu^-\mu^-)/\sigma(\mu^-)$) and/or experimental limits.

Model	Momentum cut (GeV/c)	Rate	Illustration (Figure #)	Ref.
Gluon Brems-strahlung	9.	5×10^{-6} to 2×10^{-5}	Fig.6.1a	[6.2 -6.5, 6.8]
Gluon Fusion	9.	$\sim10^{-5}$	Fig.6.1b	[6.6]
Intrinsic Charm	9.	$<2\times10^{-7*}$	Fig.6.1c	[6.6, 6.7]
Bottom Production	4.5	$<10^{-5*}$	Fig.6.1d	[6.6, 6.9,6.1]
D^0-$\bar{D}^0$ Mixing		$<2\times10^{-5*}$	Fig.6.1e	[6.10]

* limits set by the experiment based on the model.

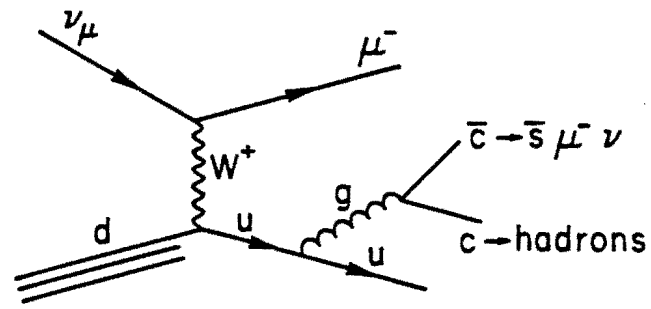

GLUON BREMSSTRAHLUNG

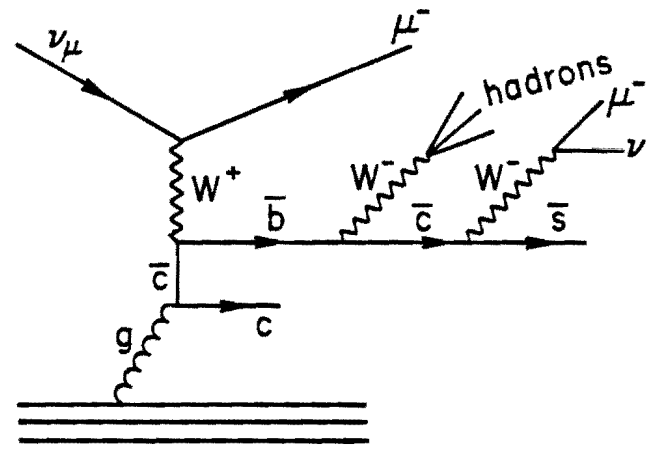

GLUON FUSION

Figure 6.1 Proposed diagrams for the production of like-sign dimuons: (a) gluon bremsstrahlung, (b) gluon fusion, (c) intrinsic charm, (d) bottom production, (e) D^0-$\bar{D}^0$ mixing, (f) diffractive associated charm production.

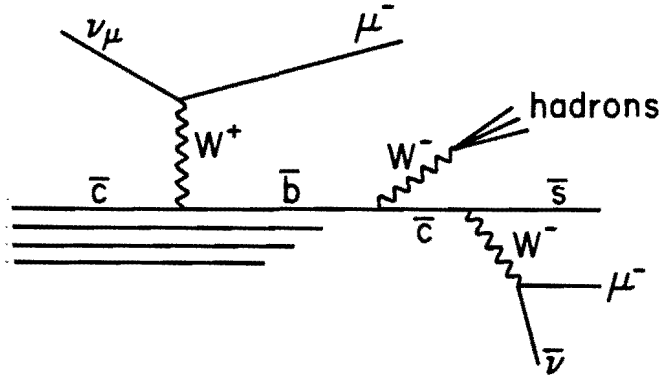

INTRINSIC CHARM

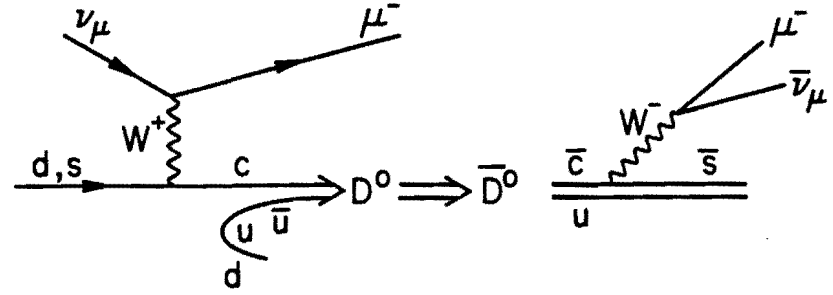

D^0- $\bar{D}^0$ MIXING

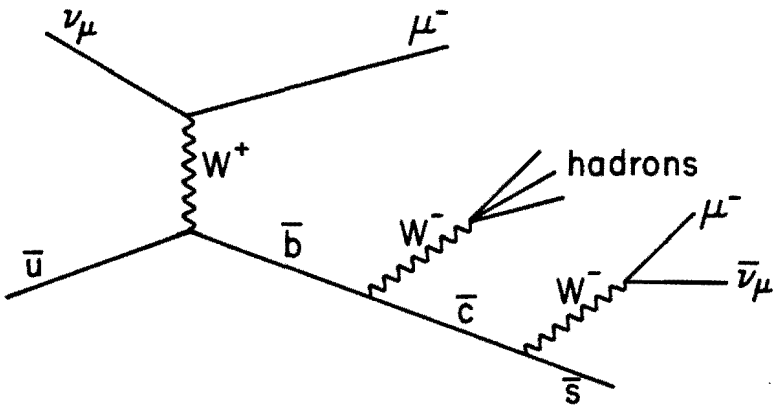

BOTTOM PRODUCTION

Figure 6.1c and d

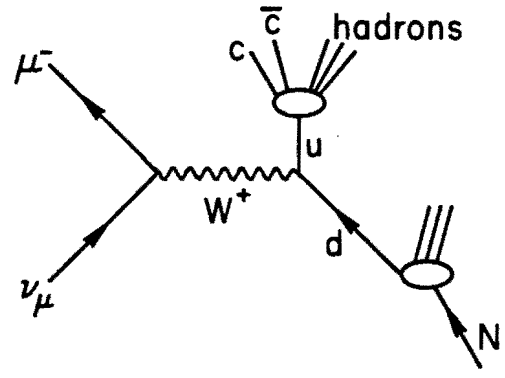

DIFFRACTIVE CHARM PRODUCTION
(PHENOMENOLOGICAL APPROACH)

Figure 6.1e and f

A mechanism not mentioned in Table 6.4 has been proposed in reference [6.11]. That model (Fig.6.1f), which assumes a very high diffractive associated charm production cross-section, is able to explain observed rates. However, there is little experimental evidence to support such an assumption.

In the absence of a model for like-sign dimuons and in order to calculate acceptance corrected rates (with respect to charged current events) it was assumed that the distribution of prompt dimuon events is the same as that of the non-prompt background. The acceptance has also been calculated using the model of associated charm production (c-$\bar{c}$ pair) [6.5] through gluon bremsstrahlung. In this model the anticharm decays into the second μ^-. Although the contribution to like-sign dimuons from D^o-$\bar{D}^o$ mixing is negligible [6.10], the acceptance using this process was also calculated.

The rates corrected for acceptance using the model of π and K decay are presented in Table 6.5a. Also shown are the rates with acceptance corrections using c-$\bar{c}$ production and D^o-$\bar{D}^o$ mixing production models. A comparison with the prompt like-sign and opposite sign rates from other experiments is shown in Table 6.6. The energy dependence of the rates of prompt like-sign dimuons to charged current

Table 6.5a Calculation of the rate of $\mu^-\mu^-/\mu^-$ for the events in Table 6.2. The μ^- events are corrected for acceptance. From left to right are shown: (1) number of charged current events (acceptance corrected), (2) number of raw $\mu\mu$ events, (3) the background from the hadron shower, (4) the background form misclassified trimuons and coincident single-muon events, (5) the raw prompt like-sign dimuon signal (after subtraction of all the background). Next three columns show the prompt $\mu\mu$ signal corrected for acceptance using: (6) a model of π/K decay and shower, (7) c-c gluon bremsstrahlung model, and (8) D^o-$\bar{D}^o$ mixing. The last column shows the $\mu\mu/\mu$ rate and its error for $p_\mu > 9$ GeV/c calculated using the π/K model. The error includes the 20% systematic error in the hadron shower background.

Energy Bin (GeV)	μ^- Events (1)	$\mu^-\mu^-$ Events (2)	Hadron Shower Bkg. (3)	Misc. Bkg. (4)	Data-Bkg. (5)
30-100	108128	2	2.0	0.2	-0.2
100-200	52930	11	5.7	0.4	4.9
200-230	16058	5	3.0	0.1	1.9
30-230	177116	18	10.7	0.7	6.6

Table 6.5a (cont'd)

Energy Bin (GeV)	Prompt (π/K) (6)	Prompt (cc) (7)	Prompt (D^o-$\bar{D}^o$) (8)	$\mu^-\mu^-/\mu^-$
30-100	-0.8	-1.0	-0.6	$(-0.1 \pm 0.5)\times10^{-4}$
100-200	12.7	13.7	9.5	$(2.4 \pm 1.7)\times10^{-4}$
200-230	3.7	3.7	2.9	$(2.3 \pm 2.8)\times10^{-4}$
30-230	17.1	15.9	13.2	$(1.0 \pm 0.7)\times10^{-4}$

Table 6.5b Calculation of the rate of $\mu^-\mu^-/\mu^-$ for the events in Table 6.2 using the prompt like-sign dimuon signal when using fits based on the BEBC/EMC fragmentation functions in the calculations of the hadron shower background. The μ^- events are corrected for acceptance. From left to right are shown: (1) number of charged current events (acceptance corrected), (2) number of raw $\mu^-\mu^-$ events, (3) the background from the hadron shower, (4) the background form misclassified trimuons and coincidence single-muon events, (5) the raw prompt like-sign dimuon signal (after subtraction of all the background). Next three columns show the prompt $\mu^-\mu^-$ signal corrected for acceptance using: (6) a model of π/K decay and shower, (7) c-$\bar{c}$ gluon bremsstrahlung model, and (8) D^o-$\bar{D}^o$ mixing. The last column shows the $\mu^-\mu^-/\mu^-$ rate and its error for $p_\mu > 9$ GeV/c calculated using the π/K model. The error includes the 20% systematic error in the hadron shower background.

Energy Bin (GeV)	μ^- Events (1)	$\mu^-\mu^-$ Events (2)	Hadron Shower Bkg. (3)	Misc. Bkg. (4)	Data-Bkg. (5)
30-100	108128	2	1.5	0.2	0.3
100-200	52930	11	4.9	0.4	5.7
200-230	16058	5	3.0	0.1	1.9
30-230	177116	18	9.4	0.7	7.9

Table 6.5b (cont'd)

Energy Bin (GeV)	Prompt (π/K) (6)	Prompt ($c\bar{c}$) (7)	Prompt (D^o-$\bar{D}^o$) (8)	$\mu^-\mu^-/\mu^-$
30-100	1.3	1.0	1.0	$(0.1 \pm 0.5)\times10^{-4}$
100-200	18.2	14.0	11.5	$(3.4 \pm 2.0)\times10^{-4}$
200-230	4.0	3.1	2.9	$(2.5 \pm 3.1)\times10^{-4}$
30-230	22.2	18.1	15.4	$(1.3 \pm 0.8)\times10^{-4}$

events is shown in Fig.6.2. The solid line in Fig.6.2 is the prompt signal calculated from the c-$\bar{c}$ gluon bremsstrahlung model [6.5], using $\alpha_s = 0.2$ and $m_c = 1.5$ GeV/c^2. The rate in this model scales with α_s^2 and predicts 0.2 events for this experiment. For completeness, Table 6.5b shows corresponding results when fits based on the BEBC/EMC fragmentation functions are used in the calculations of the hadron shower background.

Table 6.6 Comparison of prompt like-sign dimuon rates for several experiments. The beam nomenclature is: NBB for narrow band beam, WBB for wide band horn focussed beam, QTB for quadrupole triplet beam. Note that a WBB has the lower mean neutrino energy.

Experiment	Beam Type	p_μ cut (GeV/c)	$\mu^-\mu^-/\mu^-$ prompt $\times10^{-4}$	$\mu^-\mu^-/\mu^-\mu^+$ prompt $\times10^{-2}$	Ref.
CCFRR	NBB	9.	1.0±0.7	4.0±2.9	this exp.
CDHS	WBB	6.5	0.43±0.23	4.2±2.3	[1.13c]
CDHS	NBB	4.5	3±2	5±3	[1.13a]
CHARM	WBB	4.	4.5±1.6	14±5	[1.10]
HPWFOR	QTB	10.	3.0±0.8	7±4	[1.13d]
CFNRR	QTB	9.	2.0±1.1	-	[1.13f]

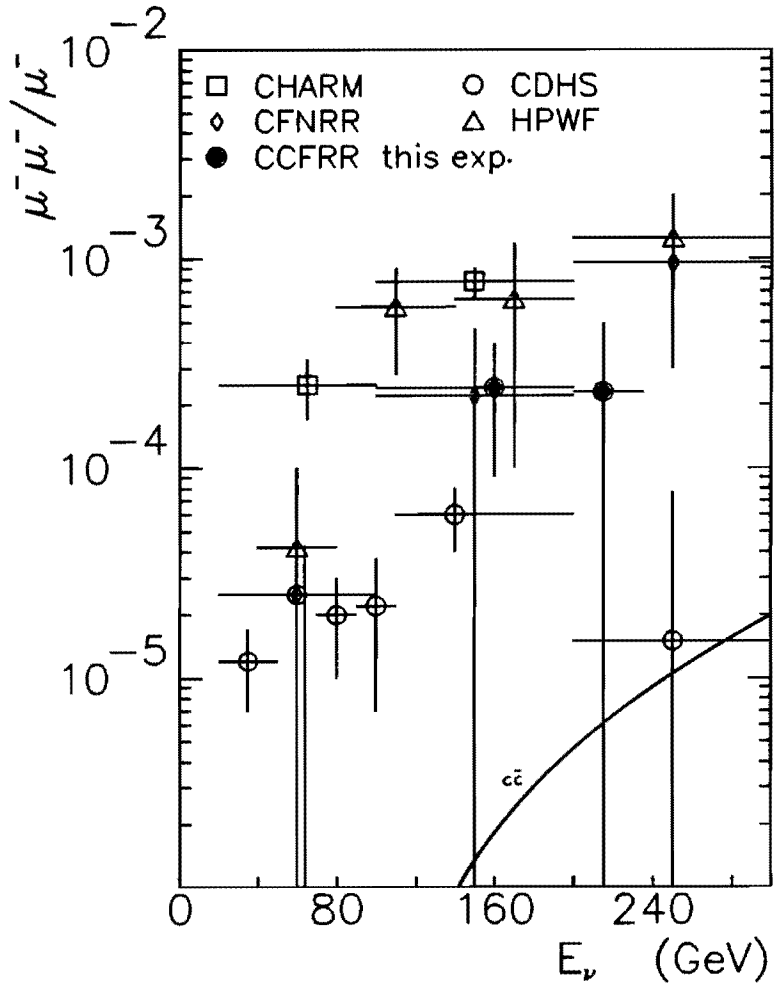

Figure 6.2 Like-sign dimuon rates. The rates for $\nu N \rightarrow \mu^- \mu^- X$ relative to the single-muon charged current cross-section are shown. References are given in Table 6.3 except for the CDHS points which are taken from ref.[6.13].

6.2 Like-Sign Dimuon Kinematics

In addition to the overall rates, the event kinematics may be used to determine whether the π/K background can be the sole explanation of the like-sign dimuon signal. Distributions of several kinematic variables for the like-sign dimuons and Monte Carlo events from π/K background are shown in Figs.6.3a-f. The π/K decay background, shown as the dashed histogram, consists of 10.7 events. The means of these distributions are shown in Table 6.7.

The distribution of the angle (ϕ_{12}) between the two muon tracks projected on a plane perpendicular to the incident neutrino direction is shown in Fig.6.3a. The peaking of this distribution near 180° indicates that the second muon is associated with the hadron shower in a large fraction of events. This is a property expected of π/K decay background.

For further comparison with the hypothesis of π/K decay, the second muon was chosen to be the muon which has the smaller momentum in the direction perpendicular to the axis of the hadron shower, p_{T2min}. The hadron shower direction is determined from the direction of the incoming ν beam and the kinematics of the chosen first muon. Fig.6.3b shows the

p_{T2min}^2 distribution. There is one event with a p_{T2min}^2 = 6.0 GeV^2/c^2, which is unlikely to be from π/K decay (this is event No. 673/3251 in Appendix H). Fig.6.3c displays the momentum of the chosen second muon.

Fig.6.3d shows the distribution of missing energy for all like-sign events originating from neutrinos from kaon decays (ν_K). The missing energy is the difference between the neutrino energy determined by the transverse vertex radius and the measured energy. Fig.6.5 shows the distribution of missing energy of single-muon data events used for like-sign dimuon analysis.

Table 6.7 Means of kinematic distributions of like-sign dimuon data, the π/K decay background, and a combination of π/K decay and $c\bar{c}$ gluon bremsstrahlung models. The $c\bar{c}$ number of events is multiplied by a factor 42 to equal the prompt like-sign dimuon signal. The errors on the means are shown in parentheses. The missing energy is calculated for identified ν_K events only, is corrected for single-muon off-set values, and its error includes an overall 1.2 GeV systematic error. The transverse second muon momentum with respect to the hadron shower is also calculated only for ν_K events. A similar comparison for opposite-sign dimuon events is shown in Table 6.8.

Quantity	Data (raw)	Hadron Sh. Bkg.	Hadron Sh.+ $c\bar{c}\times 42$
ϕ_{12}(degrees)	139(9)	133(1)	129(1)
p_{T2min}^2(GeV^2/c^2)	0.80(.35)	0.37(.02)	0.46(.03)
$p_{\mu 2}$(GeV/c)	17.1(1.3)	16.4(.3)	18.2(.2)
E_{mis}(GeV)	17.5(4.5)	7.2(1.5)	8.1(1.6)
$z_{\mu 2}$	0.21(.02)	0.21(.01)	0.19(.01)
M_{12}(GeV/c^2)	3.1(.3)	2.8(.1)	2.9(.1)

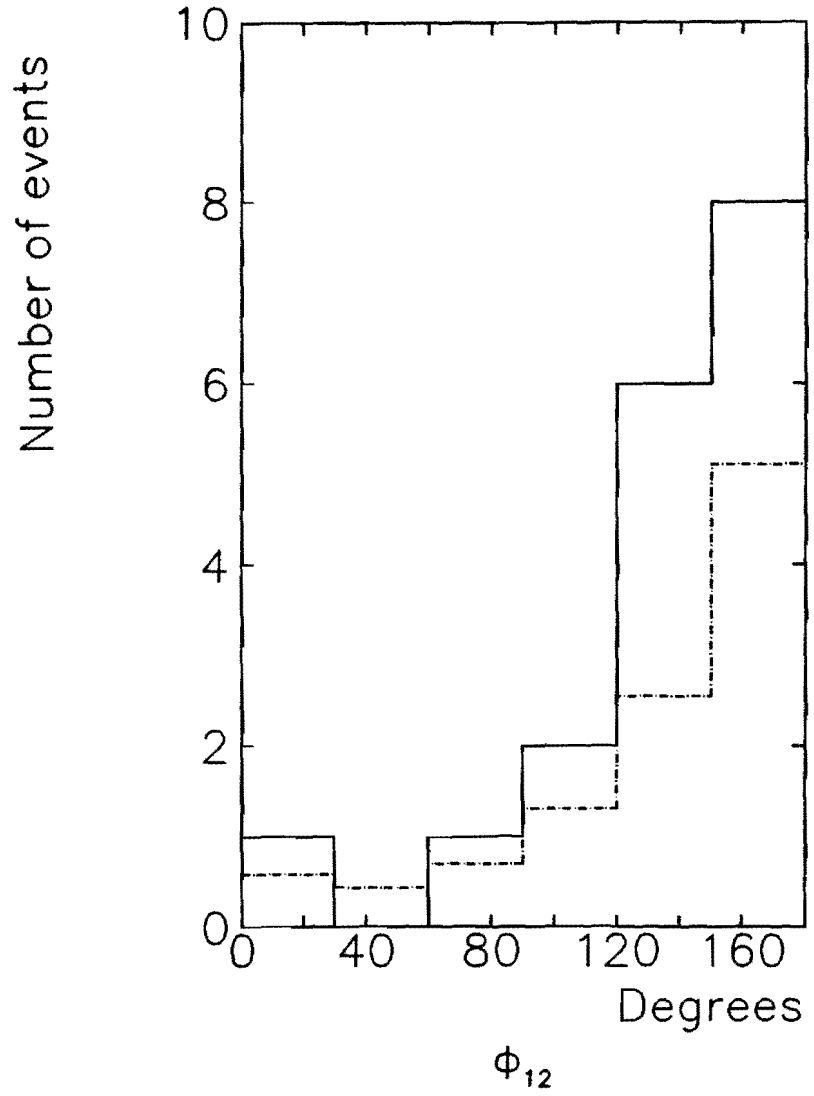

Figure 6.3 Distributions of several kinematic quantities from like-sign dimuon data (solid line), and from hadron shower background (dashed line). Fig.6.3a shows the angle between two muons in the plane perpendicular to the direction of the incident neutrino direction;

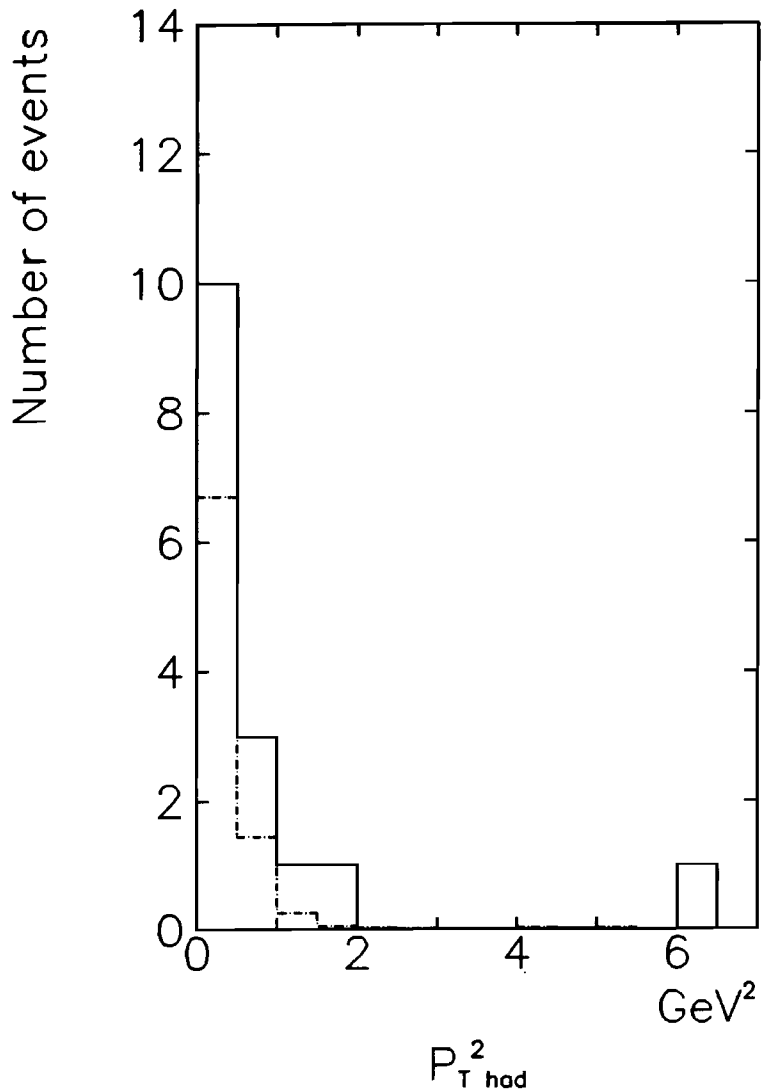

Figure 6.3b Like-sign dimuon distribution of p_T^2, the square of the transverse muon momentum with respect to the shower direction (after choosing the leading and the second muon to minimize this momentum) for ν_k events.

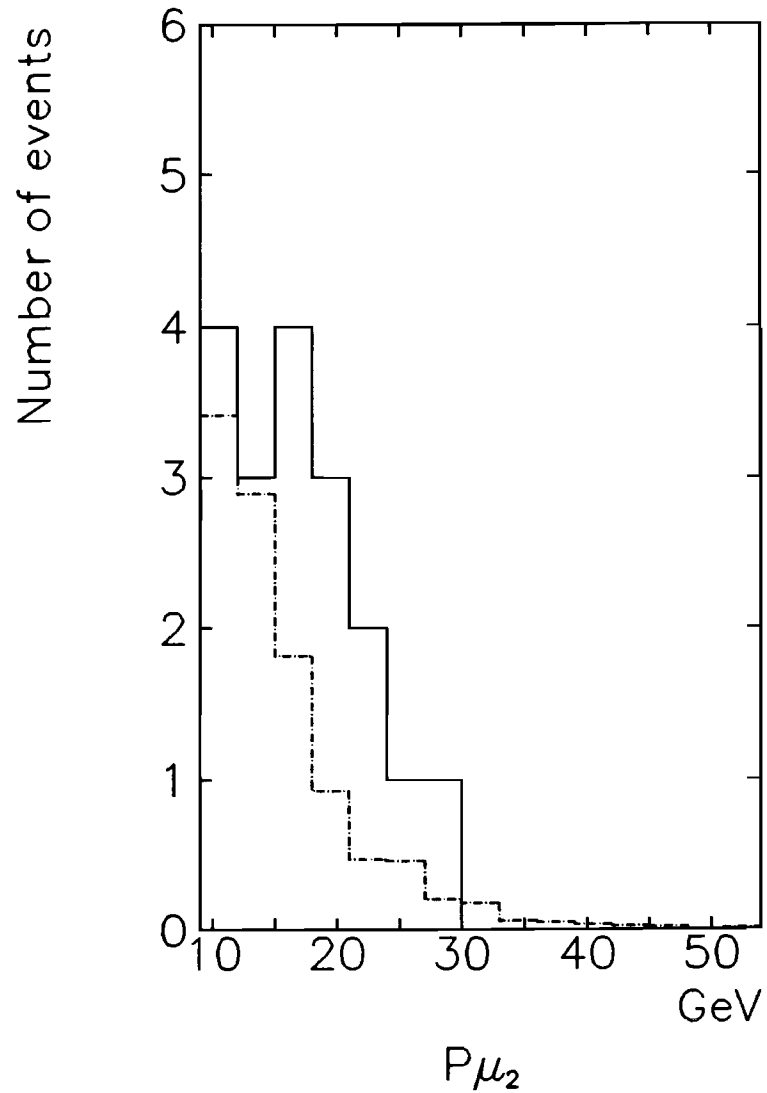

Figure 6.3c Like-sign dimuon distribution of $p_{\mu 2}$, momentum of the second muon (with the choice described in text).

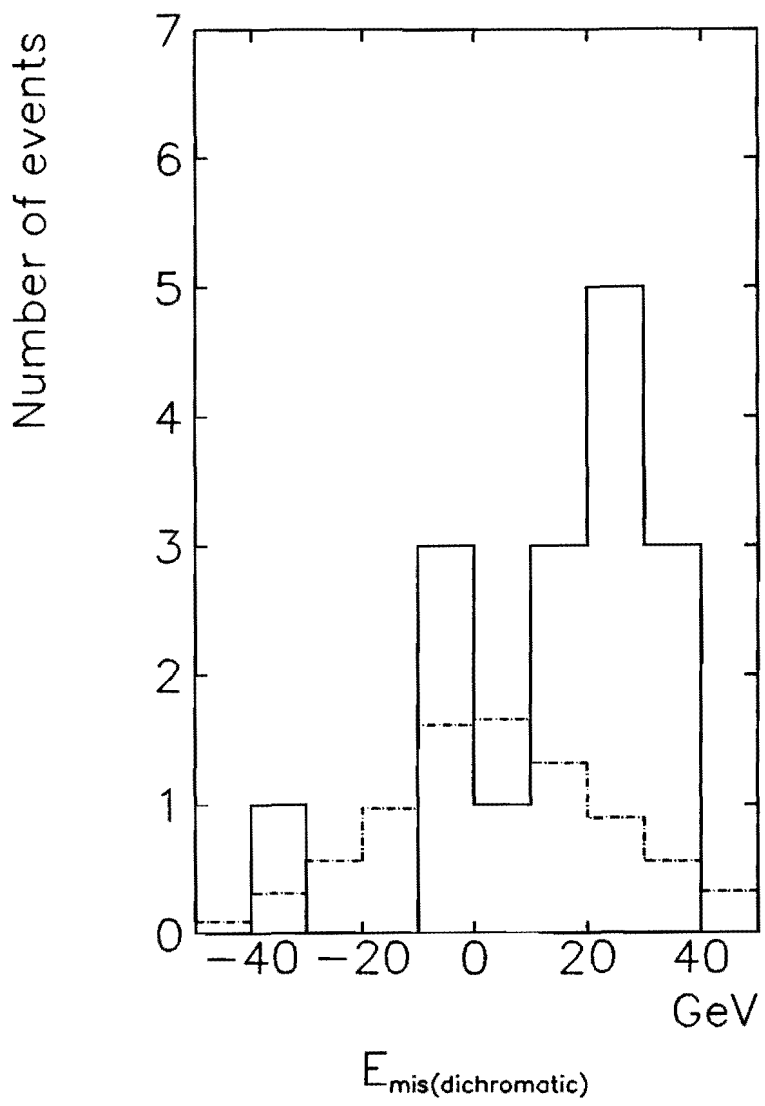

Figure 6.3d Distribution of the measured missing energy E_{mis} of like-sign dimuon ν_K events.

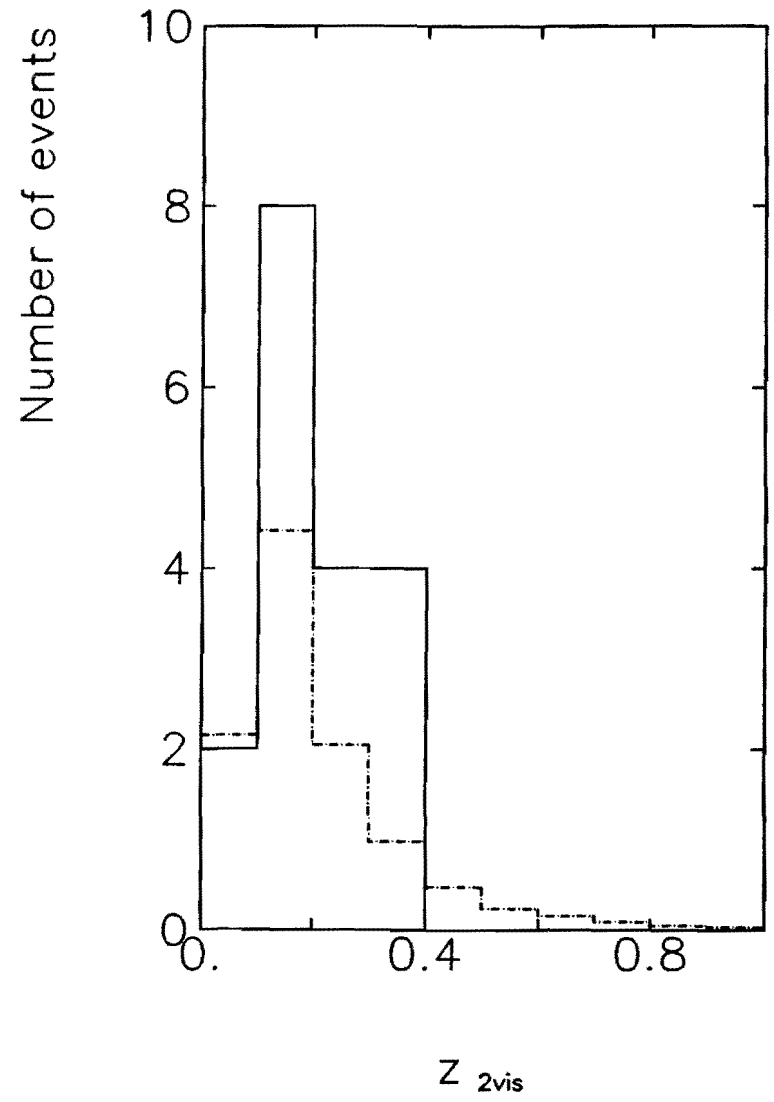

Figure 6.3e Like-sign dimuon distribution of $z_{\mu 2}$ (defined in the text).

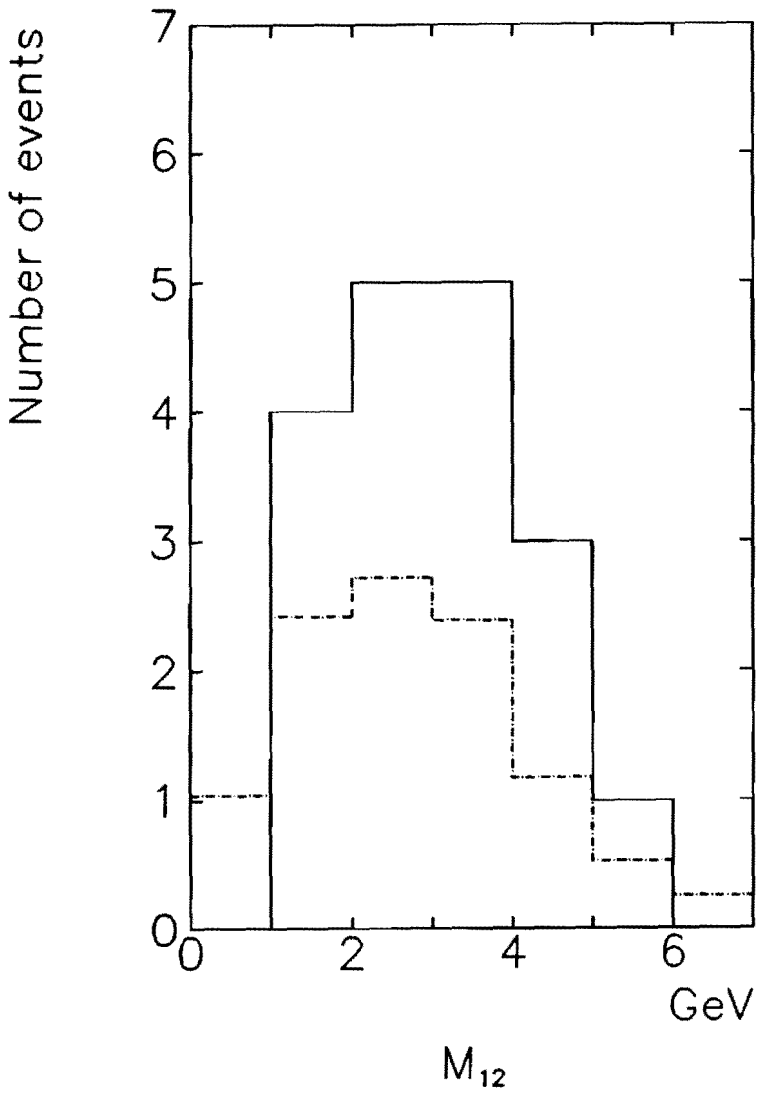

Figure 6.3f Like-sign dimuon distribution of the invariant mass M_{12} of the muon pair.

The distribution of $z_{\mu 2} = p_{\mu 2}/(E_H+p_{\mu 2})$ is shown in Fig.6.3e, and the distribution of the invariant mass of the $\mu^-\mu^-$ pair is shown in Fig.6.3f. There is no evidence for any structure in the mass distributions of the data.

It has been suggested [6.11] that an enhanced c-$\bar{c}$ production could account for the prompt like-sign dimuon signal. A comparison of the same kinematic distributions of the data in Fig.6.3 with the sum of π/K decay signal and the events from the c-$\bar{c}$ Monte Carlo normalized to equal the prompt like-sign dimuon signal of 6.6 events (which requires multiplication of c-$\bar{c}$ weights by a factor of 42) is shown in Fig. 6.4. The means of the distributions are also compared in Table 6.7. The kinematics of c-$\bar{c}$ do not differ from those of π/K decay sufficiently to attribute the prompt signal to c-$\bar{c}$ production any more than to π/K decay.

The validity of kinematic comparisons of like-sign dimuon data with the π/K decay and c-$\bar{c}$ production models can be verified by an examination of the kinematic distributions of the prompt <u>opposite sign</u> dimuon data as compared to the charm model.

Figs.6.6a-f show the same kinematic distributions for the opposite sign data as were presented in Figs.6.3 and 6.4 for the like-sign data. The data (with the π/K decay background subtracted) are shown along with the single charm

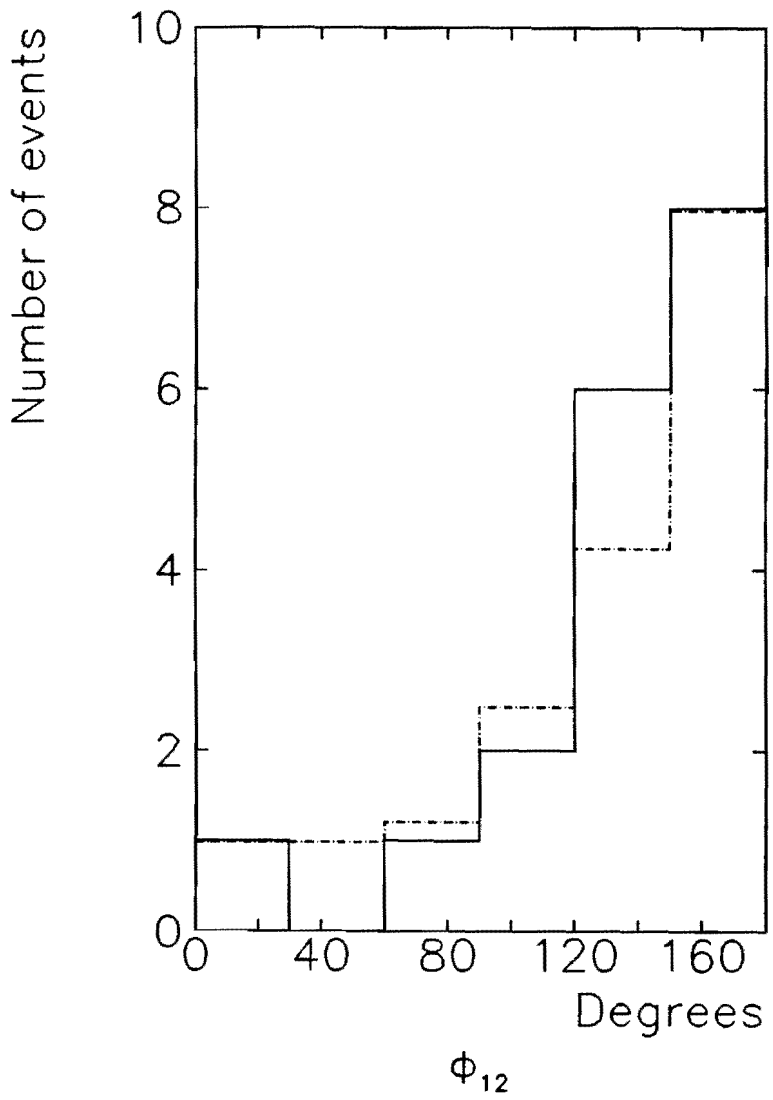

Figure 6.4 Distributions of several kinematic quantities from the like-sign dimuon data (solid_line), and from hadron shower background together with c-c gluon bremsstrahlung model (multiplied by 42) (dashed line). Fig.6.4a shows the angle between two muons in the plane perpendicular to the direction of the incident neutrino direction;

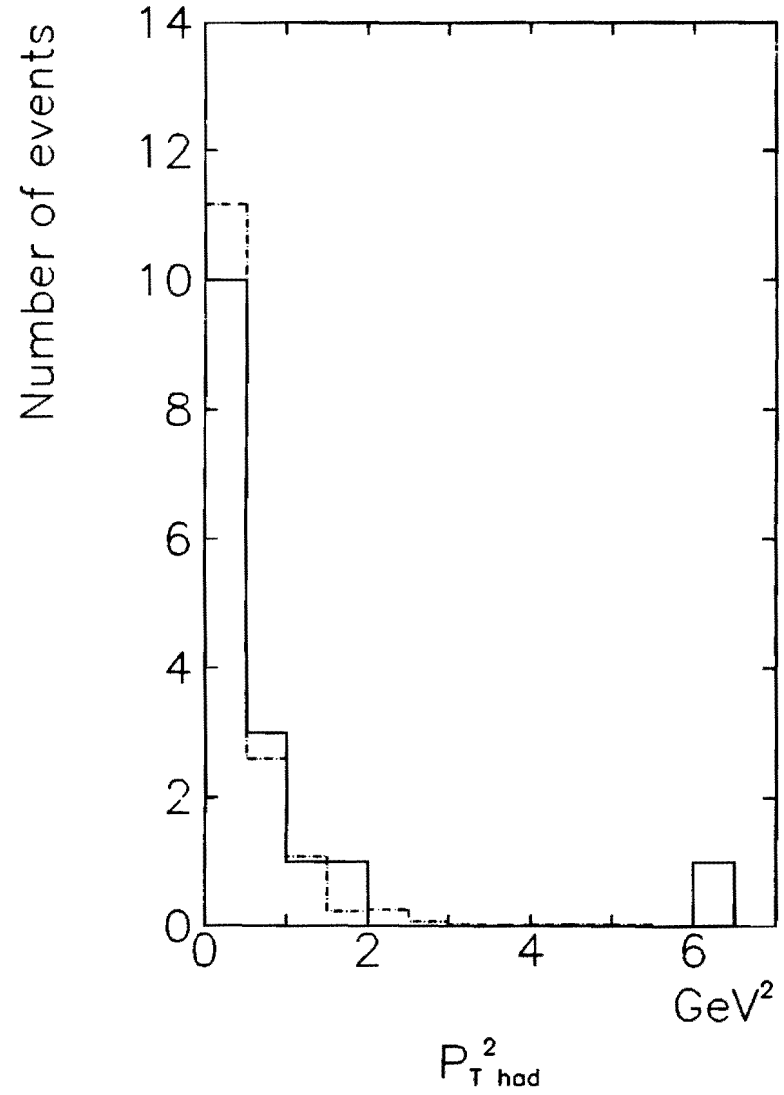

Figure 6.4b Like-sign dimuon distribution of p_T^2, square of the transverse muon momentum with respect to the shower direction (after choosing the leading and the second muon to minimize this momentum) for ν_K events.

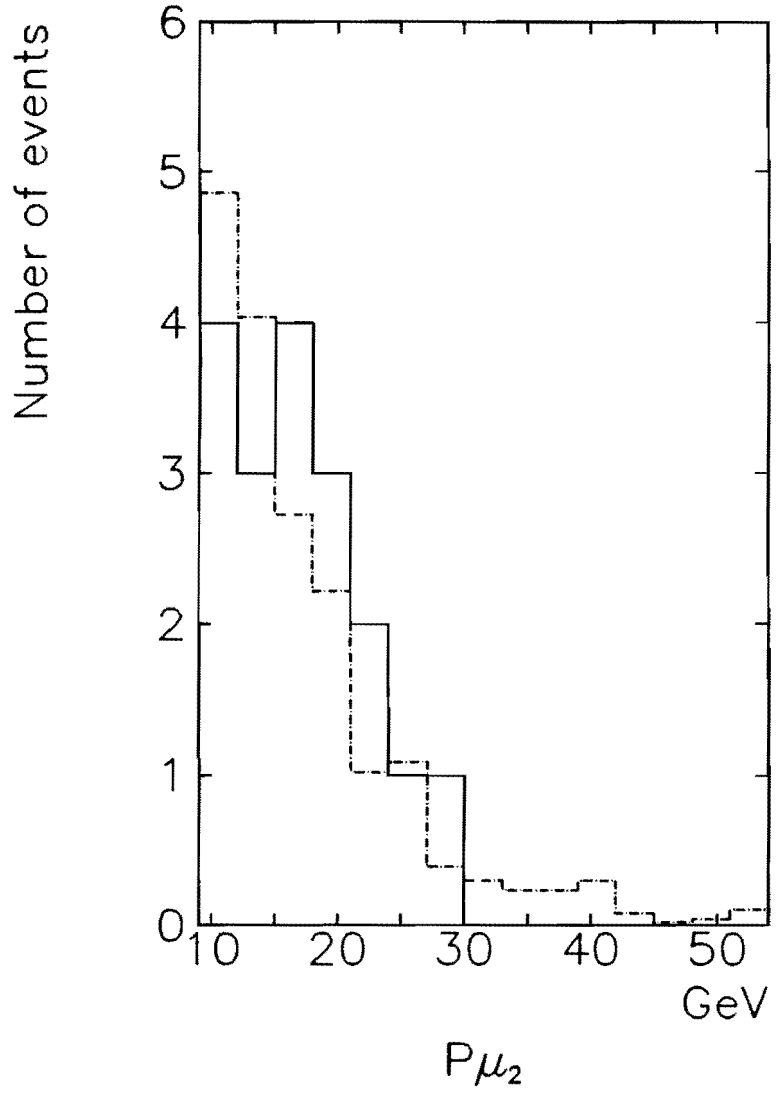

Figure 6.4c Like-sign dimuon distribution of p_{μ_2}, momentum of the second muon (with the choice described in text).

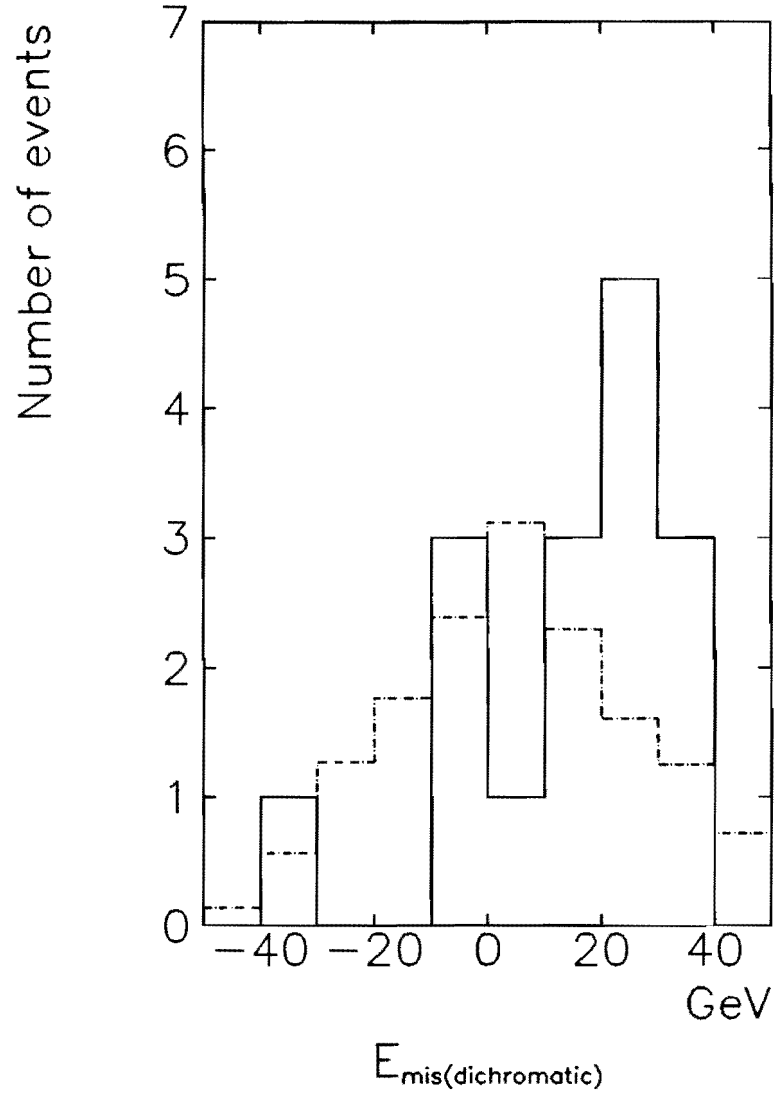

Figure 6.4d Distribution of the measured missing energy E_{mis} for like-sign ν_K events.

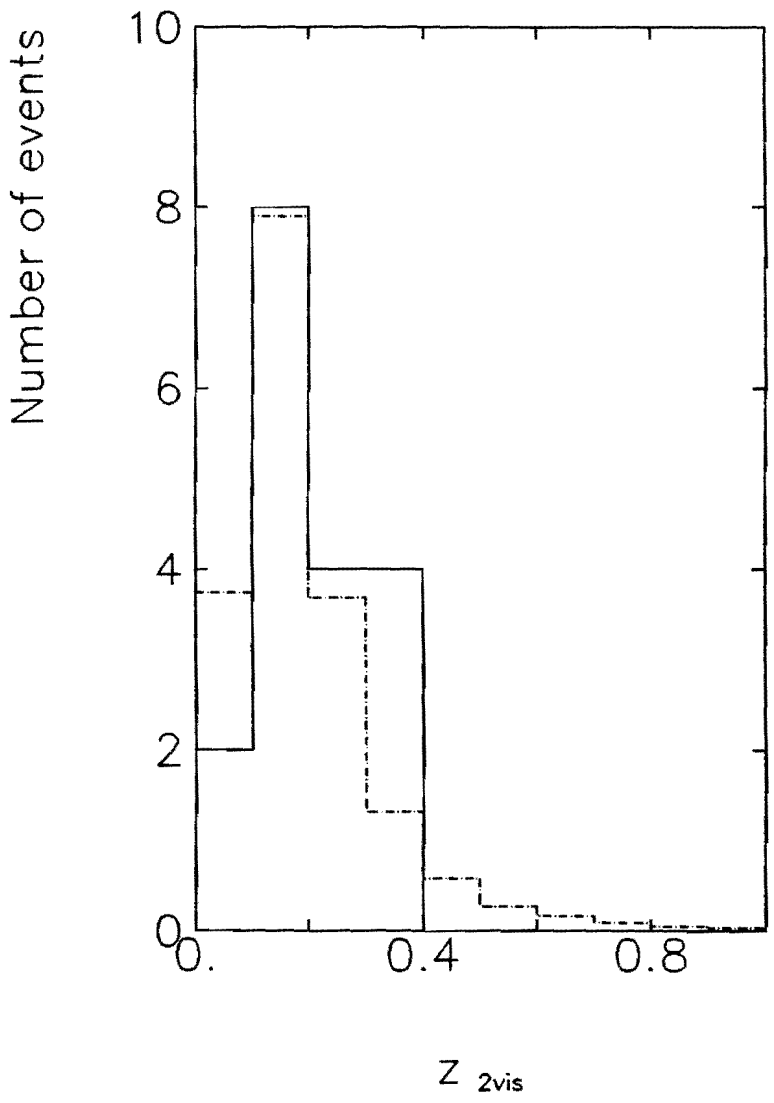

Figure 6.4e Like-sign dimuon distribution of $z_{\mu 2}$ (defined in the text).

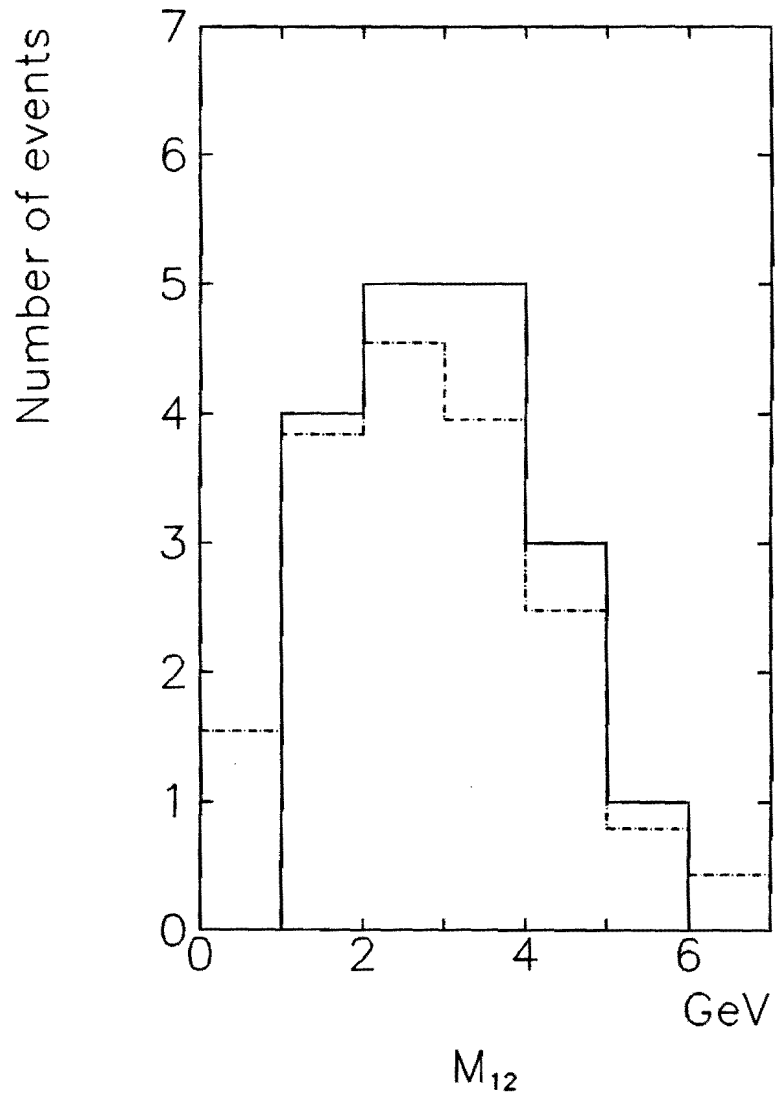

Figure 6.4f Like-sign dimuon distribution of the invariant mass M_{12} of the muon pair.

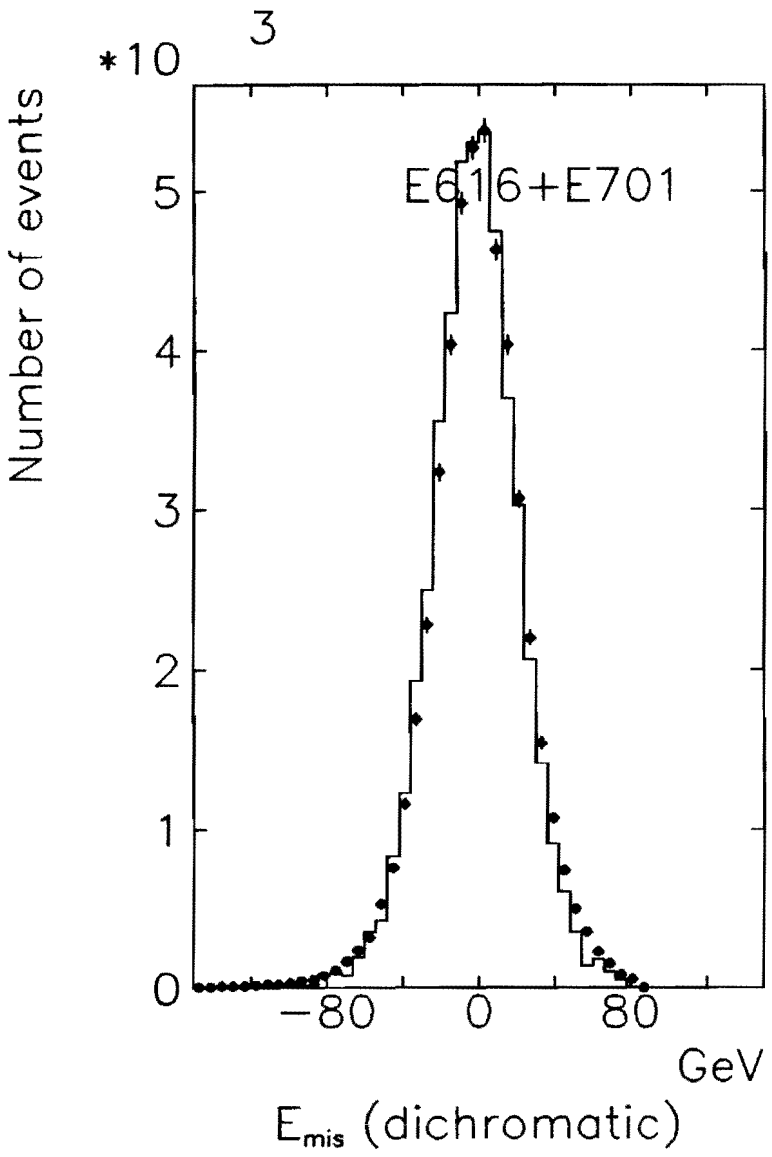

Figure 6.5 Distribution of missing energy for single-muon charged current events used in like-sign dimuon analysis. Points with error bars represent data, the histogram represents Monte Carlo events.

Monte Carlo distributions. The means of these distributions are given in Table 6.8. To provide a direct comparison with the like-sign dimuon data, the opposite sign events are also required to have both muons momentum analyzed (passing through the first toroid) with momentum $p_\mu > 9$ GeV/c, and pass all of the like-sign dimuon analysis cuts. The number of opposite sign dimuon events passing these cuts is 199. The hadron shower π/K background is 12.1 ± 2.4 events, yielding a prompt signal of 187 ± 14 events. The agreement between the model and data is good for all distributions, including the missing energy.

Table 6.8 Means of kinematic distributions of opposite sign dimuons with hadron shower background subtracted along with means of distributions of charm Monte Carlo. All events have both muons momentum magnetically analyzed with $p_\mu > 9$ GeV/c. The errors on the means are shown in parentheses. The missing energy is corrected for the single-muon off-set values, is calculated for identified ν_K events only, and its error includes an overall 1.2 GeV systematic error. The transverse momentum of the positive muon with respect to the hadron shower direction is also calculated for ν_K events.

Quantity	Data with Backgr. subtracted	Charm production Monte Carlo
ϕ_{12}(degrees)	136(3)	135(1)
$p_{T2min}{}^2$(GeV^2/c^2)	0.50(0.05)	0.47(0.01)
$p_{\mu 2}$(GeV/c)	24.4(0.4)	23.5(0.2)
E_{mis}(GeV)	14.5(2.2)	15.4(0.7)
$z_{\mu 2}$	0.31(0.01)	0.30(0.01)
M_{12}(GeV/c^2)	2.9(0.1)	3.0(0.1)

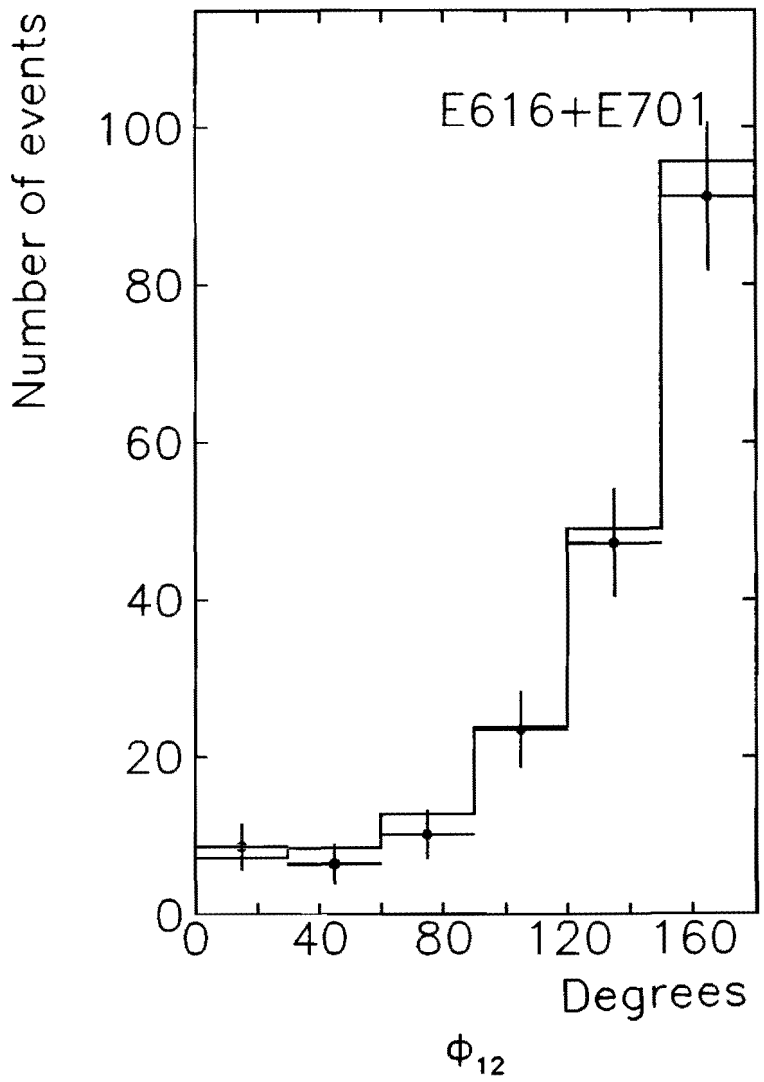

Figure 6.6 Distributions of several kinematic quantities from opposite-sign dimuon data. The points with error bars represent data after the hadron background subtraction, the histogram shows results from Monte Carlo model of charm production. Here the second muon is well defined as μ^+. Fig.6.3a shows the angle between two muons in the plane perpendicular to the direction of the incident neutrino direction.

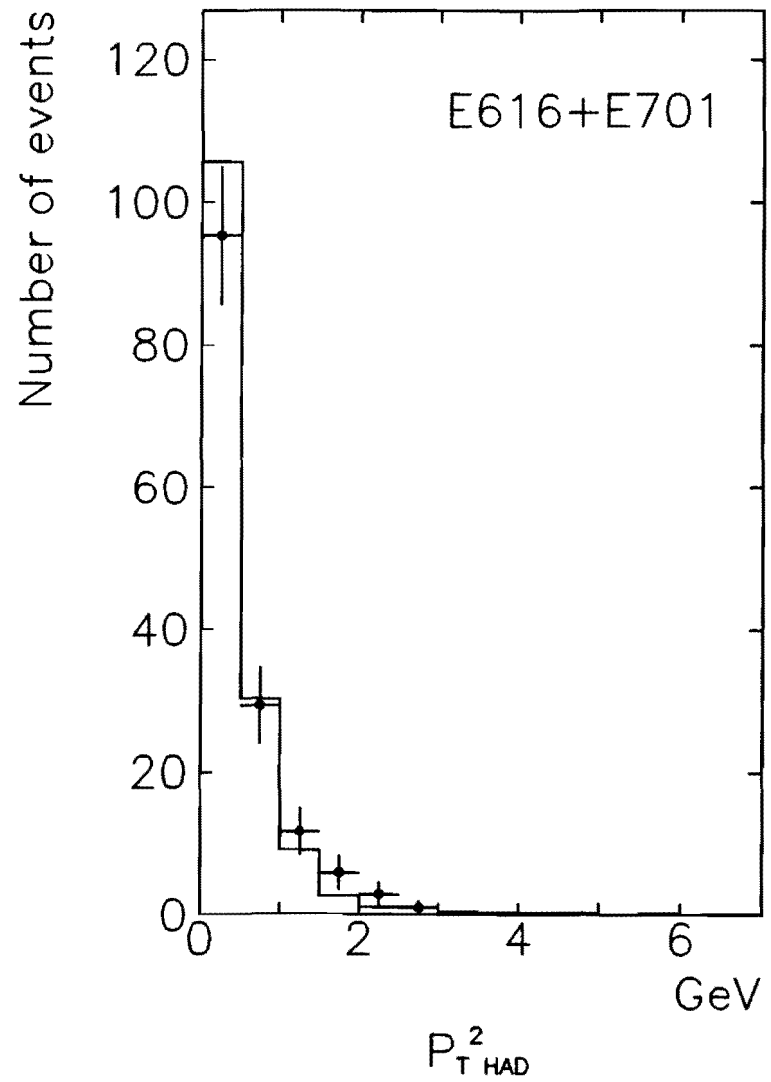

Figure 6.6b Opposite-Sign dimuon distribution of p_T^2, square of the transverse muon momentum with respect to the shower direction

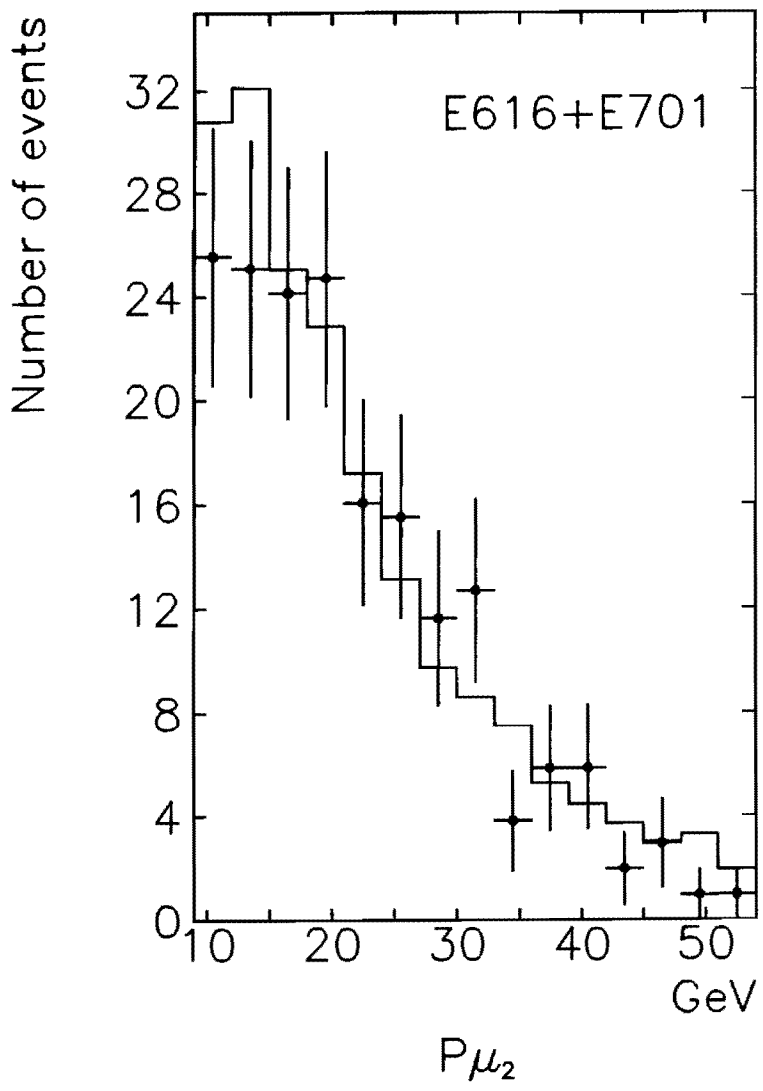

Figure 6.6c Opposite-Sign dimuon distribution of $p_{\mu 2}$, momentum of the second muon.

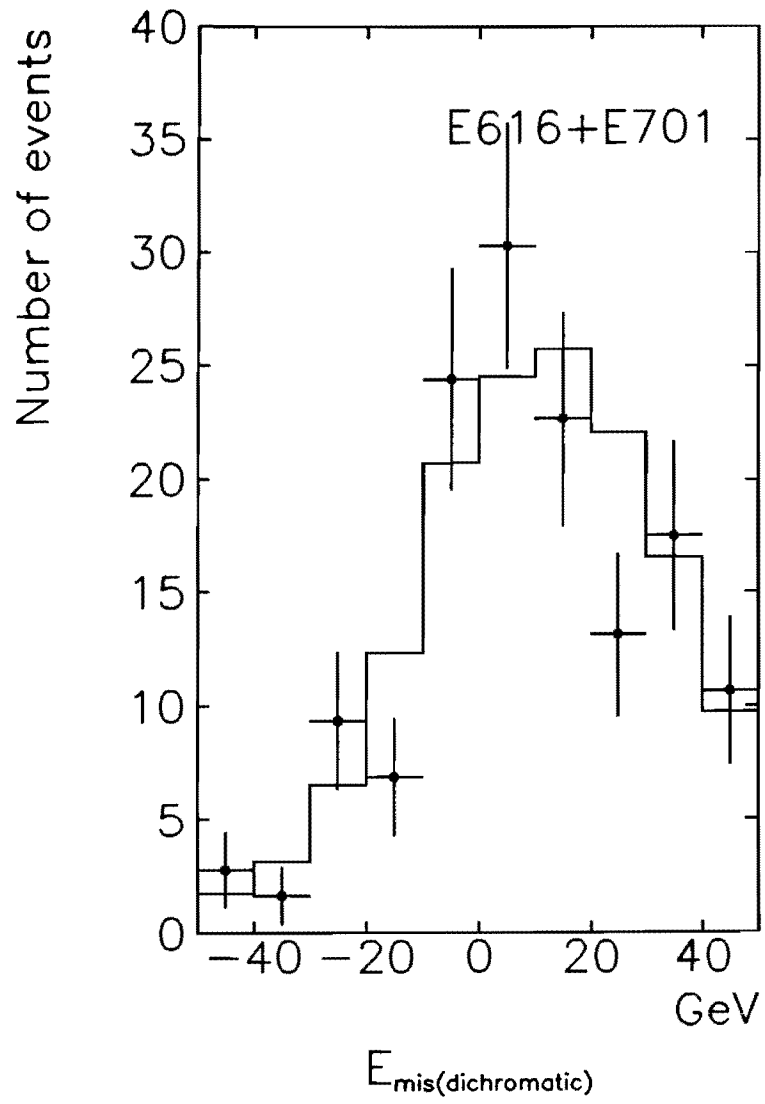

Figure 6.6d Opposite-Sign dimuon distribution of the measured missing energy E_{mis} from ν_K events.

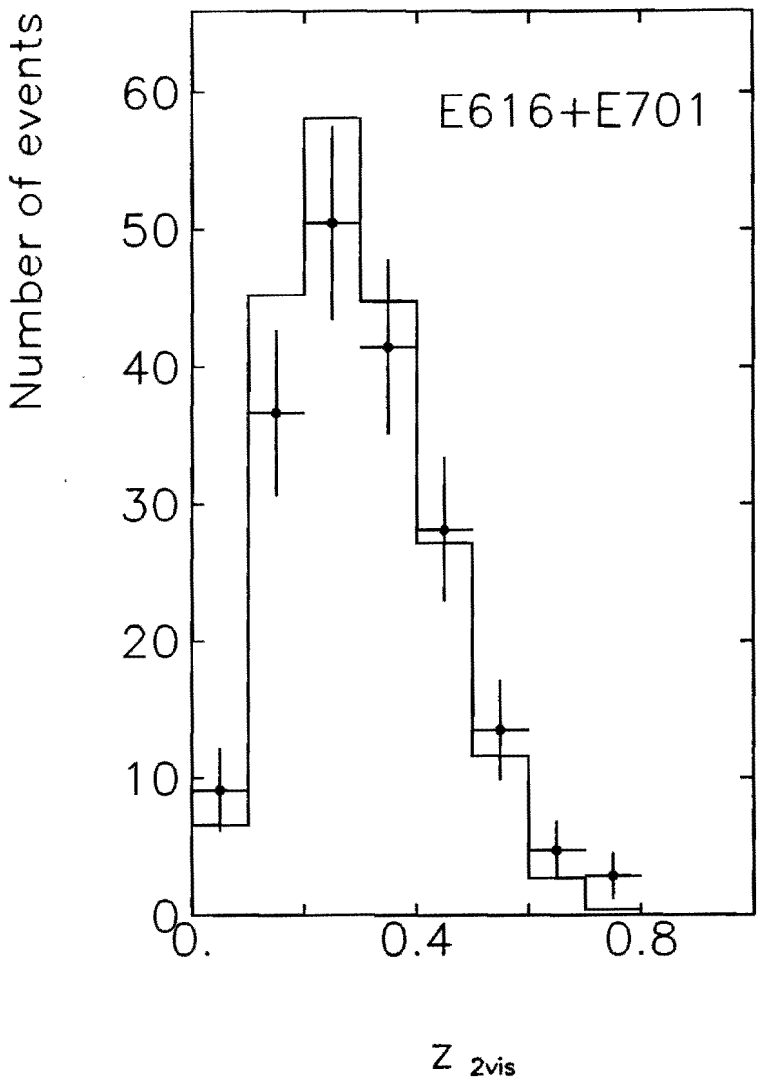

Figure 6.6e Opposite-Sign dimuon distribution of $z_{\mu 2}$ (defined in the text)

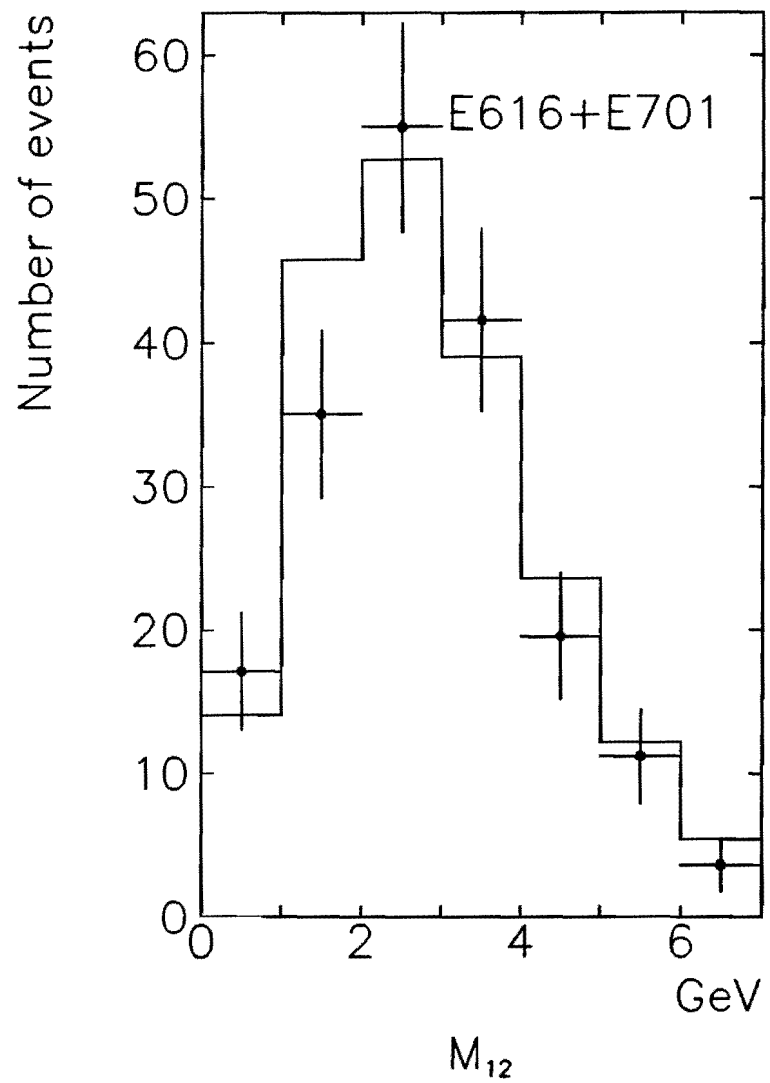

Figure 6.6f Opposite-Sign dimuon distribution of the invariant mass M_{12} of the muon pair.

The observed like-sign dimuon signal of 6.6 ± 4.8 events is about 1.5 standard deviations above the background. The hadron shower background and/or associated charm production with anticharm decaying into μ^- cannot explain the measured rates. In addition, although most distributions of the data are similar to those expected from these two sources, the missing energy and p_T kinematic distributions of the data display features which are not expected from the two models.

Chapter 7

Results on Opposite-Sign Dimuons

The predominant mechanism for the production of opposite-sign dimuons is the semileptonic decay of charm particles. The background originating from the hadronic shower accounts for about 20% of the observed events. In this experiment, dimuon events with a 4.3 GeV/c muon momentum cut on the second muon (CLASS 1, described in Chapter 3) can have a second muon with an unknown sign. This occurs in the case for which the second muon is not magnetically analyzed in the toroid. Such events comprise about 40% out of the total data sample. Therefore hadron showers can contribute to the background through μ^- or μ^+ production, and the background calculations must contain contributions from muons of both signs.

Both μ^- and μ^+ Monte Carlo background events were generated. Each background event was checked as to whether the second muon could be analyzed in the spectrometer (and have its sign determined). If this condition was satisfied, only muons with the correct sign contributed to the background.

Table 7.1a and b show the number of background events (passing all the analysis cuts) for neutrino and antineutrino induced opposite-sign dimuons with a 4.3 GeV/c muon momentum cut in energy bins.

Table 7.1a Number of background events from hadron showers for neutrino induced opposite-sign dimuon events with a muon momentum cut of 4.3 GeV/c calculated for experiments E616, E701 separately, and total in three energy bins.

Energy Bin	E616	E701	E616+E701
30-100	21.7	12.7	34.4
100-180	17.8	10.2	28.0
180-230	29.4	14.3	43.7
30-230	68.9	37.2	106.1

Table 7.1b Number of background events from hadron shower for antineutrino induced opposite-sign dimuon events with muon momentum cut of 4.3 GeV/c calculated for experiments E616, E701 separately, and total in three energy bins.

Energy Bin	E616	E701	E616+E701
30-100	3.0	1.1	4.1
100-230	2.0	0.9	2.9
30-230	5.0	2.0	7.0

7.1 Rates of Opposite-Sign Dimuons

The charm production model was used to correct for the geometric and kinematic acceptance of opposite-sign dimuon events (see eqn.3.4). The values of important parameters on which the charm production model depends (as introduced in Chapter 5) are given below:

(a) The mass of the charm quark, $m_c = 1.5$ GeV/c^2,

(b) The parameter ε in the Peterson et al. charm fragmentation function [5.17][see (5.2.16)], $\varepsilon = 0.19$,

(c) The strange sea fraction κ, as defined by (1.3.6) (the determination of κ is discussed in detail later in this chapter), $\kappa = 0.42$,

(d) The semileptonic decay branching ratio of charm particles into muons, $B_1(c \to \mu X) = 0.100$.

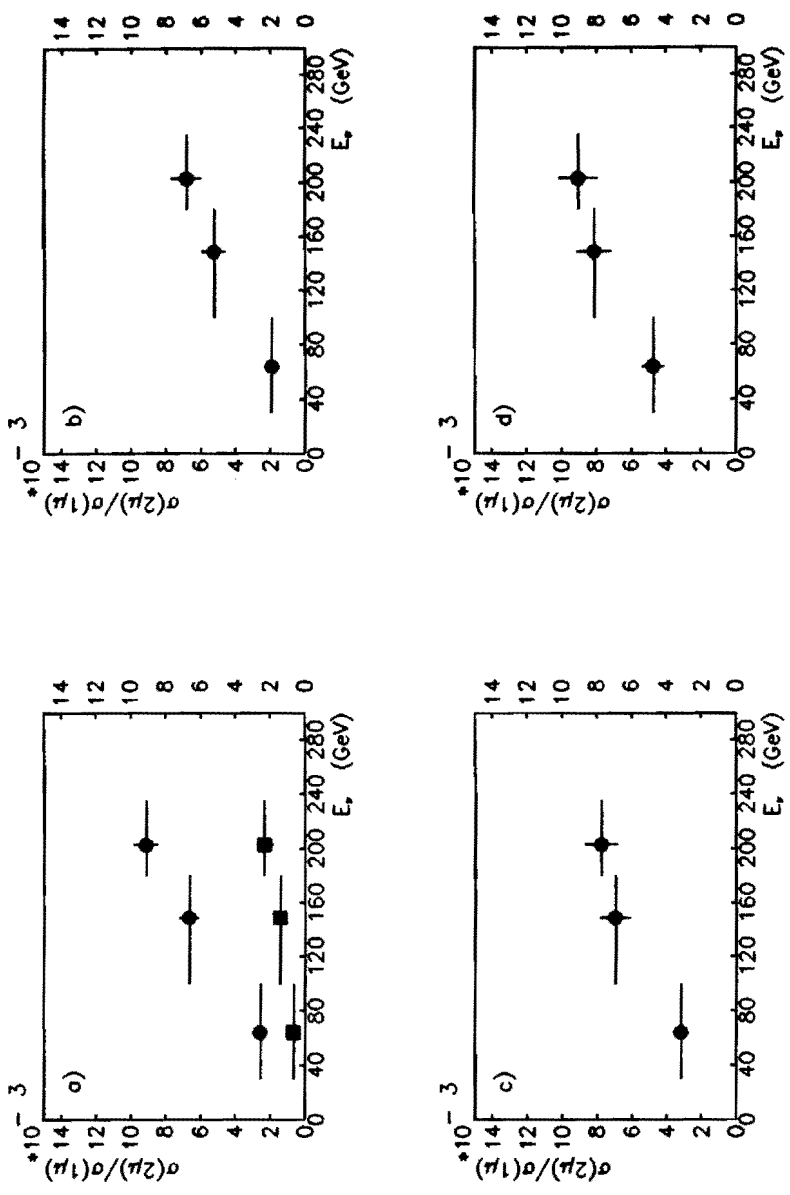

Figure 7.1 Energy dependence of neutrino induced opposite-sign dimuon rates: (a)raw data (circles) and raw background (p_μ>4.3GeV/c); (b) raw data with the background subtracted (p_μ>4.3GeV/c); (c) data with the background subtracted corrected for geometric acceptance (p_μ>4.3GeV/c); (d) as in (c) with additional correction for muon momentum cut (yielding rates for p_μ > 0 GeV/c).

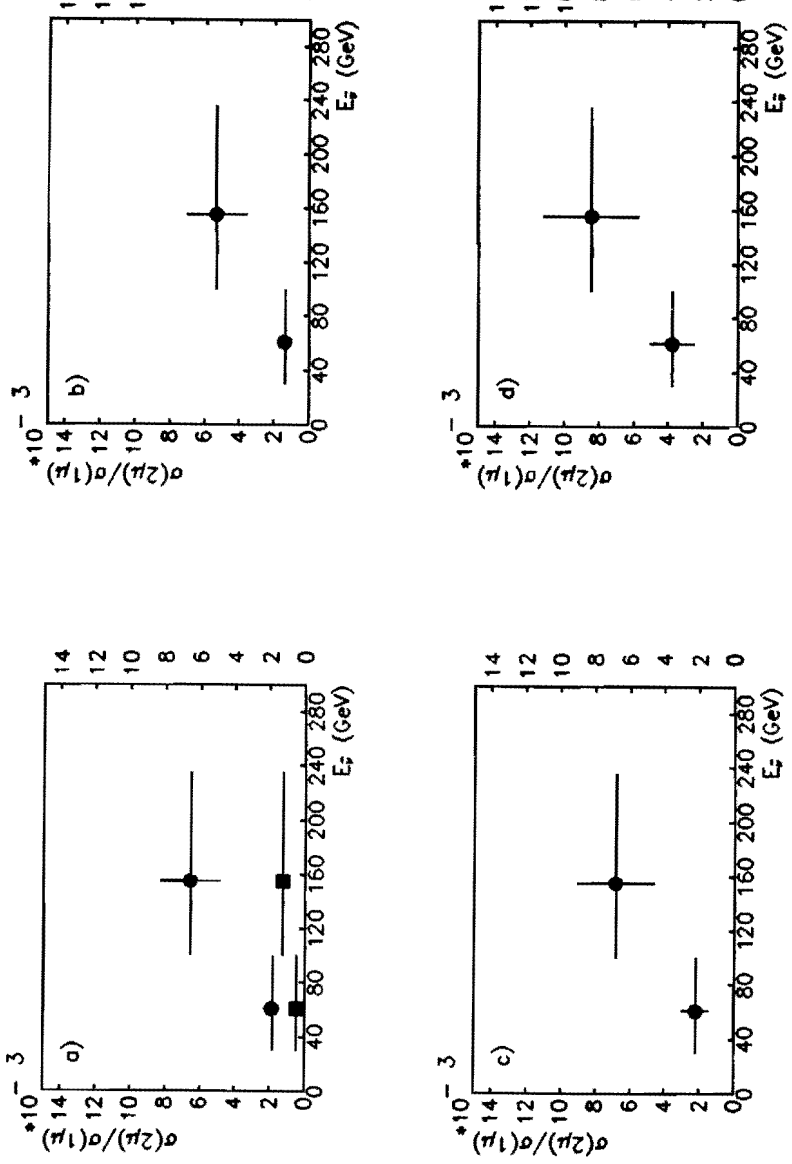

Figure 7.2 Energy dependence of antineutrino induced opposite-sign dimuon rates: (a)raw data (circles) and raw background (p_μ>4.3GeV/c); (b) raw data with the background subtracted (p_μ>4.3GeV/c); (c) data with the background subtracted corrected for geometric acceptance (p_μ>4.3GeV/c); (d) as in (c) with additional correction for muon momentum cut (yielding rates for p_μ > 0 GeV/c).

Fig.7.1a shows the raw ratio of $\sigma(\mu^-\mu^+)/\sigma(\mu^-)$ versus neutrino energy for $p_\mu > 4.3$ GeV/c. Also shown is the calculated background rate versus neutrino energy. Fig.7.1.b shows the measured $\mu^-\mu^+/\mu^-$ rate for $p_\mu > 4.3$ GeV/c after subtraction of the background. Fig.7.1c shows $\mu^-\mu^+/\mu^-$ rate for $p_\mu > 4.3$ GeV/c after subtraction of the background and corrected for geometric acceptance. Fig.7.1d shows the $\mu^-\mu^+/\mu^-$ rate after subtraction of the background, corrected for geometric acceptance and corrected for the muon momentum cut of 4.3 GeV/c (i.e. expresses the rate for $p_\mu > 0$ GeV/c). Figs.7.2 shows the same quantities for antineutrinos (because of limited statistics only two energy bins are used). Table 7.2 and 7.3 contain the numbers corresponding to points displayed in Figs.7.1 and 7.2.

The raw data and background rates rise linearly with neutrino energy. The raw data with subtracted background reaches a rate of ~0.7% at 200 GeV. The geometric factors which correct for the acceptance of the apparatus increase this rate to ~0.8% at 200 GeV. The correction for the muon momentum cut, $p_\mu > 4.3$ GeV/c, flattens the rate versus energy and yields a rate of ~0.9% in the 100 to 200 GeV range for $p_\mu > 0$ GeV/c.

Table 7.2 Calculation of opposite-sign rates from neutrino interactions. Columns represent: (1) raw data rates for $p_\mu > 4.3$ GeV/c , (2) raw background rates for $p_\mu > 4.3$ GeV/c, (3) raw data rate after the background subtraction for $p_\mu > 4.3$ GeV/c, (4) rates for $p_\mu > 4.3$ GeV/c corrected for geometric acceptance, (5) rates corrected for geometric acceptance and muon momentum cut of 4.3 GeV/c

Energy Bin (GeV)	Data raw (1)	Bkg. raw (2)	Data -Bkg. (3)	Geom. corr. (4)	Geom. + p_μ corr. (5)
	--------> in units of 10^{-3} <---------				
30-100	2.6±0.2	0.66±0.13	1.9±0.3	3.2±0.4	4.8±0.6
100-180	6.6±0.6	1.42±0.28	5.2±0.7	6.9±0.9	8.1±1.0
180-230	9.1±0.7	2.33±0.39	6.8±0.8	7.7±1.0	9.0±1.1

Table 7.3 Calculation of opposite-sign rates from antineutrino interactions. Columns represent: (1) raw data rates for $p_\mu > 4.3$ GeV/c , (2) raw background rates for $p_\mu > 4.3$ GeV/c, (3) raw data rate after the background subtraction for $p_\mu > 4.3$ GeV/c, (4) rates for $p_\mu > 4.3$ GeV/c corrected for geometric acceptance, (5) rates corrected for geometric acceptance and muon momentum cut of 4.3 GeV/c.

Energy Bin (GeV)	Data raw (1)	Bkg. raw (2)	Data -Bkg. (3)	Geom. corr. (4)	Geom. + p_μ corr. (5)
	--------> in units of 10^{-3} <---------				
30-100	1.9±0.5	0.47±0.09	1.4±0.5	2.2±0.8	3.8±1.3
100-230	6.6±1.7	1.27±0.25	5.3±1.7	6.8±2.2	8.5±2.7

In addition to corrections for geometric and kinematic inefficiencies the rates can be corrected for the threshold effect due to the mass of the charm quark (slow rescaling correction). In principle this correction should remove all the energy dependence from the dimuon rates.

Technically, this correction is obtained by taking the ratio of Monte Carlo generated dimuon events with a certain charm quark mass (eg. m_c = 1.5 GeV/c), and events generated with this mass set to zero. Fig.7.3a and Table 7.4a show the corrected rates using charm quark masses of 1.0, 1.5, and 1.9 GeV/c^2. Fig.7.3b and Table 7.4b show the corresponding rates for antineutrinos. Table 7.4

As shown, the energy dependence is not removed below the high charm quark mass of 1.9 GeV/c^2. Note that the large errors do not exclude the 1.5 GeV/c^2 value. It appears that a charm quark mass of 1.5 GeV or lower is unlikely, or that the slow scaling formalism does not fully account for threshold effects, unless a mass which is closer to the mass of the D meson is used. However, an energy dependent charm semileptonic branching ratio could also be responsible for some energy dependence. This possibility is discussed later in this chapter.

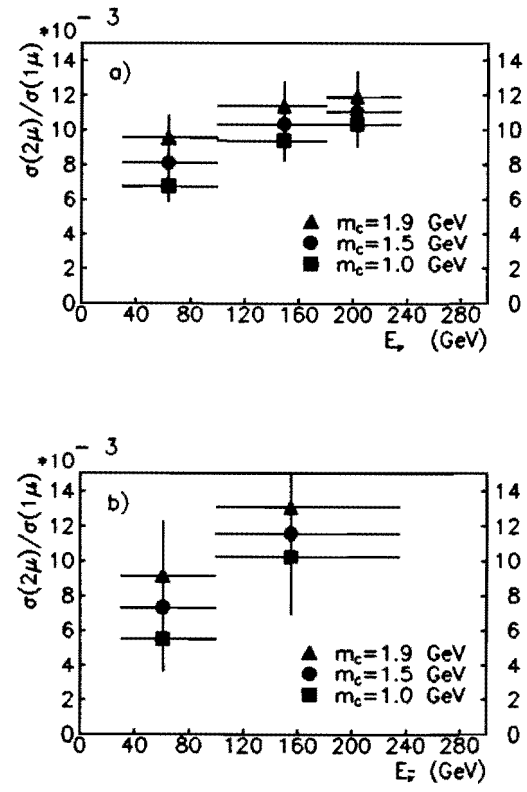

Figure 7.3 Energy dependence of (a) neutrino and (b) antineutrino induced opposite-sign dimuon rates fully corrected for geometric acceptance and muon momentum cut, and also corrected for the slow rescaling with charm quark masses of 1.0, 1.5, and 1.9 GeV/c^2..

Table 7.4a Rates of neutrino induced opposite-sign dimuon events fully corrected for geometric and kinematic acceptance, and also corrected for threshold effects (slow rescaling correction) with charm quark masses of 1.0, 1.5, and 1.9 GeV.

Energy Bin (GeV)	m_c = 1.0 GeV	m_c = 1.5 GeV	m_c = 1.9 GeV
	----------> in units of 10^{-3} <----------		
30-100	6.8±0.9	8.1±1.1	9.6±1.3
100-180	9.4±1.2	10.4±1.3	11.4±1.4
180-230	10.4±1.3	11.1±1.4	11.9±1.5

Table 7.4b Rates of antineutrino induced opposite-sign dimuon events fully corrected for geometric and kinematic acceptance, and also corrected for threshold effects (slow rescaling correction) with charm quark masses of 1.0, 1.5, and 1.9 GeV.

Energy Bin (GeV)	m_c = 1.0 GeV	m_c = 1.5 GeV	m_c = 1.9 GeV
	----------> in units of 10^{-3} <----------		
30-100	5.5±1.9	7.3±2.5	9.2±3.1
100-230	10.3±3.3	11.6±3.8	13.1±4.2

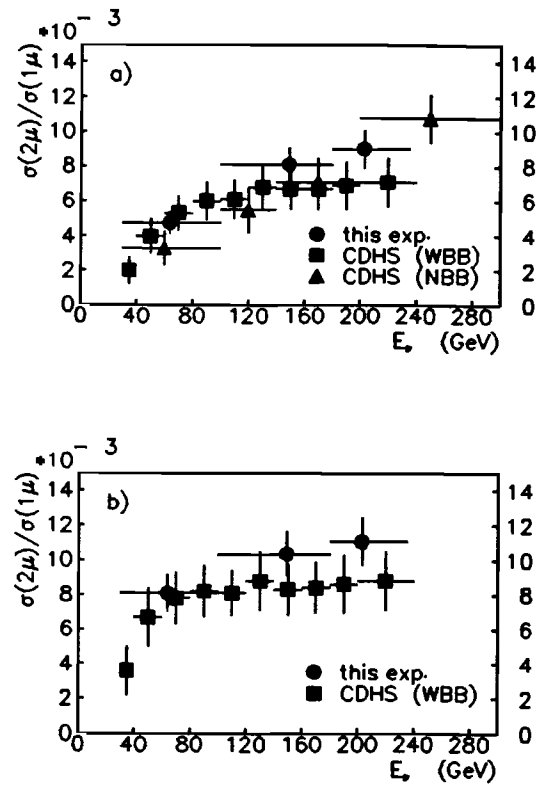

Figure 7.4 Comparison of the energy dependence of neutrino induced opposite-sign dimuon rates from this experiment and the CDHS experiment at CERN. The squares show CDHS results with the wide band beam [1.9], the triangles show the CDHS results with the narrow band beam [7.1]. Part a) presents rates corrected for geometric acceptance and the muon momentum cut, part b) shows the rates with an additional correction for slow rescaling with m_c = 1.5 GeV/c^2.

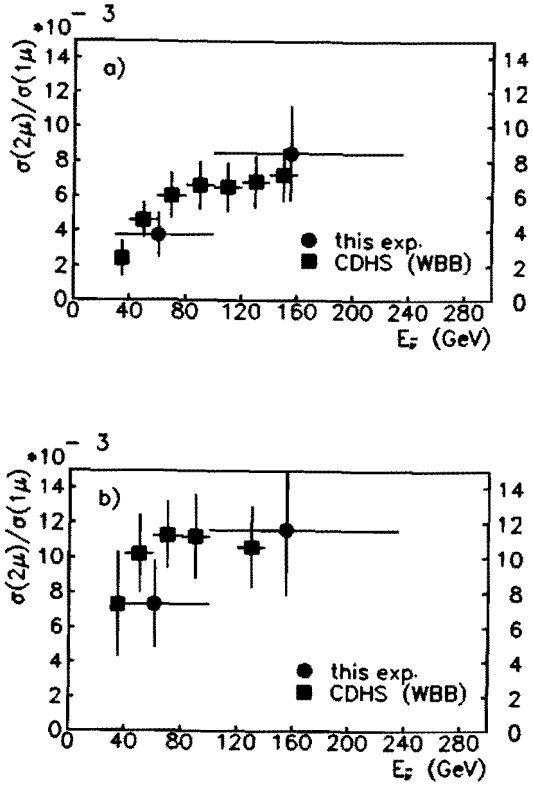

Figure 7.5 Comparison of the energy dependence of antineutrino induced opposite-sign dimuon rates from this experiment and the CDHS experiment at CERN. The squares show the CDHS results with the wide band beam [1.9]. Part a) presents rates corrected for geometric acceptance and muon momentum cut, part b) shows the rates with an additional correction for slow rescaling with $m_c = 1.5\ GeV/c^2$.

Fig.7.4a shows a comparison of rates fully corrected for geometric acceptance and the muon momentum cut with similar data from the CDHS group [1.9,7.1]. The rates from this experiment (CCFRR) are somewhat higher than the published CDHS rates from their neutrino wide band beam data (a sample of ~15 000 opposite-sign dimuon events). There is a better agreement with the CDHS rates obtained using a neutrino narrow band beam [7.1]. Fig.7.4b compares these rates with additional slow rescaling correction. The comparisons for antineutrinos are shown in Figs.7.5a and b.

7.2 The Fraction of the Strange Sea in the Nucleon

The extraction of the fraction of the strange sea in the nucleon is based on the charm Monte Carlo model which was used to generate charm D mesons as outlined in Chapter 5. The D meson energy is determined from the energy of the produced charm quark according to the Peterson et al. fragmentation distribution.

The neutrino and antineutrino x distributions from the Monte Carlo were generated using events passing all the dimuon analysis cuts and with an initial value of parameter

$\kappa = 2s(x')/(\bar{u}(x') + \bar{d}(x'))$

These distributions were compared to the corresponding x distributions for the data (after subtraction of background) by forming a χ^2 between the two distributions. The branching ratio was allowed to float with an input constraint of 10.9±1.4%. The χ^2 surface as a function of κ and B_1 was thus obtained.

The comparison of x distribution was done in 7 x bins: 0.00-0.05, 0.05-0.10, 0.10-0.15, 0.15-0.20, 0.20-0.25, 0.25-0.45, 0.45-1.00. It was therefore sensitive to both the shape and normalization of the data.

The systematic error from the 20% normalization uncertainty in the background was estimated by a reanalysis with the background multiplied by either a factor 1.2 or 0.8.

The fit resulted in (the minimum χ^2):

$$\kappa = 0.42 \begin{smallmatrix} +\,0.13 \\ -\,0.10 \end{smallmatrix} \pm 0.02$$

at $B_1(c\to\mu) = 0.100$

where the first error is statistical, and the second originates in 20% background uncertainty. Adding these errors in quadrature yields

$$\kappa = 0.42 \begin{smallmatrix} +\,0.13 \\ -\,0.10 \end{smallmatrix}$$

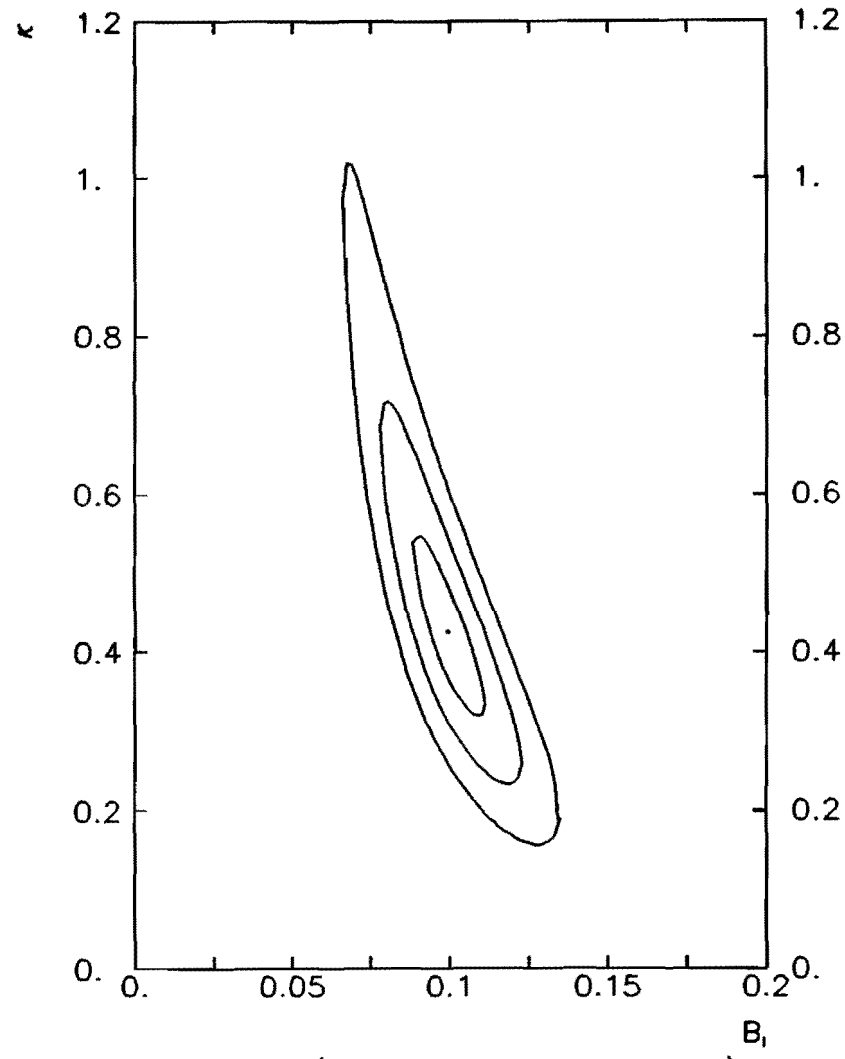

κ vs. Br. (1σ, 2σ, and 3σ contours)

Figure 7.6 Shown are 1, 2, and 3 standard deviation χ^2 contours in the κ-B_1 plane for m_c=1.5GeV/c^2 and ε=0.19.

Table 7.7 Effect of charm quark masses on the determination of the fraction of the strange sea. The first error is statistical, and the second is the systematic error due to the ±20% background uncertainty.

Energy Bin (GeV)	m_c=1.0GeV/c^2	m_c=1.5GeV/c^2	m_c=1.9GeV/c^2
	κ	κ	κ
	B_l	B_l	B_l
30-100	$.12^{+.10}_{-.08}\pm.02$	$.19^{+.13}_{-.11}\pm.04$	$.30^{+.15}_{-.12}\pm.04$
	$.103^{-.013}_{+.013}\pm.001$	$.105^{-.014}_{+.014}\pm.001$	$.106^{-.014}_{+.014}\pm.001$
100-230	$.45^{+.14}_{-.11}\pm.03$	$.52^{+.16}_{-.12}\pm.03$	$.59^{+.19}_{-.14}\pm.04$
	$.101^{-.012}_{+.012}\pm.003$	$.103^{-.012}_{+.012}\pm.003$	$.106^{-.012}_{+.012}\pm.002$
30-230	$.35^{+.11}_{-.09}\pm.02$	$.42^{+.13}_{-.10}\pm.02$	$.50^{+.15}_{-.12}\pm.03$
	$.097^{-.011}_{+.011}\pm.003$	$.100^{-.011}_{+.011}\pm.003$	$.104^{-.011}_{+.011}\pm.003$

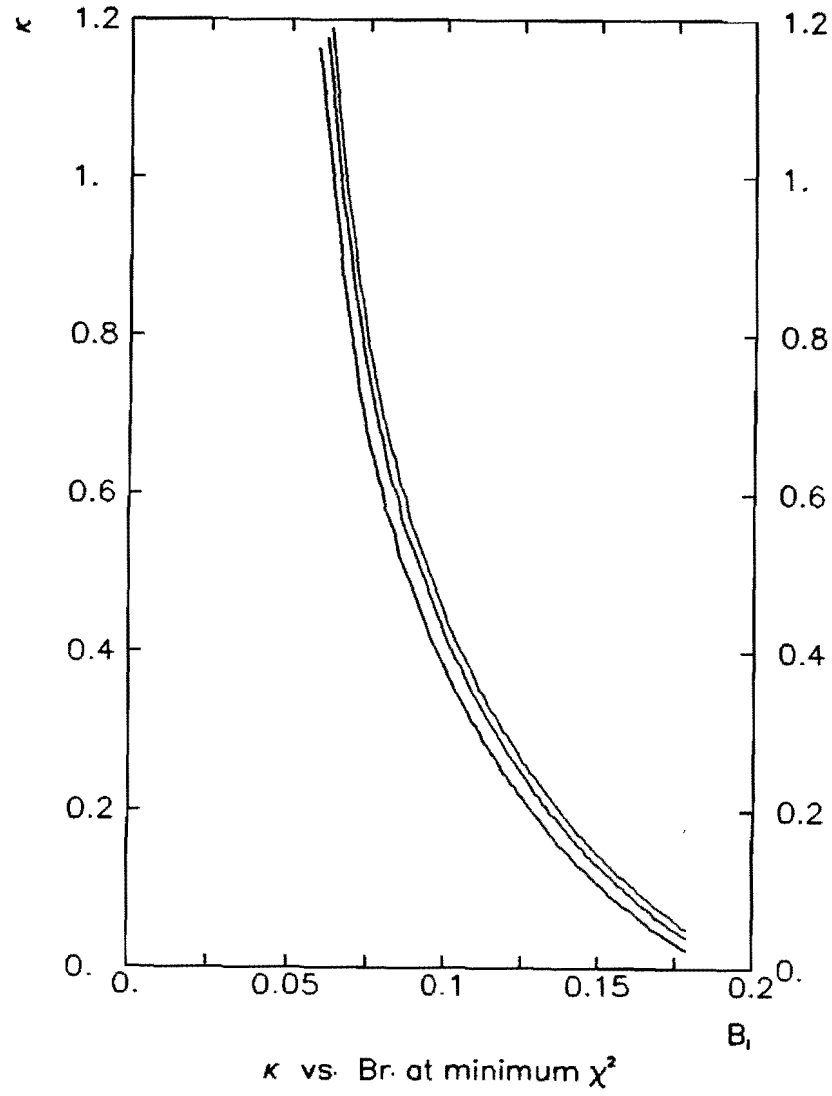

Figure 7.9 Correlation between the best fit of κ versus the semileptonic branching ratio for three different values of the parameter ε in the Peterson et al. fragmentation function; ε = 0.09 (bottom curve), ε = 0.19 (middle curve), and ε = 0.29 (top curve).

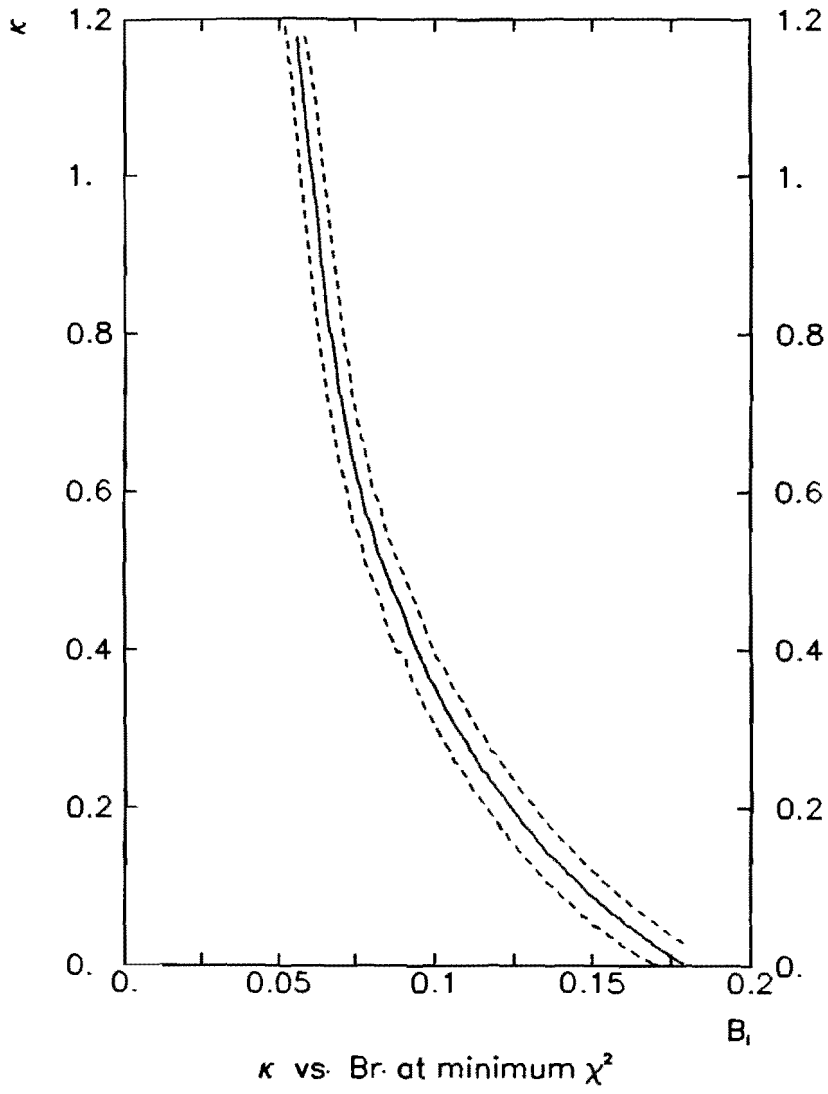

Figure 7.10 Correlation between the best fit of κ versus the semileptonic branching ratio for the charm fragmentation function equal to the delta function δ(z-0.68).

meson spectrum and a smaller value of κ. As shown in the figure, the sensitivity of the κ parameter to the value of ε is rather weak. Results of fits are summarized in Table 7.8.

A delta function form of the fragmentation function was also investigated. The use of the function δ(z-0.68) as suggested in [1.9] leads to change in κ as shown in Table 7.9. Fig.7.10 shows κ dependence versus branching ratio for δ(z-0.68)

Table 7.8 Effect of charm quark fragmentation function on the determination of the fraction of the strange sea. Fits for 3 different values of the parameter ε in the Peterson et al. fragmentation function are shown. The first error is statistical, the second the systematic due to the ±20% background uncertainty.

Energy Bin (GeV)	ε = 0.09	ε = 0.19	ε = 0.29
	κ	κ	κ
	B_1	B_1	B_1
30-100	$.15^{+.13}_{-.11}\pm.05$	$.19^{+.13}_{-.11}\pm.04$	$.24^{+.13}_{-.11}\pm.04$
	$.106^{-.015}_{+.015}\pm.001$	$.105^{-.014}_{+.014}\pm.001$	$.104^{-.014}_{+.014}\pm.0.001$
100-230	$.50^{+.15}_{-.12}\pm.03$	$.52^{+.16}_{-.12}\pm.03$	$.53^{+.16}_{-.12}\pm.03$
	$.101^{-.012}_{+.012}\pm.003$	$.103^{-.012}_{+.012}\pm.003$	$.104^{-.012}_{+.012}\pm.003$
30-230	$.41^{+.12}_{-.10}\pm.02$	$.42^{+.13}_{-.10}\pm.02$	$.44^{+.13}_{-.11}\pm.03$
	$.097^{-.011}_{+.011}\pm.003$	$.100^{-.011}_{+.011}\pm.003$	$.100^{-.011}_{+.011}\pm.003$

Table 7.9 Effect of charm quark fragmentation function on the determination of the fraction of the strange sea. Fits for ϵ=0.19 of the parameter ϵ in the Peterson et al. fragmentation function and for fragmentation function in the form of $\delta(z-0.68)$ are shown. The first error is statistical, the second is the systematic error due to the ±20% background uncertainty.

Energy Bin (GeV)	$\delta(z-0.68)$	ϵ = 0.19
	κ	κ
	B_1	B_1
30-100	$.14^{+.12}_{-.10}\pm.04$	$.19^{+.13}_{-.11}\pm.04$
	$.103^{-.015}_{+.015}\pm.001$	$.105^{-.014}_{+.014}\pm.001$
100-230	$.49^{+.15}_{-.12}\pm.03$	$.52^{+.16}_{-.12}\pm.03$
	$.100^{-.012}_{+.012}\pm.003$	$.103^{-.012}_{+.012}\pm.003$
30-230	$.39^{+.12}_{-.10}\pm.02$	$.42^{+.13}_{-.10}\pm.02$
	$.095^{-.011}_{+.011}\pm.003$	$.100^{-.011}_{-.011}\pm.004$

7.6 Effect of Like-Sign Dimuons on the Extraction of the Strange Sea

Because of the poor statistics, the like-sign dimuon data cannot decisively address the question of the existence of a prompt like-sign dimuon signal. A prompt like-sign dimuon signal can affect the determination of the κ from this experiment. Three possible scenarios were studied:

(1) If there are no prompt like-sign dimuons, than the hadron shower background calculation should have yielded about 1.6 the number of like-sign dimuon events (17.3 instead of 10.7). The factor of 1.6 is much greater than the 20% error in the background as estimated in Chapter 4. The κ determined for data with a 4.3 GeV/c muon momentum cut (where the background subtraction is important and accounts for about 20% of observed dimuon events) is consistent with the value obtained from the data sample with 9 GeV/c muon momentum cut (where the background subtraction is not important and accounts for only 5% of observed events). A factor of 1.6 increase in the background for the sample with a 4.3 GeV/c muon momentum cut leads to a change of κ from 0.42 to 0.36. This possibility is considered to be very unlikely.

(2) If the prompt like-sign dimuon signal exists, and originates from the associated charm production (c-$\bar{c}$ pair from a gluon bremsstrahlung process) then it can contribute to the opposite-sign dimuon signal (the contribution comes both from c decay, and $\bar{c}$ decays which can yield muons which are not analyzed in the spectrometer). This possible effect has been estimated by increasing the calculated c-$\bar{c}$ rate by a factor of 42 to match the number of prompt like-sign dimuon events above the calculated background (6.6 events). The c-$\bar{c}$ rates were added to the hadron background model, and the sum subtracted from the observed data. This procedure leads to a change of κ from 0.42 to the smaller value of κ=0.41 (compare Table 7.5 and 7.6).

(3) If the prompt signal of unknown origin exists then the observed ratio of prompt like-sign dimuons to prompt opposite-sign dimuons is 4.0±2.9% (see Table 6.6). If a charge conjugated process also exists at the same fractional rate, its contribution accounts for 0.040 of the opposite prompt signal. This leads to a change of κ from 0.42 to 0.41.

7.7 Kinematics of Opposite-Sign Dimuons

The distributions of kinematic quantities of the opposite-sign dimuon data sample (with the background subtracted) are compared to the distributions of the "standard" charm Monte Carlo model.

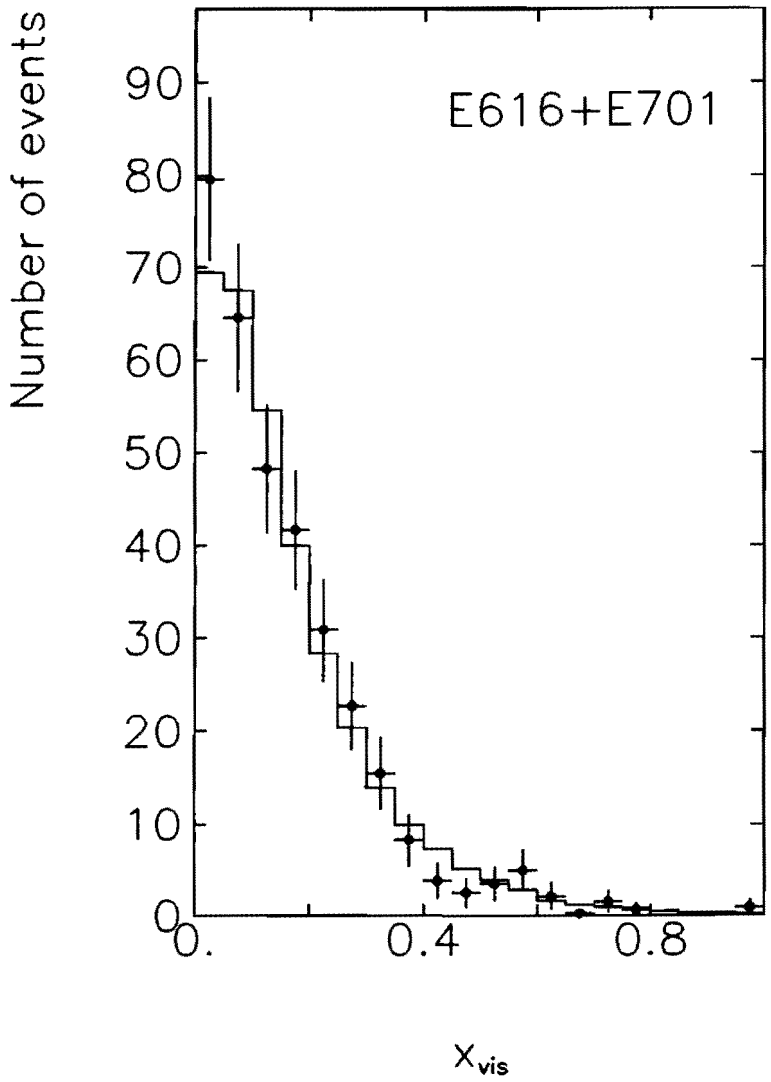

Figure 7.11 Distribution of variable x_{Bj} for data events with the subtracted background (points with error bars) and Monte Carlo generated events with κ=0.42, m_c=1.5GeV/c^2, ε=0.19, and $B_l(c\to\mu X)$=0.100 (histogram)

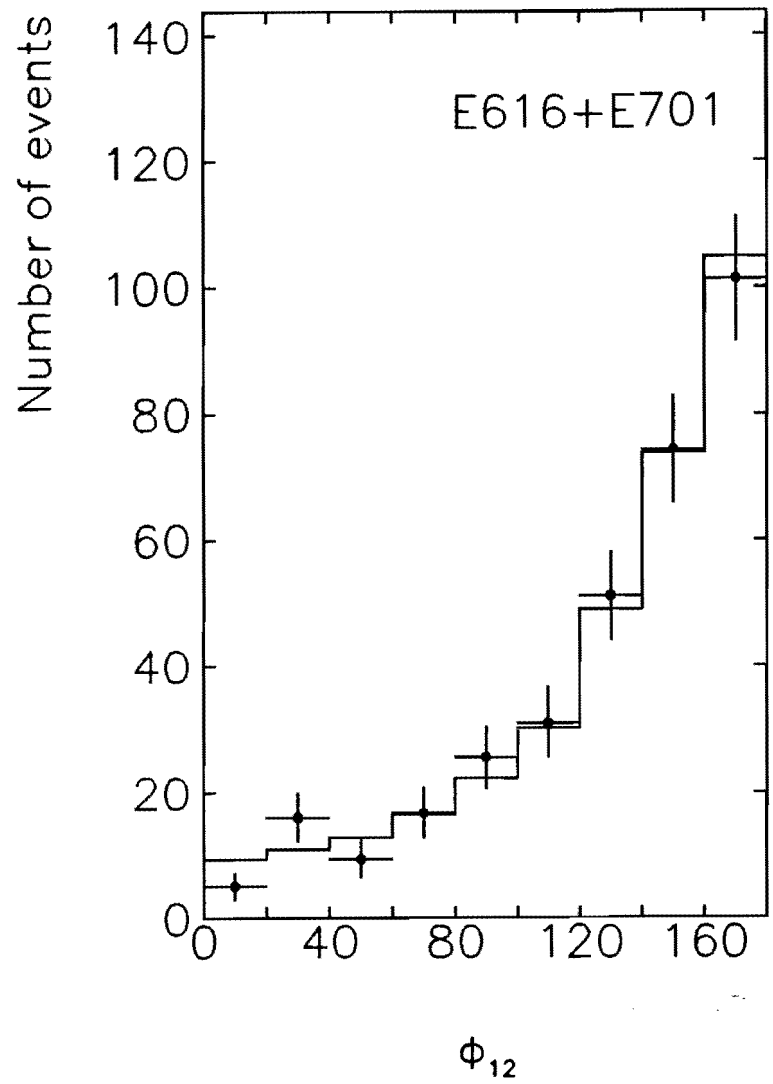

Figure 7.12 Distribution of variable ϕ_{12} (azimuthal angle between two muons projected on the plane perpendicular to the incoming neutrino direction) for data events with the subtracted background (points with error bars) and Monte Carlo generated events with κ=0.42, m_c=1.5GeV/c^2, ε=0.19, and $B_l(c\to\mu X)$=0.100 (histogram)

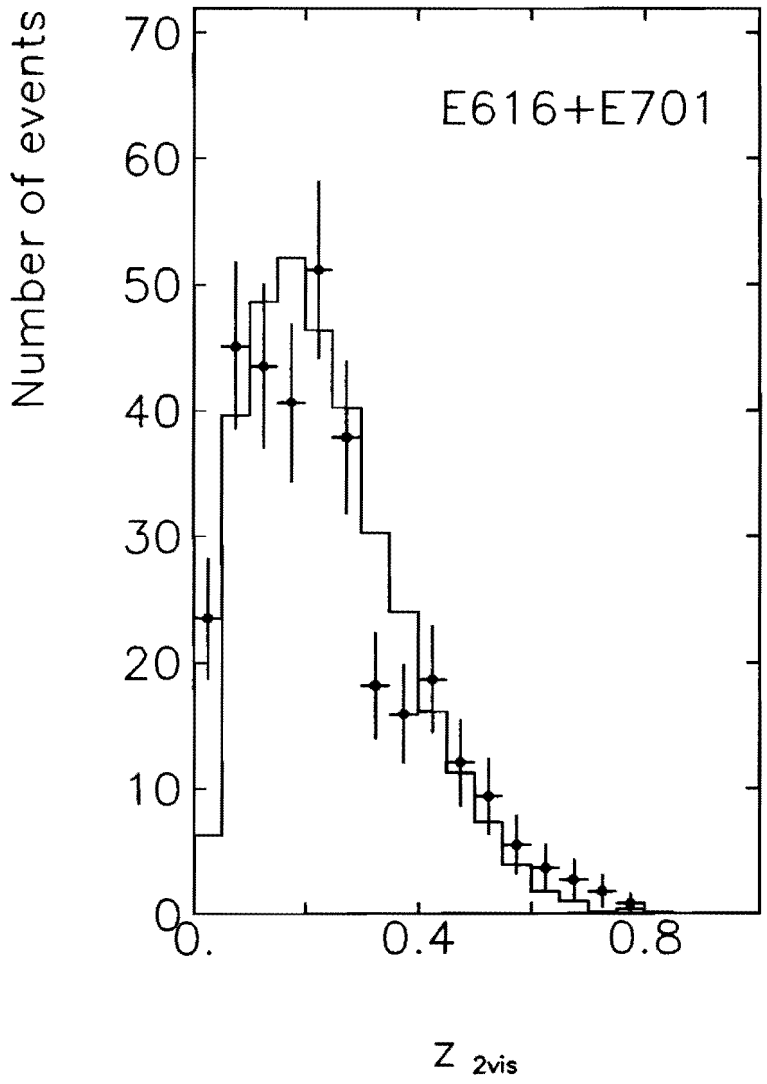

Figure 7.13 Distribution of variable $z_\mu = p_{\mu 2}/(E_H + p_{\mu 2})$ for data events with the subtracted background (points with error bars) and Monte Carlo generated events with κ=0.42, m_c=1.5GeV/c^2, ε=0.19, and $B_1(c\to\mu X)$=0.100 (histogram)

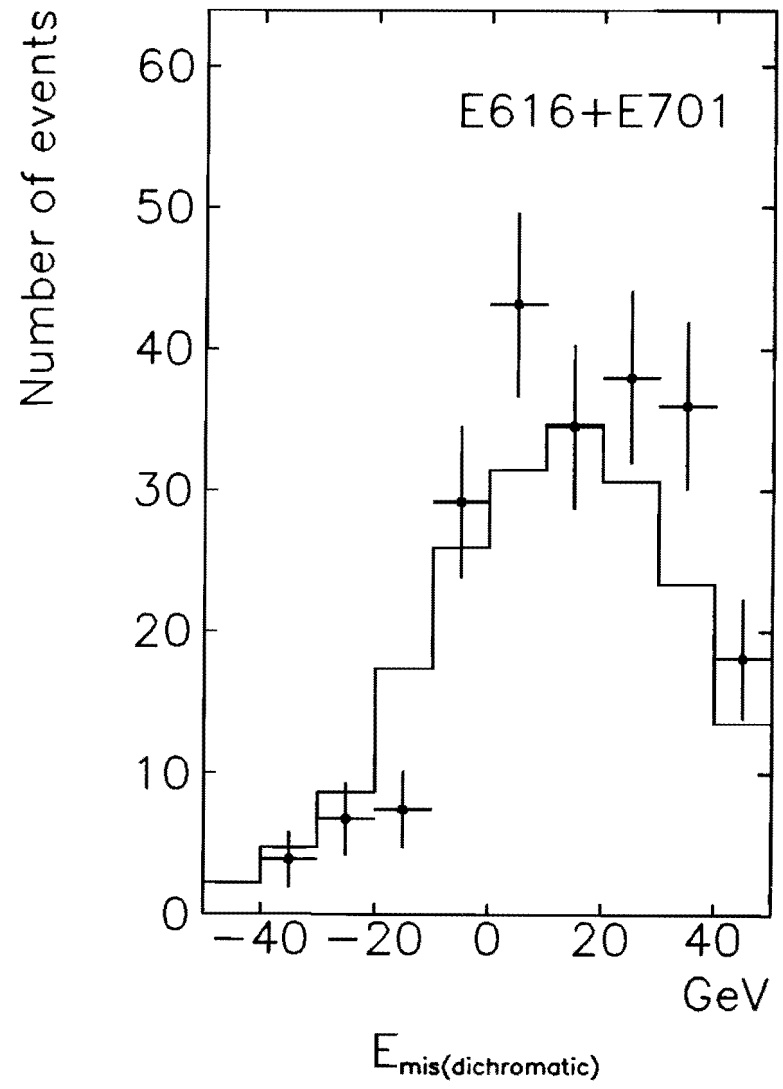

Figure 7.14 Distribution of missing energy (obtained as the difference between the measured total neutrino interaction energy and the energy determined from the radial position of the interaction) for data events with the subtracted background (points with error bars) and Monte Carlo generated events with κ=0.42, m_c=1.5GeV/c^2, ε=0.19, and $B_1(c\to\mu X)$=0.100 (histogram)

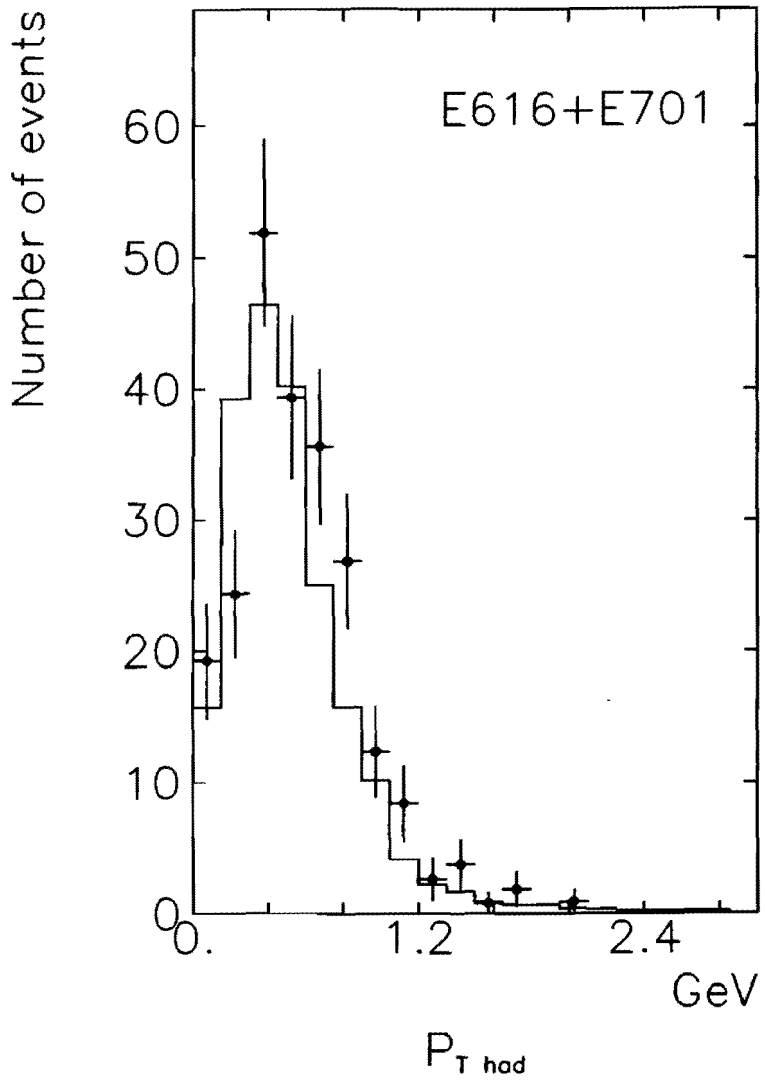

Figure 7.15 Distribution of the transverse second muon momentum with respect to the hadron shower direction for data events with the subtracted background (points with error bars) and Monte Carlo generated events with κ=0.42, m_c=1.5GeV/c^2, ε=0.19, and $B_1(c\to\mu X)$=0.100 (histogram)

7.8 Conclusions

This thesis has described the analysis of the like-sign and opposite-sign neutrino and antineutrino induced dimuon events collected in two Fermilab experiments(E616 and E701) using the Lab E detector.

The 18 observed like-sign dimuon events with muon momentum cut of 9 GeV/c have a calculated background of 11.4±2.2 events. This yields an average rate for prompt like-sign dimuon production of $1.0\pm0.7\times10^{-4}$ per single muon event. Some of the distributions of the kinematic variables indicate that the background from the hadron shower is not the only source of the like-sign dimuon events.

The observed rates and kinematic distributions of opposite-sign dimuon signal are consistent with the single charm production model in which the produced charm quarks fragment into charm particles, which subsequently decay semileptonically into muons. The fully corrected rate with respect to single muon events reaches a value of $9.0\pm1.1\times10^{-3}$ at E_ν=200 GeV.

The comparison of the data (corrected for background) and the charm production model yields a value for the fraction of the strange sea in the nucleon $\kappa = 0.42^{+0.15}_{-0.13}$, where $\kappa = 2s(x)/(\bar{u}(x)+\bar{d}(x))$, and errors include uncertainties due to statistics, hadron shower background subtraction, charm quark mass and fragmentation.

The κ parameter is found to be energy dependent. The values are $\kappa=0.19^{+0.18}_{-0.14}$ in the energy range 30-100 GeV, and $\kappa=0.52^{+0.17}_{-0.15}$ in the energy range 100 -230 GeV. The possible sources of this energy dependence were discussed.

The opposite-sign dimuon data were also used to measure the average semileptonic branching ratio of neutrino produced charm particles decaying into muons. The measured value of $0.093^{+0.022}_{-0.020}$ is consistent with the results extracted from the e^-e^+ and ν-emulsion experiments.

References:

1.1 B.Aubert et al., Proc. XIV Int. Conf. on High Energy Physics, London 1974
1.2a J.J.Aubert et al., Phys. Rev. Lett. 33,1404(1974)
1.2b J.-E.Augustin et al., Phys. Rev. Lett. 33,1406(1974)

1.3a A.Benvenuti et al., Phys. Rev. Lett. 34,419(1975)
1.3b A.Benvenuti et al., Phys. Rev. Lett. 35,1199(1975)
1.3c A.Benvenuti et al., Phys. Rev. Lett. 35,1203(1975)
1.3d B.C.Barish et al., Phys. Rev. Lett. 36,939(1976)
1.3e A.Benvenuti et al., Phys. Rev. Lett. 38,1110(1977)
1.3f M.Holder et al., Phys. Lett. 69B,377(1977)
1.3g B.C.Barish et al., Phys. Rev. Lett. 39,981(1977)

1.4 S.L.Glashow, J.Iliopoulos, and L.Maiani, Phys. Rev. D2,1285(1970)
1.5 M.K.Gaillard, NAL-Conf-74/43-THY (FNAL preprint) and Proc. IV Int. Conf. on Neutrino Physics and Astrophysics, Philadelphia, USA, 1974
1.6a L.N.Chang, E.Derman and J.N.Ng, Phys. Rev. Lett. 35,6(1975)
1.6b C.H.Albright, Fermilab-Pub-75/35-THY (1975)

1.7a R.W.Brown and J.Smith, Phys. Rev. D3,207(1971)
1.7b R.W.Brown, R.H.Hobbs and J.Smith, Phys. Rev. D4,794(1971)
1.7c S.L.Adler, J.B.Healy and I.Karliner, Princeton Univeristy preprint COO-2220-51 (1975)
1.8a V.Barger, T.Weiler and R.J.N.Phillips, University of Wisconsin preprint, COO-881459 (1975)
1.8b A.DeRujula, H.Georgi and S.L.Glashow, Phys. Rev. Lett. 35,69(1975)
1.8c H.Fritzsch and P.Minkowski, Caltech preprint CALT-68-503 (1975)
1.9 H.Abramowicz et al., Z.Phys. C15,19(1982)

1.10 M.Jonker et al., Phys. Lett. 107B,241(1981)

1.11 A.Benvenuti et al., Phys. Rev. Lett. 41,1204(1978)

1.12a C.Baltay et al., submitted to Phys. Rev. Lett.
1.12b H.C.Ballagh et al., Phys. Rev. Lett. 24,7(1981)
1.12c C.Baltay et al., Phys. Rev. Lett. 39,62(1977)
1.12d J.Blietschau et al., Phys. Lett. 60B,207(1976)
1.12e H.Deden et al., Phys. Lett. 58B,361(1975)

1.13a M.Holder et al. Phys. Lett. 70B,396(1977)
1.13b A.Benvenuti et al.,Phys. Rev. Lett. 41,725(1978)
1.13c J.G.H de Groot et al., Phys. Lett. 86B,103(1979)
1.13d T.Trinko et al., Phys. Rev. D23,1889(1981)
1.13e K.Nishikawa et al., Phys. Rev. Lett. 46,1555(1981)
1.13f K.Nishikawa et al., Phys. Rev. Lett. 54,1336(1985)

1.14a A.C.Shaffer, Ph.D. Thesis, Columbia University, 1985, Nevis report no. R-1326 (CU-356, Nevis 250)
1.14b A.Haatuft et al., CERN-EP/83-16 (1983)
1.14c V.V.Ammosov et al., Phys. Lett. 106B,151(1981)

1.15a R.M.Barnett, Phys. Rev. Lett. 36,1163(1976)
1.15b H.Georgi and H.D.Politzer, Phys. Rev. D14,1829(1976)
1.15c J.Kaplan and F.Martin, Nucl. Phys. B115,333(1976)
1.15d A.DeRujula, H.Georgi and H.D.Politzer, Phys. Rev. D15,2495(1977)
1.16 R.Brock, Phys. Rev. Lett. 44,1027(1980)

1.17 B.J.Edwards and T.D.Gottschalk, Nucl. Phys. B186,309(1981)
1.18 C.H.Lai, Phys. Rev. D18,1422(1978)

1.19 H.E.Fisk and F.Sciulli, Ann. Rev. Part. Sci. 32,499(1982)
2.1 D.A.Edwards and F.Sciulli, Fermilab TM-660 (unpublished)
2.2 R.Blair et al., Nucl. Instr. Meth. 226,281(1984)

2.3 A.Bodek et al., Z.Phys. C18,283(1983)

2.4 J.R.Lee, "Measurements of νN Charged Current Cross Sections from E_ν = 25 GeV to E_ν = 260 GeV", Ph.D. Thesis, Caltech (1980)
2.5 R.Blair, "A Total Cross Section and y Distribution Measurement for Muon Type Neutrinos and Antineutrinos on Iron",Ph.D. Thesis, Caltech (1982)

2.6 C.Haber, "A Search for the Inclusive Oscillations of Muon Neutrinos" Ph.D. Thesis, Columbia University (1985), R-1328 CU-358, NEVIS-252

2.7 B.C.Barish et al., IEEE Trans. on Nucl. Sci. NS-25,532(1978)
3.1 D.MacFarlane, "Nucleon Structure from Neutrino Interactions in an Iron Target with a Study of the Singlet Quark Distribution", Ph.D. Thesis, Caltech (1984), Nevis Preprint R#1297

3.2 M.V.Purohit, "Nucleon Structure Functions from ν_μ-Fe Interactions and a Study of the Valence Quark Distribution", Ph.D. Thesis, Caltech (1984), Nevis Preprint R#1298

4.1a P.C.Bosetti et al., Nucl. Phys. B149,13(1979)
4.1b H.Deden et al., Nucl. Phys. B198,365(1982)
4.1c BEBC collaboration, private communication.

4.2 M.Arneodo et al., Phys. Lett. 150B,458(1985)

4.3 M.Shaevitz, private communication

4.4 T.Sjostrand, Computer Physics Communications 27,243(1982)
4.5 J.P.Albanese et al., paper submitted to Cornell (#317)

4.6a J.Ritchie, "Hadronic Charm Production by Protons and Pions on Iron", Ph.D. Thesis, University of Rochester (1983), UR-861
4.6b B.Peyaud, "Experimental Study of Like-Sign Dimuon and of Trimuon Events Produced in High Energy Neutrino and Antineutrino Interactions" , Ph.D. Thesis, CEN Saclay (1981), Note CEA-N-2324

4.7a S.P.Denisov et al., Nucl. Phys. B61,61(1973)
4.7b J.C.Allaby et al., Sov. Journal of Nucl. Phys. 13,295(1971)
4.7c A.S.Carroll et al., Phys. Lett. 80B,319(1979)

4.8a D.Allasia et al., Z.Phys. C24,119(1984)
4.8b D.Allasia et al., Phys. Lett. 124B,543(1983)

4.9 P.Allen et al., Nucl. Phys. B214,369(1983)

4.10 J.P.Albanese et al., Phys. Lett. 144B,302(1984)

4.11 J.P.Albanese et al., Phys. Lett. 149B,415(1984)

4.12 A.Ardridson et al., Nucl. Phys. B246,381(1984)

4.13 T.H.Burnett et al., Phys. Lett. 77B,443(1978)

4.14 G.T.Jones et al., Z.Phys. C27,43(1985)

4.15 A.E.Brenner et al., Phys. Rev. D26,1497(1982)

4.16 A.M.Cnops et al., Proc. Rencontre de Moriond, Les Arcs, France, 1978

4.17 D.Allasia et al., Nucl. Phys. B224,1(1983)

4.18 P.Bosetti et al., Nucl. Phys. B209,29(1982)

4.19 M.Arneodo et al., Phys. Lett. 145B,156(1984)

4.20 E.Wolin, "Neutral Strange Particle Production in High-Energy Neutrino Interactions", Ph.D. Thesis, University of Washington, Seattle, VTL-PUB-98 (1984)

5.1 A.J.Buras and K.J.F.Gaemers, Nucl. Phys.B132,249(1978)

5.2a J.D.Bjorken, Phys. Rev. D17,171(1978)
5.2b M.Suzuki, Phys. Lett. 71B,189(1977)

5.3 J.M.Izen, DESY 84-104(1984) and in Proc. of the XV Symposium on Multiparticle Dynamics, Lund 1984
5.4 J.Dorfan, SLAC-PUB-3250(1983)

5.5 H.Albrecht et al., DESY 84-073(1984)

5.6 K.Kleinknecht and B.Renk, Z.Phys. C17,325(1983)

5.7 C.Peterson et al., Phys. Rev. D27,105(1983)

5.8 V.G.Kartvelishvili et al., Yad. Fiz. 38,1563(1983)

5.9a C.Bebek et al., Phys. Rev. Lett. 49,430(1982)
5.9b P.Avery et al., Phys. Rev. Lett. 51,1139(1983)

5.10 H.Yamamoto et al., SLAC-PUB-3498/CALT-68-1206(1984)

5.11 N.Ushida et al., Phys. Lett. 121B,292(1983)

5.12 N.Ushida et al., Phys. Lett. 121B,287(1983)

5.13 R.M.Baltrusaitis et al., Phys. Rev. Lett. 54,1976(1985)

5.14 R.H.Shindler et al., Phys. Rev. D24,78(1981)

5.15 G.Kalmus, Proc. XXI Int. Conf. on High Energy Physics, Paris, France, 1982

5.16a M.Aguilar-Benitez et al., Phys. Lett. 123B,98(1984)
5.16b M.Aguilar-Benitez et al., Phys. Lett. 123B,103(1984)

5.17a V.Barger and R.J.N.Phillips, Phys. Rev. D14,80(1976)
5.17b V.Barger, T.Gottschalk and R.J.N.Phillips, Phys. Rev. D16,746(1977)
5.18 M.Bacino et al., Phys. Rev. Lett. 43,1073(1979)

5.19a F.W.Brasse, Proc. XX Conference on High Energy Physics, Madison 1980
5.19b J.J.Aubert et al., Phys. Lett. 95B,306(1980)

5.20a D.Allasia et al., Z.Phys. C27,239(1985)
5.20b G.T.Jones et al., MPI-PAE/Exp.E1.128(1984)
5.20c H.Deden et al., Nucl. Phys. B181,375(1981)

6.1 T.Hansl et al., Nucl. Phys. B142,381(1978)

6.2 V.Barger, W.Y.Keung and R.J.N.Phillips, Phys. Rev. D25,1803(1982)
6.3 V.Barger, T.Gottschalk and R.J.N.Phillips, Phys. Rev. D18,2308(1978)
6.4 G.L.Kane, J.Smith and J.A.M.Vermaseren, Phys. Rev. D19,1978(1979)

6.5 B-L.Young, T.V.Walsh and T.C.Yang, Phys. Lett. 74B,111(1978)
6.6 V.Barger, W.Y.Keung and R.J.N.Phillips, Phys. Rev. D24,244(1981)

6.7 A.Bodek at al., Phys. Lett. 113B,77(1982)

6.8 H.Goldberg, Phys. Rev. Lett. 39,1598(1977)

6.9 R.J.N.Phillips, Nucl. Phys. B153,475(1979)

6.10 A.Bodek et al., Phys. Lett. 113B,82(1982)

6.11 R.M.Godbole and D.P.Roy, Phys. Rev. Lett. 48,1711(1982)

6.12a V.Barger, T.Gottschalk, D.V.Nanopulos, and R.J.N.Phillips, Phys. Rev. D16,3177(1977)
6.12b V.Barger, T.Gottschalk, and R.J.N.Phillips, Phys. Rev. D17,2284(1978)
6.12c V.Barger, T.Gottschalk, and R.J.N.Phillips, Phys. Rev. D18,2308(1978)
6.12d T.Hansl et al., Phys. Lett. 77B,114(1978)

6.13 J.Knobloch et al., Proc. XI Int. Conf. on Neutrino Physics and Astrophysics, Maui, Hawaii, vol.I, p.421, 1981

7.1 B.Renk, "Untersuchung von Multimyon-Endzustanden in Tiefinelastischer Neutrinostreuung", Ph.D. Thesis, Univeristy of Dortmund, Dortmund, West Germany, 1984.

7.2 D.MacFarlane et al., Z.Phys. C26,1(1984)

7.3 E.Eichten et al., Rev. Mod. Phys. 56,579(1984)

7.4 N.N.Nikolaev, Tokyo U. preprint INS-539, May 1985

Appendix A

Participants in the CCFRR Collaboration

A.Bodek, F.Borcherding, N.Giokaris, I.E.Stockdale, K.Lang

Department of Physics and Astronomy

University of Rochester, Rochester, New York 14627

P.Auchincloss, R.Blair, C.Haber, S.Mishra, M.Ruiz,

F.J.Sciulli, M.Shaevitz, W.H.Smith, R.Zhu

Physics Department,

Columbia University, New York, New York 10027

R.Coleman, H.E.Fisk, Y.Fukushima, Q.Kerns, B.Jin,

D.Levinthal, T.Kondo, W.Marsh, P.A.Rapidis, S.Segler,

R.Stefanski, D.Theriot, H.B.White, D.Yovanovitch

Fermi National Accelerator Laboratory,

Batavia, Illinois 60510

D.Garfinkle, F.S.Merrit, M.Oreglia, P.Reutens
Enrico Fermi Institute,
University of Chicago, Chicago, Illinois 60637

O.Fackler, K.Jenkins
Rockefeller University, New York, New York 10021

Y.K.Chu, D.B.MacFarlane, R.L.Messner, D.B.Novikoff,
M.V.Purohit
California Institute of Technology, Pasadena, CA 91125

Appendix B

Parametrization of the BEBC Fragmentation Functions

The fragmentation functions provided by the BEBC collaboration for ν-Ne interactions were parametrized by the constraining the fit so that the multiplicity in each W^2 bins remains unchanged.

For all negative particles the following form was used:

$$D^-(z,W^2)=a_3\times[\log W^2 + a_4]^{a_5} \times \exp(a_1 z+a_2 z^2)$$

where,

a_1 = -13.2687

a_2 = 5.8750

a_3 = 15.959

a_4 = -1.7337

a_5 = 0.6620

For all positive particles the following form was used:

$$D^{+}(z,W^2) = 10^{-2}\times\{a_5(\log W^2)^2 + a_6 + a_7\log W^2\}\times\exp(p(z))$$

where

$$p(z) = a_1/(a_2+z) + a_3/(a_4 + z)^2$$

and

$a_1 = -1.849$

$a_2 = 11.5261$

$a_3 = 0.1406$

$a_4 = 0.0586$

$a_5 = 0.0096$

$a_6 = 84.5339$

$a_7 = 19.7486$.

Appendix C

Multiplicities Used in the Background Calculations

Table C.1 contains multiplicities obtained with the Lund Monte Carlo with two changed parameters (E_{min}=0.2 GeV and λ=0.2, see Chapter 4 for details). For comparison, Table C.2 contains multiplicities obtained by convoluting the BEBC and EMC fragmentation functions.

Table C.1 : Mean multiplicities of particles obtained with the Lund Monte Carlo program and used in the background calculation as the function of invariant hadronic mass W^2.

W^2:	7.0	22.5	49.9	89.6	164.9 [GeV^2]
π^-_+:	0.72	1.35	1.84	2.18	2.60
π^-_-:	1.30	1.95	2.45	2.85	3.21
K_+:	0.02	0.10	0.15	0.18	0.21
K_-:	0.08	0.14	0.18	0.21	0.24
p^-:	0.00	0.03	0.07	0.09	0.12
p_-:	0.61	0.66	0.70	0.73	0.77
n^-:	0.00	0.03	0.06	0.08	0.11
n_o:	0.39	0.41	0.43	0.44	0.47
K^o_L:	0.04	0.12	0.14	0.19	0.21

Table C.2 : Mean multiplicities of particles obtained from fits to the BEBC and EMC fragmentation functions versus invariant hadronic mass W^2.

W^2:	9.5	24.0	47.0	92.0	180.0 [GeV^2]
π^-:	0.64	1.34	1.74	2.10	2.43
π^+:	2.05	2.34	2.55	2.76	2.97
K^-:	0.05	0.10	0.13	0.15	0.18
K^+:	0.17	0.20	0.22	0.23	0.25
p^-:	0.07	0.14	0.18	0.21	0.25
p_+:	0.46	0.52	0.57	0.62	0.66
n^-:	0.07	0.14	0.18	0.21	0.25
n_o:	0.46	0.52	0.57	0.62	0.66
K^o_L:	0.11	0.15	0.17	0.19	0.22

Appendix D

Muon Rates from E379

Muon production rates ($R_1(p_{cut}$, $R_2(p_{cut})$) from the Fermilab experiment E379 (at the target densities ρ_1=6.12 g/cm^3 (λ^A_{int}=1.266λ_{int}^{Fe}) and ρ_2=3.06 g/cm^3 (λ^B_{int}=2.533λ_{int}^{Fe}) are presented below. The results given for the momentum cut of 4.26 GeV/c (range of 3.11 m iron equivalent material) are the mean of μ^- and μ^+ rates because sign determination was not possible at this momentum cut.

The data were taken with a π^- beam incident on a variable density calorimeter. The muon momenta of 4.26, 8.45, 9.45, 15.45, and 20.45 GeV/c include a correction for the energy loss (dE/dx) in the iron, and are defined with respect to the beginning of the calorimeter (not with respect to the interaction point). This definition simulates muons produced in secondary interactions from primary neutrino interactions.

Table D.1 a : Sum of $\mu^+ + \mu^-$ rates from Fermilab experiment E379 for a muon momentum cut of 4.26 GeV/c (or 3.11 m of iron equivalent material) and 4 energies of the π^- beam at two target densities of ρ_1=6.12 g/cm^3 and ρ_2=3.06 g/cm^3:

Momentum cut (GeV/c)	Beam Energy (GeV)	$\mu^+ + \mu^-$ rate ρ_1 $\times 10^3$	ρ_2
4.26	40.	0.900±0.060	1.390±0.080
	75.	1.924±0.070	3.210±0.150
(3.11 of	150.	4.220±0.170	7.030±0.290
iron)	225.	6.340±0.270	11.070±0.480

Table D.1 b : μ^+ rates from Fermilab experiment E379 for a muon momentum cut of 8.45 GeV/c and 4 energies of the π^- beam at two target densities of ρ_1=6.12 g/cm^3 and ρ_2=3.06 g/cm^3:

Momentum cut (GeV/c)	Beam Energy (GeV)	μ^+ rate ρ_1 $\times 10^3$	ρ_2
8.45	40.	0.088±0.012	0.127±0.019
	75.	0.234±0.021	0.366±0.044
	150.	0.487±0.056	1.149±0.111
	225.	0.939±0.101	1.523±0.161

Table D.1 c : μ^- rates from Fermilab experiment E379 for a muon momentum cut of 8.45 GeV/c and 4 energies of the π^- beam at two target densities of ρ_1=6.12 g/cm^3 and ρ_2=3.06 g/cm^3:

Momentum cut (GeV/c)	Beam Energy (GeV)	μ^- rate ρ_1 $\times 10^3$	ρ_2
8.45	40.	0.115±0.014	0.179±0.023
	75.	0.247±0.022	0.451±0.049
	150.	0.547±0.060	0.915±0.099
	225.	0.777±0.092	1.574±0.164

Table D.1 d : μ^+ rates from Fermilab experiment E379 for a muon momentum cut of 9.45 GeV/c and 4 energies of the π^- beam at two target densities of ρ_1=6.12 g/cm^3 and ρ_2=3.06 g/cm^3:

Momentum cut (GeV/c)	Beam Energy (GeV)	μ^+ rate ρ_1 $\times 10^3$	ρ_2
9.45	40.	0.077±0.012	0.095±0.017
	75.	0.208±0.020	0.313±0.041
	150.	0.378±0.050	0.904±0.098
	225.	0.734±0.089	1.198±0.143

Table D.1 e : μ^- rates from Fermilab experiment E379 for a muon momentum cut of 9.45 GeV/c and 4 energies of the π^- beam at two target densities of ρ_1=6.12 g/cm^3 and ρ_2=3.06 g/cm^3:

Momentum cut (GeV/c)	Beam Energy (GeV)	μ^- rate ρ_1 $\times 10^3$	ρ_2
9.45	40.	0.062±0.015	0.133±0.020
	75.	0.146±0.016	0.260±0.037
	150.	0.384±0.050	0.585±0.079
	225.	0.561±0.078	0.941±0.127

Table D.1 f : μ^+ rates from Fermilab experiment E379 for a muon momentum cut of 15.45 GeV/c and 4 energies of the π^- beam at two target densities of ρ_1=6.12 g/cm^3 and ρ_2=3.06 g/cm^3:

Momentum cut (GeV/c)	Beam Energy (GeV)	μ^+ rate ρ_1 $\times 10^4$	ρ_2
15.45	40.	0.120±0.045	0.202±0.080
	75.	0.806±0.123	0.954±0.225
	150.	1.433±0.306	2.979±0.563
	225.	3.668±0.629	3.422±0.765

Table D.1 g : μ^- rates from Fermilab experiment E379 for a muon momentum cut of 15.45 GeV/c and 4 energies of the π^- beam at two target densities of ρ_1=6.12 g/cm^3 and ρ_2=3.06 g/cm^3:

Momentum cut (GeV/c)	Beam Energy (GeV)	μ^- rate ρ_1 $\times 10^4$	ρ_2
15.45	40.	-	-
	75.	0.581±0.104	1.114±0.243
	150.	1.433±0.306	1.809±0.439
	225.	3.237±0.591	4.790±0.905

Table D.1 h : μ^+ rates from Fermilab experiment E379 for a muon momentum cut of 20.45 GeV/c and 3 energies of the π^- beam at two target densities of ρ_1=6.12 g/cm^3 and ρ_2=3.06 g/cm^3:

Momentum cut (GeV/c)	Beam Energy (GeV)	μ^+ rate ρ_1 $\times 10^4$	ρ_2
20.45	40.	-	-
	75.	0.337±0.077	0.636±0.184
	150.	0.717±0.216	1.383±0.384
	225.	1.942±0.458	1.882±0.567

Table D.1 i : μ^- rates from Fermilab experiment E379 for a muon momentum cut of 20.45 GeV/c and 4 energies of the π^- beam at two target densities of ρ_1=6.12 g/cm^3 and ρ_2=3.06 g/cm^3:

Momentum cut (GeV/c)	Beam Energy (GeV)	μ^- rate ρ_1 $\times 10^4$	ρ_2
20.45	40.	-	-
	75.	0.112±0.046	0.265±0.119
	150.	0.717±0.216	1.170±0.353
	225.	2.266±0.494	3.422±0.765

Muon rates ($R(p_{cut})$) measured by the Fermilab experiment E379 interpolated to the density ρ=4.27 g/cm^3 (λ_{int}^{LE} = 1.764 λ_{int}^{Fe}) of the present experiment (Lab E apparatus) are shown in Table D.2. The expression

$$R(p_{cut}))=R_{prompt}(p_{cut}))+(\lambda^{LE}_{int}/\lambda^{A}_{int})R_{np}(p_{cut})$$

which is equivalent to

$$R(p_{cut})=R_1(p_{cut})+[R_1(p_{cut})-R_1(p_{cut})][\lambda^{LE}_{int}/(\lambda^{A}_{int}-\lambda_{Bint})]$$

was used. For momentum cut 4.26 GeV/c, where there were no sign determination, equal rates for μ^- and μ^+ were assumed.

Table D.2 : Muon rates for 5 momenta cuts and 4 beam energies from the Fermilab experiment E379 translated to the density of the Lab E apparatus of ρ=4.27 g/cm^3.

($\lambda_{int}^{LE} = 1.764\ \lambda_{int}^{Fe}$)

Momentum cut (GeV/c)	Beam Energy (GeV)	μ^+ rate	μ^- rate
		$\times 10^3$	
4.26	40.	0.597±0.036	0.597±0.036
	75.	1.348±0.062	1.348±0.062
(3.11 of	150.	2.953±0.125	2.953±0.125
iron)	225.	4.589±0.205	4.589±0.205
8.45	40.	0.111±0.017	0.153±0.020
	75.	0.313±0.037	0.369±0.040
	150.	0.884±0.093	0.768±0.086
	225.	1.289±0.140	1.255±0.140
9.45	40.	0.088±0.015	0.105±0.018
	75.	0.271±0.034	0.214±0.030
	150.	0.694±0.082	0.505±0.069
	225.	1.012±0.124	0.789±0.110
		$\times 10^4$	
15.45	40.	0.169±0.068	-
	75.	0.895±0.191	0.901±0.199
	150.	2.361±0.477	1.659±0.391
	225.	3.520±0.714	4.169±0.794
20.45	40.	-	-
	75.	0.516±0.151	0.204±0.097
	150.	1.117±0.327	0.989±0.307
	225.	1.906±0.526	2.960±0.670

Table D.3 contains fit parameters to the results in Table D.2. The rates have been parametrized in a simple form:

$$\text{rate} = a\times(1-p_{cut}/p_\pi)\times E_\pi^{\ b} \quad ,$$

where E_π and p_π are the pion beam energy and momentum, and a,b are constants.

Table D.3 : Parametrization constants for total muon rate versus energy from E379 translated to the density of Lab E deetector.

(ρ_{LE} = 4.27 g/cm^3 and $\lambda_{int}^{LE} = 1.764\ \lambda_{int}^{Fe}$)

(rate = $a\times(1-p_{cut}/p_\pi)\times E_\pi^{\ b}$)

Momentum cut (GeV/c)	μ^+ rate (total) $\times 10^3$	μ^- rate (total) $\times 10^3$
4.26 (3.11 of iron)	$a=(1.117\pm0.026)\times10^{-5}$ $b=1.118\pm0.005$	$a=(1.117\pm0.026)\times10^{-5}$ $b=1.118\pm0.005$
8.45	$a=(0.121\pm0.007)\times10^{-5}$ $b=1.307\pm0.012$	$a=(0.370\pm0.021)\times10^{-5}$ $b=1.082\pm0.012$
9.45	$a=(0.120\pm0.008)\times10^{-5}$ $b=1.265\pm0.014$	$a=(0.267\pm0.019)\times10^{-5}$ $b=1.057\pm0.015$
15.45	$a=(0.0205\pm0.0024)\times10^{-5}$ $b=1.408\pm0.024$	$a=(0.0544\pm0.0068)\times10^{-5}$ $b=1.208\pm0.025$
20.45	$a=(0.1030\pm0.0147)\times10^{-5}$ $b=0.975\pm0.029$	$a=(0.000132\pm0.000019)\times10^{-5}$ $b=2.286\pm0.030$

For completeness parameters for $\mu^- + \mu^+$ rate parametrized in the same form rate = $a\times(1-p_{cut}/p_\pi)\times E_\pi^{\ b}$ are shown in the next table.

Table D.4 : Parametrization constants for mean muon rates ($\mu^- + \mu^+$) from E379 at density of Lab E detector.

(ρ_{LE} =4.27 g/cm^3 and $\lambda_{int}^{LE} = 1.764\ \lambda_{int}^{Fe}$)

(rate = $a\times(1-p_{cut}/p_\pi)\times E_\pi^{\ b}$)

Momentum cut (GeV/c)	Fit parameters for rate($\mu^-+\mu^+$) = $a\times(1-p_{cut}/p_\pi)\times E_\pi^{\ b}$
4.26	$a=2\times(1.117\pm0.026)\times10^{-5}$ $b= 1.118\pm0.005$
8.45	$a=(0.431\pm0.018)\times10^{-5}$ $b= 1.192\pm0.009$
9.45	$a=(0.357\pm0.017)\times10^{-5}$ $b= 1.164\pm0.010$
15.45	$a=(0.143\pm0.012)\times10^{-5}$ $b= 1.164\pm0.017$
20.45	$a=(0.0117\pm0.0012)\times10^{-5}$ $b= 1.546\pm0.019$

Appendix E

Decay and Interaction Lengths of Pions and Kaons

The scaling of inelastic cross sections measured on copper [4.7] yields

$\sigma(\pi^+Fe) = \sigma(\pi^-Fe) = 584$ mb $\qquad p > 22$ GeV/c

$= (678 - 4.2p)$ mb $\qquad p \leq 22$ GeV/c

where p is pion momentum in GeV/c.

and

$\sigma(K^+Fe) = 509$ mb

$\sigma(K^-Fe) = 528$ mb

with no momentum dependence.

These numbers correspond to the following values of interaction (absorption) lengths:

$\lambda(\pi^\pm Fe) = 20.23$ cm $\qquad p > 22$ GeV/c

$= 1.182\times10^4/(678-4.2p)$ cm $\qquad p \leq 22$ GeV/c

where p is pion momentum in GeV/c. At 10 GeV/c λ is 18.58 cm. For kaons

$\lambda(K^+Fe) = 23.21$ cm

$\lambda(K^-Fe) = 22.38$ cm

The above results translated to the density of the Lab E apparatus of $\rho_{LE} = 4.27\ g/cm^3$ ($\lambda_{int}=1.764\lambda_{int}^{Fe}$) give:

$$\lambda(\pi^{\pm}) = 35.69\ cm \qquad p > 22\ GeV/c$$
$$= 2.085 \times 10^4/(678-4.2p)\ cm \qquad p \leq 22\ GeV/c$$
$$\lambda(K^+) = 40.94\ cm$$
$$\lambda(K^-) = 39.48\ cm$$

Note that a correction to account for the fact that 8.5% of the material in the lab E detector consisted of scintillator and other low atomic mass materials was applied (i.e. $\lambda_{int}=1.764\lambda_{int}^{Fe}$ and not $(\rho_{Fe}/\rho_{LE})\times\lambda_{int}$ where $\rho_{Fe}=7.87\ g/cm^3$).

To calculate ratio of interaction length to decay length the values $c\tau(C)=780.4$ cm and $c\tau(K)=370.9$ cm were taken. This gave:

$$\pi: \quad \lambda_{int}/\lambda_{decay} = (6.384/E_{\pi}) \times 10^{-3} \qquad p_{\pi} > 22\ GeV/c$$
$$= 3.730/(E_{\pi}(678-4.2E_{\pi})) \qquad p_{\pi} \leq 22\ GeV/c$$

In the case of kaons two decay modes were taken into account

$K^{\pm} \rightarrow \mu^{\pm}\nu$ with branching ratio 63.5%,

$K^{\pm} \rightarrow \pi^{\pm}\pi^{o}$ with branching ratio 21.16%.

but $\pi^{\pm} \rightarrow \mu^{\pm}\nu$ with ≈100% branching ratio. Neglecting the mass difference between charged and neutral pions it was

assumed that the charged pion carries 50% of kaon momentum. Therefore:

$$K^+: \frac{\lambda_{int}}{\lambda_{decay}} = 0.635 \times \frac{5.449\times10^{-2}}{E_K} + 0.212 \times \left(\frac{\lambda_{int}}{\lambda_{decay}}\right)\Bigg|_{@E_{\pi}=0.5E_K}^{\pi}$$

$$K^-: \frac{\lambda_{int}}{\lambda_{decay}} = 0.635 \times \frac{5.255\times10^{-2}}{E_K} + 0.212 \times \left(\frac{\lambda_{int}}{\lambda_{decay}}\right)\Bigg|_{@E_{\pi}=0.5E_K}^{\pi}$$

Appendix F

Mean x Values Used in the Background Calculation

Seven intervals in x ($x=x_{Bj}$) were used. The calculated mean value of x_{Bj} in each interval is

$$\langle x \rangle = \int x F_2(x)\, dx$$

where

$$F_2(x) = 37.8x(1-x)^5 + 0.6(1-x)^5$$

$F_2(x)$ is the nucleon structure function normalized such that $\int x F_2(x) dx = 1$ (integrated from x=0 to x=1). The table below shows the x intervals and the mean x values.

Table F.1 : The 7 x intervals used for the background calculations and the mean values of x.

Interval	< x >
0.000-0.050	0.029
0.050-0.100	0.076
0.100-0.150	0.125
0.150-0.200	0.174
0.200-0.250	0.225
0.250-0.450	0.334
0.450-1.000	0.537

Appendix G

Final Tables and Fits of the Muon Rates from Neutrino and Antineutrino Showers

The final muon rates from neutrino and antineutrino showers were parametrized as a function of the hadron shower energy E_H and momentum cut of the muon p_{cut} in the following form:

$$P(\mu) = 10^{-4}\, A\, E_H^{\,B} \exp(-f\, p_{cut})$$

where, $f = C/E_H + D$, and A,B,C,D are constants.

As described in Chapter 4, the calculations were performed in 7 x_{Bj} bins for neutrino and antineutrino induced showers. Tables G.1-G.8 contain all the fit parameters for the rates calcualated with the Lund Monte Carlo fragmentation functions (with E_{min}=0.2 GeV and λ=0.2, as discussed in Chapter4) and with data from the Fermilab experiment E379 (see Appendix D). These are for a density

$\rho_{LE} = 4.27$ g/cm^3 ($\lambda_{int}^{LE} = 1.764\ \lambda_{int}^{Fe}$). Note that the results for all values of x are similar, and that the use of the x=0.2 parametrization yields a good description of the calculation at all values of x.

These tables are followed by detailed tables containing results from the hadron shower background calculation (at $x_{Bj} = 0.175$). Shown are rates of muons due to various particles from primary decays and secondary interactions. (all for the Lab E detector density of $\rho_{LE} = 4.27$ g/cm^3).

TABLE G.1 : CONSTANTS USED TO PARAMETRIZE POSITIVE MUON RATES FROM NEUTRINO INDUCED SHOWERS FOR 7 X BINS FOR MUON MOMENTUM CUT IN THE RANGE 4.26-9.45 GEV/C.

X BIN	A	B	C	D
.000-.049	7.2336	.4443	4.8086	.2284
.050-.099	7.2683	.4433	4.7868	.2285
.100-.149	7.3354	.4416	4.7649	.2288
.150-.199	7.4163	.4389	4.7470	.2286
.200-.249	7.4855	.4370	4.7251	.2287
.250-.449	7.7355	.4297	4.6838	.2286
.450-1.00	8.4489	.4097	4.6350	.2274

TABLE G.2 : CONSTANTS USED TO PARAMETRIZE NEGATIVE MUON RATES FROM NEUTRINO INDUCED SHOWERS FOR 7 X BINS FOR MUON MOMENTUM CUT IN THE RANGE 4.26-9.45 GEV/C.

X BIN	A	B	C	D
.000-.049	5.6228	.4930	6.6581	.2343
.050-.099	5.6585	.4911	6.6412	.2340
.100-.149	5.6445	.4918	6.6120	.2341
.150-.199	5.6760	.4902	6.5901	.2339
.200-.249	5.6880	.4897	6.5634	.2338
.250-.449	5.7273	.4876	6.5050	.2335
.450-1.00	5.7160	.4845	6.3939	.2315

TABLE G.3 : CONSTANTS USED TO PARAMETRIZE POSITIVE MUON RATES FROM NEUTRINO INDUCED SHOWERS FOR 7 X BINS FOR MUON MOMENTUM CUT IN THE RANGE 9.45-20.45 GEV/C.

X BIN	A	B	C	D
.000-.049	8.0084	.1799	6.3917	.0892
.050-.099	8.1272	.1768	6.3783	.0892
.100-.149	7.9497	.1810	6.3362	.0893
.150-.199	8.0383	.1786	6.3136	.0893
.200-.249	8.0591	.1781	6.2820	.0895
.250-.449	8.1573	.1746	6.2119	.0895
.450-1.00	8.6548	.1609	6.0609	.0896

TABLE G.4 : CONSTANTS USED TO PARAMETRIZE NEGATIVE MUON RATES FROM NEUTRINO INDUCED SHOWERS FOR 7 X BINS FOR MUON MOMENTUM CUT IN THE RANGE 9.45-20.45 GEV/C.

X BIN	A	B	C	D
.000-.049	4.2157	.2993	7.8943	.0933
.050-.099	4.2484	.2977	7.8701	.0933
.100-.149	4.2377	.2980	7.8381	.0934
.150-.199	4.2574	.2969	7.8077	.0934
.200-.249	4.2697	.2964	7.7721	.0935
.250-.449	4.2972	.2944	7.6928	.0935
.450-1.00	4.4322	.2861	7.5256	.0932

TABLE G.5 : CONSTANTS USED TO PARAMETRIZE POSITIVE MUON RATES FROM ANTINEUTRINO INDUCED SHOWERS FOR 7 X BINS FOR MUON MOMENTUM CUT IN THE RANGE 4.26-9.45 GEV/C.

X BIN	A	B	C	D
.000-.049	8.1619	.4168	7.0216	.2255
.050-.099	8.0723	.4190	6.9930	.2254
.100-.149	8.0047	.4209	6.9620	.2254
.150-.199	7.9331	.4235	6.9254	.2259
.200-.249	7.8452	.4258	6.8890	.2259
.250-.449	7.6653	.4311	6.8010	.2263
.450-1.00	7.1888	.4444	6.5942	.2270

TABLE G.6 : CONSTANTS USED TO PARAMETRIZE NEGATIVE MUON RATES FROM ANTINEUTRINO INDUCED SHOWERS FOR 7 X BINS FOR MUON MOMENTUM CUT IN THE RANGE 4.26-9.45 GEV/C.

X BIN	A	B	C	D
.000-.049	6.5052	.4644	5.2526	.2319
.050-.099	6.5140	.4645	5.2256	.2322
.100-.149	6.5079	.4654	5.1937	.2326
.150-.199	6.5155	.4654	5.1633	.2328
.200-.249	6.5222	.4656	5.1301	.2330
.250-.449	6.5828	.4641	5.0581	.2332
.450-1.00	6.8345	.4563	4.9084	.2332

TABLE G.7 : CONSTANTS USED TO PARAMETRIZE POSITIVE MUON RATES FROM ANTINEUTRINO INDUCED SHOWERS FOR 7 X BINS FOR MUON MOMENTUM CUT IN THE RANGE 9.45-20.45 GEV/C.

X BIN	A	B	C	D
.000-.049	8.9139	.1586	8.4950	.0894
.050-.099	8.8756	.1600	8.4690	.0895
.100-.149	8.7151	.1637	8.4339	.0895
.150-.199	8.6467	.1655	8.4021	.0896
.200-.249	8.5443	.1684	8.3654	.0898
.250-.449	8.2415	.1755	8.2735	.0898
.450-1.00	7.5784	.1919	8.0507	.0902

TABLE G.8 : CONSTANTS USED TO PARAMETRIZE NEGATIVE MUON RATES FROM ANTINEUTRINO INDUCED SHOWERS FOR 7 X BINS FOR MUON MOMENTUM CUT IN THE RANGE 9.45-20.45 GEV/C.

X BIN	A	B	C	D
.000-.049	6.7765	.2035	6.7998	.0888
.050-.099	6.9886	.1965	6.8058	.0883
.100-.149	6.7292	.2053	6.7464	.0889
.150-.199	6.7114	.2060	6.7177	.0890
.200-.249	6.6976	.2067	6.6841	.0891
.250-.449	6.6668	.2084	6.6025	.0895
.450-1.00	6.7984	.2047	6.4222	.0899


```
*****************************************************************************
********** MOMENTUM CUT =  4 26          MEAN X =    1748 **********
*****************************************************************************

--> HADRON ENERGY =  10.0     ---> MEAN WSQ =  16 360

          PRIMARY-MU+          PRIMARY-MU-          SHOWER-MU+          SHOWER-MU-          SUM-MU+          SUM-MU-
PIMIN   0.                   32403E-04            43598E-06            11911E-05           43598E-06        33594E-04
PIPOS   0.  82143E-04     0                       31891E-05            12252E-05           85332E-04        12252E-05
KAMIN   0.                0  10363E-04           10194E-06            29537E-06           10194E-06        10658E-04
KAPOS   0.  38394E-04     0                       11711E-05            45336E-06           39569E-04        45336E-06
PRMIN   0.                0                       10641E-07            88809E-07           10641E-07        88809E-07
PRPOS   0                 0                       10135E-05            12043E-06           10135E-05        12043E-06
NEMIN   0                 0                       22718E-07            62745E-07           22718E-07        62745E-07
NEPOS   0                 0                       25831E-06            88898E-07           25831E-06        88898E-07
KZERO   0.  22603E-07                             15771E-06            44674E-06           18032E-06        44752E-06
                                                                                                                
ALL NEGATIVE: DECAY   42767E-04   SHOWER   39727E-05   TOTAL   46739E-04
ALL POSITIVE: DECAY   12056E-03   SHOWER   63609E-05   TOTAL   12692E-03
SUMMARY PCUT-EHAD-X-WSQ   4 260   10 000   175   16 360   MU-/MU+/TOTAL   46739E-04   12692E-03   17366E-03

--> HADRON ENERGY =  15 0     ---> MEAN WSQ =  24 100

          PRIMARY-MU+          PRIMARY-MU-          SHOWER-MU+          SHOWER-MU-          SUM-MU+          SUM-MU-
PIMIN   0                    84269E-04            19353E-05            42695E-05           19353E-05        88539E-04
PIPOS   0   17617E-03     0                       10419E-04            50413E-05           18658E-03        50413E-05
KAMIN   0                 0  36008E-04           54857E-06            12825E-05           54857E-06        37291E-04
KAPOS   0   81055E-04     0                       35246E-05            17171E-05           84580E-04        17171E-05
PRMIN   0                 0                       36892E-07            38404E-06           36892E-07        38404E-06
PRPOS   0                 0                       31589E-05            49587E-06           31589E-05        49587E-06
NEMIN   0                 0                       12194E-06            27102E-06           12194E-06        27102E-06
NEPOS   0                 0                       85725E-06            38524E-06           85725E-06        38524E-06
KZERO   0   24753E-06                            73630E-06            16649E-05           98384E-06        17780E-05
                                                                                                                
ALL NEGATIVE  DECAY   12039E-03   SHOWER   15512E-04   TOTAL   13590E-03
ALL POSITIVE  DECAY   25747E-03   SHOWER   21359E-04   TOTAL   27883E-03
SUMMARY PCUT-EHAD-X-WSQ   4 260   15 000   175   24 100   MU-/MU+/TOTAL   13590E-03   27883E-03   41473E-03

--> HADRON ENERGY =  20 0     ---> MEAN WSQ =  31 840

          PRIMARY-MU+          PRIMARY-MU-          SHOWER-MU+          SHOWER-MU-          SUM-MU+          SUM-MU-
PIMIN   0                    13550E-03            47368E-05            91800E-05           47368E-05        14468E-03
PIPOS   0   25007E-03     0                       20931E-04            11604E-04           27100E-03        11604E-04
KAMIN   0                 0  65229E-04           14428E-05            29417E-05           14428E-05        68171E-04
KAPOS   0   11326E-03     0                       65705E-05            36683E-05           11983E-03        36683E-05
PRMIN   0                 0                       14837E-06            87768E-06           14837E-06        87768E-06
PRPOS   0                 0                       58254E-05            10860E-05           58254E-05        10860E-05
NEMIN   0                 0                       31545E-06            61353E-06           31545E-06        61353E-06
NEPOS   0                 0                       16567E-05            87840E-06           16567E-05        97840E-06
KZERO   0   38918E-06                            23690E-06            35061E-05           21732E-05        37430E-05
                                                                                                                
ALL NEGATIVE  DECAY   20096E-03   SHOWER   34356E-04   TOTAL   23532E-03
ALL POSITIVE  DECAY   36373E-03   SHOWER   43411E-04   TOTAL   40714E-03
SUMMARY PCUT-EHAD-X-WSQ   4 260   20 000   175   31 840   MU-/MU+/TOTAL   23532E-03   40714E-03   64245E-03
```

********** MOMENTUM CUT = 4.26 MEAN X = 1748 **********

--> HADRON ENERGY = 30.0 ---> MEAN WSQ = 47 320

	PRIMARY-MU+	PRIMARY-MU-	SHOWER-MU+	SHOWER-MU-	SUM-MU+	SUM-MU-
PIMIN	0	22555E-03	13984E-04	23235E-04	13984E-04	24878E-03
PIPOS	35905E-03	0	48424E-04	31413E-04	40747E-03	31413E-04
KAMIN	0	11703E-03	44111E-05	75941E-05	44111E-05	12462E-03
KAPOS	15516E-03	0	13467E-04	88125E-05	16862E-03	88125E-05
PRMIN	0	0	45795E-06	23059E-05	45795E-06	23059E-05
PRPOS	0	0	11443E-04	26021E-05	11443E-04	26021E-05
NEMIN	0	0	95490E-06	15817E-05	95490E-06	15817E-05
NEPOS	0	0	34147E-05	21918E-05	34147E-05	21918E-05
KZERO	13475E-05	93372E-06	49895E-05	82804E-05	63370E-05	92141E-05

ALL NEGATIVE DECAY 34351E-03 SHOWER 88016E-04 TOTAL 43153E-03
ALL POSITIVE DECAY 51555E-03 SHOWER 10155E-03 TOTAL 61710E-03
SUMMARY PCUT-EHAD-X-WSQ 4 260 30.000 175 47 320 MU-/MU+/TOTAL 43153E-03 61710E-03 10486E-02

--> HADRON ENERGY = 40 0 ---> MEAN WSQ = 62 800

	PRIMARY-MU+	PRIMARY-MU-	SHOWER-MU+	SHOWER-MU-	SUM-MU+	SUM-MU-
PIMIN	0	29651E-03	27074E-04	40628E-04	27074E-04	33714E-03
PIPOS	43649E-03	0	80570E-04	57603E-04	51706E-03	57603E-04
KAMIN	0.	15416E-03	84599E-05	13015E-04	84599E-05	16718E-03
KAPOS	17969E-03	0	20462E-04	14761E-04	20015E-03	14761E-04
PRMIN	0	0	90462E-06	40990E-05	90462E-06	40990E-05
PRPOS	0	0	16770E-04	42898E-05	16770E-04	42898E-05
NEMIN	0	0	18607E-05	27785E-05	18607E-05	27785E-05
NEPOS	0	0	50991E-05	36788E-05	50991E-05	36788E-05
KZERO	29385E-05	30436E-05	91445E-05	13615E-04	12083E-04	16658E-04

ALL NEGATIVE DECAY 45372E-03 SHOWER 15447E-03 TOTAL 60818E-03
ALL POSITIVE DECAY 61911E-03 SHOWER 17035E-03 TOTAL 78946E-03
SUMMARY PCUT-EHAD-X-WSQ 4 260 40 000 175 62 800 MU-/MU+/TOTAL 60818E-03 .78946E-03 13976E-02

--> HADRON ENERGY = 75 0 ---> MEAN WSQ = 116 98

	PRIMARY-MU+	PRIMARY-MU-	SHOWER-MU+	SHOWER-MU-	SUM-MU+	SUM-MU-
PIMIN	0.	.41675E-03	.91959E-04	.11769E-03	91959E-04	53444E-03
PIPOS	.55801E-03	0	.21457E-03	17788E-03	77259E-03	17788E-03
KAMIN	0	.20748E-03	26408E-04	33814E-04	26408E-04	24129E-03
KAPOS	21040E-03	0	44625E-04	37418E-04	25503E-03	37418E-04
PRMIN	0	0	31794E-05	12119E-04	31794E-05	12119E-04
PRPOS	0	0	.36440E-04	10999E-04	36440E-04	10999E-04
NEMIN	0.	0.	64281E-05	81163E-05	64281E-05	81163E-05
NEPOS	0	0	11540E-04	98294E-05	11540E-04	98294E-05
KZERO	60114E-05	48372E-05	26789E-04	33499E-04	32801E-04	38337E-04

ALL NEGATIVE DECAY .62906E-03 SHOWER 44136E-03 TOTAL 10704E-02
ALL POSITIVE DECAY 77443E-03 SHOWER 46194E-03 TOTAL 12364E-02
SUMMARY PCUT-EHAD-X-WSQ 4.260 75 000 175 116 981 MU-/MU+/TOTAL 10704E-02 12364E-02 23068E-02

********** MOMENTUM CUT = 4 26 MEAN X = 1748 **********

--> HADRON ENERGY = 100.0 ---> MEAN WSQ = 155 68

	PRIMARY-MU+	PRIMARY-MU-	SHOWER-MU+	SHOWER-MU-	SUM-MU+	SUM-MU-
PIMIN	0	53424E-03	14861E-03	17941E-03	14861E-03	71365E-03
PIPOS	68804E-03	0	32006E-03	27857E-03	10081E-02	27857E-03
KAMIN	0	23915E-03	40397E-04	48422E-04	40397E-04	28758E-03
KAPOS	23886E-03	0.	61477E-04	54078E-04	30003E-03	54078E-04
PRMIN	0.	0	51867E-05	18577E-04	51867E-05	18577E-04
PRPOS	0.	0	54126E-04	17012E-04	54126E-04	17012E-04
NEMIN	0	0	.10469E-04	12460E-04	10469E-04	12460E-04
NEPOS	0	0	17336E-04	15505E-04	17336E-04	15505E-04
KZERO	.65300E-05	.55518E-05	40274E-04	47414E-04	46804E-04	52966E-04

ALL NEGATIVE: DECAY .77895E-03 SHOWER 67144E-03 TOTAL 14504E-02
ALL POSITIVE. DECAY 93343E-03 SHOWER 69794E-03 TOTAL 16314E-02
SUMMARY PCUT-EHAD-X-WSQ 4.260 100 000 175 155 681 MU-/MU+/TOTAL 14504E-02 .16314E-02 30818E-02

--> HADRON ENERGY = 150 0 ---> MEAN WSQ = 233 08

	PRIMARY-MU+	PRIMARY-MU-	SHOWER-MU+	SHOWER-MU-	SUM-MU+	SUM-MU-
PIMIN	0.	60000E-03	27607E-03	31376E-03	27607E-03	91376E-03
PIPOS	.74899E-03	0	.54587E-03	49823E-03	12949E-02	49823E-03
KAMIN	0	.24700E-03	.69084E-04	.77355E-04	69084E-04	32436E-03
KAPOS	25002E-03	0	95575E-04	.88003E-04	34559E-03	88003E-04
PRMIN	0	0	.96085E-05	32235E-04	96085E-05	32235E-04
PRPOS	0	0.	.10237E-03	33116E-04	10237E-03	33116E-04
NEMIN	0	0	.19401E-04	.21716E-04	.19401E-04	21716E-04
NEPOS	0.	0	32911E-04	30641E-04	32911E-04	30641E-04
KZERO	61030E-05	.68267E-05	67608E-04	74933E-04	73711E-04	81760E-04

ALL NEGATIVE. DECAY 85383E-03 SHOWER .11700E-02 TOTAL 20238E-02
ALL POSITIVE. DECAY .10051E-02 SHOWER 12185E-02 TOTAL 22236E-02
SUMMARY PCUT-EHAD-X-WSQ 4 260 150 000 175 233 082 MU-/MU+/TOTAL 20238E-02 22236E-02 42474E-02

--> HADRON ENERGY = 200 0 ---> MEAN WSQ = 310 48

	PRIMARY-MU+	PRIMARY-MU-	SHOWER-MU+	SHOWER-MU-	SUM-MU+	SUM-MU-
PIMIN	0	53987E-03	41446E-03	45463E-03	41446E-03	99450E-03
PIPOS	66404E-03	0	77837E-03	72930E-03	14424E-02	.72930E-03
KAMIN	0	.22947E-03	.97993E-04	10577E-03	97993E-04	.33524E-03
KAPOS	23433E-03	0.	12963E-03	12232E-03	36395E-03	.12232E-03
PRMIN	0	0	14205E-04	.45982E-04	14205E-04	45982E-04
PRPOS	0.	0.	.16707E-03	54783E-04	.16707E-03	.54783E-04
NEMIN	0.	0	.28677E-04	31046E-04	28677E-04	.31046E-04
NEPOS	0	0.	52791E-04	.50249E-04	52791E-04	50249E-04
KZERO	.63067E-05	.63067E-05	.94735E-04	10166E-03	.10104E-03	10797E-03

ALL NEGATIVE: DECAY .77564E-03 SHOWER .16957E-02 TOTAL .24714E-02
ALL POSITIVE. DECAY .90467E-03 SHOWER .17779E-02 TOTAL 26826E-02
SUMMARY PCUT-EHAD-X-WSQ 4.260 200.000 175 310 483 MU-/MU+/TOTAL .24714E-02 26826E-02 .51540E-02

********** MOMENTUM CUT = 4 26 MEAN X = .1748 **********

--> HADRON ENERGY = 250.0 ---> MEAN WSQ = 387.88

	PRIMARY-MU+	PRIMARY-MU-	SHOWER-MU+	SHOWER-MU-	SUM-MU+	SUM-MU-
PIMIN	0	.73262E-03	.56070E-03	60602E-03	56070E-03	13386E-02
PIPOS	86021E-03	0	.10195E-02	96598E-03	18797E-02	96598E-03
KAMIN	0.	25513E-03	.12715E-03	13499E-03	12715E-03	39012E-03
KAPOS	27645E-03	0	.16487E-03	15705E-03	44132E-03	15705E-03
PRMIN	0	0	.18808E-04	59810E-04	18808E-04	59810E-04
PRPOS	0	0	24932E-03	81960E-04	24932E-03	81960E-04
NEMIN	0	0	.37924E-04	40379E-04	37924E-04	40379E-04
NEPOS	0.	0	.77026E-04	73719E-04	77026E-04	73719E-04
KZERO	.50380E-05	82935E-05	12169E-03	12886E-03	12673E-03	.13715E-03

ALL NEGATIVE DECAY 99603E-03 SHOWER 22488E-02 TOTAL 32448E-02
ALL POSITIVE. DECAY 11417E-02 SHOWER .23770E-02 TOTAL 35187E-02
SUMMARY PCUT-EHAD-X-WSQ 4.260 250 000 175 387 883 MU-/MU+/TOTAL 32448E-02 35187E-02 67635E-02

********** MOMENTUM CUT = 8 45 MEAN X = .1748 **********

--> HADRON ENERGY = 10 0 ---> MEAN WSQ = 16 360

	PRIMARY-MU+	PRIMARY-MU-	SHOWER-MU+	SHOWER-MU-	SUM-MU+	SUM-MU-
PIMIN	0	41744E-06	27654E-08	13419E-07	27654E-08	43085E-06
PIPOS	.14550E-05	0	45577E-07	94463E-08	15006E-05	94463E-08
KAMIN	0	83729E-07	51173E-09	25147E-08	51173E-09	86244E-07
KAPOS	74069E-06	0	19476E-07	40531E-08	76017E-06	40531E-08
PRMIN	0.	0	56818E-10	82745E-09	56818E-10	82745E-09
PRPOS	0	0	78932E-08	53134E-09	78932E-08	53134E-09
NEMIN	0	0	13213E-09	.64472E-09	13213E-09	64472E-09
NEPOS	0	0	16665E-08	33135E-09	16665E-08	33135E-09
KZERO	0	0	85484E-09	42056E-08	85484E-09	42056E-08

ALL NEGATIVE DECAY 50116E-06 SHOWER 35973E-07 TOTAL 53714E-06
ALL POSITIVE OECAY 21957E-05 SHOWER 78933E-07 TOTAL 22746E-05
SUMMARY PCUT-EHAD-X-WSQ 8 450 10 000 175 16 360 MU-/MU+/TOTAL 53714E-06 22746E-05 28118E-05

--> HADRON ENERGY = 15 0 ---> MEAN WSQ = 24 100

	PRIMARY-MU+	PRIMARY-MU-	SHOWER-MU+	SHOWER-MU-	SUM-MU+	SUM-MU-
PIMIN	0	49515E-05	.38947E-07	14333E-06	38947E-07	50948E-05
PIPOS	15093E-04	0	43650E-06	12252E-06	15529E-04	12252E-06
KAMIN	0	15694E-05	10390E-07	39785E-07	10390E-07	16092E-05
KAPOS	73130E-05	0	17942E-06	50839E-07	74924E-05	50839E-07
PRMIN	0	0	.10102E-08	11399E-07	10102E-08	11399E-07
PRPOS	0	0	.11464E-06	10159E-07	11464E-06	10159E-07
NEMIN	0	0	.23428E-08	87459E-08	23428E-08	87459E-08
NEPOS	0	0	.27048E-07	69549E-08	.27048E-07	69549E-08
KZERO	0	0	15436E-07	58620E-07	15436E-07	58620E-07

ALL NEGATIVE OECAY 65209E-05 SHOWER 45235E-06 TOTAL .69732E-05
ALL POSITIVE DECAY 22406E-04 SHOWER 82573E-06 TOTAL 23231E-04
SUMMARY PCUT-EHAD-X-WSQ 8 450 15 000 175 24 100 MU-/MU+/TOTAL 69732E-05 23231E-04 30204E-04

--> HAOHON ENERGY = 20 0 ---> MEAN WSQ = 31 840

	PRIMARY-MU+	PRIMARY-MU-	SHOWER-MU+	SHOWER-MU-	SUM-MU+	SUM-MU-
PIMIN	0	14105E-04	15627E-06	47937E-06	15627E-06	14584E-04
PIPOS	37123E-04	0	13435E-05	46138E-06	38466E-04	46138E-06
KAMIN	0	56105E-05	48385E-07	15581E-06	.48385E-07	57663E-05
KAPOS	17432E-04	0	52389E-06	18169E-06	17956E-04	18169E-06
PRMIN	0	0	44018E-08	41785E-07	44018E-08	41785E-07
PRPOS	0	0	37076E-06	41153E-07	37076E-06	41153E-07
NEMIN	0	0	10091E-07	31426E-07	10091E-07	31426E-07
NEPOS	0	0	92875E-07	29561E-07	92875E-07	29561E-07
KZERO	25134E-07	35038E-09	66171E-07	20909E-06	91305E-07	20944E-06

ALL NEGATIVE DECAY 19716E-04 SHOWER .16313E-05 TOTAL 21347E-04
ALL POSITIVE DECAY 54579E-04 SHOWER 26163E-05 TOTAL 57196E-04
SUMMARY PCUT-EHAD-X-WSQ 8 450 20.000 175 31 840 MU-/MU+/TOTAL 21347E-04 57196E-04 78543E-04

********** MOMENTUM CUT = 8 45 MEAN X = 1748 **********

--> HADRON ENERGY = 30 0 ---> MEAN WSQ = 47 320

	PRIMARY-MU+	PRIMARY-MU-	SHOWER-MU+	SHOWER-MU-	SUM-MU+	SUM-MU-
PIMIN	0	40223E-04	77511E-06	19112E-05	77511E-06	42134E-04
PIPOS	85223E-04	0	47820E-05	20860E-05	90005E-04	20860E-05
KAMIN	0	19269E-04	26865E-06	69443E-06	26865E-06	19964E-04
KAPOS	38072E-04	0	16787E-05	73938E-06	39751E-04	73938E-06
PRMIN	0	0	23374E-07	17899E-06	23374E-07	17899E-06
PRPOS	0	0	12385E-05	18445E-06	12385E-05	18445E-06
NEMIN	0	0	52221E-07	13023E-06	52221E-07	13023E-06
NEPOS	0	0	32770E-06	13819E-06	32770E-06	13819E-06
KZERO	74922E-07	33601E-07	33285E-06	83422E-06	40778E-06	86782E-06

ALL NEGATIVE DECAY 59526E-04 SHOWER 68971E-05 TOTAL 66423E-04
ALL POSITIVE DECAY 12337E-03 SHOWER 94790E-05 TOTAL 13285E-03
SUMMARY PCUT-EHAD-X-WSQ 8 450 30 000 175 47 320 MU-/MU+/TOTAL 66423E-04 13285E-03 19927E-03

--> HADRON ENERGY = 40 0 ---> MEAN WSQ = 62 800

	PRIMARY-MU+	PRIMARY-MU-	SHOWER-MU+	SHOWER-MU-	SUM-MU+	SUM-MU-
PIMIN	0	68167E-04	19991E-05	43009E-05	19991E-05	72468E-04
PIPOS	12671E-03	0	10052E-04	50583E-05	13676E-03	50583E-05
KAMIN	0	34831E-04	71336E-06	15961E-05	71336E-06	36427E-04
KAPOS	54593E-04	0	32276E-05	16398E-05	57821E-04	16398E-05
PRMIN	0	0	62400E-07	41549E-06	62400E-07	41549E-06
PRPOS	0	0	23938E-05	42632E-06	23938E-05	42632E-06
NEMIN	0	0	13683E-06	29635E-06	13683E-06	29635E-06
NEPOS	0	0	64785E-06	32503E-06	64785E-06	32503E-06
KZERO	11128E-06	14612E-06	83686E-06	18096E-05	94815E-06	19557E-05

ALL NEGATIVE DECAY 10314E-03 SHOWER 15868E-04 TOTAL 11901E-03
ALL POSITIVE DECAY 18141E-03 SHOWER 20070E-04 TOTAL 20148E-03
SUMMARY PCUT-EHAD-X-WSQ 8 450 40 000 175 62 800 MU-/MU+/TOTAL 11901E-03 20148E-03 32049E-03

--> HADRON ENERGY = 75 0 ---> MEAN WSQ = 116 98

	PRIMARY-MU+	PRIMARY-MU-	SHOWER-MU+	SHOWER-MU-	SUM-MU+	SUM-MU-
PIMIN	0	14925E-03	10720E-04	18212E-04	10720E-04	16746E-03
PIPOS	22645E-03	0	37801E-04	23960E-04	26425E-03	23960E-04
KAMIN	0	77068E-04	37112E-05	63998E-05	37112E-05	83468E-04
KAPOS	88245E-04	0	98165E-05	62865E-05	98062E-04	62865E-05
PRMIN	0	0	35835E-06	18548E-05	35835E-06	18548E-05
PRPOS	0	0	76230E-05	17907E-05	76230E-05	17907E-05
NEMIN	0	0	76053E-06	12873E-05	76053E-06	12873E-05
NEPOS	0	0	21676E-05	14342E-05	21676E-05	14342E-05
KZERO	12560E-05	16581E-05	39890E-05	66725E-05	52450E-05	83306E-05

ALL NEGATIVE DECAY 22797E-03 SHOWER 67897E-04 TOTAL 29587E-03
ALL POSITIVE DECAY 31595E-03 SHOWER 76948E-04 TOTAL 39289E-03
SUMMARY PCUT-EHAD-X-WSQ 8 450 75 000 175 116 981 MU-/MU+/TOTAL 29587E-03 39289E-03 68877E-03

********** MOMENTUM CUT = 8 45 MEAN X = 1748 **********

--> HADRON ENERGY = 100 0 ---> MEAN WSQ = 155 68

	PRIMARY-MU+	PRIMARY-MU-	SHOWER-MU+	SHOWER-MU-	SUM-MU+	SUM-MU-
PIMIN	0	19236E-03	20198E-04	31577E-04	20198E-04	22393E-03
PIPOS	27420E-03	0	62793E-04	42994E-04	33699E-03	42994E-04
KAMIN	0	95317E-04	66916E-05	10513E-04	66916E-05	10583E-03
KAPOS	10126E-03	0	14847E-04	10278E-04	11611E-03	10278E-04
PRMIN	0	0	69086E-06	32670E-05	69086E-06	32670E-05
PRPOS	0	0	12424E-04	31744E-05	12424E-04	31744E-05
NEMIN	0	0	14526E-05	22540E-05	14526E-05	22540E-05
NEPOS	0	0	36292E-05	26143E-05	36292E-05	26143E-05
KZERO	17313E-05	15799E-05	69803E-05	10684E-04	87117E-05	12264E-04

ALL NEGATIVE DECAY 28925E-03 SHOWER 11736E-03 TOTAL 40661E-03
ALL POSITIVE. DECAY 37719E-03 SHOWER 12971E-03 TOTAL 50690E-03
SUMMARY PCUT-EHAD-X-WSQ 8 450 100 000 175 155 681 MU-/MU+/TOTAL 40661E-03 50690E-03 91351E-03

--> HADRON ENERGY = 150.0 ---> MEAN WSQ = 233.08

	PRIMARY-MU+	PRIMARY-MU-	SHOWER-MU+	SHOWER-MU-	SUM-MU+	SUM-MU-
PIMIN	0.	24117E-03	44586E-04	63352E-04	44586E-04	30453E-03
PIPOS	32337E-03	0	11938E-03	89444E-04	44275E-03	89444E-04
KAMIN	0.	11203E-03	13632E-04	19221E-04	13632E-04	13125E-03
KAPOS	11331E-03	0	25079E-04	19036E-04	13839E-03	19036E-04
PRMIN	0	0	15436E-05	65763E-05	15436E-05	65763E-05
PRPOS	0.	0	25242E-04	71290E-05	25242E-04	71290E-05
NEMIN	0	0	32190E-05	45142E-05	32190E-05	45142E-05
NEPOS	0.	0	75742E-05	60121E-05	75742E-05	60121E-05
KZERO	29845E-05	16983E-05	13741E-04	18981E-04	16725E-04	20679E-04

ALL NEGATIVE: DECAY 35490E-03 SHOWER 23427E-03 TOTAL 58917E-03
ALL POSITIVE: DECAY 43967E-03 SHOWER 25399E-03 TOTAL 69367E-03
SUMMARY PCUT-EHAD-X-WSQ 8 450 150 000 175 233.082 MU-/MU+/TOTAL 58917E-03 69367E-03 12828E-02

--> HADRON ENERGY = 200.0 ---> MEAN WSQ = 310 48

	PRIMARY-MU+	PRIMARY-MU-	SHOWER-MU+	SHOWER-MU-	SUM-MU+	SUM-MU-
PIMIN	0	29327E-03	73975E-04	98636E-04	73975E-04	39190E-03
PIPOS	37600E-03	0	17973E-03	14301E-03	55573E-03	14301E-03
KAMIN	0.	12587E-03	21255E-04	27944E-04	21255E-04	15381E-03
KAPOS	12626E-03	0	35222E-04	28434E-04	16148E-03	28434E-04
PRMIN	0.	0	25385E-05	10116E-04	25385E-05	10116E-04
PRPOS	0.	0	42421E-04	12837E-04	42421E-04	12837E-04
NEMIN	0.	0	52730E-05	69229E-05	52730E-05	69229E-05
NEPOS	0.	0	12705E-04	10779E-04	12705E-04	10779E-04
KZERO	35759E-05	35759E-05	20987E-04	27120E-04	24562E-04	30696E-04

ALL NEGATIVE DECAY 42271E-03 SHOWER 36580E-03 TOTAL 78851E-03
ALL POSITIVE: DECAY 50583E-03 SHOWER 39411E-03 TOTAL 89994E-03
SUMMARY: PCUT-EHAD-X-WSQ 8 450 200 000 175 310 483 MU-/MU+/TOTAL 78851E-03 89994E-03 16884E-02

********** MOMENTUM CUT = 8 45 MEAN X = 1748 **********

--> HADRON ENERGY = 250 0 ---> MEAN WSQ = 387 88

	PRIMARY-MU+	PRIMARY-MU-	SHOWER-MU+	SHOWER-MU-	SUM-MU+	SUM-MU-
PIMIN	0	33403E-03	10717E-03	13694E-03	10717E-03	47097E-03
PIPOS	41456E-03	0	24263E-03	20139E-03	65719E-03	20139E-03
KAMIN	0	13175E-03	29331E-04	36733E-04	29331E-04	16848E-03
KAPOS	13342E-03	0	45427E-04	38326E-04	17885E-03	38326E-04
PRMIN	0	0	36130E-05	13758E-04	36130E-05	13758E-04
PRPOS	0	0	63967E-04	20390E-04	63967E-04	20390E-04
NEMIN	0	0	74821E-05	93867E-05	74821E-05	93867E-05
NEPOS	0	0	18901E-04	16829E-04	18901E-04	16829E-04
KZERO	24103E-05	28470E-05	28522E-04	35181E-04	30933E-04	38028E-04

ALL NEGATIVE DECAY 46862E-03 SHOWER 50893E-03 TOTAL 97756E-03
ALL POSITIVE DECAY .55039E-03 SHOWER 54704E-03 TOTAL 10974E-02
SUMMARY PCUT-EHAD-X-WSQ 8 450 250 000 175 387 883 MU-/MU+/TOTAL 97756E-03 10974E-02 20750E-02

********** MOMENTUM CUT = 9 45 MEAN X = 1748 **********

--> HADRON ENERGY = 10 0 ---> MEAN WSQ = 16 360

	PRIMARY-MU+	PRIMARY-MU-	SHOWER-MU+	SHOWER-MU-	SUM-MU+	SUM-MU-
PIMIN	0.	83721E-07	73953E-09	28516E-08	73953E-09	86573E-07
PIPOS	30009E-06	0	10096E-07	26217E-08	31018E-06	26217E-08
KAMIN	0.	15406E-07	12436E-09	48133E-09	12436E-09	15888E-07
KAPOS	15524E-06	0	44086E-08	.11464E-08	15964E-06	11464E-08
PRMIN	0	0	14282E-10	16425E-09	14282E-10	16425E-09
PRPOS	0	0	13246E-08	11429E-09	13246E-08	11429E-09
NEMIN	0	0	.34020E-10	13142E-09	34020E-10	13142E-09
NEPOS	0	0	26188E-09	67051E-10	26188E-09	67051E-10
KZERO	0.	0	20585E-09	79737E-09	20585E-09	79737E-09

ALL NEGATIVE DECAY 99127E-07 SHOWER 83754E-08 TOTAL 10750E-06
ALL POSITIVE. DECAY 45532E-06 SHOWER 17209E-07 TOTAL 47253E-06
SUMMARY PCUT-EHAD-X-WSQ 9 450 10 000 175 16 360 MU-/MU+/TOTAL 10750E-06 47253E-06 58003E-06

--> HADRON ENERGY = 15 0 ---> MEAN WSQ = 24.100

	PRIMARY-MU+	PRIMARY-MU-	SHOWER-MU+	SHOWER-MU-	SUM-MU+	SUM-MU-
PIMIN	0	24946E-05	.19295E-07	56430E-07	19295E-07	25510E-05
PIPOS	.80650E-05	0	18015E-06	63031E-07	82452E-05	63031E-07
KAMIN	0	73512E-06	49621E-08	14973E-07	49621E-08	75009E-06
KAPOS	39739E-05	0	.76047E-07	26833E-07	40500E-05	26833E-07
PRMIN	0	0	48231E-09	43006E-08	48231E-09	43006E-08
PRPOS	0.	0.	.44125E-07	48997E-08	44125E-07	48997E-08
NEMIN	0	0	.11417E-08	33796E-08	11417E-08	33796E-08
NEPOS	0	0	10021E-07	.32444E-08	10021E-07	32444E-08
KZERO	0	0	74782E-08	22484E-07	74782E-08	22484E-07

ALL NEGATIVE DECAY 32297E-05 SHOWER 19957E-06 TOTAL 34293E-05
ALL POSITIVE. DECAY 12039E-04 SHOWER 34370E-06 TOTAL 12383E-04
SUMMARY PCUT-EHAD-X-WSQ 9 450 15 000 .175 24 100 MU-/MU+/TOTAL 34293E-05 12383E-04 15812E-04

--> HADRON ENERGY = 20 0 ---> MEAN WSQ = 31 840

	PRIMARY-MU+	PRIMARY-MU-	SHOWER-MU+	SHOWER-MU-	SUM-MU+	SUM-MU-
PIMIN	0	84683E-05	90235E-07	22101E-06	90235E-07	86894E-05
PIPOS	.23831E-04	0	.64292E-06	.27497E-06	24474E-04	27497E-06
KAMIN	0	31935E-05	27629E-07	70797E-07	27629E-07	32643E-05
KAPOS	11282E-04	0	25823E-06	11163E-06	11540E-04	11163E-06
PRMIN	0	0	24775E-08	.18757E-07	24775E-08	18757E-07
PRPOS	0	0	17497E-06	24038E-07	17497E-06	24038E-07
NEMIN	0	0	57725E-08	14354E-07	57725E-08	14354E-07
NEPOS	0	0.	42754E-07	16878E-07	42754E-07	16878E-07
KZERO	0	0	38351E-07	96823E-07	38351E-07	96823E-07

ALL NEGATIVE DECAY 11662E-04 SHOWER 84927E-06 TOTAL 12511E-04
ALL POSITIVE DECAY 35113E-04 SHOWER .12833E-05 TOTAL 36396E-04
SUMMARY PCUT-EHAD-X-WSQ 9 450 20 000 175 31 840 MU-/MU+/TOTAL 12511E-04 36396E-04 48907E-04

********** MOMENTUM CUT = 9 45 MEAN X = 1748 **********

--> HADRON ENERGY = 30 0 ---> MEAN WSQ = 47 320

	PRIMARY-MU+	PRIMARY-MU-	SHOWER-MU+	SHOWER-MU-	SUM-MU+	SUM-MU-
PIMIN	0.	27718E-04	50010E-06	96291E-06	50010E-06	28681E-04
PIPOS	62493E-04	0	25064E-05	13930E-05	64999E-04	13930E-05
KAMIN	0	12938E-04	17427E-06	35150E-06	17427E-06	13289E-04
KAPOS	28098E-04	0	91310E-06	51244E-06	29011E-04	51244E-06
PRMIN	0.	0	14755E-07	88280E-07	14755E-07	88280E-07
PRPOS	0	0	65909E-06	12391E-06	65909E-06	12391E-06
NEMIN	0	0	33509E-07	65300E-07	33509E-07	65300E-07
NEPOS	0	0	17023E-06	90798E-07	17023E-06	90798E-07
KZERO	12513E-07	19264E-07	21962E-06	43122E-06	23213E-06	45049E-06

ALL NEGATIVE DECAY 40675E-04 SHOWER 40193E-05 TOTAL 44694E-04
ALL POSITIVE DECAY 90603E-04 SHOWER 51911E-05 TOTAL 95794E-04
SUMMARY PCUT-EHAD-X-WSQ 9 450 30 000 175 47 320 MU-/MU+/TOTAL 44694E-04 95794E-04 14049E-03

--> HADRON ENERGY = 40 0 ---> MEAN WSQ = 62 800

	PRIMARY-MU+	PRIMARY-MU-	SHOWER-MU+	SHOWER-MU-	SUM-MU+	SUM-MU-
PIMIN	0.	50225E-04	13787E-05	23096E-05	13787E-05	52534E-04
PIPOS	98430E-04	0	55810E-05	36021E-05	10401E-03	36021E-05
KAMIN	0.	25260E-04	49963E-06	87156E-06	49963E-06	26131E-04
KAPOS	.42539E-04	0	18620E-05	12138E-05	44401E-04	12138E-05
PRMIN	0	0	42294E-07	21989E-06	42294E-07	21989E-06
PRPOS	0	0	13607E-05	30893E-06	13607E-05	30893E-06
NEMIN	0.	0	94098E-07	15887E-06	94098E-07	15887E-06
NEPOS	0	0	36052E-06	23067E-06	36052E-06	23067E-06
KZERO	96824E-07	12982E-06	59499E-06	10047E-05	69181E-06	11345E-05

ALL NEGATIVE DECAY 75614E-04 SHOWER 99202E-05 TOTAL 85535E-04
ALL POSITIVE DECAY .14107E-03 SHOWER 11774E-04 TOTAL 15284E-03
SUMMARY PCUT-EHAD-X-WSQ 9 450 40 000 175 62 800 MU-/MU+/TOTAL .85535E-04 15284E-03 23837E-03

--> HADRON ENERGY = 75 0 ---> MEAN WSQ = 116 98

	PRIMARY-MU+	PRIMARY-MU-	SHOWER-MU+	SHOWER-MU-	SUM-MU+	SUM-MU-
PIMIN	0	12096E-03	80997E-05	10631E-04	80997E-05	.13159E-03
PIPOS	.18937E-03	0	22601E-04	.18533E-04	21197E-03	.18533E-04
KAMIN	0	62221E-04	28896E-05	38545E-05	28896E-05	66076E-04
KAPOS	73841E-04	0	60977E-05	50506E-05	.79939E-04	50506E-05
PRMIN	0.	0	26849E-06	10762E-05	.26849E-06	10762E-05
PRPOS	0	0.	47008E-05	14251E-05	47008E-05	14251E-05
NEMIN	0	0	.57524E-06	75301E-06	57524E-06	75301E-06
NEPOS	0	0	13147E-05	11248E-05	13147E-05	11248E-05
KZERO	81040E-06	58113E-06	31385E-05	40610E-05	39489E-05	46421E-05

ALL NEGATIVE DECAY 18376E-03 SHOWER 46509E-04 TOTAL 23027E-03
ALL POSITIVE DECAY .26402E-03 SHOWER 49685E-04 TOTAL 31371E-03
SUMMARY PCUT-EHAD-X-WSQ 9 450 75 000 175 116 981 MU-/MU+/TOTAL 23027E-03 .31371E-03 54398E-03

********** MOMENTUM CUT = 9 45 MEAN X = 1748 **********

--> HADRON ENERGY = 100 0 ---> MEAN WSQ = 155 68

	PRIMARY-MU+	PRIMARY-MU-	SHOWER-MU+	SHOWER-MU-	SUM-MU+	SUM-MU-
PIMIN	0	15434E-03	15656E-04	18960E-04	15656E-04	17350E-03
PIPOS	22675E-03	0	38367E-04	33902E-04	26511E-03	33902E-04
KAMIN	0	78262E-04	53627E-05	65288E-05	53627E-05	84791E-04
KAPOS	85361E-04	0	94052E-05	83998E-05	94766E-04	83998E-05
PRMIN	0	0	53302E-06	19549E-05	53302E-06	19549E-05
PRPOS	0	0	77864E-05	25600E-05	77864E-05	25600E-05
NEMIN	0	0	11280E-05	13565E-05	11280E-05	13565E-05
NEPOS	0	0	22472E-05	20880E-05	22472E-05	20880E-05
KZERO	18635E-05	93859E-06	56343E-05	66818E-05	74978E-05	76204E-05

ALL NEGATIVE DECAY 23374E-03 SHOWER 82432E-04 TOTAL 31617E-03
ALL POSITIVE DECAY 31397E-03 SHOWER 86120E-04 TOTAL 40009E-03
SUMMARY PCUT-EHAD-X-WSQ 9 450 100 000 175 155 681 MU-/MU+/TOTAL 31617E-03 40009E-03 71626E-03

--> HADRON ENERGY = 150 0 ---> MEAN WSQ = 233 08

	PRIMARY-MU+	PRIMARY-MU-	SHOWER-MU+	SHOWER-MU-	SUM-MU+	SUM-MU-
PIMIN	0	20267E-03	.35211E-04	.38509E-04	35211E-04	24118E-03
PIPOS	27672E-03	0	73686E-04	71385E-04	35041E-03	71385E-04
KAMIN	0	96757E-04	.11150E-04	12136E-04	11150E-04	10889E-03
KAPOS	.98695E-04	0	.16011E-04	.15685E-04	11471E-03	15685E-04
PRMIN	0	0	12187E-05	.40046E-05	12187E-05	40046E-05
PRPOS	0	0	15896E-04	57563E-05	15896E-04	57563E-05
NEMIN	0	0	25495E-05	27591E-05	25495E-05	27591E-05
NEPOS	0	0	47195E-05	.48327E-05	47195E-05	48327E-05
KZERO	23535E-05	29845E-05	11276E-04	12035E-04	13629E-04	15019E-04

ALL NEGATIVE DECAY 30241E-03 SHOWER 16710E-03 TOTAL 46952E-03
ALL POSITIVE DECAY 37777E-03 SHOWER 17172E-03 TOTAL 54949E-03
SUMMARY PCUT-EHAD-X-WSQ 9 450 150 000 175 233 082 MU-/MU+/TOTAL 46952E-03 54949E-03 10190E-02

--> HADRON ENERGY = 200 0 ---> MEAN WSQ = 310 48

	PRIMARY-MU+	PRIMARY-MU-	SHOWER-MU+	SHOWER-MU-	SUM-MU+	SUM-MU-
PIMIN	0	.25837E-03	59009E-04	61148E-04	59009E-04	31952E-03
PIPOS	33456E-03	0	11235E-03	11467E-03	44691E-03	11467E-03
KAMIN	0.	11091E-03	17519E-04	17927E-04	17519E-04	12884E-03
KAPOS	.11166E-03	0	.22679E-04	23448E-04	.13434E-03	23448E-04
PRMIN	0	0	20269E-05	62782E-05	20269E-05	62782E-05
PRPOS	0	0	26801E-04	10322E-04	26801E-04	10322E-04
NEMIN	0	0	42149E-05	43050E-05	.42149E-05	43050E-05
NEPOS	0	0	79874E-05	86629E-05	79874E-05	86629E-05
KZERO	19215E-05	22265E-05	17314E-04	17427E-04	19235E-04	19654E-04

ALL NEGATIVE DECAY 37151E-03 SHOWER 26419E-03 TOTAL 63570E-03
ALL POSITIVE DECAY 44815E-03 SHOWER 26990E-03 TOTAL 71805E-03
SUMMARY PCUT-EHAD-X-WSQ 9 450 200 000 175 310 483 MU-/MU+/TOTAL 63570E-03 71805E-03 13537E-02

********** MOMENTUM CUT = 9 45 MEAN X = 1748 **********

--> HADRON ENERGY = 250 0 ---> MEAN WSQ = 387 88

	PRIMARY-MU+	PRIMARY-MU-	SHOWER-MU+	SHOWER-MU-	SUM-MU+	SUM-MU-
PIMIN	0	27506E-03	85733E-04	85309E-04	85733E-04	36037E-03
PIPOS	34621E-03	0	15208E-03	16151E-03	49829E-03	16151E-03
KAMIN	0	11389E-03	24191E-04	23643E-04	24191E-04	13753E-03
KAPOS	11466E-03	0	29254E-04	31514E-04	14392E-03	31514E-04
PRMIN	0	0	28954E-05	.85877E-05	.28954E-05	85877E-05
PRPOS	0.	0	.40349E-04	16305E-04	40349E-04	16305E-04
NEMIN	0	0.	59958E-05	58655E-05	59958E-05	58655E-05
NEPOS	0	0	11885E-04	13481E-04	11885E-04	13481E-04
KZERO	28470E-05	40899E-05	23516E-04	22655E-04	26363E-04	26745E-04

ALL NEGATIVE DECAY .39304E-03 SHOWER 36887E-03 TOTAL 76191E-03
ALL POSITIVE DECAY 46372E-03 SHOWER 37590E-03 TOTAL 83962E-03
SUMMARY PCUT-EHAD-X-WSQ 9 450 250 000 175 387 883 MU-/MU+/TOTAL 76191E-03 83962E-03 16015E-02

********** MOMENTUM CUT = 15 45 MEAN X = 1748 **********

--> HADRON ENERGY = 20 0 ---> MEAN WSQ = 31 840

	PRIMARY-MU+	PRIMARY-MU-	SHOWER-MU+	SHOWER-MU-	SUM-MU+	SUM-MU-
PIMIN	0	32210E-06	43156E-08	12058E-07	43156E-08	33415E-06
PIPOS	11803E-05	0	42794E-07	15442E-07	12231E-05	15442E-07
KAMIN	0	88804E-07	11455E-08	32383E-08	11455E-08	92042E-07
KAPOS	59805E-06	0	19198E-07	69638E-08	61725E-06	69638E-08
PRMIN	0.	0	10020E-09	84216E-09	10020E-09	84216E-09
PRPOS	0	0	.91081E-08	10750E-08	91081E-08	10750E-08
NEMIN	0	0	25861E-09	72618E-09	25861E-09	72618E-09
NEPOS	0	0	18557E-08	64482E-09	18557E-08	64482E-09
KZERO	0	0	16664E-08	47159E-08	16664E-08	47159E-08

ALL NEGATIVE DECAY .41090E-06 SHOWER 45706E-07 TOTAL 45661E-06
ALL POSITIVE DECAY 17784E-05 SHOWER 80442E-07 TOTAL 18588E-05
SUMMARY PCUT-EHAD-X-WSQ 15 450 20 000 175 31 840 MU-/MU+/TOTAL 45661E-06 18588E-05 23155E-05

--> HADRON ENERGY = 30 0 ---> MEAN WSQ = 47.320

	PRIMARY-MU+	PRIMARY-MU-	SHOWER-MU+	SHOWER-MU-	SUM-MU+	SUM-MU-
PIMIN	0	32362E-05	50219E-07	11401E-06	50219E-07	33503E-05
PIPOS	99164E-05	0	34736E-06	15883E-06	10264E-04	15883E-06
KAMIN	0	12532E-05	17506E-07	40907E-07	17506E-07	12941E-05
KAPOS	46333E-05	0	.14483E-06	67000E-07	47781E-05	67000E-07
PRMIN	0	0.	13430E-08	93620E-08	13430E-08	93620E-08
PRPOS	0	0	94282E-07	14156E-07	94282E-07	14156E-07
NEMIN	0.	0	32773E-08	75107E-08	32773E-08	75107E-08
NEPOS	0	0	21949E-07	94971E-08	21949E-07	94971E-08
KZERO	0	0	.23401E-07	54212E-07	23401E-07	54212E-07

ALL NEGATIVE: DECAY 44894E-05 SHOWER .47549E-06 TOTAL 49649E-05
ALL POSITIVE. DECAY 14550E-04 SHOWER 70417E-06 TOTAL 15254E-04
SUMMARY: PCUT-EHAD-X-WSQ 15 450 30 000 175 47 320 MU-/MU+/TOTAL 49649E-05 15254E-04 20219E-04

--> HADRON ENERGY = 40 0 ---> MEAN WSQ = 62 800

	PRIMARY-MU+	PRIMARY-MU-	SHOWER-MU+	SHOWER-MU-	SUM-MU+	SUM-MU-
PIMIN	0	90252E-05	18142E-06	35847E-06	18142E-06	93837E-05
PIPOS	23514E-04	0	98894E-06	.53015E-06	24503E-04	53015E-06
KAMIN	0	40760E-05	69667E-07	14212E-06	69667E-07	42181E-05
KAPOS	10473E-04	0	.38354E-06	20831E-06	10857E-04	20831E-06
PRMIN	0	0	51787E-08	31665E-07	51787E-08	31665E-07
PRPOS	0	0	26184E-06	47785E-07	26184E-06	47785E-07
NEMIN	0.	0	12218E-07	.24338E-07	12218E-07	24338E-07
NEPOS	0	0	.63980E-07	33214E-07	.63980E-07	33214E-07
KZERO	0	.74952E-09	87519E-07	17529E-06	.87519E-07	17604E-06

ALL NEGATIVE DECAY .13102E-04 SHOWER 15513E-05 TOTAL 14653E-04
ALL POSITIVE DECAY 33988E-04 SHOWER 20543E-05 TOTAL 36042E-04
SUMMARY PCUT-EHAD-X-WSQ 15 450 40 000 175 62.800 MU-/MU+/TOTAL .14653E-04 36042E-04 50695E-04

```
*****************************************************************************************************
********** MOMENTUM CUT =  15.45          MEAN X =    .1748 **********
*****************************************************************************************************

--> HADRON ENERGY =  75 0      ---> MEAN WSQ =  116 98

          PRIMARY-MU+        PRIMARY-MU-        SHOWER-MU+         SHOWER-MU-         SUM-MU+            SUM-MU-
PIMIN    0.                   38368E-04          .15084E-05         23216E-05          15084E-05          40689E-04
PIPOS     .72713E-04         0                    54466E-05          .37714E-05         78160E-04          37714E-05
KAMIN    0.                   .19766E-04         .61183E-06         .95656E-06         61183E-06          .20722E-04
KAPOS     .29383E-04         0.                   .17361E-05         12147E-05          31119E-04          .12147E-05
PRMIN    0.                  0                    .48158E-07         .22717E-06         48158E-07          22717E-06
PRPOS    0.                  0                     12765E-05         32057E-06          12765E-05          32057E-06
NEMIN    0.                  0                     10739E-06         16521E-06          10739E-06          16521E-06
NEPOS    0.                  0                    .33398E-06         23867E-06          33398E-06          .23867E-06
KZERO     .10592E-06          14417E-06           .69049E-06         10529E-05          79640E-06          .11971E-05

ALL NEGATIVE:  DECAY    .58278E-04   SHOWER    10269E-04   TOTAL    68547E-04
ALL POSITIVE:  DECAY    10220E-03    SHOWER   .11760E-04   TOTAL    11396E-03
SUMMARY.PCUT-EHAD-X-WSQ   15.450  75 000   175   116 981   MU-/MU+/TOTAL    68547E-04    11396E-03    18251E-03
-----------------------------------------------------------------------------------------------------

--> HADRON ENERGY = 100 0      ---> MEAN WSQ =  155.68

          PRIMARY-MU+        PRIMARY-MU-        SHOWER-MU+         SHOWER-MU-         SUM-MU+            SUM-MU-
PIMIN    0.                   .58627E-04         .32493E-05         46236E-05          32493E-05          63251E-04
PIPOS     99695E-04          0                    .10210E-04         76131E-05          .10990E-03         76131E-05
KAMIN    0                    .30357E-04          12850E-05         18417E-05          .12850E-05         32199E-04
KAPOS     38756E-04          0                    29543E-05         .22245E-05         .41711E-04         22245E-05
PRMIN    0                   0                    .10773E-06         .46641E-06         .10773E-06         46641E-06
PRPOS    0                   0                    .23533E-05         64122E-06          23533E-05          64122E-06
NEMIN    0.                  0.                   23575E-06         .33416E-06         .23575E-06         33416E-06
NEPOS    0                   0.                   .63597E-06         .49466E-06         .63597E-06         49466E-06
KZERO     .40317E-06          21791E-06           13924E-05         19507E-05          17956E-05          21686E-05

ALL NEGATIVE.  DECAY    89202E-04   SHOWER   .20190E-04   TOTAL   .10939E-03
ALL POSITIVE:  DECAY    13885E-03   SHOWER   .22424E-04   TOTAL   .16128E-03
SUMMARY PCUT-EHAD-X-WSQ   15 450 100.000   .175   155.681   MU-/MU+/TOTAL    10939E-03    .16128E-03    .27067E-03
-----------------------------------------------------------------------------------------------------

--> HADRON ENERGY = 150 0      ---> MEAN WSQ =  233 08

          PRIMARY-MU+        PRIMARY-MU-        SHOWER-MU+         SHOWER-MU-         SUM-MU+            SUM-MU-
PIMIN    0                    90014E-04          .82233E-05         .10609E-04         82233E-05          10062E-03
PIPOS     13617E-03          0.                   21942E-04         17884E-04          .15811E-03         17884E-04
KAMIN    0                    .45178E-04          30360E-05         .39137E-05         30360E-05          49092E-04
KAPOS     50252E-04          0                    55905E-05         45964E-05          55842E-04          .45964E-05
PRMIN    0                   0.                   28000E-06         .10894E-05         .28000E-06         10894E-05
PRPOS    0                   0                    54368E-05         16246E-05          54368E-05          .16246E-05
NEMIN    0                   0                    .60257E-06         .77161E-06         .60257E-06         .77161E-06
NEPOS    0.                  0                    .15113E-05         .12911E-05         .15113E-05         .12911E-05
KZERO     .86540E-06          .72313E-06          .31411E-05         39800E-05          40065E-05          47031E-05

ALL NEGATIVE:  DECAY    .13592E-03   SHOWER   .45760E-04   TOTAL    18167E-03
ALL POSITIVE:  DECAY    .18729E-03   SHOWER    49763E-04   TOTAL   .23705E-03
SUMMARY PCUT-EHAD-X-WSQ   15 450 150 000   175   233.082   MU-/MU+/TOTAL   .18167E-03    23705E-03    41873E-03
-----------------------------------------------------------------------------------------------------
```



```
*****************************************************************************************************
********** MOMENTUM CUT =  15 45          MEAN X =    1748 **********
*****************************************************************************************************

--> HADRON ENERGY = 200 0      ---> MEAN WSQ =  310 48

          PRIMARY-MU+        PRIMARY-MU-        SHOWER-MU+         SHOWER-MU-         SUM-MU+            SUM-MU-
PIMIN    0.                   11635E-03          14852E-04         18281E-04          14852E-04          13463E-03
PIPOS     16375E-03          0                    36002E-04         30762E-04          19975E-03          30762E-04
KAMIN    0.                   55478E-04          51406E-05         .62810E-05         51406E-05          61759E-04
KAPOS     .58104E-04         0                    84459E-05         72893E-05          66550E-04          72893E-05
PRMIN    0.                  0                    50473E-06         18651E-05          50473E-06          18651E-05
PRPOS    0                   0                    98791E-05         31287E-05          98791E-05          31287E-05
NEMIN    0                   0                    10766E-05         13104E-05          .10766E-05         13104E-05
NEPOS    0                   0                    27585E-05         24875E-05          27585E-05          24875E-05
KZERO     .85937E-06          10672E-05           51700E-05         62206E-05          60293E-05          72878E-05

ALL NEGATIVE   DECAY    .17289E-03   SHOWER    77626E-04   TOTAL    25052E-03
ALL POSITIVE   DECAY    22272E-03    SHOWER    83829E-04   TOTAL    30654E-03
SUMMARY PCUT-EHAD-X-WSQ   15 450 200 000   175   310 483   MU-/MU+/TOTAL    25052E-03    30654E-03    55706E-03
-----------------------------------------------------------------------------------------------------

--> HADRON ENERGY = 250 0      ---> MEAN WSQ =  387 88

          PRIMARY-MU+        PRIMARY-MU-        SHOWER-MU+         SHOWER-MU-         SUM-MU+            SUM-MU-
PIMIN    0                    12864E-03          22558E-04         .26497E-04         22558E-04          .15514E-03
PIPOS     .17375E-03         0                    .50730E-04         45256E-04          22448E-03          .45256E-04
KAMIN    0                    .60077E-04          74165E-05         .86316E-05         74165E-05          68708E-04
KAPOS     .61401E-04         0.                   11270E-04         10156E-04          .72671E-04         10156E-04
PRMIN    0.                  0                    75681E-06         26638E-05          75681E-06          26638E-05
PRPOS    0                   0                    15634E-04         .51902E-05         15634E-04          51902E-05
NEMIN    0.                  0.                   .16064E-05         .18642E-05         16064E-05          18642E-05
NEPOS    0.                  0                    42994E-05         .40612E-05         42994E-05          40612E-05
KZERO     .15248E-05          15248E-05           73165E-05         84033E-05          88413E-05          99281E-05

ALL NEGATIVE:  DECAY    19024E-03   SHOWER    11272E-03   TOTAL    30296E-03
ALL POSITIVE.  DECAY    .23668E-03   SHOWER   12159E-03   TOTAL    35826E-03
SUMMARY PCUT-EHAD-X-WSQ   15 450 250 000   .175   387 883   MU-/MU+/TOTAL   .30296E-03    35826E-03    66123E-03
-----------------------------------------------------------------------------------------------------
```

```
*****************************************************************************************************
********** MOMENTUM CUT =  20 45          MEAN X =     1748 **********
*****************************************************************************************************

--> HADRON ENERGY =  30 0      ---> MEAN WSQ =  47 320

          PRIMARY-MU+        PRIMARY-MU-        SHOWER-MU+         SHOWER-MU-         SUM-MU+            SUM-MU-
PIMIN    0.                   51549E-06          .16517E-07         42700E-08          16517E-07          51976E-06
PIPOS      18650E-05          0                   15183E-07         59440E-07          18802E-05          59440E-07
KAMIN    0                    17138E-06          .52713E-08         13804E-08          52713E-08          17276E-06
KAPOS      91721E-06          0                   68496E-08         26979E-07          92406E-06          26979E-07
PRMIN    0                    0                   38822E-09         30273E-09          38822E-09          30273E-09
PRPOS    0                    0                   37764E-08         48550E-08          37764E-08          48550E-08
NEMIN    0                    0                   10394E-08         26989E-09          10394E-08          26989E-09
NEPOS    0                    0                   76234E-09         28743E-08          76234E-09          28743E-08
KZERO    0                    0                   72848E-08         19088E-08          72848E-08          19088E-08

ALL NEGATIVE  DECAY    68687E-06   SHOWER    10228E-06   TOTAL    78915E-06
ALL POSITIVE  DECAY    27822E-05   SHOWER    57072E-07   TOTAL    28393E-05
SUMMARY PCUT-EHAD-X-WSQ   20 450  30 000   175    47 320   MU-/MU+/TOTAL    78915E-06     28393E-05     36284E-05
-----------------------------------------------------------------------------------------------------

--> HADRON ENERGY =  40 0      ---> MEAN WSQ =  62.800

          PRIMARY-MU+        PRIMARY-MU-        SHOWER-MU+         SHOWER-MU-         SUM-MU+            SUM-MU-
PIMIN    0                    22933E-05          .91591E-07         21362E-07          91591E-07          23146E-05
PIPOS      71963E-05          0                   .66382E-07         29508E-06          72627E-05          29508E-06
KAMIN    0                    94211E-06          34697E-07         82798E-08          34697E-07          95039E-06
KAPOS      33425E-05          0                   .27841E-07         12524E-06          33703E-05          12524E-06
PRMIN    0                    0                   .24206E-08         17294E-08          24206E-08          17294E-08
PRPOS    0                    0                   .18430E-07         27263E-07          18430E-07          27263E-07
NEMIN    0                    0                   60769E-08         14259E-08          60769E-08          14259E-08
NEPOS    0                    0                   41489E-08         .17673E-07         41489E-08          17673E-07
KZERO    0                    0                   45339E-07         10741E-07          45339E-07          10741E-07

ALL NEGATIVE  DECAY   .32354E-05   SHOWER   .50880E-06   TOTAL   .37442E-05
ALL POSITIVE  DECAY   10539E-04   SHOWER    29693E-06   TOTAL    10836E-04
SUMMARY PCUT-EHAD-X-WSQ   20 450  40 000   175    62 800   MU-/MU+/TOTAL    37442E-05     10836E-04     14580E-04
-----------------------------------------------------------------------------------------------------

--> HADRON ENERGY =  75 0      ---> MEAN WSQ =  116.98

          PRIMARY-MU+        PRIMARY-MU-        SHOWER-MU+         SHOWER-MU-         SUM-MU+            SUM-MU-
PIMIN    0                    16278E-04          10127E-05         21589E-06          10127E-05          16493E-04
PIPOS      35856E-04          0                   57510E-06         26632E-05          36431E-04          .26632E-05
KAMIN    0.                   83489E-05          43832E-06         92507E-07          43832E-06          84414E-05
KAPOS      14994E-04          0                   20311E-06         93913E-06          15197E-04          93913E-06
PRMIN    0                    0                   .31499E-07         19870E-07          31499E-07          19870E-07
PRPOS    0                    0                   15407E-06         23879E-06          15407E-06          23879E-06
NEMIN    0                    0                   72122E-07         15385E-07          72122E-07          15385E-07
NEPOS    0                    0                   36596E-07         17368E-06          36596E-07          17368E-06
KZERO      17187E-07          25394E-07          50774E-06         10668E-06          52493E-06          13207E-06

ALL NEGATIVE  DECAY    24652E-04   SHOWER    44652E-05   TOTAL    29117E-04
ALL POSITIVE  DECAY    50867E-04   SHOWER   .30313E-05   TOTAL    53898E-04
SUMMARY PCUT-EHAD-X-WSQ   20 450  75 000  .175   116 981   MU-/MU+/TOTAL    29117E-04     53898E-04     83015E-04
-----------------------------------------------------------------------------------------------------
```



```
*****************************************************************************************************
********** MOMENTUM CUT =  20 45          MEAN X =     1748 **********
*****************************************************************************************************

--> HADRON ENERGY = 100 0      ---> MEAN WSQ =  155 68

          PRIMARY-MU+        PRIMARY-MU-        SHOWER-MU+         SHOWER-MU-         SUM-MU+            SUM-MU-
PIMIN    0                    28691E-04          22835E-05         52428E-06          22835E-05          29215E-04
PIPOS      55148E-04          0.                  13478E-05         54914E-05          56496E-04          54914E-05
KAMIN    0                    15051E-04          98112E-06         22044E-06          98112E-06          15272E-04
KAPOS     .22085E-04          0                   43575E-06         17571E-05          22521E-04          17571E-05
PRMIN    0                    0                   74944E-07         49714E-07          74944E-07          49714E-07
PRPOS    0                    0                   38326E-06         47417E-06          38326E-06          47417E-06
NEMIN    0                    0                   16598E-06         38304E-07          16598E-06          38304E-07
NEPOS    0                    0                   91249E-07         36470E-06          91249E-07          36470E-06
KZERO      37405E-07          14380E-06          10797E-05         24577E-06          11171E-05          38957E-06

ALL NEGATIVE  DECAY   .43886E-04   SHOWER    91659E-05   TOTAL    53052E-04
ALL POSITIVE  DECAY   .77271E-04   SHOWER    68432E-05   TOTAL    84114E-04
SUMMARY PCUT-EHAD-X-WSQ   20 450 100 000   175   155 681   MU-/MU+/TOTAL    53052E-04     84114E-04     13717E-03
-----------------------------------------------------------------------------------------------------

--> HADRON ENERGY = 150.0      ---> MEAN WSQ =  233 08

          PRIMARY-MU+        PRIMARY-MU-        SHOWER-MU+         SHOWER-MU-         SUM-MU+            SUM-MU-
PIMIN    0                    50476E-04          59325E-05         16644E-05          59325E-05          52141E-04
PIPOS      83397E-04          0                   .41145E-05         12765E-04          .87512E-04         12765E-04
KAMIN    0                    26284E-04          .23976E-05         66050E-06          23976E-05          26945E-04
KAPOS      31867E-04          0                   .11782E-05         .35684E-05         33045E-04          35684E-05
PRMIN    0                    0                   20303E-06         16101E-06          20303E-06          16101E-06
PRPOS    0                    0                   13974E-05         11135E-05          13974E-05          11135E-05
NEMIN    0                    0.                  43428E-06         12429E-06          43428E-06          12429E-06
NEPOS    0                    0                   33097E-06         90905E-06          33097E-06          90905E-06
KZERO      23948E-06          26296E-06          .24800E-05         70974E-06          27195E-05          97270E-06

ALL NEGATIVE  DECAY   .77024E-04   SHOWER    21676E-04   TOTAL    98699E-04
ALL POSITIVE  DECAY   11550E-03   SHOWER    18468E-04   TOTAL    13397E-03
SUMMARY PCUT-EHAD-X-WSQ   20 450 150.000   175   233 082   MU-/MU+/TOTAL    98699E-04     13397E-03     23267E-03
-----------------------------------------------------------------------------------------------------

--> HADRON ENERGY = 200 0      ---> MEAN WSQ =  310 48

          PRIMARY-MU+        PRIMARY-MU-        SHOWER-MU+         SHOWER-MU-         SUM-MU+            SUM-MU-
PIMIN    0                    68114E-04          10336E-04         35120E-05          10336E-04          71626E-04
PIPOS      10309E-03          0                   85493E-05         20935E-04          11164E-03          20935E-04
KAMIN    0                    34379E-04          39229E-05         13296E-05          39229E-05          35708E-04
KAPOS      38156E-04          0                   22716E-05         53686E-05          40428E-04          53686E-05
PRMIN    0.                   0                   35483E-06         33848E-06          35483E-06          33848E-06
PRPOS    0                    0                   .35111E-05         19669E-05          35111E-05          19669E-05
NEMIN    0                    0                   .74731E-06         26335E-06          74731E-06          26335E-06
NEPOS    0                    0                   81295E-06         16310E-05          81295E-06          16310E-05
KZERO      71416E-06          75616E-06          .39225E-05         13999E-05          46367E-05          21561E-05

ALL NEGATIVE  DECAY   10325E-03   SHOWER    36745E-04   TOTAL    13999E-03
ALL POSITIVE  DECAY   14196E-03   SHOWER    34429E-04   TOTAL    17639E-03
SUMMARY PCUT-EHAD-X-WSQ   20 450 200 000  .175   310 483   MU-/MU+/TOTAL    13999E-03     17639E-03     31638E-03
-----------------------------------------------------------------------------------------------------
```

```
*****************************************************************************************
********** MOMENTUM CUT =  20.45          MEAN X =    .1748 **********
*****************************************************************************************

--> HADRON ENERGY = 250.0      ---> MEAN WSQ =  387.88

          PRIMARY-MU+        PRIMARY-MU-        SHOWER-MU+        SHOWER-MU-        SUM-MU+           SUM-MU-
PIMIN    0.                  .85269E-04         15466E-04         .62298E-05        .15466E-04         91499E-04
PIPOS     .12083E-03         0.                 .14853E-04         .29825E-04        .13569E-03         29825E-04
KAMIN    0                   .40953E-04         .55293E-05         .22633E-05         55293E-05         .43217E-04
KAPOS     43276E-04          0.                 .37444E-05         71836E-05         .47020E-04         .71836E-05
PRMIN    0.                  0                  .52499E-06         .59416E-06        .52499E-06         59416E-06
PRPOS    0.                  0.                  71876E-05         .30309E-05        .71876E-05         .30309E-05
NEMIN    0.                  0                  .10925E-05         .46338E-06        .10925E-05         46338E-06
NEPOS    0.                  0                  .16192E-05         25129E-05         .16192E-05         .25129E-05
KZERO     .59811E-06          65924E-06         .53923E-05         23392E-05         .59904E-05         29984E-05

ALL NEGATIVE  DECAY   .12688E-03   SHOWER   .54442E-04   TOTAL    18132E-03
ALL POSITIVE  DECAY   .16471E-03   SHOWER    55409E-04   TOTAL    .22012E-03
SUMMARY:PCUT-EHAD-X-WSQ   20 450 250.000  .175   387.883   MU-/MU+/TOTAL    18132E-03     22012E-03     40144E-03
-----------------------------------------------------------------------------------------
```


Appendix H

Like Sign Dimuon Sample

Computer drawn event displays of 18 like sign dimuon events from this experiment are shown. All the information about geometry and kinematics of these events is also provided.

Information shown in the pictures is the first approximation of final values. The quantities displayed are:

P1 - the momentum at the front of the first toroid of the muon marked by circles (in GeV/c);
P2 - the momentum at the front of the second toroid of the muon marked by squares (in GeV/c);
TH1 - the polar angle of the muon marked by circles (in radians);
TH2 - the polar angle of the muon marked by squares (in radians);
VX,Y - transverse vertex position in the apparatus (in inches)
HAD10 - hadron energy (in GeV);
PLACE - the counter number of the first counter downstream of the interaction point (counter 82 is the most upstream counter);

The final values of kinematic and geometric quantities (after the choice of the leading and the second muon) are shown in the form of event summaries. Names used for the important characteristics are:

SMOM - the momentum setting of the train,
IKN = 1 for K, IKN = 2 for π events,
RAD = the radius of the vertex (in inches),
ANG1 = the polar angle (with respect to the incoming neutrino direction) of the first muon (in radians),
ANG2 = the polar angle (with respect to the incoming neutrino direction) of the second muon (in radians),
PTOT1 = the total momentum of the first muon (in GeV/c),
PTOT2 = the total momentum of the second muon (in GeV/c),
EMEAS = the total measured energy of the interaction (in GeV),
EHAD = the total hadron shower energy (in GeV),
XVIS = the Bjorken x determined from the measured values,
YVIS = the scaling y variable determined from the measured values,
VNUVIS = ν determined from the measured values (in GeV),
QSQVIS = Q^2 determined from the measured values (in GeV^2/c^2),
WWVIS = W^2 determined from the measured values (in GeV^2/c^4),
VERTX = the x position of the vertex (in inches),
VERTY = the y position of the vertex (in inches),
ENEU = the neutrino energy as determined from the radial position of the vertex (in GeV),
PHI12 = the azimuthal angel between the two muons in the plane transverse to the incoming neutrino direction (in radians),
QSQ = Q^2 determined using the energy of the interaction determined form the radial position of the vertex (in GeV^2/c^2),
VNU = ν determined using the energy of the interaction determined form the radial position of the vertex (in GeV),
WW = W^2 determined using the energy of the interaction determined form the radial position of the vertex (in GeV^2/c^4),
XRAD = x determined using the energy of the interaction determined form the radial position of the vertex,
PHI = the azimuthal angle of the first muon (in radians),
ZM2VIS = PTOT2/(EHAD+PTOT2)

ZMU2 = as ZM2VIS using the radial position of the interaction,
PMUHD = the transverse momentum of the second muon with respect to the hadron shower direction (in GeV/c),
VERTZ = the longitudinal position of the vertex.

RUN	1353	EVENT	2099	SMOM	250	PLACE	17	IFILE	1	IKAON	-1	ISAMSN	-1
IFR,SC	1 1	IBM,SL	0 0	EFFICY	.2430	EFFSGN	.2693	EFFKNM	.1904	RAD	54.10	ANG1	.1301
ANG2	.2735E-01	PTOT1	20.41	PTOT2	10.08	EMEAS	149.4	EHAD	119.2	XVIS	.2131	YVIS	.7978
VNUVIS	129.0	QSQVIS	51.63	WWVIS	13.83	PMUTR	-.1670	PH	150.4	VERTX	44.56	VERTY	35.15
ENEU	170.6	PHI12	2.558	QSQ	58.96	VNU	150.2	WW	14.96	XRAD	.2073	PHI	2.398
ZMU2	.6713E-01	ZM2VIS	.7816E-01	PMUHD	.1739	WEI	0.	WMUZ	9999.	PTOT3	0.	ANG3	0.
EFF2	.2693	EFF1	0.	IEHT	1	N67	1 IKN 1	IG1	-2 IG2 -2	IFDMC2	0	VERTZ	-147.3

RUN	1476	EVENT	794	SMOM	165	PLACE	40	IFILE	3	IKAON	-1	ISAMSN	-1
IFR,SC	0 0	IBM,SL	0 0	EFFICY	.5020	EFFSGN	.7635	EFFKNM	.4835	RAD	51.31	ANG1	.7020E-01
ANG2	.4405E-01	PTOT1	60.38	PTOT2	29.09	EMEAS	139.4	EHAD	50.69	XVIS	.2795	YVIS	.3635
VNUVIS	79.05	QSQVIS	41.49	WWVIS	10.38	PMUTR	-.3406	PH	79.29	VERTX	-44.26	VERTY	21.35
ENEU	139.4	PHI12	2.912	QSQ	41.48	VNU	79.03	WW	10.38	XRAD	.2717	PHI	4.584
ZMU2	.3681	ZM2VIS	.3680	PMUHD	.4741	WEI	0.	WMUZ	1.910	PTOT3	0.	ANG3	0.
EFF2	.7635	EFF1	.5237	IEHT	1	N67	1 IKN 1	IG1	-2 IG2 -2	IFDMC2	0	VERTZ	-335.3

RUN	1599	EVENT	1547	SMOM	250	PLACE	46	IFILE	1	IKAON	-1	ISAMSN	-1
IFR,SC	1 1	IBM,SL	1 0	EFFICY	.6566	EFFSGN	.5165	EFFKNM	.5958	RAD	46.66	ANG1	.9123E-01
ANG2	.4876E-01	PTOT1	82.22	PTOT2	24.67	EMEAS	215.2	EHAD	109.1	XVIS	.5894	YVIS	.5072
VNUVIS	133.0	QSQVIS	147.2	WWVIS	10.16	PMUTR	-.7792	PH	102.0	VERTX	-28.91	VERTY	-33.19
ENEU	183.6	PHI12	2.474	QSQ	125.6	VNU	101.4	WW	8.097	XRAD	.6524	PHI	5.723
ZMU2	.2434	ZM2VIS	.1855	PMUHD	1.178	WEI	0.	WMUZ	9999.	PTOT3	0.	ANG3	0.
EFF2	.5165	EFF1	0.	IEHT	1	N67	1 IKN 1	IG1	-2 IG2 -2	IFDMC2	0	VERTZ	-383.5

RUN	1677	EVENT	2795	SMOM	140	PLACE	27	IFILE	4	IKAON	0	ISAMSN	-1
IFR,SC	0 0	IBM,SL	0 0	EFFICY	.8373	EFFSGN	.5466	EFFKNM	.6997	RAD	17.73	ANG1	.1527
ANG2	.4882E-01	PTOT1	16.27	PTOT2	18.05	EMEAS	63.54	EHAD	29.68	XVIS	.2712	YVIS	.4670
VNUVIS	47.28	QSQVIS	24.07	WWVIS	8.095	PMUTR	-.2691E-01	PH	35.13	VERTX	19.82	VERTY	2.991
ENEU	51.12	PHI12	3.099	QSQ	19.37	VNU	34.86	WW	6.850	XRAD	.2886	PHI	4.758
ZMU2	.5180	ZM2VIS	.3819	PMUHD	.3936	WEI	0.	WMUZ	4.037	PTOT3	0.	ANG3	0.
EFF2	.5466	EFF1	.2477	IEHT	1	N67	1 IKN 2	IG1	-2 IG2 -2	IFDMC2	0	VERTZ	-229.3

RUN	1762	EVENT	2024	SMOM	200	PLACE	44	IFILE	2	IKAON	-1	ISAMSN	-1
IFR,SC	0 0	IBM,SL	0 0	EFFICY	.2901	EFFSGN	.4665	EFFKNM	.5162	RAD	59.86	ANG1	.1704E-01
ANG2	.5763E-01	PTOT1	96.98	PTOT2	10.33	EMEAS	146.5	EHAD	39.92	XVIS	.4445E-01	YVIS	.2725
VNUVIS	49.48	QSQVIS	4.130	WWVIS	9.466	PMUTR	-.5609E-01	PH	49.39	VERTX	-47.25	VERTY	-31.21
ENEU	146.3	PHI12	3.042	QSQ	4.126	VNU	49.35	WW	9.454	XRAD	.3887E-01	PHI	3.675
ZMU2	.2092	ZM2VIS	.2087	PMUHD	.2916	WEI	0.	WMUZ	1.128	PTOT3	0.	ANG3	0.
EFF2	.4665	EFF1	.8862	IEHT	1	N67	1 IKN 1	IG1	-2 IG2 -2	IFDMC2	0	VERTZ	-367.0

RUN	1971	EVENT	5251	SMOM	250	PLACE	24	IFILE	1	IKAON	0	ISAMSN	-1
IFR,SC	1 1	IBM,SL	0 0	EFFICY	.2755	EFFSGN	.1992	EFFKNM	.2446	RAD	6.662	ANG1	.2397
ANG2	.5243E-01	PTOT1	9.782	PTOT2	17.92	EMEAS	100.1	EHAD	72.83	XVIS	.3307	YVIS	.7273
VNUVIS	90.35	QSQVIS	56.11	WWVIS	10.69	PMUTR	.2486	PH	87.78	VERTX	8.405	VERTY	.7499E-01
ENEU	97.25	PHI12	3.406	QSQ	54.49	VNU	87.47	WW	10.51	XRAD	.3318	PHI	5.377
ZMU2	.2048	ZM2VIS	.1983	PMUHD	.5008	WEI	0.	WMUZ	9999.	PTOT3	0.	ANG3	0.
EFF2	.1992	EFF1	0.	IEHT	1	N67	1 IKN 2	IG1	-2 IG2 -2	IFDMC2	0	VERTZ	-204.8

RUN	2070	EVENT	1941	SMOM	250	PLACE	60	IFILE	1	IKAON	-1	ISAMSN	-1
IFR,SC	1 0	IBM,SL	0 0	EFFICY	1.000	EFFSGN	.9680	EFFKNM	.9115	RAD	32.17	ANG1	.5965E-01
ANG2	.5431E-01	PTOT1	62.38	PTOT2	22.69	EMEAS	171.5	EHAD	87.50	XVIS	.1858	YVIS	.5102
VNUVIS	109.1	QSQVIS	38.07	WWVIS	12.94	PMUTR	-.6246	PH	145.4	VERTX	-12.78	VERTY	30.38
ENEU	207.7	PHI12	2.629	QSQ	46.11	VNU	145.3	WW	15.08	XRAD	.1687	PHI	2.707
ZMU2	.1562	ZM2VIS	.2080	PMUHD	.8042	WEI	0.	WMUZ	1.225	PTOT3	0.	ANG3	0.
EFF2	.9680	EFF1	.8163	IEHT	1	N67	1 IKN 1	IG1	-2 IG2 -2	IFDMC2	0	VERTZ	-498.6

RUN	1580	EVENT	465	SMOM	250	PLACE	55	IFILE	1	IKAON	-1	ISAMSN	-1
IFR,SC	1 0	IBM,SL	0 1	EFFICY	1.000	EFFSGN	.6146	EFFKNM	.9160	RAD	21.50	ANG1	.7640E-01
ANG2	.6984E-01	PTOT1	31.69	PTOT2	12.75	EMEAS	192.1	EHAD	148.6	XVIS	.1181	YVIS	.7734
VNUVIS	160.4	QSQVIS	35.57	WWVIS	16.32	PMUTR	.1820	PH	190.7	VERTX	10.02	VERTY	-18.14
ENEU	222.3	PHI12	3.335	QSQ	41.16	VNU	190.6	WW	17.81	XRAD	.1150	PHI	3.417
ZMU2	.6693E-01	ZM2VIS	.7951E-01	PMUHD	.7323	WEI	0.	WMUZ	1.203	PTOT3	0.	ANG3	0.
EFF2	.6146	EFF1	.8315	IEHT	1	N67	1 IKN 1	IG1	-2 IG2 -2	IFDMC2	0	VERTZ	-458.5

RUN	1855	EVENT	374	SMOM	250	PLACE	34	IFILE	1	IKAON	-1	ISAMSN	-1
IFR,SC	1 0	IBM,SL	0 1	EFFICY	.5853	EFFSGN	.3223	EFFKNM	.5748	RAD	45.18	ANG1	.1527E-01
ANG2	.9399E-01	PTOT1	136.3	PTOT2	9.730	EMEAS	169.8	EHAD	24.39	XVIS	.8579E-01	YVIS	.1436
VNUVIS	33.52	QSQVIS	5.400	WWVIS	7.641	PMUTR	-.4998	PH	49.90	VERTX	26.41	VERTY	39.80
ENEU	186.2	PHI12	2.556	QSQ	5.920	VNU	49.85	WW	9.408	XRAD	.6325E-01	PHI	.9161
ZMU2	.1952	ZM2VIS	.2903	PMUHD	.6391	WEI	0.	WMUZ	1.000	PTOT3	0.	ANG3	0.
EFF2	.3223	EFF1	1.000	IEHT	1	N67	1 IKN 1	IG1	-2 IG2 -2	IFDMC2	0	VERTZ	-285.8

RUN	1715	EVENT	6079	SMOM	165	PLACE	61	IFILE	3	IKAON	-1	ISAMSN	-1
IFR,SC	0 0	IBM,SL	0 1	EFFICY	1.000	EFFSGN	.8517	EFFKNM	.9230	RAD	29.26	ANG1	.3545E-01
ANG2	.6231E-01	PTOT1	72.52	PTOT2	20.66	EMEAS	129.9	EHAD	37.76	XVIS	.1100	YVIS	.2908
VNUVIS	57.33	QSQVIS	11.84	WWVIS	9.830	PMUTR	-1.227	PH	81.45	VERTX	18.19	VERTY	-23.95
ENEU	153.9	PHI12	1.886	QSQ	14.04	VNU	81.36	WW	11.81	XRAD	.8965E-01	PHI	5.534
ZMU2	.2539	ZM2VIS	.3604	PMUHD	1.249	WEI	0.	WMUZ	1.021	PTOT3	0.	ANG3	0.
EFF2	.8517	EFF1	.9790	IEHT	1	N67	1 IKN 1	IG1	-2 IG2 -2	IFDMC2	0	VERTZ	-506.8

RUN	354	EVENT	9238	SMOM	165	PLACE	28	IFILE	3	IKAON	-1	ISAMSN	-1
IFR,SC	1 1	IBM,SL	0 0	EFFICY	1.000	EFFSGN	.9719	EFFKNM	1.000	RAD	29.22	ANG1	.4193E-01
ANG2	.3268E-01	PTOT1	63.36	PTOT2	12.23	EMEAS	161.6	EHAD	86.47	XVIS	.9768E-01	YVIS	.5352
VNUVIS	98.20	QSQVIS	18.01	WWVIS	12.93	PMUTR	.3464	PH	90.63	VERTX	-20.70	VERTY	-12.92
ENEU	153.9	PHI12	4.240	QSQ	17.16	VNU	90.54	WW	12.39	XRAD	.1018	PHI	5.216
ZMU2	.1350	ZM2VIS	.1245	PMUHD	.3864	WEI	0.	WMUZ	1.050	PTOT3	0.	ANG3	0.
EFF2	.9719	EFF1	.9524	IEHT	0	N67	2 IKN 1	IG1	-2 IG2 -2	IFDMC2	0	VERTZ	-237.0

RUN	489	EVENT	6076	SMOM	250	PLACE	29	IFILE	1	IKAON	-1	ISAMSN	-1
IFR,SC	1 1	IBM,SL	0 0	EFFICY	1.000	EFFSGN	.7307	EFFKNM	1.000	RAD	18.05	ANG1	.1447
ANG2	.2847E-01	PTOT1	15.04	PTOT2	20.05	EMEAS	192.7	EHAD	158.1	XVIS	.1821	YVIS	.8204
VNUVIS	177.6	QSQVIS	60.72	WWVIS	16.54	PMUTR	.5376	PH	211.2	VERTX	-13.28	VERTY	8.683
ENEU	226.1	PHI12	5.074	QSQ	71.25	VNU	211.0	WW	18.04	XRAD	.1798	PHI	.3412E-01
ZMU2	.9500E-01	ZM2VIS	.1129	PMUHD	.6790	WEI	0.	WMUZ	2.039	PTOT3	0.	ANG3	0.
EFF2	.7307	EFF1	.4904	IEHT	0	N67	2 IKN 1	IG1	-2 IG2 -2	IFDMC2	0	VERTZ	-244.8

RUN	567	EVENT	229	SMOM	200	PLACE	17	IFILE	2	IKAON	-1	ISAMSN	-1
IFR,SC	1 1	IBM,SL	0 1	EFFICY	1.000	EFFSGN	.8969	EFFKNM	.9881	RAD	33.14	ANG1	.5804E-01
ANG2	.5660E-01	PTOT1	81.56	PTOT2	14.84	EMEAS	172.5	EHAD	76.40	XVIS	.2775	YVIS	.4429
VNUVIS	90.94	QSQVIS	47.39	WWVIS	11.14	PMUTR	-.2796	PH	93.57	VERTX	29.45	VERTY	-17.53
ENEU	174.9	PHI12	2.774	QSQ	48.05	VNU	93.31	WW	11.31	XRAD	.2756	PHI	4.236
ZMU2	.1590	ZM2VIS	.1632	PMUHD	.2822	WEI	0.	WMUZ	1.072	PTOT3	0.	ANG3	0.
EFF2	.8969	EFF1	.9325	IEHT	0	N67	2 IKN 1	IG1	-2 IG2 -2	IFDMC2	0	VERTZ	-147.3
RUN	661	EVENT	5844	SMOM	200	PLACE	34	IFILE	2	IKAON	-1	ISAMSN	-1
IFR,SC	1 1	IBM,SL	0 0	EFFICY	1.000	EFFSGN	.9840	EFFKNM	1.000	RAD	25.39	ANG1	.3732E-01
ANG2	.6410E-02	PTOT1	35.40	PTOT2	15.88	EMEAS	165.1	EHAD	114.4	XVIS	.3359E-01	YVIS	.6928
VNUVIS	129.7	QSQVIS	8.179	WWVIS	15.36	PMUTR	-.7927E-01	PH	146.0	VERTX	22.62	VERTY	-13.70
ENEU	181.3	PHI12	2.298	QSQ	8.986	VNU	145.9	WW	16.30	XRAD	.3285E-01	PHI	6.043
ZMU2	.1088	ZM2VIS	.1225	PMUHD	.1026	WEI	0.	WMUZ	1.027	PTOT3	0.	ANG3	0.
EFF2	.9840	EFF1	.9734	IEHT	0	N67	2 IKN 1	IG1	-2 IG2 -2	IFDMC2	0	VERTZ	-285.8
RUN	673	EVENT	3251	SMOM	140	PLACE	23	IFILE	4	IKAON	-1	ISAMSN	-1
IFR,SC	1 1	IBM,SL	1 0	EFFICY	.5410	EFFSGN	.4454	EFFKNM	.5400	RAD	19.63	ANG1	.1951
ANG2	.8798E-01	PTOT1	12.59	PTOT2	23.10	EMEAS	95.29	EHAD	59.99	XVIS	.2935	YVIS	.6295
VNUVIS	82.70	QSQVIS	45.57	WWVIS	10.51	PMUTR	.8441	PH	121.1	VERTX	3.450	VERTY	-17.55
ENEU	133.4	PHI12	5.852	QSQ	63.83	VNU	120.9	WW	12.80	XRAD	.2814	PHI	5.999
ZMU2	.1911	ZM2VIS	.2793	PMUHD	2.451	WEI	0.	WMUZ	9999.	PTOT3	0.	ANG3	0.
EFF2	.4454	EFF1	0.	IEHT	0	N67	2 IKN 1	IG1	-2 IG2 -2	IFDMC2	0	VERTZ	-196.8
RUN	799	EVENT	7539	SMOM	100	PLACE	27	IFILE	6	IKAON	-1	ISAMSN	-1
IFR,SC	1 1	IBM,SL	1 1	EFFICY	.1269	EFFSGN	.7212	EFFKNM	.1867	RAD	51.93	ANG1	.1041
ANG2	.7819E-01	PTOT1	24.44	PTOT2	17.23	EMEAS	70.78	EHAD	29.58	XVIS	.2153	YVIS	.4179
VNUVIS	46.34	QSQVIS	18.74	WWVIS	8.313	PMUTR	.1726	PH	65.76	VERTX	-4.133	VERTY	-49.72
ENEU	90.01	PHI12	3.246	QSQ	23.84	VNU	65.58	WW	10.01	XRAD	.1895	PHI	2.744
ZMU2	.2627	ZM2VIS	.3717	PMUHD	.6863	WEI	0.	WMUZ	1.909	PTOT3	0.	ANG3	0.
EFF2	.7212	EFF1	.5238	IEHT	0	N67	2 IKN 1	IG1	-2 IG2 -2	IFDMC2	0	VERTZ	-229.3
RUN	839	EVENT	2209	SMOM	250	PLACE	42	IFILE	1	IKAON	-1	ISAMSN	-1
IFR,SC	1 1	IBM,SL	0 1	EFFICY	1.000	EFFSGN	.7668	EFFKNM	1.000	RAD	21.22	ANG1	.3075E-01
ANG2	.6082E-01	PTOT1	116.5	PTOT2	10.52	EMEAS	199.0	EHAD	72.72	XVIS	.1416	YVIS	.3654
VNUVIS	82.51	QSQVIS	21.93	WWVIS	11.57	PMUTR	.3256	PH	106.2	VERTX	-17.70	VERTY	1.700
ENEU	222.6	PHI12	3.683	QSQ	24.53	VNU	106.1	WW	13.24	XRAD	.1288	PHI	5.829
ZMU2	.9921E-01	ZM2VIS	.1275	PMUHD	.3753	WEI	0.	WMUZ	1.088	PTOT3	0.	ANG3	0.
EFF2	.7668	EFF1	.9191	IEHT	0	N67	2 IKN 1	IG1	-2 IG2 -2	IFDMC2	0	VERTZ	-351.0
RUN	888	EVENT	200	SMOM	250	PLACE	42	IFILE	1	IKAON	-1	ISAMSN	-1
IFR,SC	1 1	IBM,SL	1 1	EFFICY	1.000	EFFSGN	.9780	EFFKNM	.9936	RAD	27.70	ANG1	.6807E-01
ANG2	.6581E-01	PTOT1	75.40	PTOT2	17.75	EMEAS	187.1	EHAD	94.69	XVIS	.3116	YVIS	.5061
VNUVIS	111.7	QSQVIS	65.36	WWVIS	12.05	PMUTR	.7550	PH	139.1	VERTX	6.183	VERTY	-25.48
ENEU	214.2	PHI12	3.866	QSQ	74.84	VNU	138.8	WW	13.66	XRAD	.2909	PHI	.1619
ZMU2	.1279	ZM2VIS	.1589	PMUHD	.7889	WEI	0.	WMUZ	1.079	PTOT3	0.	ANG3	0.
EFF2	.9780	EFF1	.9270	IEHT	0	N67	2 IKN 1	IG1	-2 IG2 -2	IFDMC2	0	VERTZ	-351.0

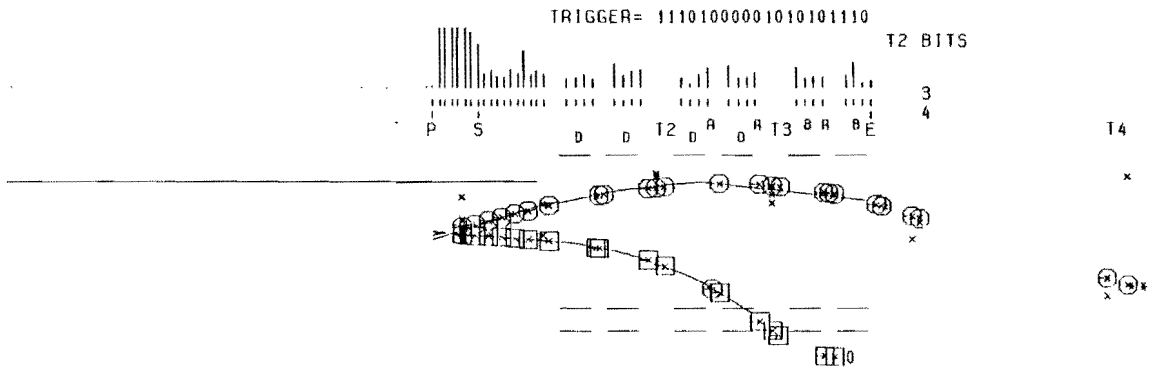

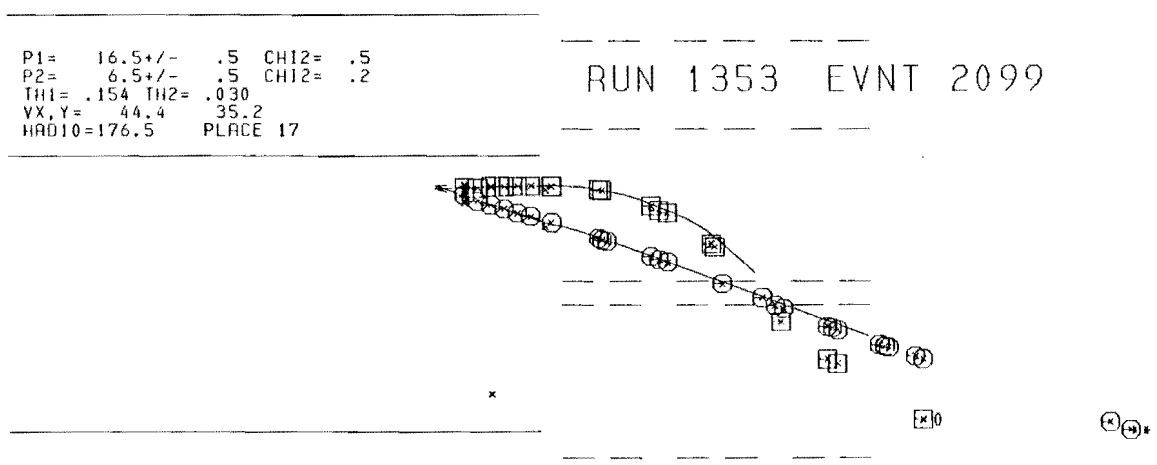

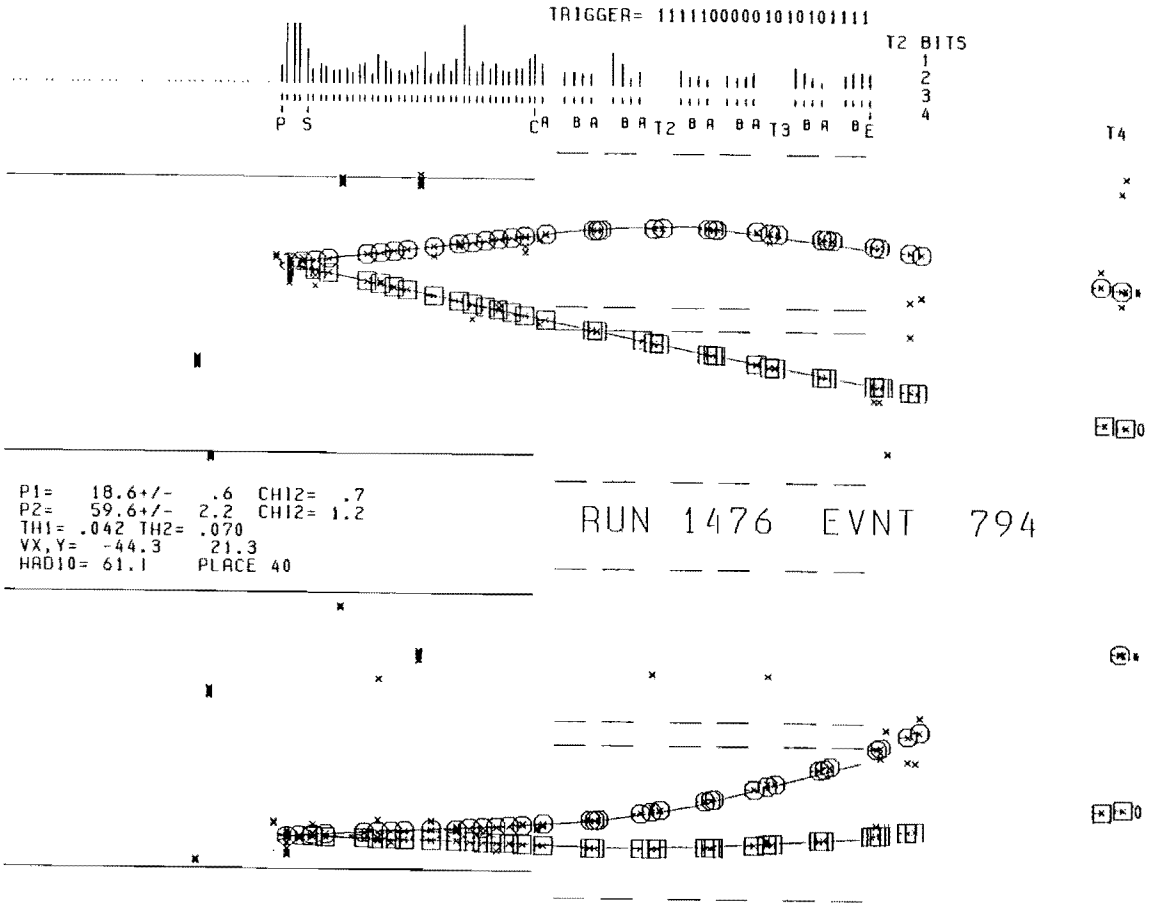
TRIGGER= 1111100000101010111 1
T2 BITS
1
2
3
4
P S
C A B A B A T2 B A B A T3 B A B E
T4
P1= 18.6+/- .6 CHI2= .7
P2= 59.6+/- 2.2 CHI2= 1.2
TH1= .042 TH2= .070
VX,Y= -44.3 21.3
HAD10= 61.1 PLACE 40
RUN 1476 EVNT 794

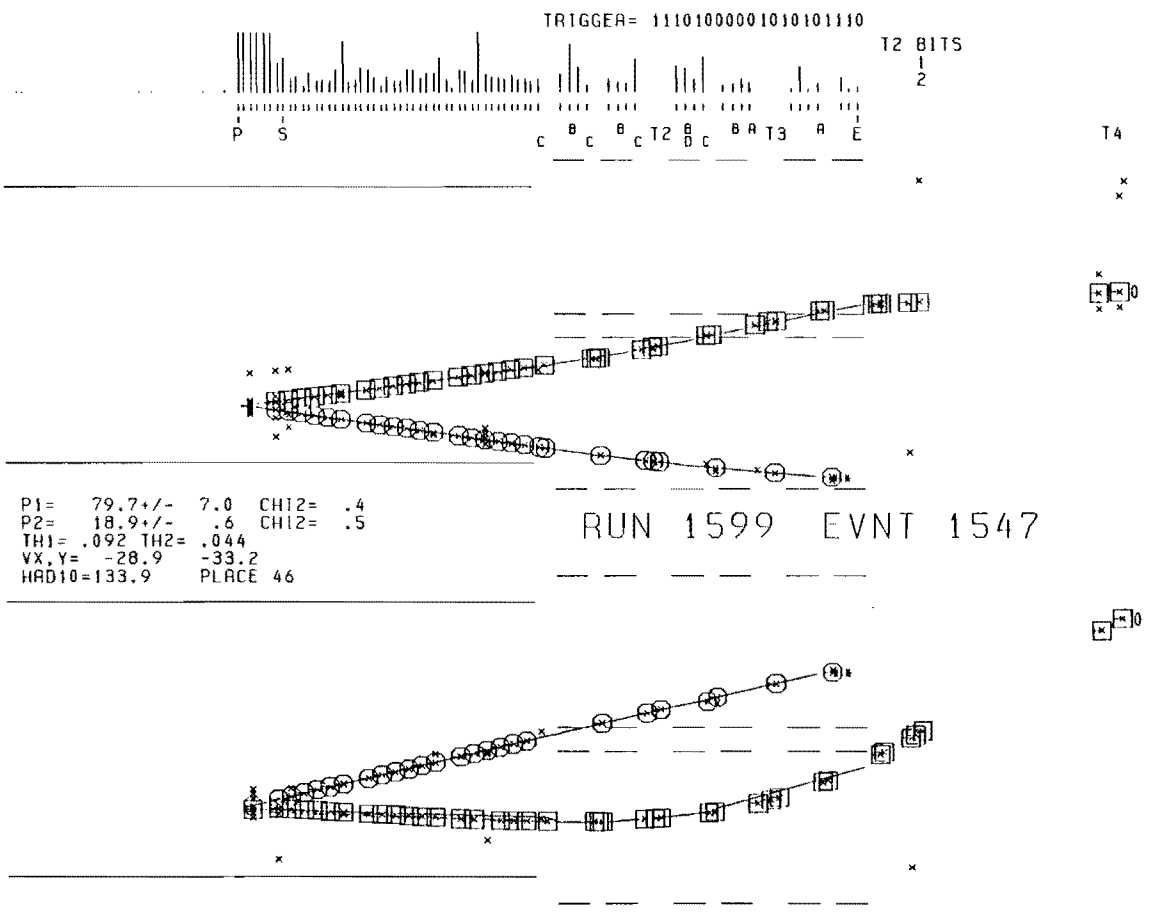
TRIGGER= 1110100000101010110
T2 BITS
1
2
P S
C B C B C T2 B D C B A T3 A E
T4
P1= 79.7+/- 7.0 CHI2= .4
P2= 18.9+/- .6 CHI2= .5
TH1= .092 TH2= .044
VX,Y= -28.9 -33.2
HAD10=133.9 PLACE 46
RUN 1599 EVNT 1547

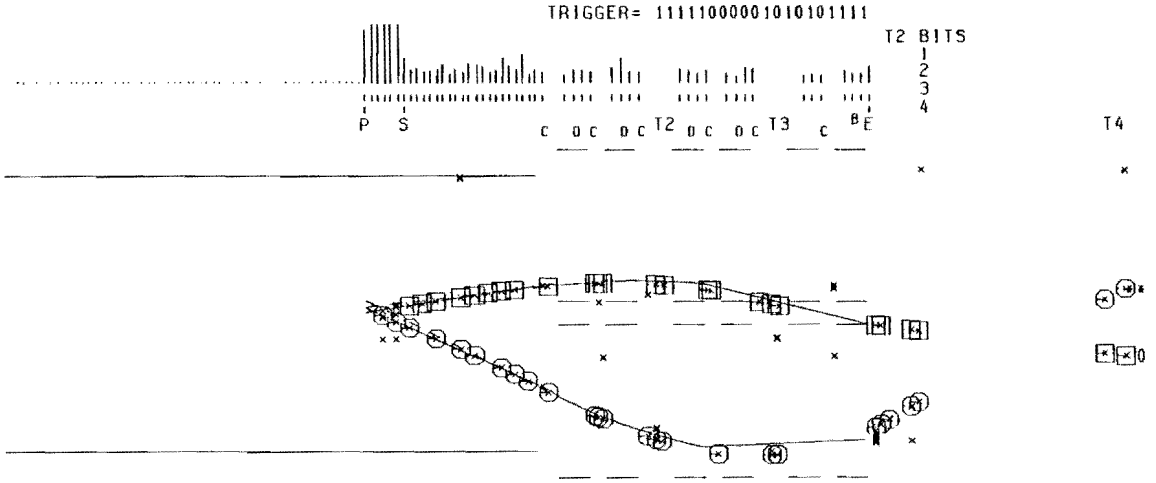

P1= 11.8+/- .3 CHI2= 1.1
P2= 11.6+/- .7 CHI2= .9
TH1= .151 TH2= .053
VX,Y= 19.8 3.0
HAD10= 31.1 PLACE 27

RUN 1677 EVNT 2795

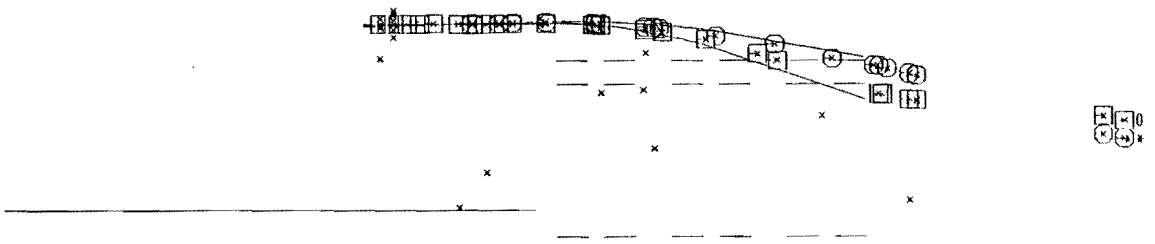

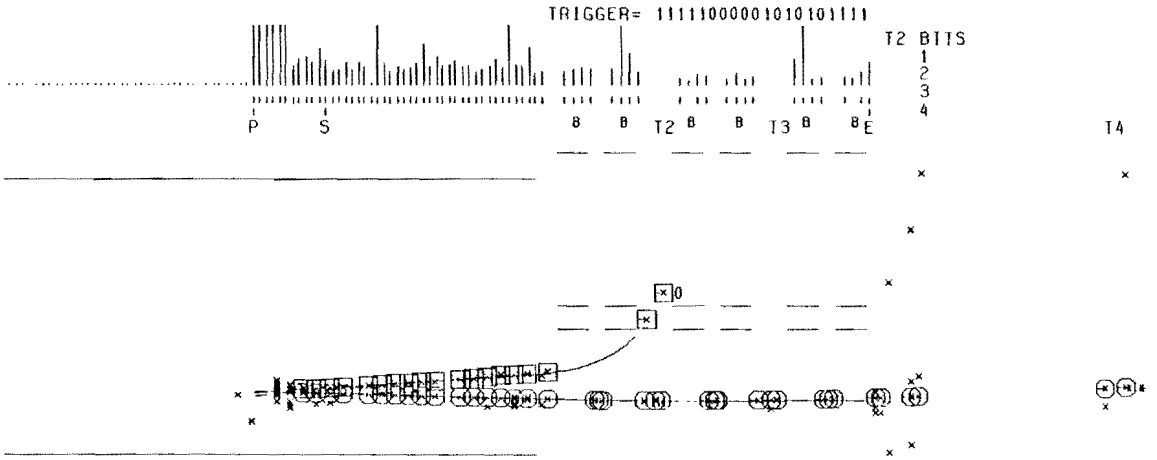

P1= 97.1+/- 3.9 CHI2= 1.2
P2= 3.0+/- .1 CHI2= .2
TH1= .016 TH2= .053
VX,Y= -47.2 -31.2
HAD10= 57.0 PLACE 44

RUN 1762 EVNT 2024

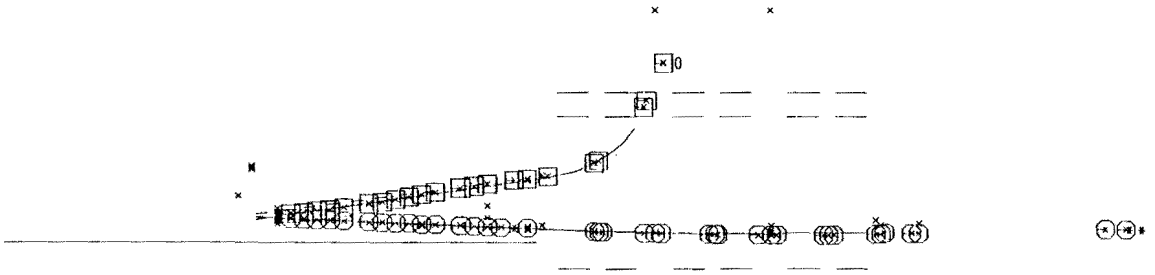

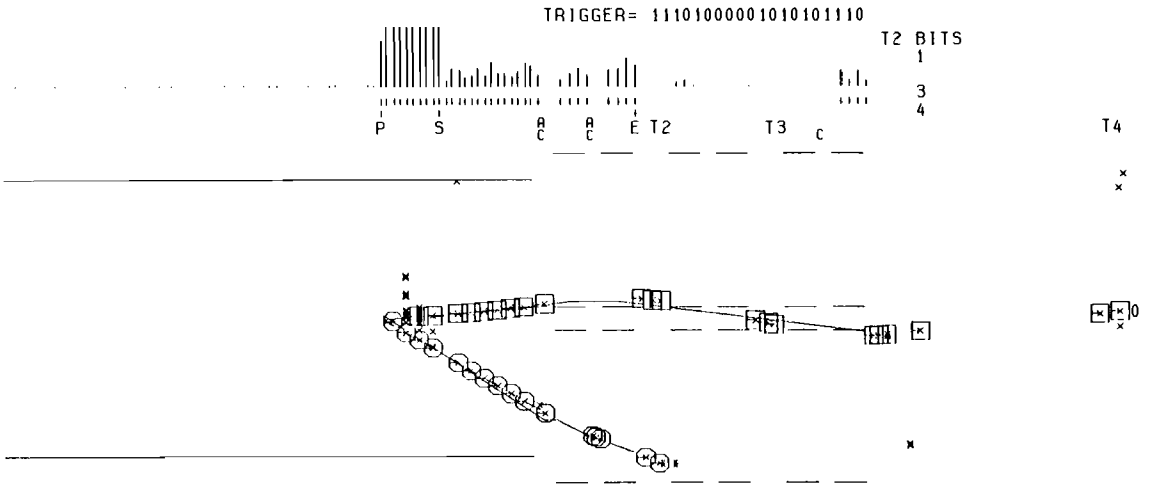
TRIGGER= 11101000001010101110
T2 BITS
1
3
4
P
S
A
C
A
C
E
T2
T3
C
T4

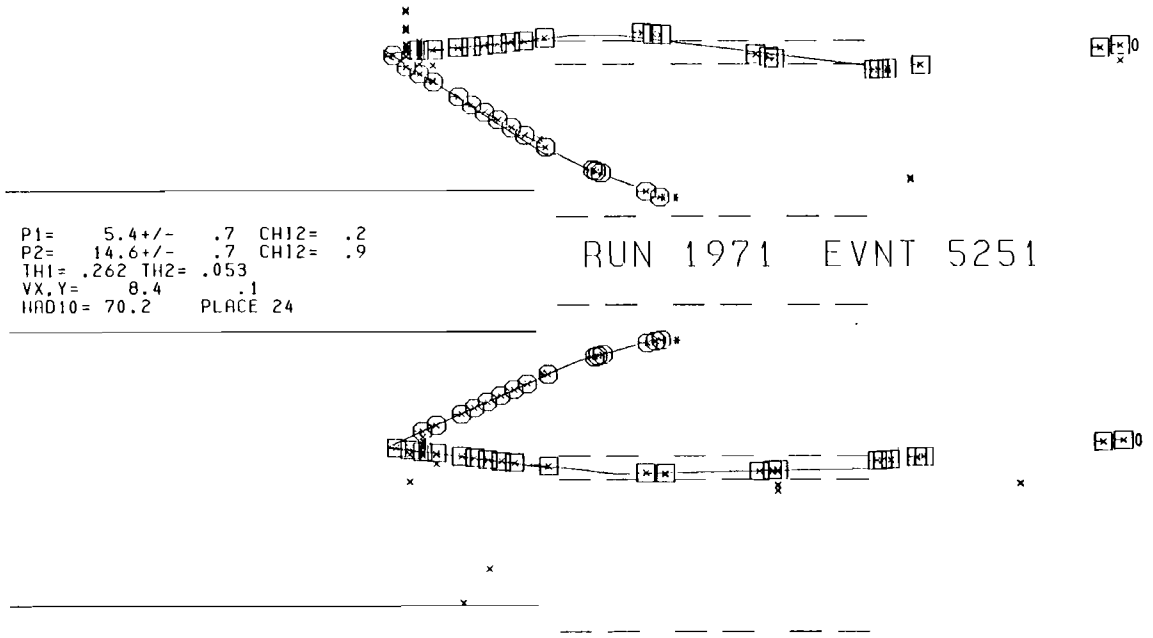
P1= 5.4+/- .7 CHI2= .2
P2= 14.6+/- .7 CHI2= .9
TH1= .262 TH2= .053
VX,Y= 8.4 .1
HAD10= 70.2 PLACE 24
RUN 1971 EVNT 5251

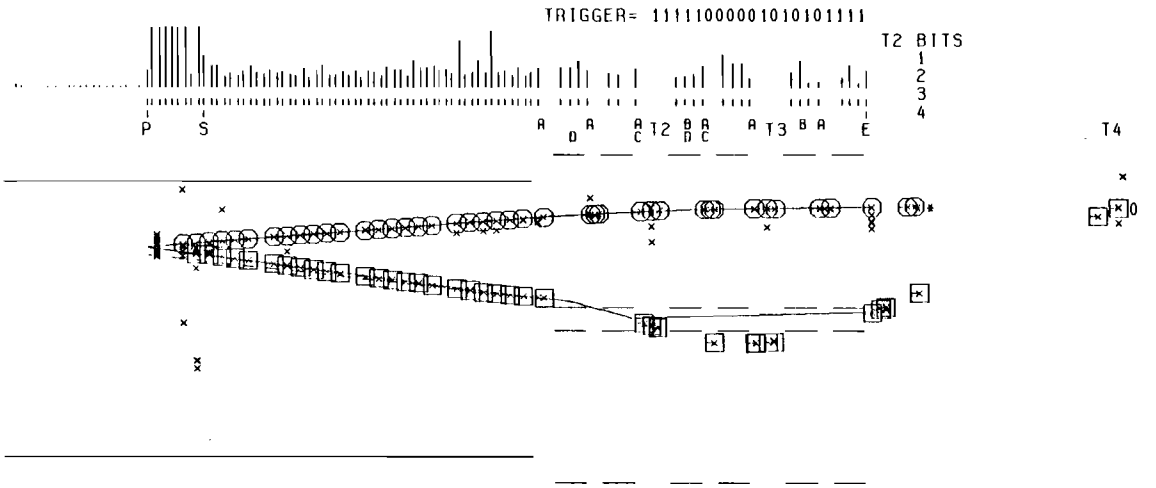
TRIGGER= 11111000001010101111
T2 BITS
1
2
3
4
P
S
A
D
A
A
C
T2
B
D
A
C
A
T3
B
A
E
T4

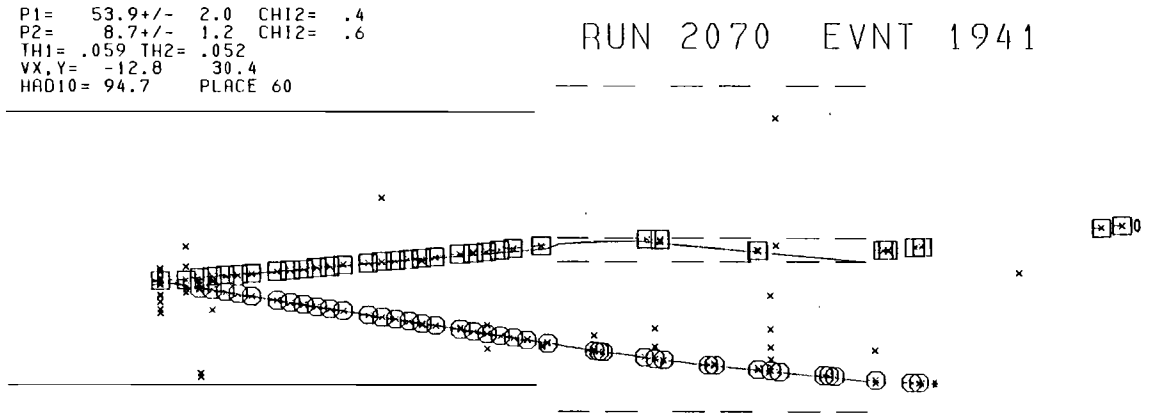
P1= 53.9+/- 2.0 CHI2= .4
P2= 8.7+/- 1.2 CHI2= .6
TH1= .059 TH2= .052
VX,Y= -12.8 30.4
HAD10= 94.7 PLACE 60
RUN 2070 EVNT 1941

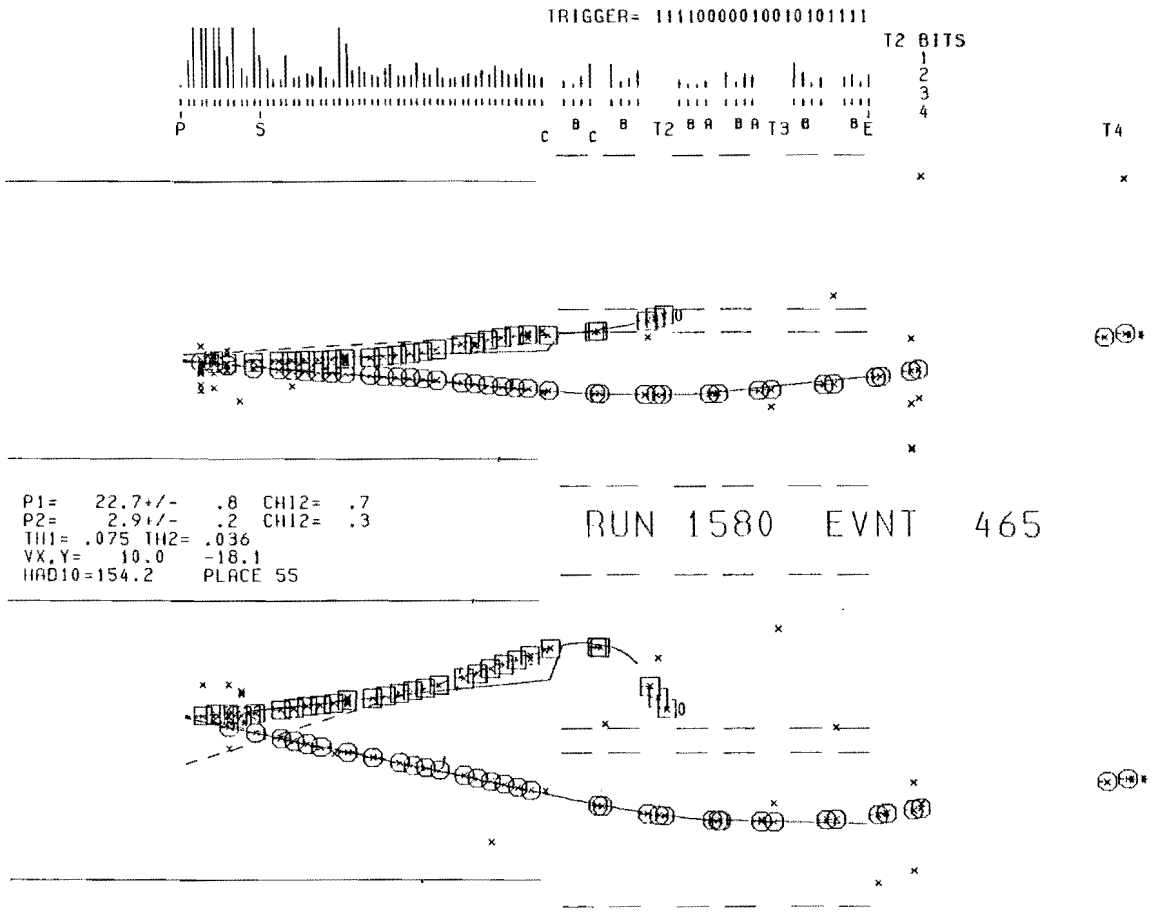
TRIGGER= 11110000010010101111
T2 BITS
1
2
3
4
P
S
C
B
C
B
T2
B
A
B
A
T3
B
B
E
T4
P1= 22.7+/- .8 CH12= .7
P2= 2.9+/- .2 CH12= .3
TH1= .075 TH2= .036
VX,Y= 10.0 -18.1
HAD10=154.2 PLACE 55
RUN 1580 EVNT 465

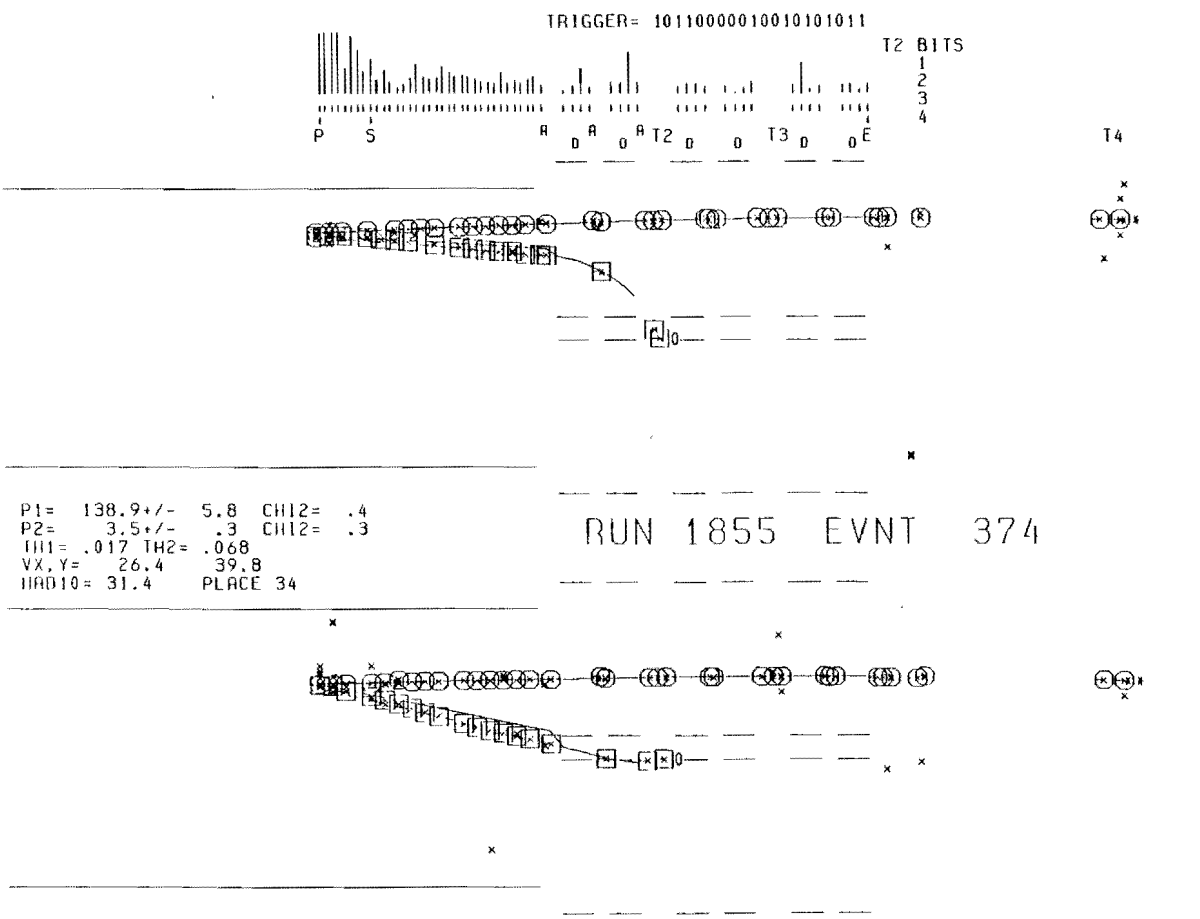
TRIGGER= 10110000010010101011
T2 BITS
1
2
3
4
P
S
A
D
A
D
A
T2
D
D
T3
D
D
E
T4
P1= 138.9+/- 5.8 CH12= .4
P2= 3.5+/- .3 CH12= .3
TH1= .017 TH2= .068
VX,Y= 26.4 39.8
HAD10= 31.4 PLACE 34
RUN 1855 EVNT 374

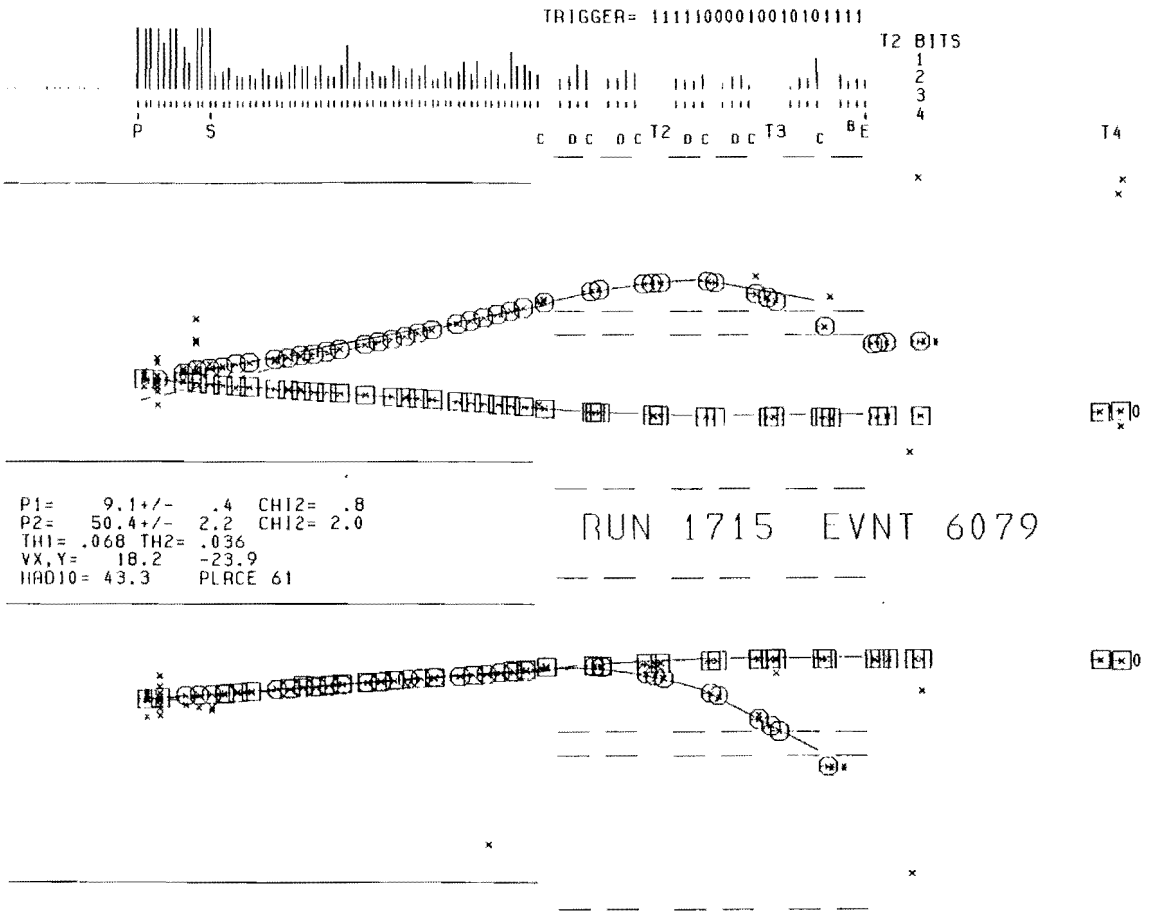
TRIGGER= 11111000010010101111
T2 BITS
1
2
3
4
P
S
T2
T3
T4
P1= 9.1+/- .4 CHI2= .8
P2= 50.4+/- 2.2 CHI2= 2.0
TH1= .068 TH2= .036
VX,Y= 18.2 -23.9
HAD10= 43.3 PLACE 61
RUN 1715 EVNT 6079

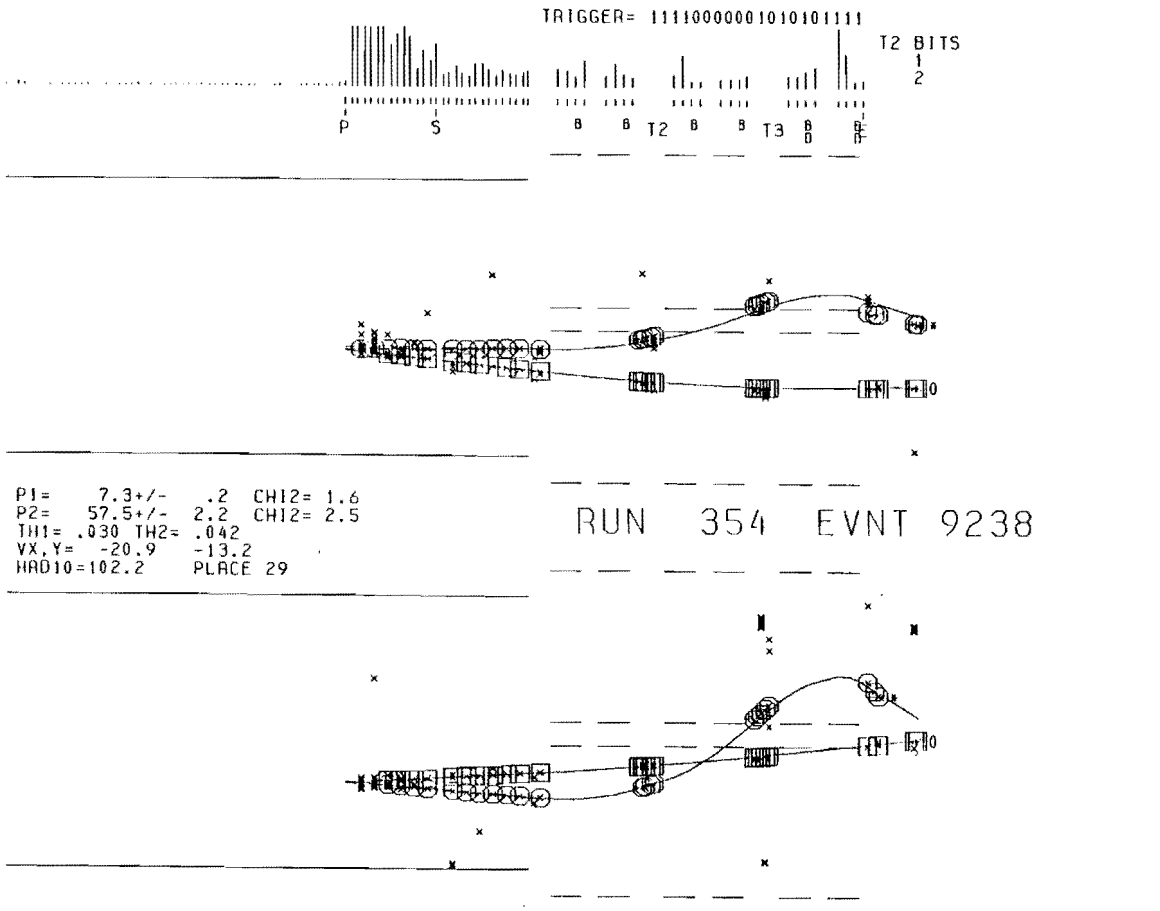
TRIGGER= 11110000001010101111
T2 BITS
1
2
P
S
T2
T3
P1= 7.3+/- .2 CHI2= 1.6
P2= 57.5+/- 2.2 CHI2= 2.5
TH1= .030 TH2= .042
VX,Y= -20.9 -13.2
HAD10=102.2 PLACE 29
RUN 354 EVNT 9238

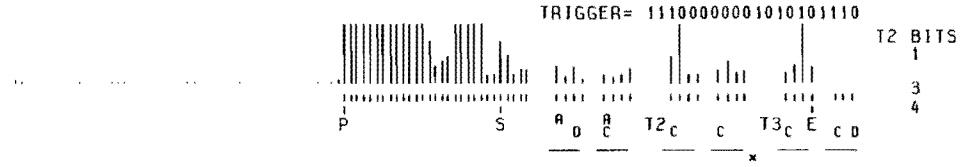

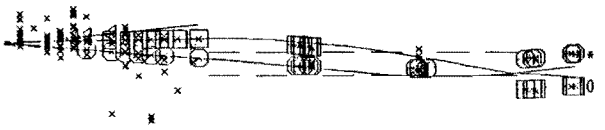

P1= 14.8+/- 1.8 CHI2= 1.4
P2= 9.8+/- .2 CHI2= 1.1
TH1= .030 TH2= .144
VX,Y= -13.3 8.7
HAD10=163.4 PLACE 29

RUN 489 EVNT 6076

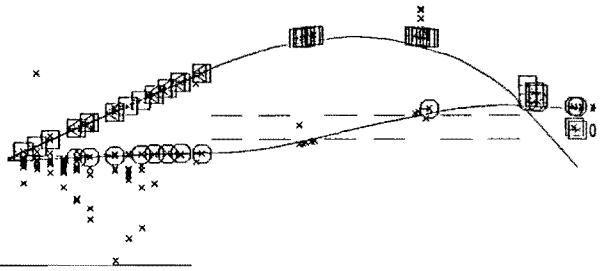

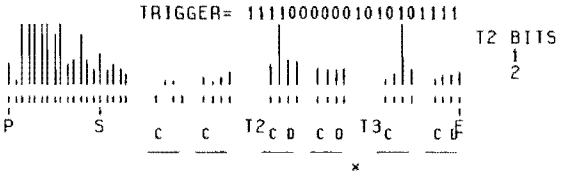

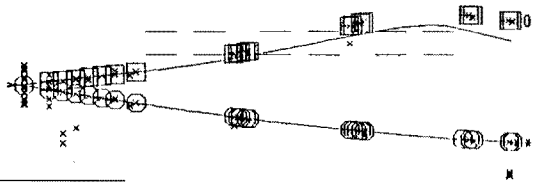

P1= 77.7+/- 3.4 CHI2= 1.0
P2= 11.5+/- .3 CHI2= 1.4
TH1= .057 TH2= .056
VX,Y= 29.8 -16.6
HAD10= 76.0 PLACE 19

RUN 567 EVNT 229

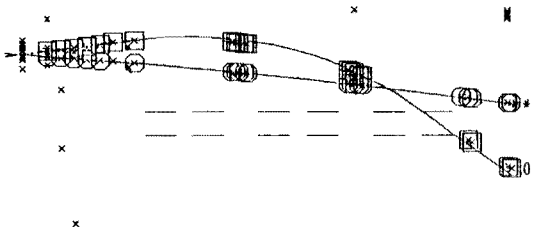

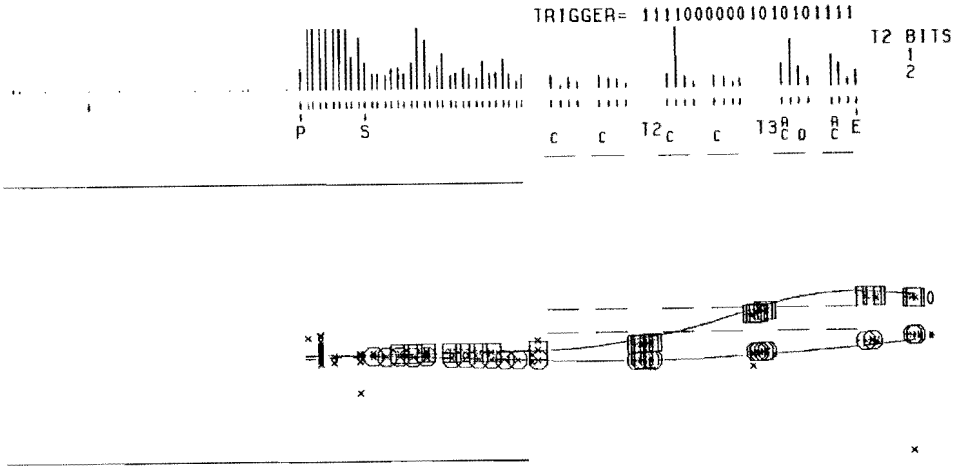

P1= 28.7+/- 1.1 CHI2= .7
P2= 9.7+/- .5 CHI2= 1.6
TH1= .039 TH2= .006
VX,Y= 22.1 -13.5
HAD10=131.4 PLACE 35

RUN 661 EVNT 5844

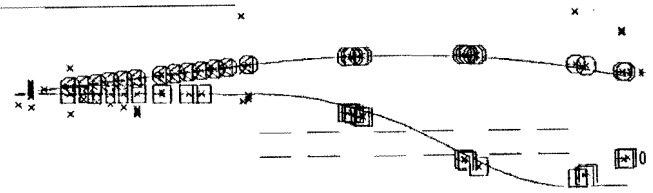

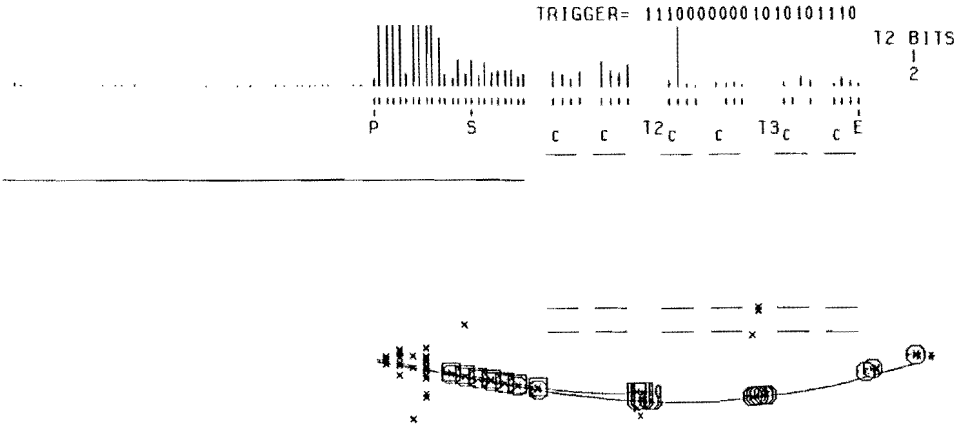

P1= 18.6+/- .7 CHI2= 1.7
P2= 8.3+/- .8 CHI2= .5
TH1= .087 TH2= .197
VX,Y= 3.1 -17.2
HAD10= 64.7 PLACE 24

RUN 673 EVNT 3251

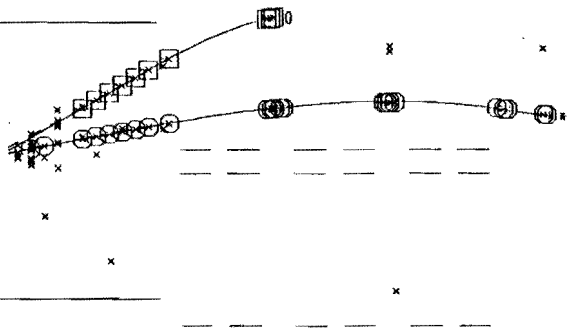

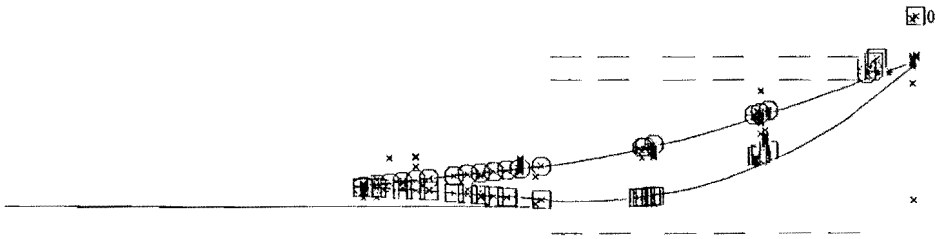

P1= 19.2+/- .7 CHI2= 2.0
P2= 12.2+/- .5 CHI2= 1.8
TH1= .104 TH2= .074
VX,Y= -3.2 -49.8
HAD10= 33.5 PLACE 28

RUN 799 EVNT 7539

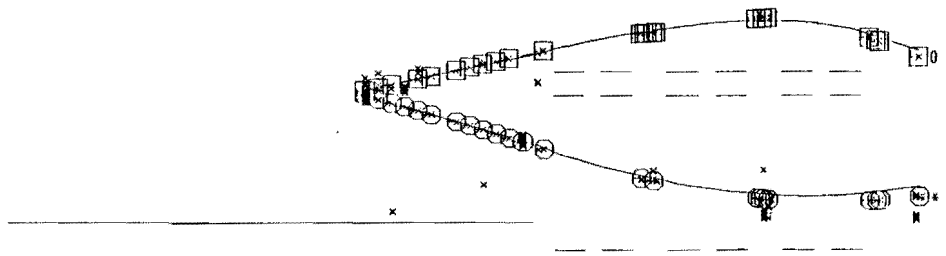

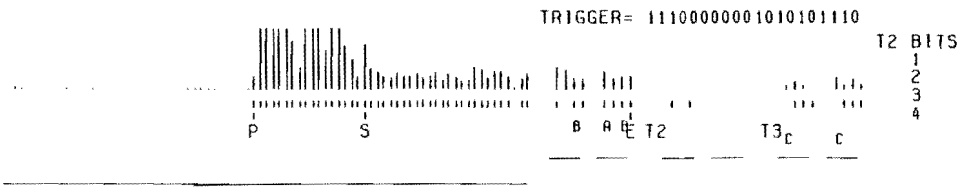

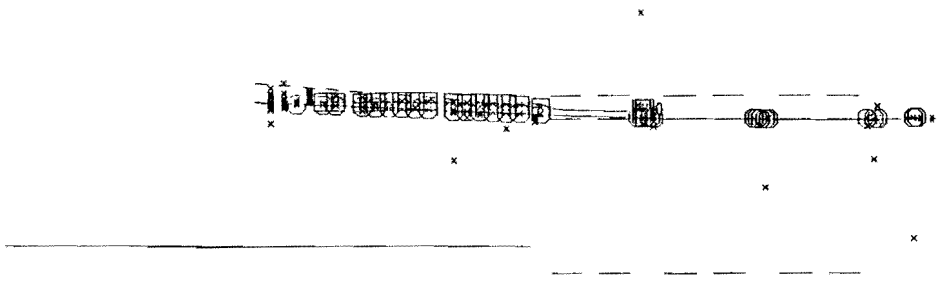

P1= 109.4+/- 5.3 CHI2= .9
P2= 3.3+/- .1 CHI2= .3
TH1= .030 TH2= .059
VX,Y= -17.9 1.8
HAD10= 79.5 PLACE 43

RUN 839 EVNT 2209

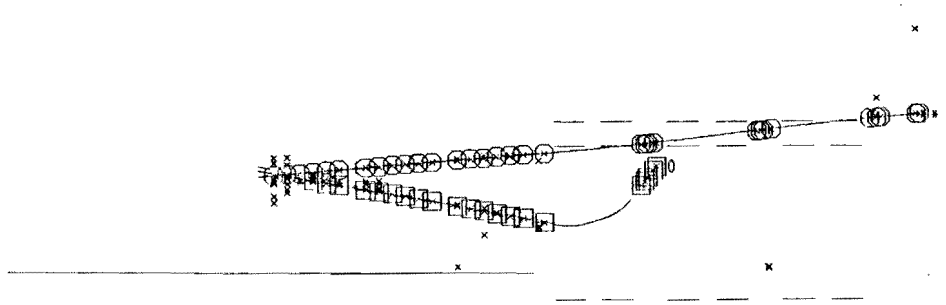

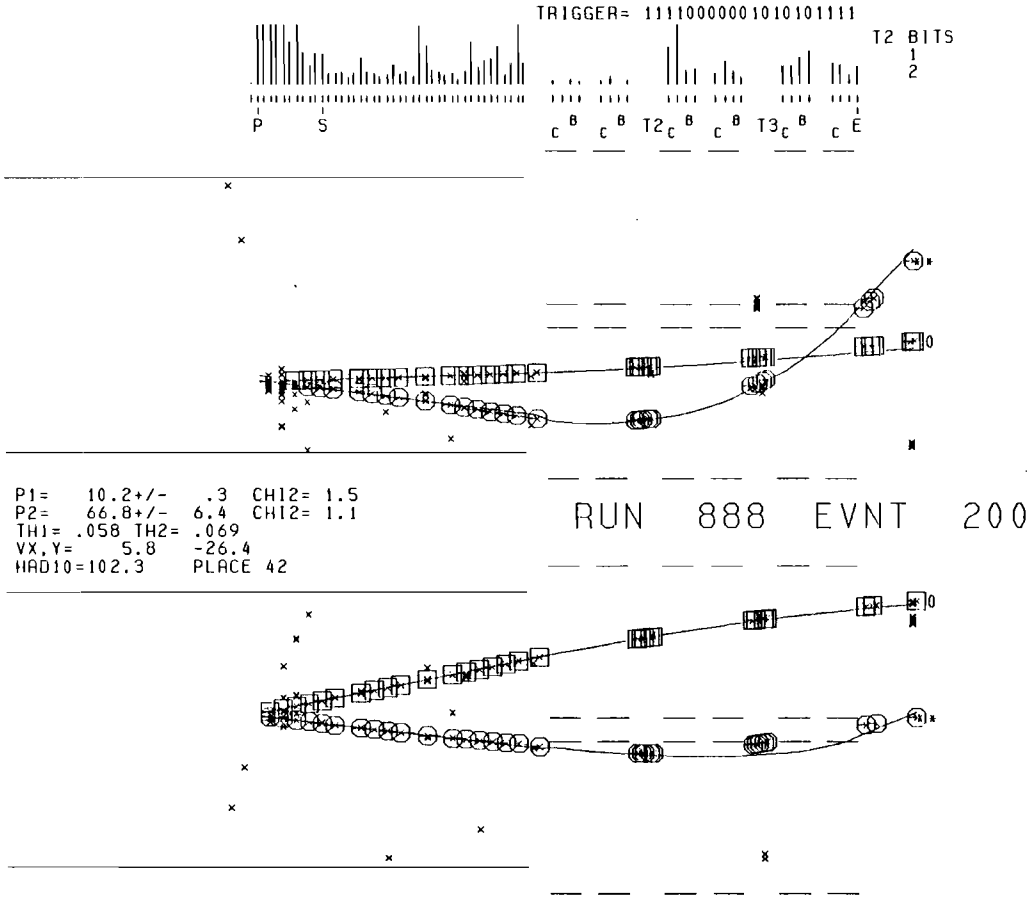
TRIGGER= 1111000000101010111 1
T2 BITS
1
2
P
S
C B C B T2 C B C B T3 C B C E
P1= 10.2+/- .3 CHI2= 1.5
P2= 66.8+/- 6.4 CHI2= 1.1
TH1= .058 TH2= .069
VX,Y= 5.8 -26.4
HAD10=102.3 PLACE 42
RUN 888 EVNT 200